Structural Behavior of a Prototype Ultra-High Performance Concrete Pi-Girder

November 2009

NTIS Accession No. PB2009-115495

FHWA Publication No. FHWA-HRT-10-027

U.S. Department of Transportation
Federal Highway Administration

FOREWORD

With the ever increasing congestion and deterioration of our nation's highway system, a need exists to develop highly durable and rapidly constructed infrastructure systems. Durable bridge structures that would require less intrusive maintenance and would exhibit longer life spans thus maximizing the use of the facility are highly desirable. Expediting bridge construction can minimize traffic flow disruptions. Ultra-high performance concrete (UHPC) is an advanced construction material which affords new opportunities to envision the future of the high infrastructure. The Federal Highway Administration has been engaged in research into the optimal uses of UHPC in the highway bridge infrastructure since 2001 through its Bridge of the Future initiative. This report presents results of a study aimed at developing a bridge superstructure system which facilitates rapid construction and long service life through the use of UHPC. The decked prestressed concrete girder which was developed and tested is expected to, with a few refinements, provide bridge owners with a new solution that meets many of their demands.

This report corresponds to the TechBrief titled, "Structural Behavior of a Prototype UHPC Pi-Girder" (FHWA-HRT-09-068). This report is being distributed through the National Technical Information Service for informational purposes. The content in this report is being distributed "as is" and may contain editorial or grammatical errors.

TECHNICAL REPORT DOCUMENTATION PAGE

1. Report No. FHWA-HRT-10-027	2. Government Accession No. PB2009-115495	3. Recipient's Catalog No.
4. Title and Subtitle Structural Behavior of a Prototype Ultra-High Performance Concrete Pi-Girder		5. Report Date November 2009 6. Performing Organization Code:
7. Author(s) Benjamin A. Graybeal		8. Performing Organization Report No.
9. Performing Organization Name and Address Office of Infrastructure Research & Development Federal Highway Administration 6300 Georgetown Pike McLean, VA 22101-2296		10. Work Unit No. 11. Contract or Grant No.
12. Sponsoring Agency Name and Address Office of Infrastructure Research & Development Federal Highway Administration 6300 Georgetown Pike McLean, VA 22101-2296		13. Type of Report and Period Covered Final Report: 2003-2008 14. Sponsoring Agency Code HRDI-06
15. Supplementary Notes		

16. Abstract

Ultra-high performance concrete (UHPC) is an advanced cementitious composite material which has been developed in recent decades. When compared to more conventional cement-based concrete materials, UHPC tends to exhibit superior properties such as increased durability, strength, and long-term stability. This experimental investigation focused on the structural behavior of a newly developed highway bridge girder cross section, namely the pi-girder. This girder was developed and optimized specifically to exploit the advanced mechanical and durability properties of UHPC. Structural testing was completed on girders and sections of girders so as to investigate the flexural response, the shear response, the transverse flexural response, and the lateral load distribution capabilities of the girder. The knowledge gained through this study present a path forward to a viable structurally-optimized UHPC bridge superstructure system. Further development of the pi-girder system is underway.

17. Key Words Ultra-high performance concrete, UHPC, fiber-reinforced concrete, bridges, precast concrete, prestressed concrete, bridge design, accelerated construction, durable infrastructure systems.	18. Distribution Statement No restrictions. This document is available through the National Technical Information Service, Springfield, VA 22161.		
19. Security Classif. (of this report) Unclassified	20. Security Classif. (of this page) Unclassified	21. No. of Pages 146	22. Price A 08

Form DOT F 1700.7 (8-72) Reproduction of completed page authorized

SI* (MODERN METRIC) CONVERSION FACTORS

APPROXIMATE CONVERSIONS TO SI UNITS

Symbol	When You Know	Multiply By	To Find	Symbol
		LENGTH		
in	inches	25.4	millimeters	mm
ft	feet	0.305	meters	m
yd	yards	0.914	meters	m
mi	miles	1.61	kilometers	km
		AREA		
in^2	square inches	645.2	square millimeters	mm^2
ft^2	square feet	0.093	square meters	m^2
yd^2	square yard	0.836	square meters	m^2
ac	acres	0.405	hectares	ha
mi^2	square miles	2.59	square kilometers	km^2
		VOLUME		
fl oz	fluid ounces	29.57	milliliters	mL
gal	gallons	3.785	liters	L
ft^3	cubic feet	0.028	cubic meters	m^3
yd^3	cubic yards	0.765	cubic meters	m^3
		NOTE: volumes greater than 1000 L shall be shown in m^3		
		MASS		
oz	ounces	28.35	grams	g
lb	pounds	0.454	kilograms	kg
T	short tons (2000 lb)	0.907	megagrams (or "metric ton")	Mg (or "t")
		TEMPERATURE (exact degrees)		
^oF	Fahrenheit	5 (F-32)/9 or (F-32)/1.8	Celsius	^oC
		ILLUMINATION		
fc	foot-candles	10.76	lux	lx
fl	foot-Lamberts	3.426	candela/m^2	cd/m^2
		FORCE and PRESSURE or STRESS		
lbf	poundforce	4.45	newtons	N
lbf/in^2	poundforce per square inch	6.89	kilopascals	kPa

APPROXIMATE CONVERSIONS FROM SI UNITS

Symbol	When You Know	Multiply By	To Find	Symbol
		LENGTH		
mm	millimeters	0.039	inches	in
m	meters	3.28	feet	ft
m	meters	1.09	yards	yd
km	kilometers	0.621	miles	mi
		AREA		
mm^2	square millimeters	0.0016	square inches	in^2
m^2	square meters	10.764	square feet	ft^2
m^2	square meters	1.195	square yards	yd^2
ha	hectares	2.47	acres	ac
km^2	square kilometers	0.386	square miles	mi^2
		VOLUME		
mL	milliliters	0.034	fluid ounces	fl oz
L	liters	0.264	gallons	gal
m^3	cubic meters	35.314	cubic feet	ft^3
m^3	cubic meters	1.307	cubic yards	yd^3
		MASS		
g	grams	0.035	ounces	oz
kg	kilograms	2.202	pounds	lb
Mg (or "t")	megagrams (or "metric ton")	1.103	short tons (2000 lb)	T
		TEMPERATURE (exact degrees)		
^oC	Celsius	1.8C+32	Fahrenheit	^oF
		ILLUMINATION		
lx	lux	0.0929	foot-candles	fc
cd/m^2	candela/m^2	0.2919	foot-Lamberts	fl
		FORCE and PRESSURE or STRESS		
N	newtons	0.225	poundforce	lbf
kPa	kilopascals	0.145	poundforce per square inch	lbf/in^2

*SI is the symbol for the International System of Units. Appropriate rounding should be made to comply with Section 4 of ASTM E380.
(Revised March 2003)

TABLE OF CONTENTS

LIST OF FIGURES

LIST OF TABLES

CHAPTER 1. INTRODUCTION

INTRODUCTION

Ultra-high performance concrete (UHPC) is an advanced cementitious composite material which has been developed in recent decades. When compared to more conventional cement-based concrete materials, UHPC tends to exhibit superior properties such as increased strength, durability, long-term stability.

This experimental investigation focused on the structural behavior of a newly developed highway bridge girder cross section, namely the pi-girder. This girder was developed and optimized specifically to exploit the advanced mechanical and durability properties of UHPC. Structural testing was completed on girders and sections of girders so as to investigate the flexural response, the shear response, the transverse flexural response, and the lateral load distribution capabilities of the girder.

OBJECTIVE

The objective of this research program is to evaluate a prototype UHPC pi-girder cross section intended for use in short-to-medium span highway bridge applications.

SUMMARY OF APPROACH

The research discussed herein includes two phases. The first phase focused on the fabrication of four UHPC pi-girders. These 0.91-m (33-inch) deep, 2.4-m (8 foot) wide, 21.3-m (70-foot) long prestressed girders were fabricated at a conventional precast bridge girder production plant. The second phase of the research focused on the physical testing of these full-scale girders through the application of structural loads. Primary flexure, primary shear, transverse flexure, and load distribution tests were conducted. The results of the tests were then analyzed and are presented herein.

OUTLINE OF REPORT

This report is divided into seven chapters. Chapters 1 and 2 provide an introduction to the study and relate relevant background information necessary in understanding the study's results. Chapter 3 presents the compressive and tensile mechanical properties of the UHPC tested in this study. Information regarding the fabrication of and the experimental methods associated with the girders tested in this study is presented in Chapter 4. The results of the structural tests are presented in Chapter 5. Chapter 6 presented a summary and discussion of the results presented in Chapter 5. Finally, Chapter 7 presents the conclusions of this research program.

CHAPTER 2. BACKGROUND

INTRODUCTION

This chapter provides background information relevant to the focus of the research effort. A general discussion of UHPC constituent materials and material properties is presented first. The development of the concept for the UHPC pi-girder cross section studied in this research effort is presented next. Finally, results of prior full-scale structural testing focused on UHPC bridge components are presented.

UHPC CONSTITUENT MATERIALS

The specific UHPC investigated in this study is a product of a major worldwide construction materials manufacturer and supplier. It is currently the only product of this type that is widely available in the U.S. in the quantities necessary for large scale infrastructure applications. Table 1 provides a typical UHPC composition[(1)].

As reported in reference (1), the constituent material proportions were determined, in part, based on an optimization of the granular mixture. This method allows for a finely graded and highly homogeneous concrete matrix. Fine sand, generally between 150 and 600 micrometers (μm), is dimensionally the largest granular material. The next largest particle is cement with an average diameter of approximately 15 μm. Of similar size is the crushed quartz with an average diameter of 10 μm. The smallest particle, the silica fume, has a diameter small enough to fill the interstitial voids between the cement and the crushed quartz particles. Dimensionally, the largest constituent in the mix is the steel fiber reinforcement. In this study, the fibers in the mix had a diameter of 0.2 mm (0.008 inch), a length of 12.7 mm (0.5 inch), and a minimum tensile strength of 2600 MPa (377 ksi). The fibers were included in the mix at two percent by volume. Given the relative sizes of the sand and the fibers, the steel fibers are able to reinforce the concrete matrix on the micro level.

Table 1. Typical UHPC composition.

Material	Amount (kg/m^3 (lb/yd^3))	Percent by Weight
Portland Cement	712 (1,200)	28.5
Fine Sand	1,020 (1,720)	40.8
Silica Fume	231 (390)	9.3
Ground Quartz	211 (355)	8.4
Superplasticizer	30.7 (51.8)	1.2
Accelerator	30.0 (50.5)	1.2
Steel Fibers	156 (263)	6.2
Water	109 (184)	4.4

UHPC MATERIAL PROPERTIES

The research program associated with reference (1) addressed the materials properties of the UHPC investigated in this study. A brief summary of the relevant results is presented in Table 2.

Table 2. Typical UHPC material properties.

Material Characteristic	Average Result
Compressive Strength (ASTM C39; 28-day strength)	193 MPa
Modulus of Elasticity (ASTM C469; 28-day modulus)	52.4 GPa
Split Cylinder Cracking Strength (ASTM C496)	11.7 MPa
Prism Flexure Cracking Strength (ASTM C1018; 305-mm span; corrected)	9.0 MPa
Mortar Briquette Cracking Strength (AASHTO T132)	8.3 MPa
Direct Tension Cracking Strength (Axial tensile load)	9.7–11.0 MPa
Prism Flexural Tensile Toughness (ASTM C1018; 305-mm span)	$I_{30} = 53$
Long-Term Creep Coefficient (ASTM C512; 77 MPa sustained load)	0.29
Long-Term Shrinkage (ASTM C157; initial reading after set)	766 microstrain
Total Shrinkage (Embedded vibrating wire gage)	850 microstrain
Coefficient of Thermal Expansion (AASHTO TP60–00)	15.6×10^{-6}
Chloride Ion Penetrability (ASTM C1202; 28-day test)	18 coulombs
Chloride Ion Permeability (AASHTO T259; 12.7-mm depth)	< 0.06 kg/m^3
Scaling Resistance (ASTM C672)	No Scaling
Abrasion Resistance (ASTM C944 2x weight; ground surface)	0.17 grams lost
Freeze-Thaw Resistance (ASTM C666A; 600 cycles)	RDM = 96%
Alkali-Silica Reaction (ASTM C1260; tested for 28 days)	Innocuous

1 MPa = 145 psi
1 kg/m^3 = 1.69 lb/yd^3
1 g = 0.035 ounce

DEVELOPMENT OF PROTOTYPE UHPC PI-GIRDER

The concept of using decked-girder members for bridge applications in transportation and infrastructure is not new. The deck-bulb-Tee pretensioned concrete girder has been frequently implemented in various parts of the U.S., most notably in the Pacific Northwest. The double-Tee pretensioned concrete beam is widely used around the world in parking structures. In New England, governmental and industry partners are working to develop a pretensioned double-Tee suitable for short to medium span highway bridges.

It is also the case that bridge designs are inherently a function of the mechanical and durability properties of the materials from which the bridge is to be constructed. In the case of reinforced or prestressed concrete bridges, these properties and the related design specifications have resulted in bridge component geometries which make efficient use of the material properties.

The development of new materials or the significant modification of the properties of existing materials results in the need for the development of new structural forms. The use of existing geometries for materials with advanced properties, although simple to implement, results in

inefficient designs and less cost effective solutions. Advanced material properties bring about the possibility of new design solutions which heretofore may not have been possible.

The advanced properties of UHPC provide opportunities for the development of new structural forms focused on addressing any number of important focus areas. Straightforward topics such as creating longer-life bridges through enhanced durability or allowing for the spanning of longer distances with shallower superstructures can be addressed through the use of UHPC. In a systematic sense, UHPC also presents the opportunity to create new structural forms which facilitate accelerated construction and rapid renewal of the highway infrastructure.

The development of a prototype decked girder member which utilized UHPC as the primary structural component was initiated during the early stages of the FHWA UHPC research program, results of which are presented in references (1) and (2). It was evident that UHPC's mechanical and durability properties would allow for beneficial modifications to conventional concrete bridge component solutions as well as development of heretofore not feasible components. Given the exceptional durability properties of UHPC and its comparatively high compressive and tensile strengths, the development of a decked pretensioned girder with slender cross sectional dimensions was an appropriate choice.

The geometric concept for the pi-girder also draws on construction of the Peace Footbridge in Seoul, Korea[3]. This arch bridge uses post-tensioned construction and the pi-girder cross sectional shape to span 120 meters (394 feet). Although significantly different than conventional highway bridges in the U.S. both in terms of bridge type and loading, this footbridge clearly demonstrated the opportunities that UHPC presents for slender, decked members.

The cross sectional dimensions of the prototype UHPC pi-girder were set through an analytical study completed at the Massachusetts Institute of Technology[4,5,6]. This research group was selected for this effort as they had completed prior work developing analytical models for the mechanical response of UHPC[7]. The models implemented in the design included one, two, and three dimensional analyses of the predicted response of the girder to the loadings prescribed in the AASHTO LRFD Bridge Design Specification[8].

FHWA FULL-SCALE UHPC I-GIRDER TESTING

As detailed in reference (2), full-scale structural behavior testing has previously been completed by FHWA. In the test program, AASHTO Type II pretensioned concrete bridge girders were cast using the same UHPC investigated in the current study. Other than the twenty-four 12.7 mm (0.5 inch), 1860 MPa (270 ksi) prestressing strands in their bottom bulb and the two additional strands in their top flange, these girders did not contain any mild steel reinforcement.

A flexure test was completed wherein a girder was subjected to four-point loading over a 23.9 m (78.5 foot) span. The ultimate dead plus live load capacity of the girder was 4800 kN-m (42480 kip-inches).

Three shear tests were completed wherein a girder was subjected to three-point bending with shear span-to-depth ratios ranging from 2.0 to 2.5. These test setups had varying levels of restraint provided to strands near the reaction location so as to consider the effect of strand slip

on shear capacity results. The lowest ultimate dead plus live load shear capacity recorded was 1710 kN (384 kips) while the highest was 2230 kN (502 kips).

CHAPTER 3. CONCRETE MATERIAL PROPERTIES

INTRODUCTION

The material properties of the UHPC in the prototype pi-girder specimens were obtained through the testing of cylinders cast along side the girder specimens. These material properties are reported herein.

CONCRETE MATERIAL PROPERTIES

During the casting of the pi-girder specimens, 76-mm (3-inch) and 102-mm (4-inch) diameter cylinder specimens were cast in order to allow for material property characterization. These cylinders were cast in the field alongside the girders using UHPC obtained from the trucks which were casting the girders. As the concrete for each leg of the girder came from an individual truck which held specific a specific batch of UHPC, cylinders were made from each truck's concrete. After casting, the cylinders were stored with the girders during curing and heat treatment.

The cylinders were prepared for testing by grinding both ends to create parallel surfaces through the use of an end grinder. After preparation, the cylinders exhibited length to diameter ratios of approximately 1.9. Four tests were carried out on the cylinders, namely density, modulus of elasticity, compressive strength, and split cylinder tensile strength. Density measurements were obtained through conventional means by measuring weight of each cylinder and dividing by the volume. The average density of the UHPC was 2515 kg/m^3 (157 lb/ft^3).

The compressive strength tests were completed according to ASTM C39[(9)], except that the load rate was increased to 1MPa/sec (150 psi/sec). Modulus of elasticity tests were completed according to ASTM C469[(10)] following the procedure described in reference (1). The test was modified in that the load rate for the cylinder was increased to 1 MPa/sec (150 psi/sec), the deformation values were captured continuously throughout each test, and the modulus was calculated based on the load range from 10 to 30 percent of the actual compressive strength of the specimen. Each modulus of elasticity test was run through compressive failure so as to obtain the compressive strength result.

The compressive strength and modulus of elasticity results are presented in Table 3. The tests were completed during the timeframe when the girders were being tested. In general, the cylinders were 5 to 7 months old. Overall, the compressive strength of the UHPC used in the girders was approximately 220MPa (32.1 ksi). The modulus of elasticity was approximately 56.3 GPa (8170 ksi).

Table 3. Compressive strength and modulus of elasticity.

Girder Casting	Test Age (days)	Compressive Strength (MPa)			Modulus of Elasticity (GPa)		
		No.	Ave.	St. Dev.	No.	Ave.	St. Dev.
ASTM C39 Compressive Test Only							
P1 North	241	3	230	13.3			
P1 South	241	3	225	9.6			
P2 North	233	3	229	22.8			
P2 South	233	3	235	6.2			
P3 North	170	3	221	10.4			
P3 South	170	3	200	22.8			
P4 North	156	3	230	4.4			
P4 South	156	3	213	3.4			
ASTM C469 and C39							
P1 North	249	3	228	5.6	3	59.1	1.5
P1 South	249	3	212	24.5	3	57.2	3.1
P2 North	241	2	233	3.6	2	60.5	6.0
P2 South	241	1	241	---	1	56.3	---
P3 North	178	2	229	5.3	2	57.3	1.7
P3 South	178	2	217	8	2	56.0	3.4
P4 North	164	3	235	7.2	3	56.2	2.0
P4 South	164	3	220	5.0	3	56.9	3.1

1 MPa = 145 psi
1 GPa = 145,000 psi

The split cylinder tensile strength tests were completed according to the procedure described briefly in reference (1) and more fully in reference (11). The procedure is the same as that described in ASTM C496[12] with the exception of an increased load rate (3.45 MPa/min (500 psi/min)) and extra data collection allowing for determination of lateral specimen expansion throughout the test. A single 102-mm (4-inch) diameter cylinder was tested from the concrete in the north and south legs of each girder. Results from these tests are presented in Table 4. The cracking tensile strength is approximately 10.3 MPa (1.5 ksi).

Table 4. Split cylinder tensile test results.

Girder Casting	Test Age (days)	Cracking Strength (MPa (ksi))	Peak Strength (MPa (ksi))
P1†	281	10.1 (1.46)	27.5 (3.99)
P1†	281	11.6 (1.68)	26.9 (3.90)
P2 North	273	10.3 (1.50)	24.5 (3.56)
P2 South	273	11.4 (1.65)	27.4 (3.97)
P3 North	210	11.7 (1.69)	24.2 (3.51)
P3 South	210	10.8 (1.57)	20.2 (2.93)
P4 North	196	10.4 (1.51)	20.3 (2.94)
P4 South	196	10.6 (1.54)	23.4 (3.40)

† North/South was not differentiated on specimens from P1.

CHAPTER 4. GIRDER DESIGN, FABRICATION, AND TESTING METHODS

INTRODUCTION

The experimental program is described in this chapter. The girder design is described first. The girder fabrication process is then presented, followed by a discussion of the test matrix and the test setups. The specific details of each girder specimen and the instrumentation plan for each girder test are then presented.

GIRDER DESIGN

The pi-girder was developed to efficiently utilize the advanced material properties of UHPC. Its design is based on resisting the loadings prescribed in the AASHTO LRFD Bridge Design Specification[8]. The concept for the design was described previously in Chapter 2. Analytical calculations completed as part of the design effort were primarily conducted through the use of 1D, 2D, and 3D computer analyses.

The specific cross section investigated in this study was designed to span between 21.3 and 30.5 m (70 to 100 feet). This cross section is shown in Figure 1. The girder is 0.84 m (33 inches) deep, 2.44 m (8 feet) wide, and can contain up to 15 prestressing strands in each bulb. The integral deck of the girder is 76 mm (3 inches) thick, and the webs range from 64 to 84 mm (2.5 to 3.3 inches) thick. A 156 mm (6.1 inch) deep shear key runs the length of each flange tip to allow for connection of the modular components once on site. Basic properties of the girder include an area of 0.392 m^2 (609 in^2), strong axis moment of inertia of 37.07x10^9 mm^4 (89,060 in^4), and a self-weight of 978 kg/m (657 lb/ft).

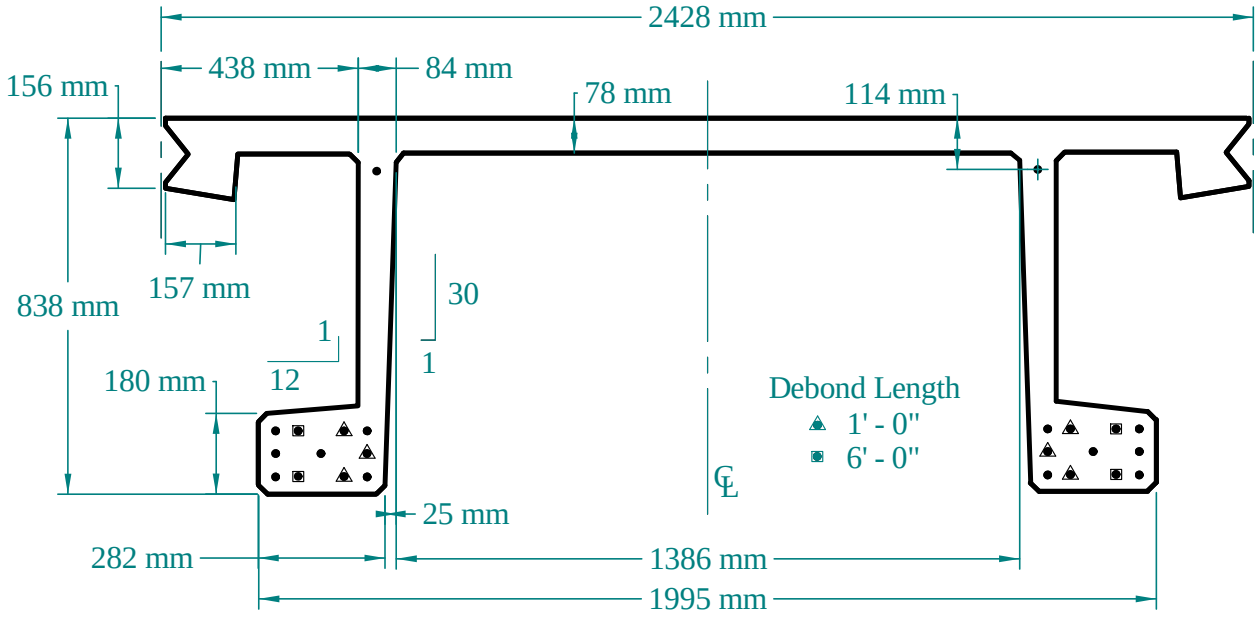

Figure 1. Illustration. Girder cross section and strand pattern.

GIRDER FABRICATION

Four UHPC pi-girders were fabricated at Prestress Services of Kentucky, Inc., in Lexington, Kentucky. These girders were designed to efficiently utilize the advanced material properties exhibited by concrete from which they were composed.

The formwork used for the fabrication of the four girders was fabricated by Helser Industries, Inc. of Tualatin, Oregon. A pair of approximately 11-m (36-ft) long forms were fabricated and installed end-to-end on a girder casting bed at Prestress Services. This casting bed was wide enough to allow for the entire girder width to be supported as well as to allow for the exterior side forms to be slid back from the girder during assembly and disassembly. Figure 2 shows the formwork during assembly for a trial casting. As can be observed in the figure, the left and right form pieces which support the underside of the concrete deck adjacent to the form's center post can articulate down and toward the middle so as to allow for unrestrained transverse dimensional changes in the girder during setting and hydration.

Figure 2. Photo. Girder formwork.

The process of preparing the form for casting included: 1) assembling and locking in place the center portion of the form, 2) installing the bulkheads at the ends of the form, 3) pulling the prestressing strands through the form, 4) sealing gaps in the form using silicone caulk, 5) installing the side forms, and 6) installing the Styrofoam covered wooden blockouts on top of the side forms to create the void in the underside of the overhang deck. Extra care was taken to ensure that, to the greatest extent possible, the forms were securely bolted to the prestressing bed and any gaps in the formwork were sealed.

The girders were prestressed through the use of 12.7-mm (0.5-inch) diameter, 1860 MPa (270 ksi) low-relaxation prestressing strands. Other than these strands, the girders contained no discrete steel reinforcement. Four girders were fabricated and will be referred to in this report as

Girders P1, P2, P3, and P4. Girders P1 and P2 contained 22 strands, 11 in each of the two bulbs. Girders P3 and P4 contained two additional strands, one each located near the top of each web of these girders. The strands were all stressed to 130 kN (29.2 kips). Figure 1 shows the girder cross-section along with the strand pattern. As noted in the figure, six of the strands were debonded for 0.3 m (12 inch) from each end of the girder and another 4 strands were debonded for 1.8 m (72 inch) from each end of the girder. Note that this strand pattern was modified for one end of Girder P4 wherein the three strands on the inside of each bulb were draped up into the web. On this end of this girder, no strands were debonded for 0.3 m (12 inch), the draping began at a distance of 6.5 m (21.33 ft) from the end of the girder, and the bottom draped strands exited the girder at 0.56 m (22 inch) up from the bottom of the girder.

The UHPC for each girder was mixed in the precaster's central batch plant. Four batches of approximately 2.7 m^3 (3.5 yd^3) each were mixed for each girder. The mix design for each batch is presented in Table 5. The mix design includes a water to cementitious materials ratio of approximately 0.18. Discontinuous, dispersed steel fibers are included in the mix at 2 percent by volume. These steel fibers were 13 mm (0.5 inch) long and had a diameter of 0.2 mm (0.008 inch). The mixing of each batch was completed in approximately 25 to 30 minutes from first water addition to mixer discharge.

Table 5. Mix design.

Constituent	Quantity
Premix	2190 kg/m^3 (3692 lb/yd^3)
Glenium 3000 NS Superplasticizer	30 kg/m^3 (50.5 lb/yd^3)
Water	128.7 kg/m^3 (217 lb/yd^3)
Steel Fibers	156 kg/m^3 (262.5 lb/yd^3)

After the mixing of each batch, the concrete was discharged into a ready mix truck for holding and transport to the casting bed. The first and fourth batches were placed into one truck, while the second and third batches were placed into a second truck. The truck drums were kept out direct sunlight and were slowly rotated. For each girder, the time from mix initiation of the first batch until start of placing was approximately 3.5 hours. As there was only one formwork available, the process of girder casting was repeated four times on four separate days.

After the mixing of the fourth batch, the trucks transported the concrete to the form. The filling of the bulbs and webs was completed through one truck on each side of the formwork discharging concrete into the top of the web opening. As the concrete is self-consolidating, the concrete was discharged beginning at one end of the girder and allowed to flow toward the other end. The discharge point moved along the girder length as the form began to fill up, but always remained behind the leading edge of the flowing concrete. Once both webs of the form were full to approximately two-thirds of their height, a trough was inserted in the placement stream to allow for uniform dispersion of the concrete across the deck width. Figure 3 presents photographs of the concrete placing process. Short duration bursts of external form vibration were used infrequently during the placing process. This vibration was intended to facilitate the expulsion of air trapped in the concrete during the placing process. Plastic sheeting was placed

over the concrete immediately behind the trough. The plastic was in contact with the concrete and served to retard dehydration of the top surface of the girder.

After concrete placement was complete, each girder was covered by an insulating tent in order to control the environment and facilitate initial curing. As the girders were cast during colder months, live steam was released under the girders beginning a few hours after casting. This served to keep the environment surrounding the girders at a high humidity level and at a temperature of approximately 38ºC (100ºF).

The girders were monitored during initial setting of the concrete in order to determine the proper timing for formwork release. Thermocouples were embedded in the concrete during casting in order to monitor the temperature of the deck and bulbs during initial setting. Embedded vibrating wire strain gages were also monitored. Finally, the penetration resistance of the exposed surface of the deck was monitored. The penetration resistance was used as a primary mechanism to determine whether the interior and exterior forms could be released. The timing of the form release was critical as an early release would result in sloughing of the wet concrete while late release would result in shrinkage cracking of the deck.

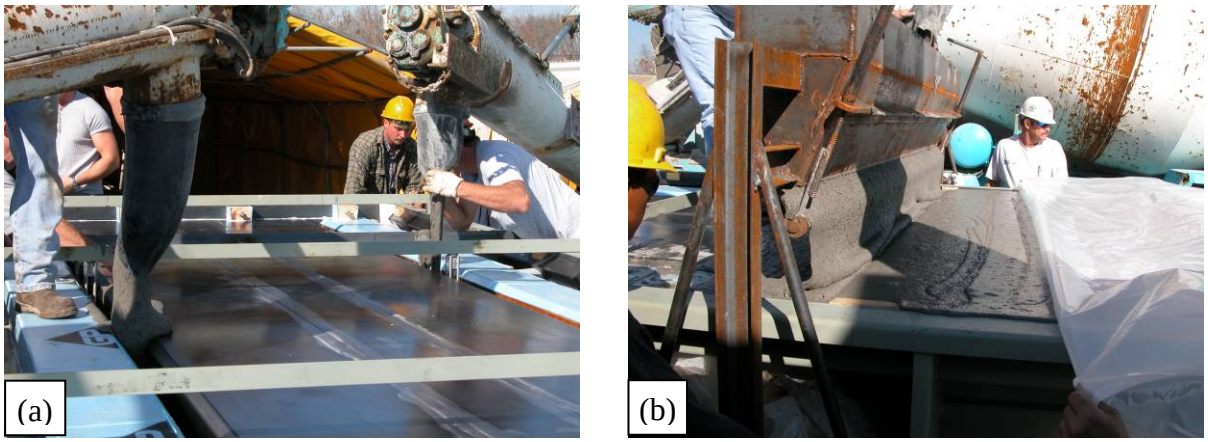

Figure 3. Photo. Concrete placement, including (a) directly into formwork and (b) through trough into formwork.

After form release, the concrete was allowed to continue to cure until match cast cylinders demonstrated that the compressive strength of the concrete was at least 80 MPa (11.6 ksi). Once this strength was reached, the prestressing strands were detensioned by flame-cutting individual strands on each end of the girder.

After strand detensioning, each girder was moved to a temporary storage location where a solid UHPC diaphragm could be cast onto each end of each girder. In each case, this diaphragm was 102 mm (4 inches) thick and enclosed the end of the girder as shown in Figure 4.

Figure 4. Photo. Fabricated girder with diaphragm prior to steam treatment.

After the diaphragms were demolded, each girder was moved to a casting bed which had been arranged for application of a steam treatment. The steam treatment consisted of releasing live steam under the girder which was insulated by multiple layers of insulating tarps. The volume of steam released was ramped up and down so as not to thermally shock the girders. The environment surrounding each girder was maintained at a temperature of at least 90 ºC (194 ºF) for at least 48 hours. After the application of the steam treatment for all four girders, the girders were transported to the FHWA's Turner-Fairbank Highway Research Center.

Note that Girders P1, P3, and P4 met all fabrication requirements and were considered to accurately reflect the design of the pi-girder. A negative flexural crack was observed in Girder P2 at midspan as it was being removed from its formwork immediately after detensioning. This crack extended through the girder deck and down into both webs. It is suspected that this crack resulted from insufficient tensile capacity in the top flange of the girder at strand release. The future structural testing of this girder was designed so as to minimize the impact that this crack would have on the test results.

BRIDGE ERECTION AND TEST PROCEDURE

Girders P1 and P3 were erected to form a test bridge immediately upon arrival at TFHRC. One crane was stationed at each end of the bridge span to facilitate the girder placement. Figure 5 shows a photo of the placing of the second girder. After placement, the longitudinal joint between the girders was bolted together through the use of stainless steel threaded rods spaced at 0.91 m (3 feet) along the length of the bridge. The detail for this connection is shown in Figure 6. After the bolting of the connection, the shear key was filled with a non-shrink structural grout. As this bridge does not require the casting of an additional structural deck or overlay, the grouting of the longitudinal joint completed the construction of the main structural elements of the bridge. Were this bridge being placed into service, the approaches, riding surface, and barriers would also need to be completed prior to opening to traffic. The erection of the girders, bolting of the joint, and casting of the shear key was completed within 8 hours, demonstrating the speed with which modular components of this type can be constructed to form a bridge.

Figure 5. Photo. Erection of test bridge.

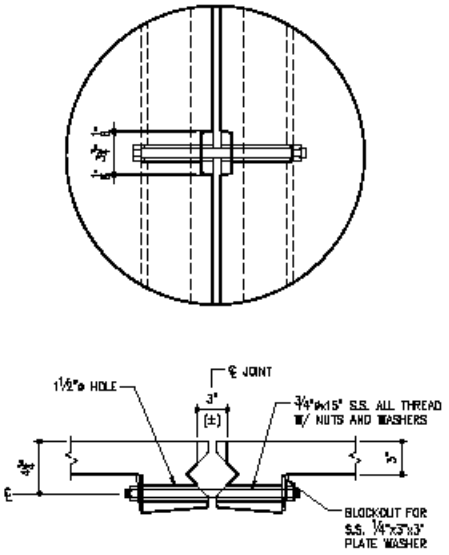

Figure 6. Illustration. Longitudinal joint connection detail.

The load testing of the bridge was focused on the service load level response of the structure. The test procedure was devised to load the bridge both symmetrically and asymmetrically, thus providing information related to the load distribution behavior of the structure. Figure 7 shows the concept of the loading setup wherein hydraulic jacks pull down on spreader beams which are placed above the deck. The spreader beams are attached to the jacks through high strength steel threaded rods which pass through 76 mm (3 inch) diameter core holes in the deck. In order to

study the behavior of the longitudinal joint, independent spreader beams were used above each girder. The setup shown relates to symmetric loading of the bridge; however, through simple modification of spreader beam and point load locations unsymmetric loading configurations were created.

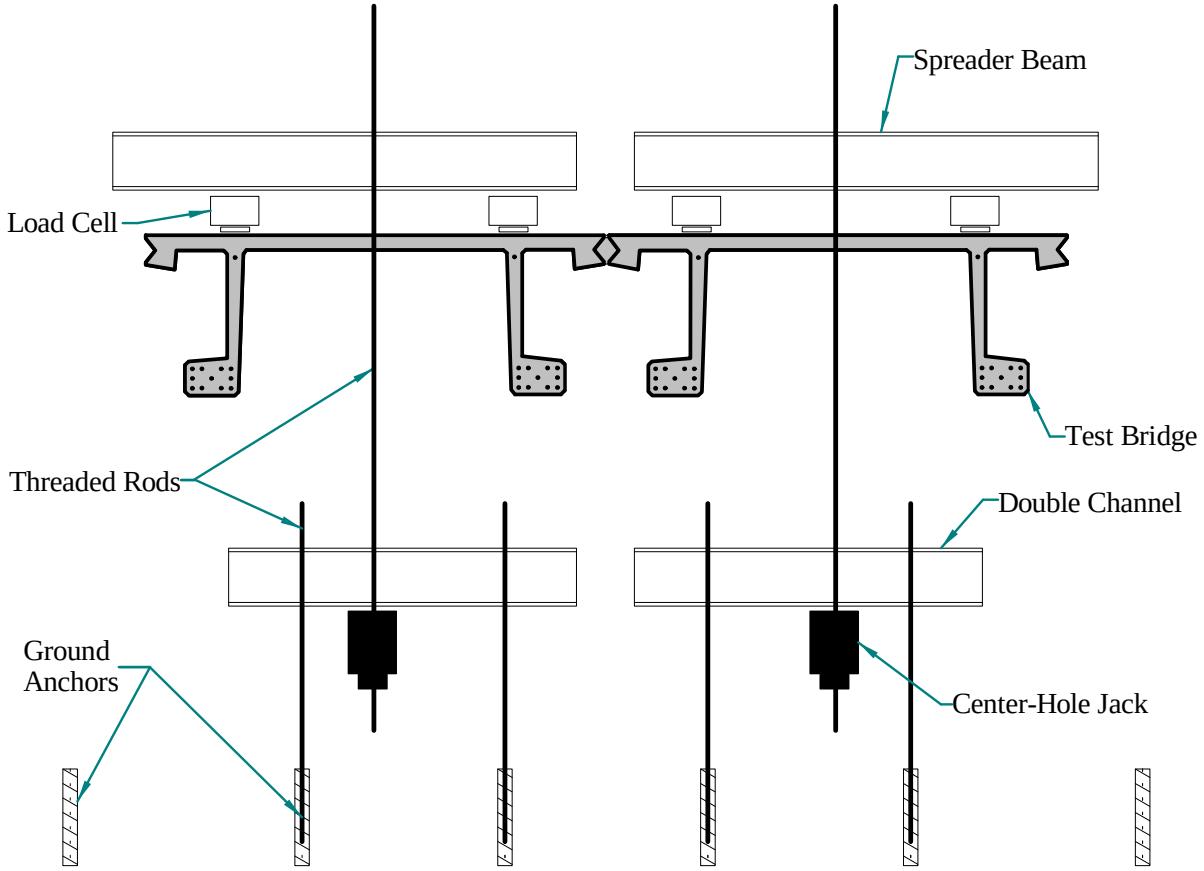

Figure 7. Illustration. Cross-section of loading setup near midspan of test bridge.

GIRDER TEST PROCEDURE

Upon delivery to TFHRC, Girders P2 and P4 were brought into the Structural Testing Laboratory. Seven full-scale destructive investigations of structural behavior were completed through the use of these two girders. Table 6 provides details on these seven tests, with the tests being completed in the order shown in the table. The primary focus of the tests is also provided along with the center-to-center of bearing span over which the tests were completed. Figure 8 provides an illustration of the origin of the test specimens originating from Girder P2. Figure 9 provides similar origination information for Girder P4 specimens. Both of these figures demonstrate the progression of test specimens from the full girders as delivered through the completion of testing. In all seven tests, the loads were applied by hydraulic jacks pushing vertically downward on the top of the deck.

Table 6. Girder tests.

Test Identifier	Girder	Span	Behavioral Focus
P2-70F	P2	21 m	Primary flexure
P2-21S	P2	6.4 m	Primary shear with debonded strands
P4-57Ss	P4	17.4 m	Primary shear with debonded strands
P4-57Sh	P4	17.4 m	Primary shear with harped strands
P4-45F	P4	13.7 m	Primary flexure
P4-24T	P4	7.3 m	Transverse flexure
P4-24D	P4	7.3 m	Transverse flexure

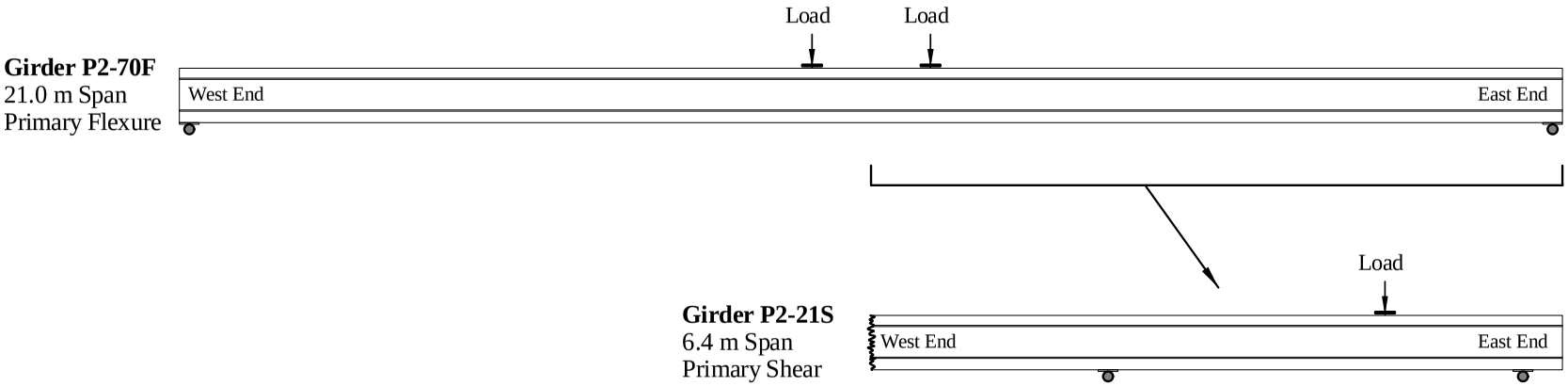

Figure 8. Illustration. Origin of Girder P2-70F and P2-21S test specimens.

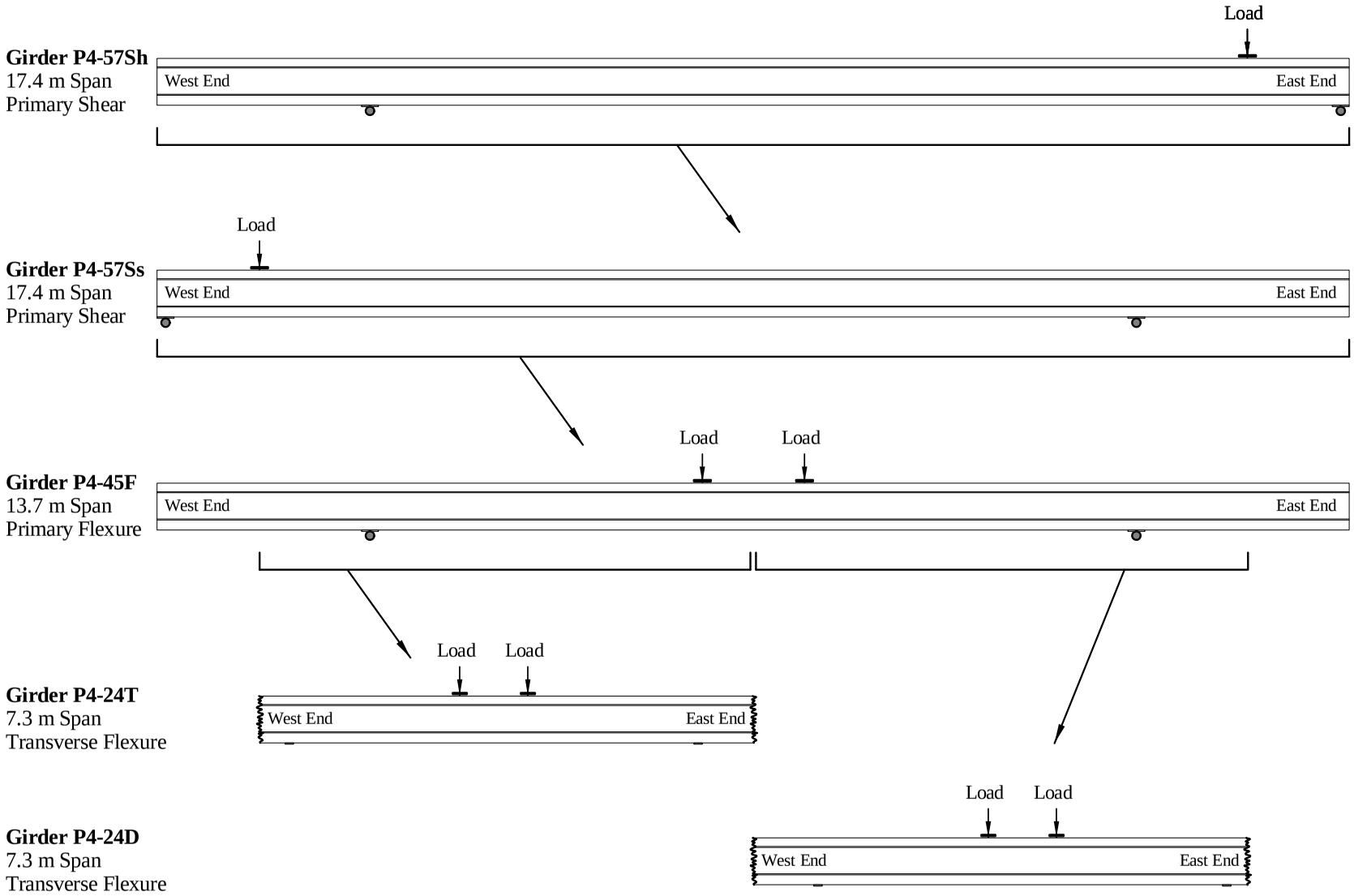

Figure 9. Illustration. Origin of Girder P4-57Ss, P4-57Sh, P4-45F, P4-24T, and P4-24D test specimens.

TEST SETUP AND INSTRUMENTATION

Bridge Load Distribution Test

Four tests were completed on the test bridge. During each test, loads were applied along two lines, each equidistant from midspan. Table 7 and Figure 10 provide details of the four loading configurations. Load Configuration (LC) 1 was symmetric loading of the bridge, while LC 2W, 2D, and 3 were asymmetric. Loads at locations A, B, C, and D were applied through 0.23 m (9 inch) diameter steel plates grouted to the surface of the deck, while loads at location E were applied through 0.25 m by 0.51 m (10 inch by 20 inch) elastomeric pads placed on the deck. LC 2D differs from the other load configurations as it was designed to simulate wheels from a pair of rear axles on a truck. The four tests were conducted according to the order listed in Table 7.

Table 7. Test bridge load configurations.

Load Configuration	Description	Locations Loaded (Figure 10)	Load Distances from Midspan
1	Both Girders	A,B,C,D	0.91 m (3 feet)
2W	South Girder Webs	A,B	0.91 m (3 feet)
2D	South Girder Deck	E	0.61 m (2 feet)
3	South Leg of South Girder	A	0.91 m (3 feet)

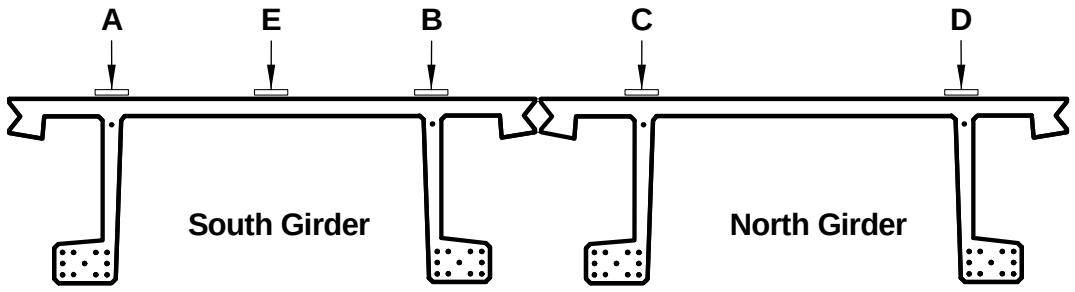

Figure 10. Illustration. Test bridge load locations.

The loading of the test bridge was completed in a stepwise static fashion wherein the applied forces at the load points were increased periodically then held as data and observations were gathered. The entirety of the loading of this bridge was intended to be elastic. Preliminary analyses indicated that loads of 50 kips at points A, B, C, and D in Figure 10 might result in flexural cracking of the girders. As such, loads at points A through E were limited to 30 kips. (Recall that the load at any point shown in Figure 10 is actually applied through two points equidistant from midspan.)

The behavior of the test bridge was captured through the use of visual and audible observations, electrical resistance strain gages, LVDTs, linear potentiometers, and tiltmeters. The instrumentation was focused on the midspan cross-section of the bridge. Figure 11 presents the locations of the 40 strain gages that were affixed to the surface of the bridge. For visualization

purposes, the gages are shown as rotated 90 degrees outward from the surface of the girders. Figure 12 presents the locations of the 10 potentiometers, 6 LVDTs, and 4 tiltmeters installed on the midspan cross-section. Note that the LVDTs were affixed to the surface over predefined gage lengths of approximately 0.25 m (10 inches) to allow for a measure of distributed strain in potentially cracked regions. Also, four of the potentiometers measured relative movement between girder legs, while the remaining six measured absolute vertical deflection of the bridge at discrete locations.

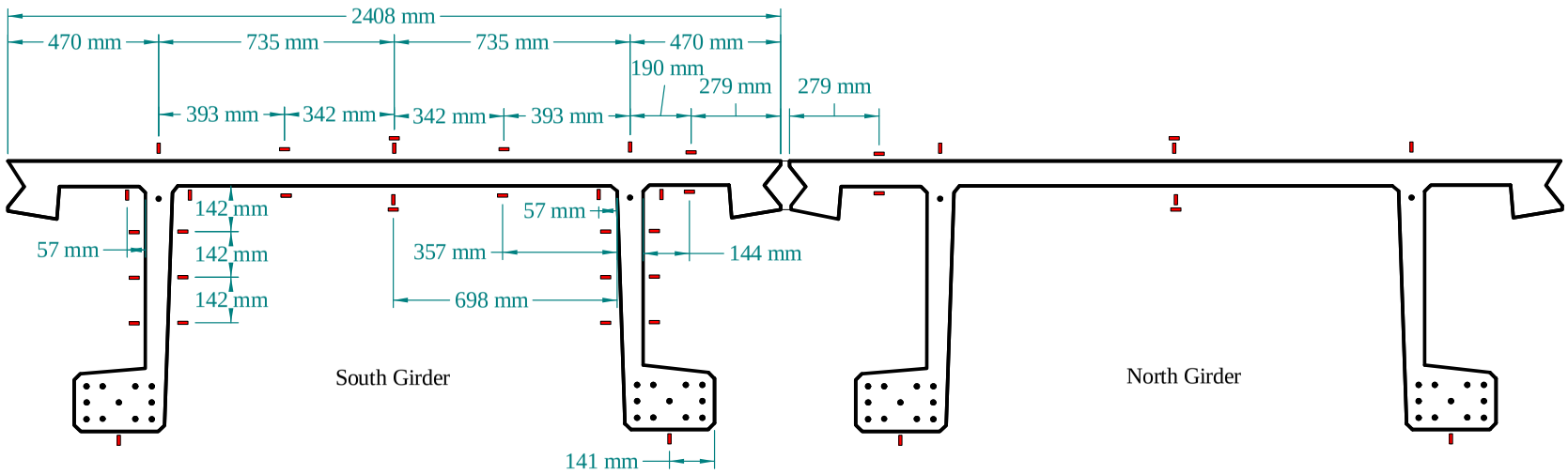

Figure 11. Illustration. Midspan strain gage locations for bridge load distribution test.

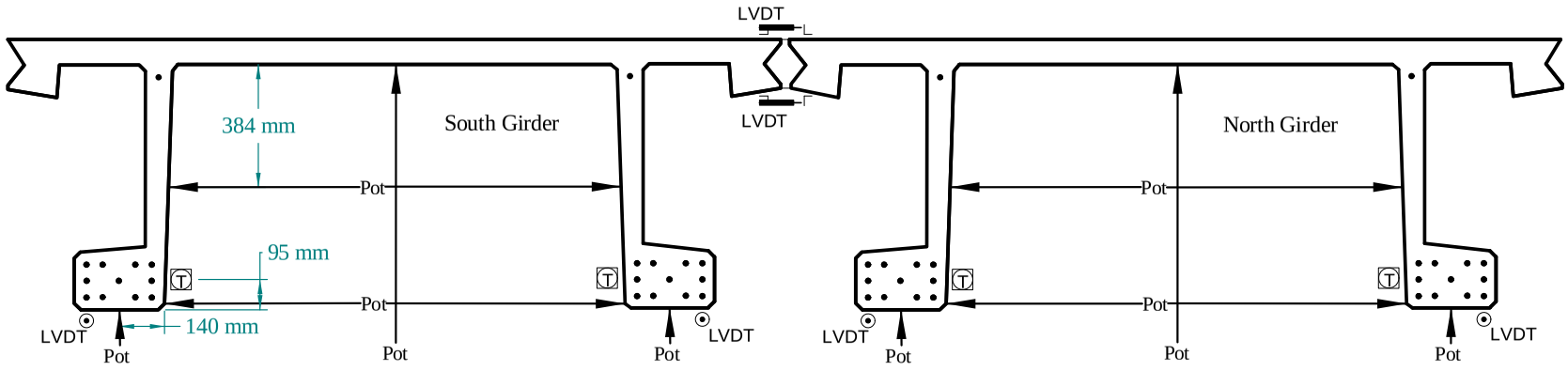

Figure 12. Illustration. Midspan potentiometer, LVDT, and tiltmeter locations for bridge load distribution test.

Test P2-70F

The loading setup for test P2-70F is shown in Figure 13. This 21.34 m (70 ft) girder was loaded in four-point bending over a span of 21 m (69 ft). The load points were located 0.91 m (3 ft) east and west of midspan.

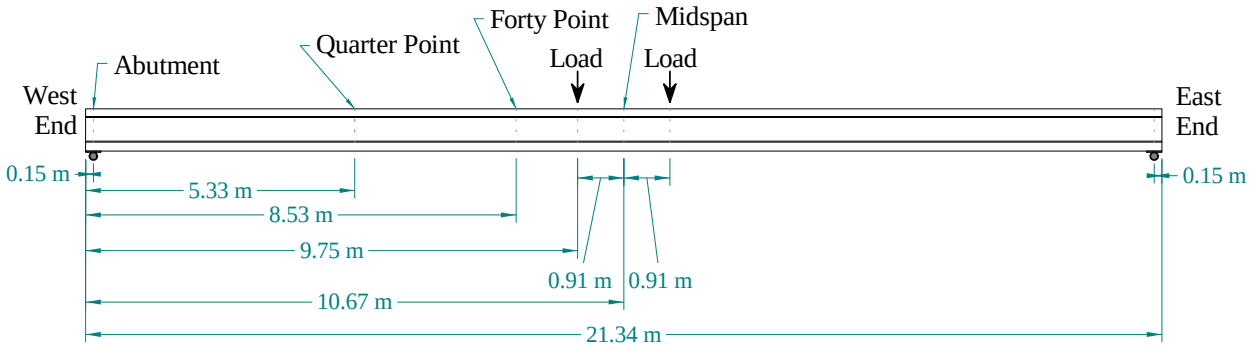

Figure 13. Illustration. Loading setup for Girder P2-70F.

Two series of tests were completed on this girder in this test configuration. First, a set of load distribution tests were completed wherein the loads were placed at various locations along the width of the deck and the reaction forces at supports were monitored. Five load configurations were used in the six load distribution tests that were completed. These load configurations are described in Table 8 and shown in Figure 14. In the baseline test, Configuration A, the loads were applied through 229 mm (9 inch) diameter steel plates that were grouted to the surface of the deck. In tests B through F, the loads were applied through 25 mm by 254 mm by 508 mm (1 inch by 10 inch by 20 inch) elastomeric pads. In all cases, loads were applied along two load lines each 0.91 m (3 ft) from midspan and the girder was supported by steel plates resting on load cells. The load distribution tests were completed in the order shown in Table 8.

Table 8. P2-70F load configurations.

Load Config.	Loading Description	Loading Application Mechanism	Peak Load Applied to Girder
A	Above Both Webs	Grouted Steel Plates	272 kN (61.1 kips)
B	Above South Web	Elastomeric Pads	131 kN (29.4 kips)
C	Along South Overhang	Elastomeric Pads	90 kN (20.3 kips)
D	At Quarter Span Between Webs	Elastomeric Pads	136 kN (30.5 kips)
E	At Middeck	Elastomeric Pads	86 kN (19.4 kips)
F	At Middeck (Beyond Cracking)	Elastomeric Pads	134 kN (30.1 kips)

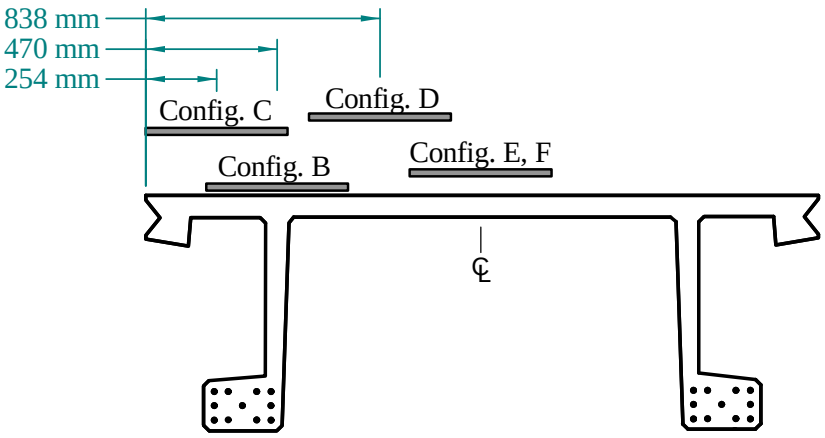

Figure 14. Illustration. Load configurations for P2-70F load distribution tests.

The second of the tests performed on P2-70F focused on global flexural response of the girder. Loads were applied at four locations on the deck, each 0.91 m (3 ft) from midspan and centered over a web. Loads were applied to the deck through 0.23 m (9 inch) diameter steel plates which were grouted to the deck surface. The girder was supported over its 21 m (69 ft) span on 0.18 m (7 inch) diameter steel rollers.

For both series of tests, load cells recorded the load applied by each hydraulic jack. Discrete instrumentation was also installed at the quarter and forty points west of midspan and at midspan. (Note that, just as the terms quarter point refers to a location at 25% of the span length from the bearing, the term forty point refers to a location at 40% of the span length from the bearing.) Fifty electrical resistance strain gages were installed at midspan as shown in Figure 15, and twelve more were installed at both the west quarter and forty points as shown in Figure 16. A total of 13 potentiometers, 6 LVDTs, and 2 tiltmeters were also installed on these three instrumentation lines as shown in Figure 17 and Figure 18. All of the instrumentation results were recorded periodically by an electronic data acquisition system throughout the test.

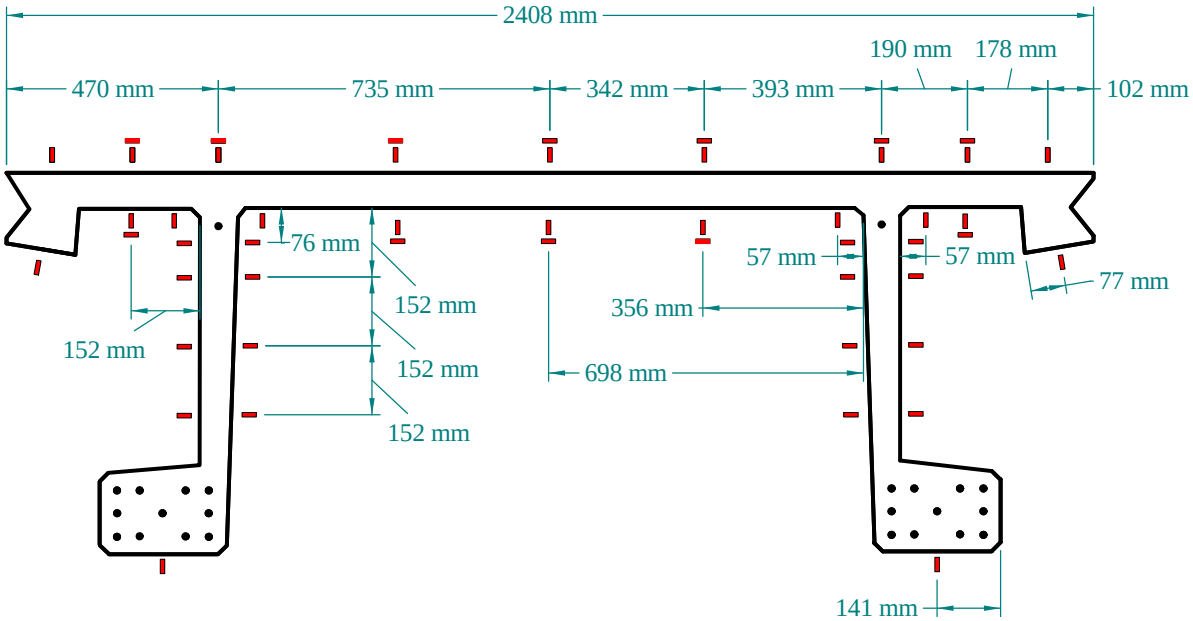

Figure 15. Illustration. Midspan strain gage locations for Girder P2-70F.

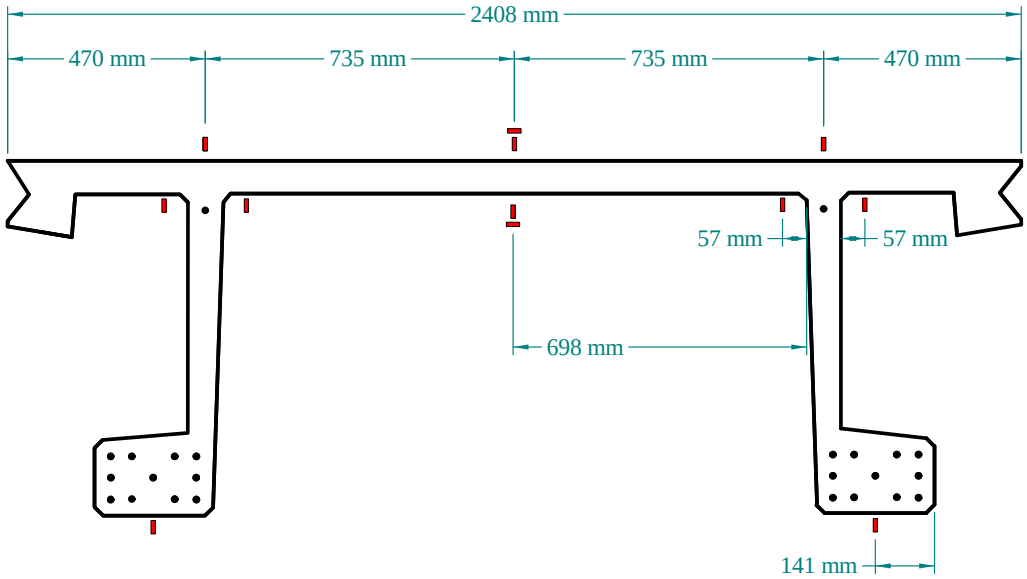

Figure 16. Illustration. Forty and quarter point strain gage locations for Girder P2-70F.

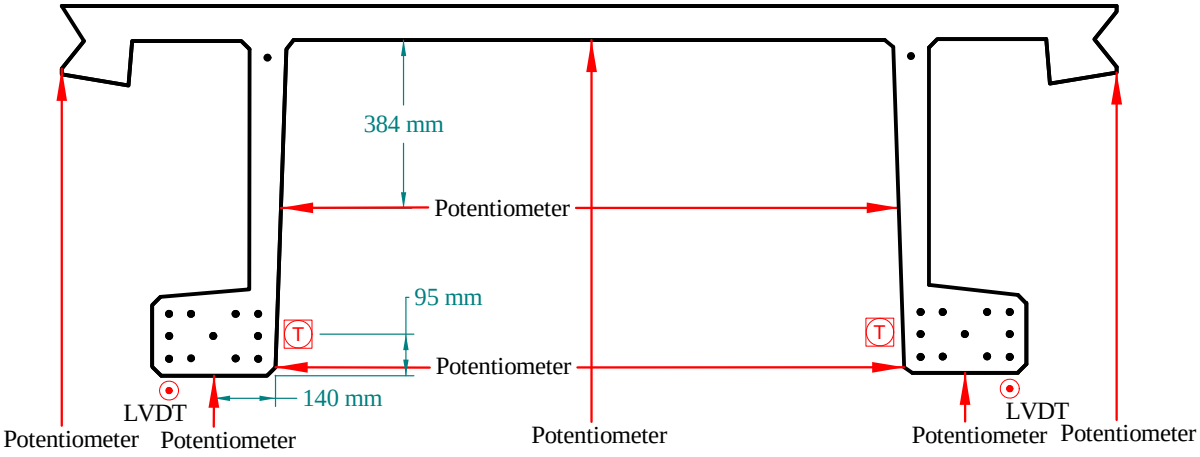

Figure 17. Illustration. Midspan potentiometer, LVDT, and tilt meter locations for Girder P2-70F.

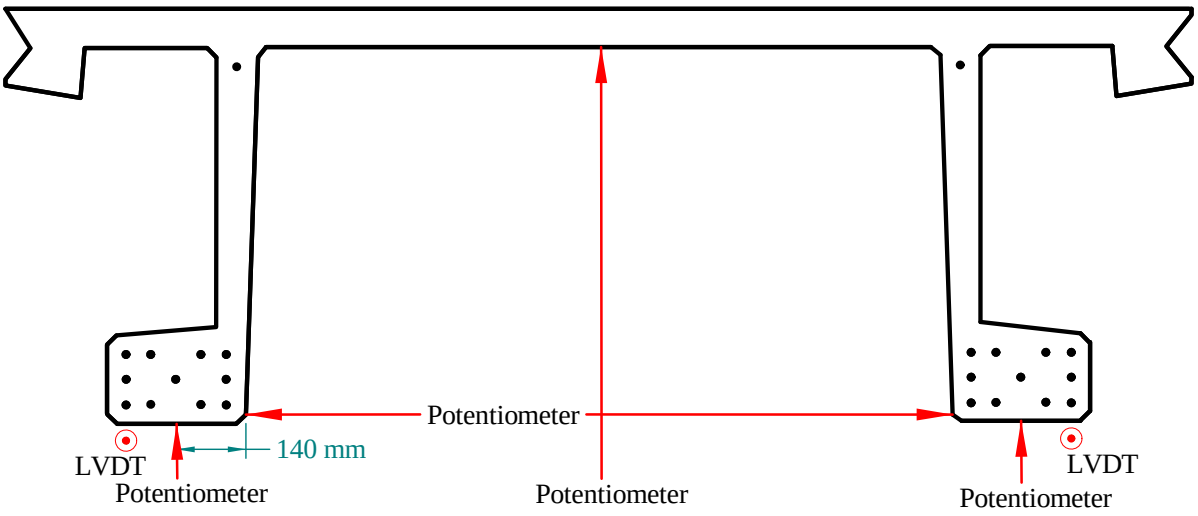

Figure 18. Illustration. Forty and quarter point potentiometer and LVDT locations for Girder P2-70F.

Test P4-45F

The loading setup for test P4-45F is shown in Figure 19. This 21.34 m (70 ft) girder was loaded in four-point bending over a span of 13.7 m (45 ft). Loads were applied at four locations on the deck, each 0.91 m (3 ft) from midspan and centered over a web. Loads were applied to the deck through 0.23 m (9 inch) diameter steel plates which were grouted to the deck surface. The girder was supported over its 13.7 m (45 ft) span on 0.18 m (7 inch) diameter steel rollers. A 3.81 m (12.5 ft) length of girder overhung both the east and west ends support locations. Figure 19 presents the test setup.

The overhang regions on the west and east ends of the girder contained areas that were significantly damaged during Tests P4-57Ss and P4-57Sh, respectively. These damaged areas were concentrated beyond the test P4-45F reaction points and thus were not anticipated to significantly affect the test.

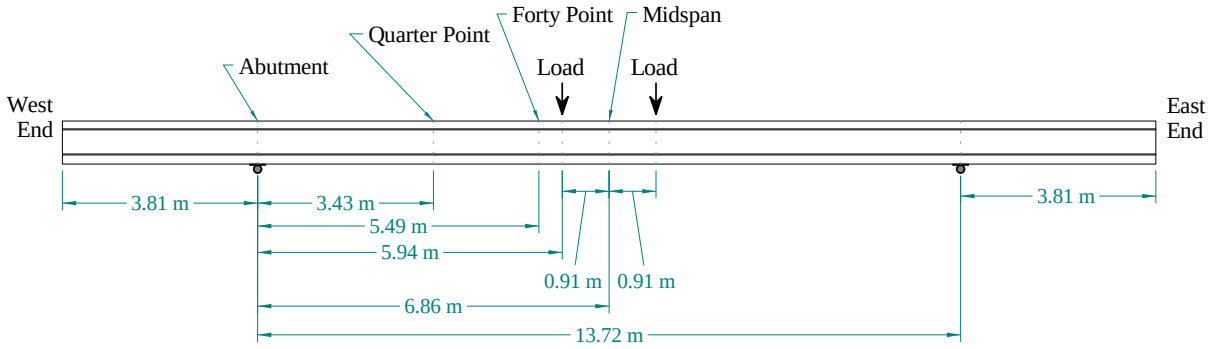

Figure 19. Illustration. Loading setup for Test P4-45F.

The instrumentation setup for this girder was very similar to that used for Test P2-70F. Load cells again captured the applied load at each load point. A total of 66 strain gages, 15 potentiometers, and 6 LVDTs were installed on the three instrumentation lines. Figure 20, Figure 21, Figure 22, and Figure 23 provide the details on the instrumentation installed for this test.

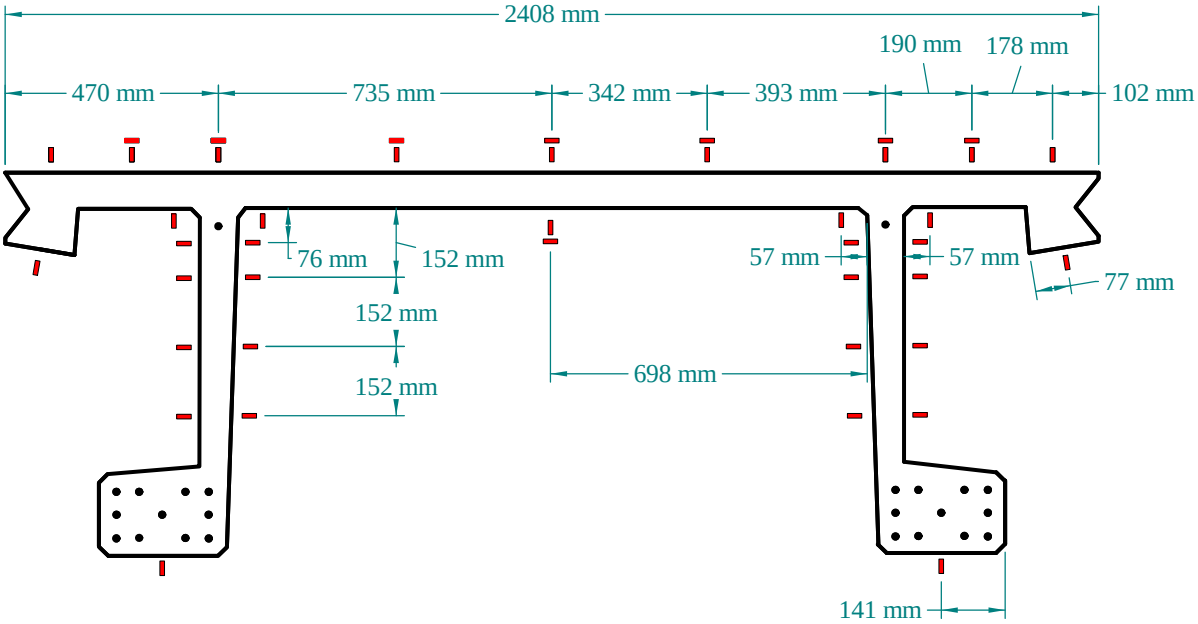

Figure 20. Illustration. Midspan strain gage locations for Test P4-45F.

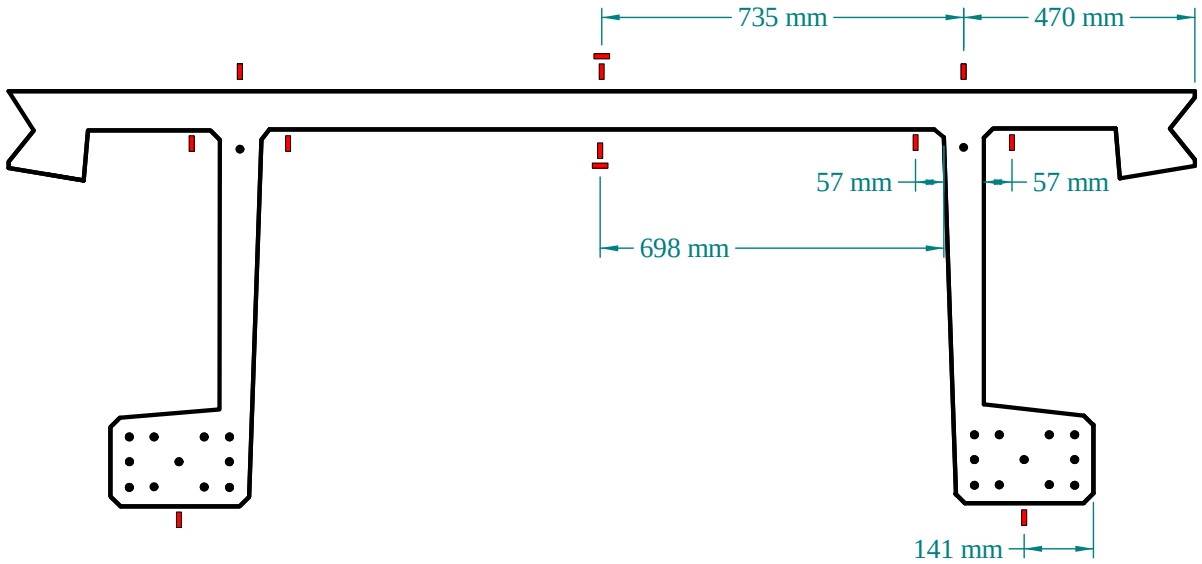

Figure 21. Illustration. Forty and quarter point strain gage locations for Test P4-45F.

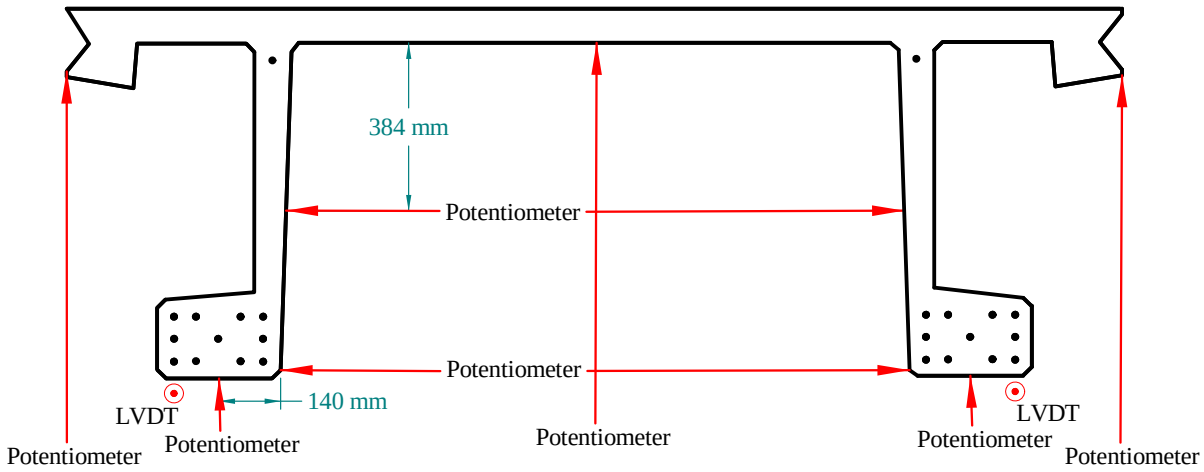

Figure 22. Illustration. Midspan potentiometer, LVDT, and tilt meter locations for Test P4-45F.

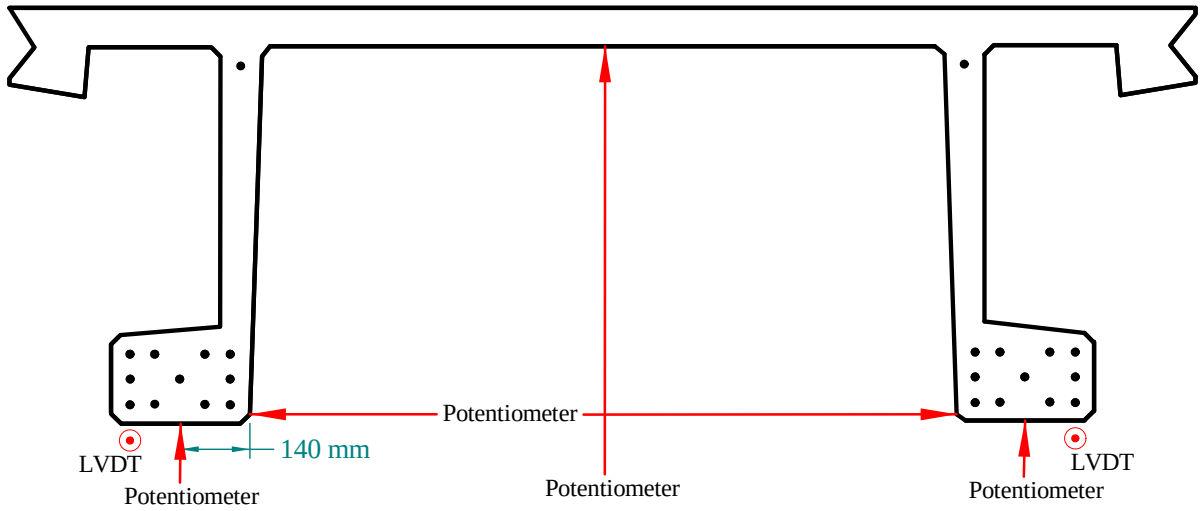

Figure 23. Illustration. Forty and quarter point potentiometer and LVDT locations for Test P4-45F.

Test P2-21S

Test P2-21S was focused on determining the shear response of this girder shape when subjected to large point loads applied above the girder webs. The test was completed on the east end of Girder P2 after this girder had been subjected to and failed under the loading of Test P2-70F. The test setup for Test P2-21S is shown in Figure 24. Loads were applied along a line located 2.13 m (7 ft) from the east support, which was itself centered 0.61 m (2 ft) from the east end of the girder. The overall span for the test was 6.4 m (21 ft) and a 3.6 m (11.8 ft) section of girder overhung the west support.

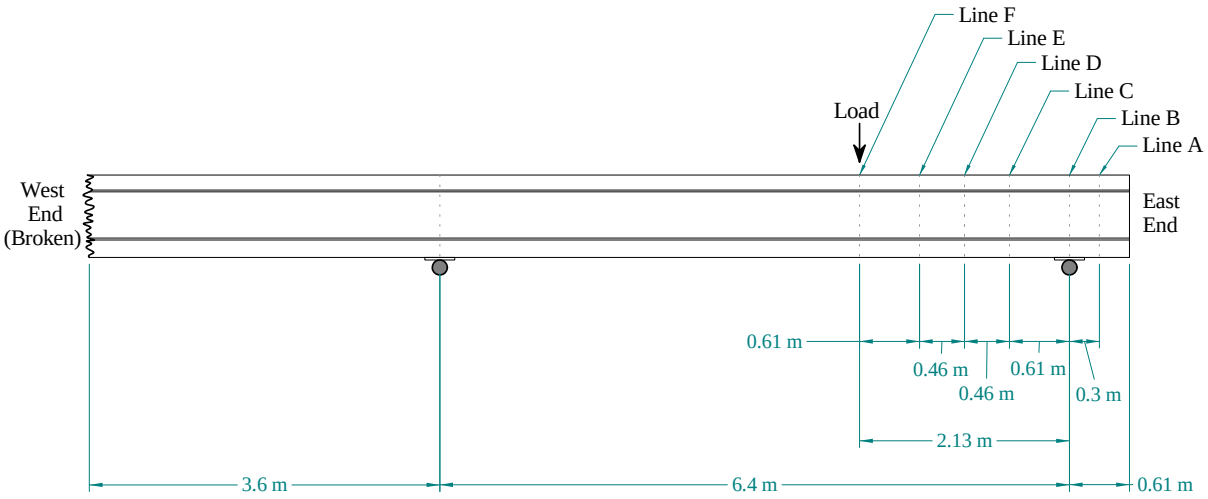

Figure 24. Illustration. Loading setup for Test P2-21S.

Two loading configurations were applied during this test. In the first configuration, a single point load was applied above the south web of the girder through a 0.23 m (9 inch) diameter plate which was grouted to the deck surface. Load cells were placed at the reaction points and above the hydraulic jack such that the load and reactions were all monitored throughout the test. In the second configuration, point loads were applied above both webs through 0.23 m (9 inch) diameter plates grouted to the deck surface. Loads were reacted through 0.18 m (7 inch) diameter steel rollers placed at all four support locations. Loads were monitored through load cells placed above the hydraulic jacks. Figure 25 provides a photograph of the test setup for the second load configuration.

Figure 25. Photo. Setup for second load configuration of Test P2-21S.

Strain gages, potentiometers, and LVDTs were used to capture the behavior of this girder throughout the application of loads in this test. The instrumentation was applied to Instrumentation Lines A through F whose locations are shown in Figure 24 and to the strands emanating from the south bulb on the east end of the girder. Figure 26, Figure 27, Figure 28, Figure 29, and Figure 30 show the locations of strain gages applied to the surface of the girder. Figure 31, Figure 32, and Figure 33 show the locations of the linear potentiometers and LVDTs. Note that all LVDTs are affixed such that they measure axial deformation along a surface of the girder over a predefined gage length thus allowing for a measurement of distributed strain after cracking. Also note that the LVDTs shown on the inside of the webs are orientated at 39 degrees clockwise from vertical if viewed from the south. The LVDTs were installed at this angle as it was consistent with the orientation of the principal tensile strain as reported by the strain rosettes when the girder was subjected to elastic-level loads. All of the strands emanating from the south bulb at the east end of the girder were instrumented with LVDTs. Figure 34 shows the LVDT identifiers and Figure 35 provides a photograph of the instrumented strands.

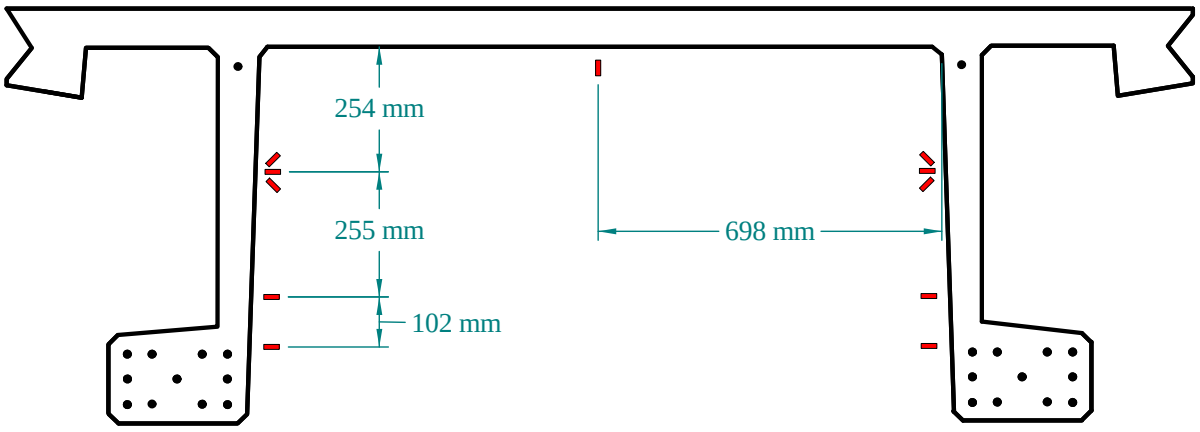

Figure 26. Illustration. Lines A and C strain gage locations for Test P2-21S.

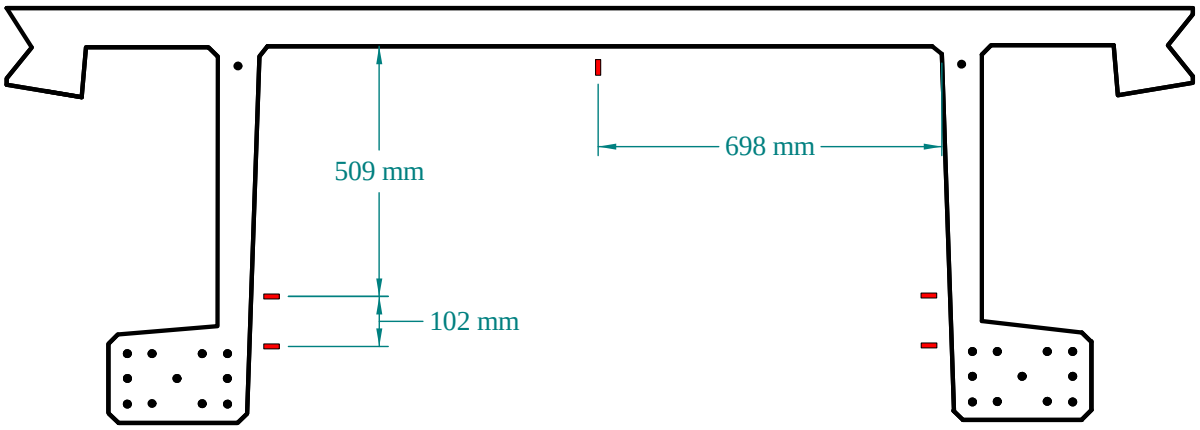

Figure 27. Illustration. Line B strain gage locations for Test P2-21S.

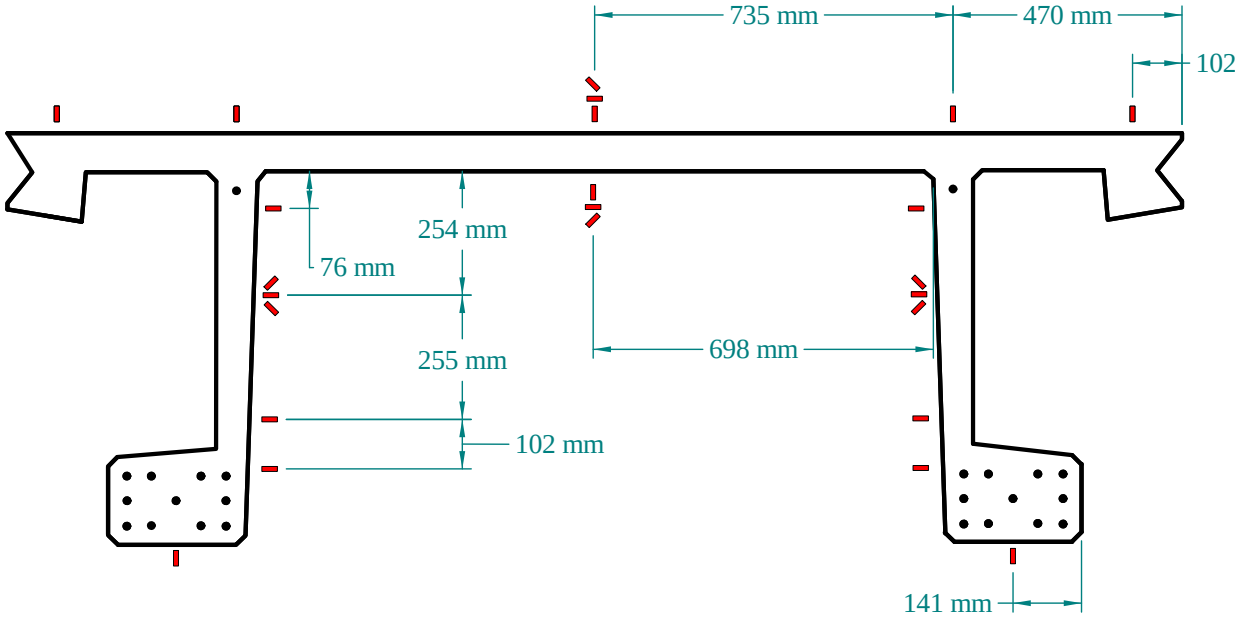

Figure 28. Illustration. Line D strain gage locations for Test P2-21S.

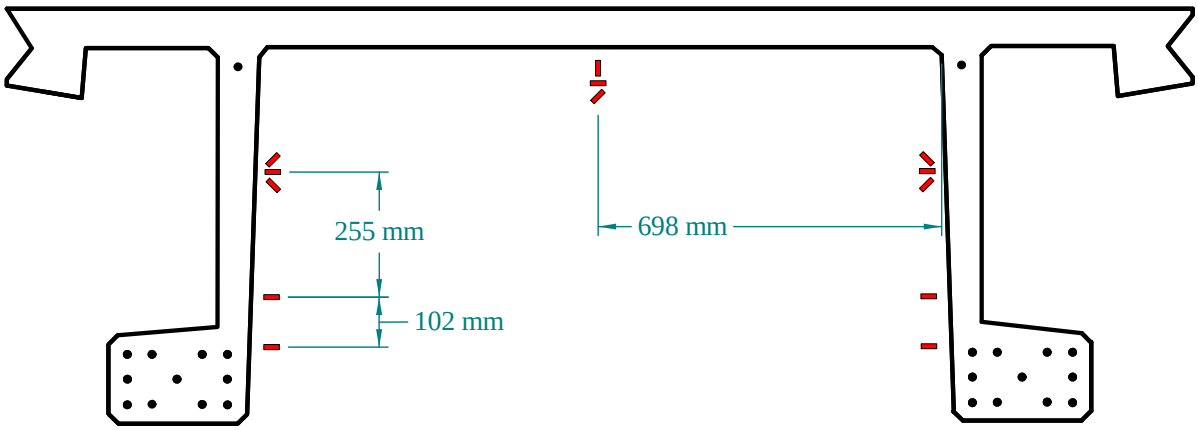

Figure 29. Illustration. Line E strain gage locations for Test P2-21S.

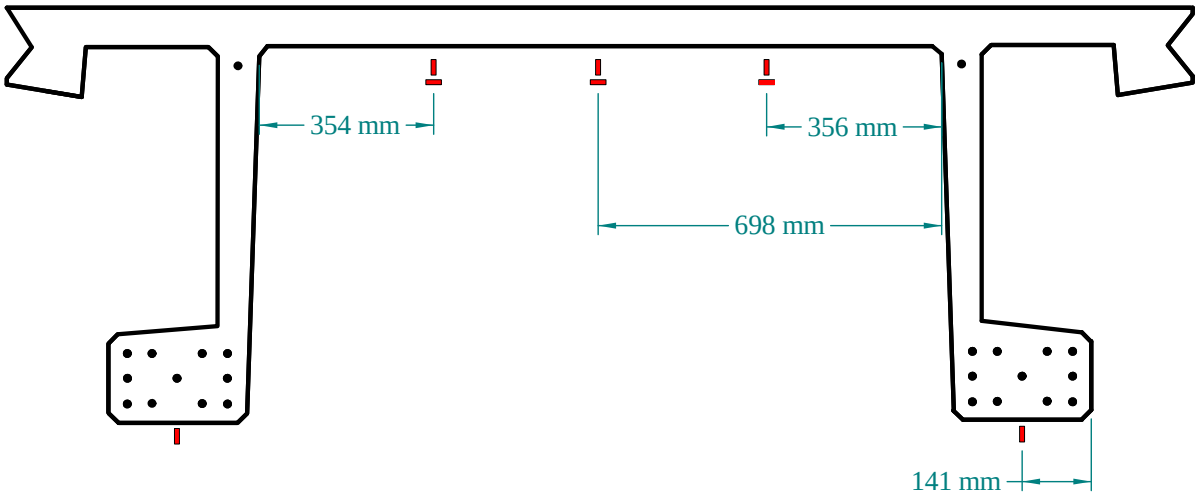

Figure 30. Illustration. Line F strain gage locations for Test P2-21S.

Figure 31. Illustration. Lines C and E LVDT locations for Test P2-21S.

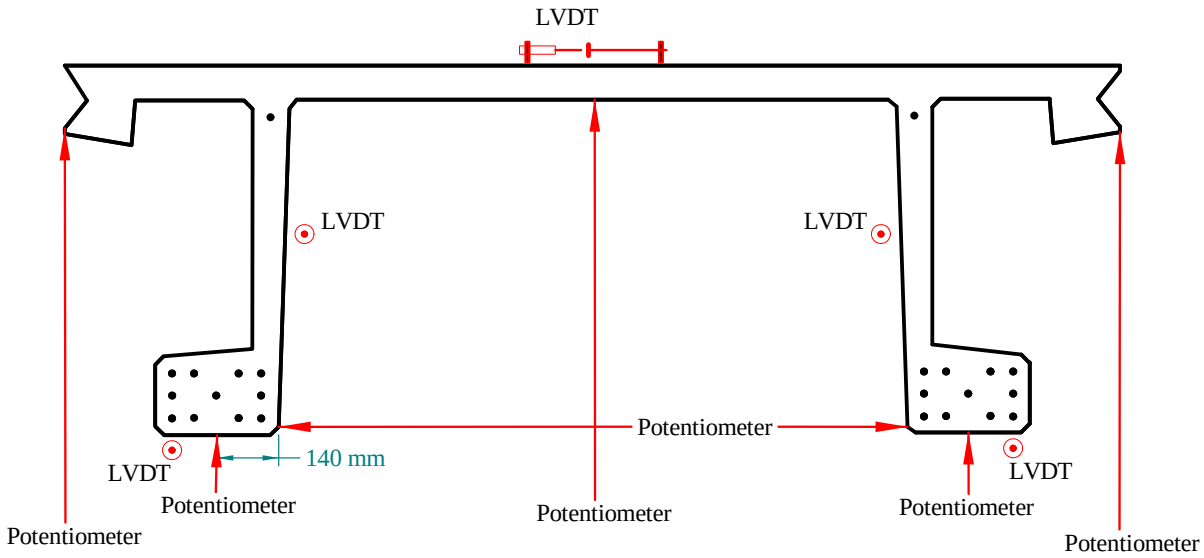

Figure 32. Illustration. Line D potentiometer and LVDT locations for Test P2-21S.

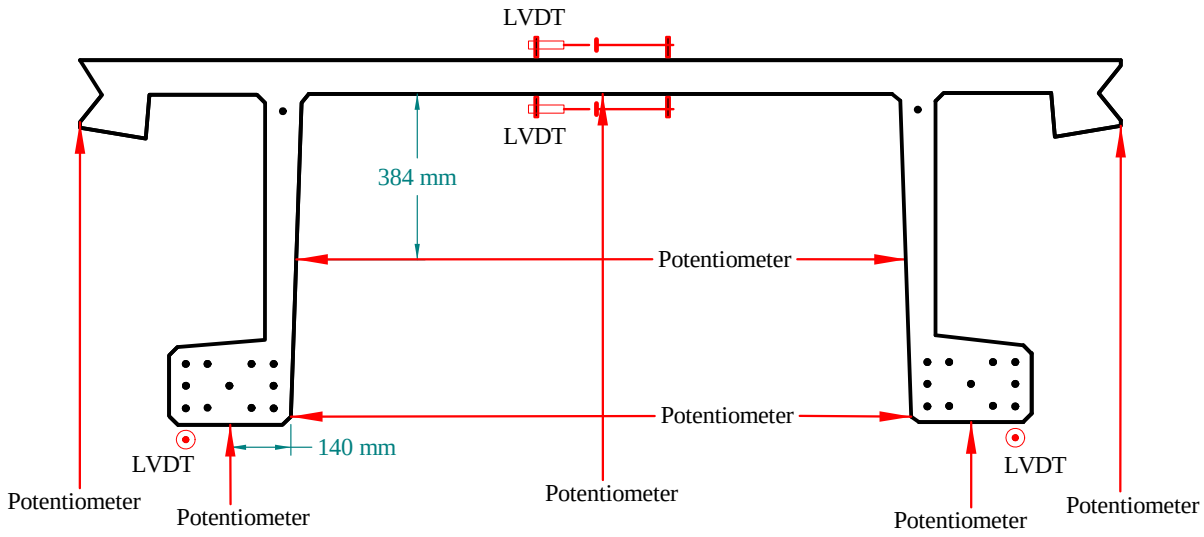

Figure 33. Illustration. Line F potentiometer and LVDT locations for Test P2-21S.

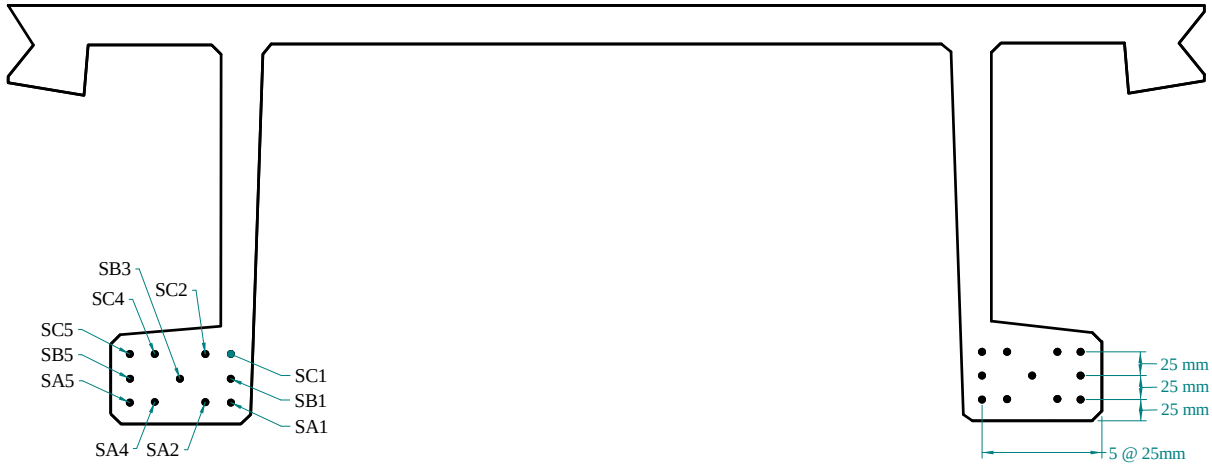

Figure 34. Illustration. Prestressing strand locations and identifiers.

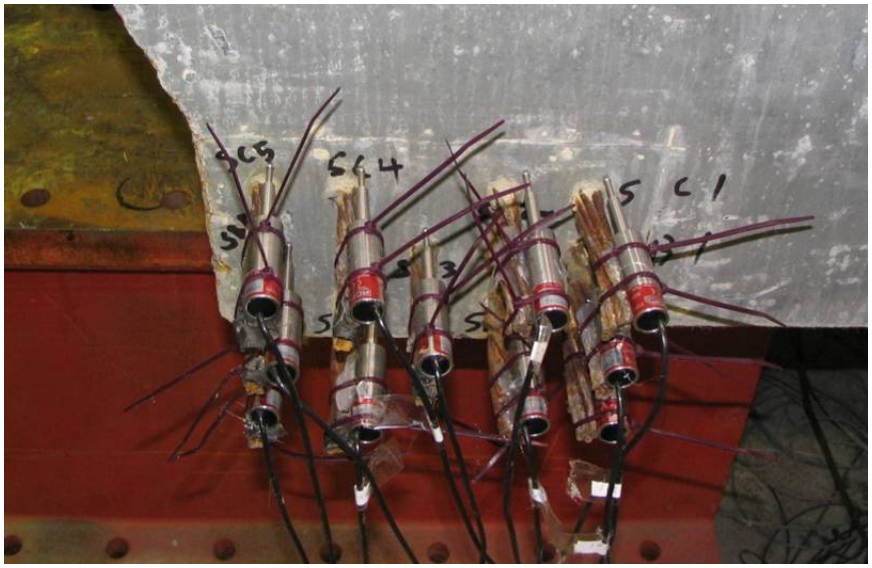

Figure 35. Photo. Prestressing strand instrumentation.

Test P4-57Sh

Test P4-57Sh was focused on determining the shear response of this girder shape when subjected to large point loads applied above the girder webs. Recall that three strands from each bulb of this girder were harped up into the webs of the girder within the region being tested. Test P4-57Sh was completed on the east end of Girder P4, a girder which had previously not been tested. The test setup for Test P4-57Sh is shown in Figure 36. Loads were applied along a line located 1.83 m (6 ft) from the east support, which was itself centered 0.15 m (6 inches) from the east end of the girder. The overall span for the test was 17.4 m (57 ft) and a 3.8 m (12.5 ft) section of girder overhung the west support.

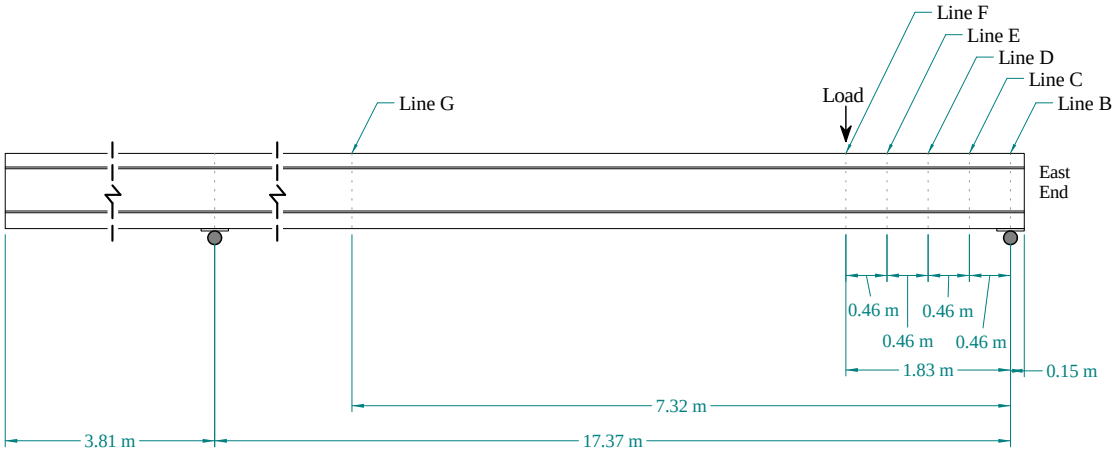

Figure 36. Illustration. Loading setup for Test P4-57Sh.

Loads were applied to the girder through two hydraulic jacks placed above the deck of the girder. The applied loads were captured by load cells placed above the jacks. The jacks bore on 0.3 m by 0.3 m (12 inch by 12 inch) steel plates which were grouted to the deck surface and centered over the webs. The top surface of the steel plates created an arc segment from a 0.91 m (36 inch) radius cylinder, thus allowing for 10 degrees of deck rotation under the vertically applied loads. These plates ranged in thickness from 38 to 51 mm (1.5 to 2 inch). Loads were reacted through 0.18 m (7 inch) diameter steel rollers placed at all four support locations. Figure 37 provides a photograph of the east end of Girder P4 prior to the initiation of Test P4-57Sh.

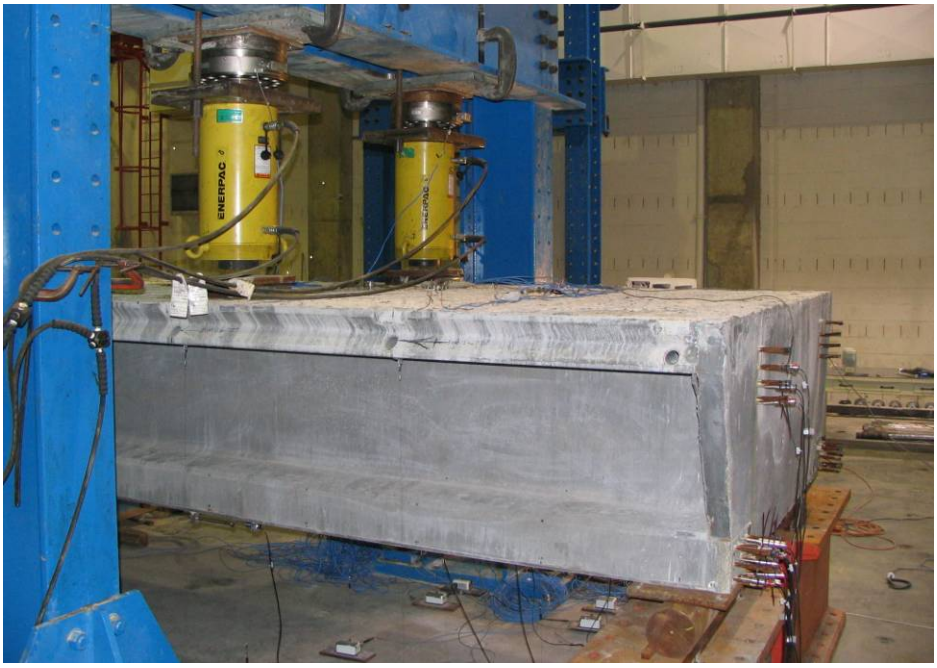

Figure 37. Photo. Setup for Test P4-57Sh.

Strain gages, potentiometers, and LVDTs were used to capture the behavior of this girder throughout the application of loads in this test. The instrumentation was applied to Instrumentation Lines B through G whose locations are shown in Figure 36 and to the strands emanating from the south bulb on the east end of the girder. Figure 38, Figure 39, Figure 40, and Figure 41 show the locations of strain gages applied to the surface of the girder. Figure 42, Figure 43, and Figure 44 show the locations of the linear potentiometers and LVDTs. Note that all LVDTs are affixed such that they measure axial deformation along a surface of the girder over a predefined gage length thus allowing for a measurement of distributed strain after cracking. Also note that the LVDTs shown on the inside of the webs are orientated at 45 degrees from vertical. All of the strands emanating from the south bulb at the east end of the girder were instrumented with LVDTs. The same LVDT identifiers used for Test P2-21S were used again here, with the harped strands retaining their names but being located higher in the cross-section.

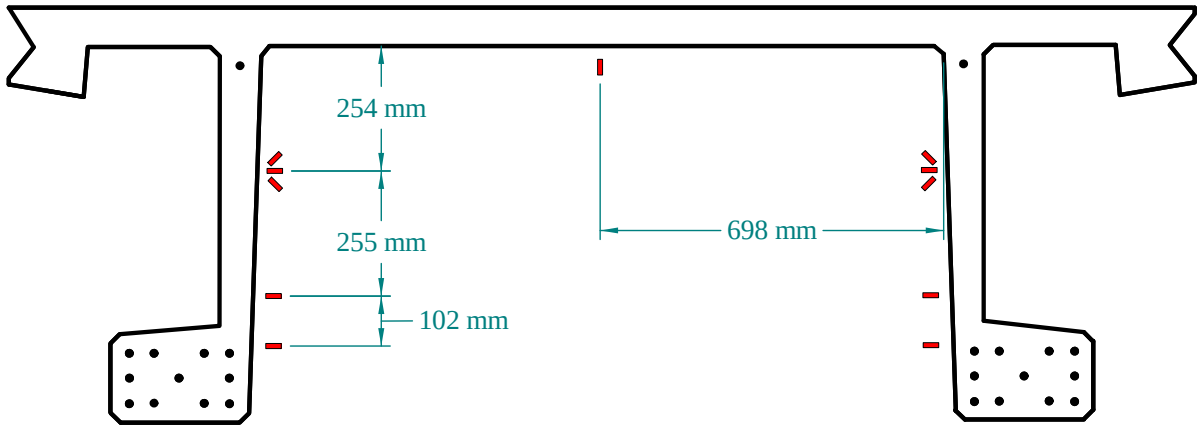

Figure 38. Illustration. Line C strain gage locations for Tests P4-57Sh and P4-57Ss.

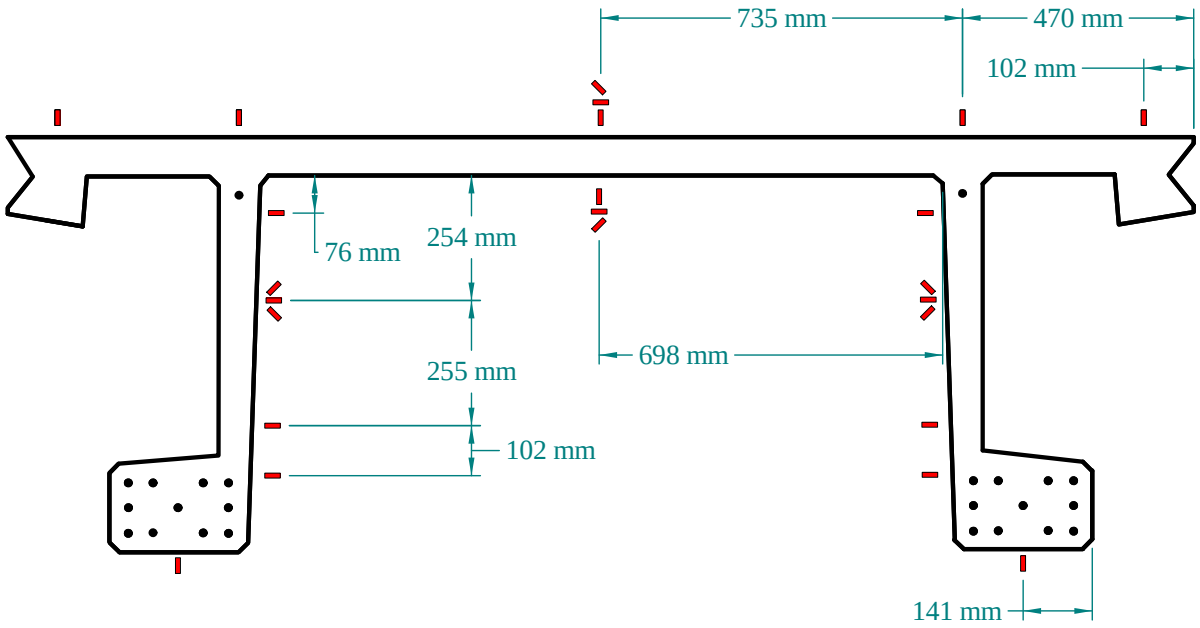

Figure 39. Illustration. Line D strain gage locations for Tests P4-57Sh and P4-57Ss.

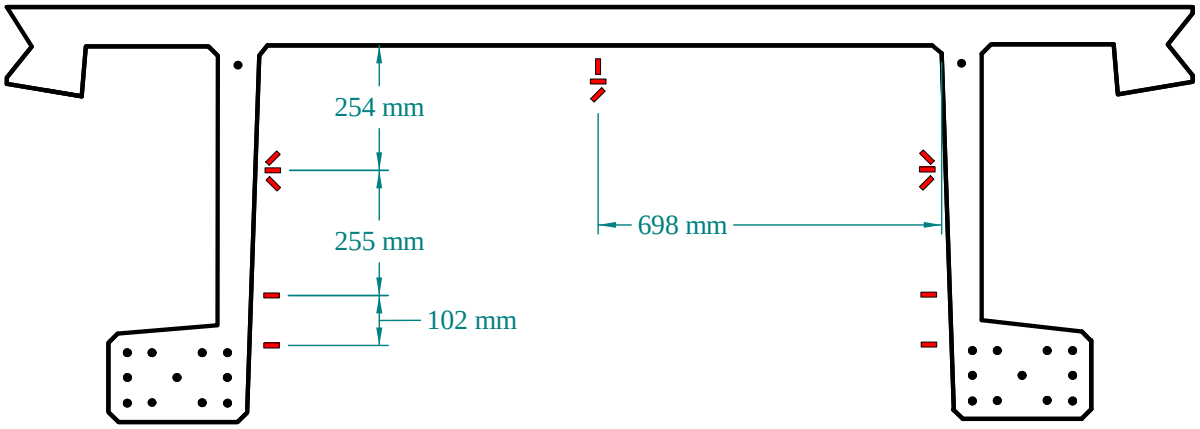

Figure 40. Illustration. Line E strain gage locations for Tests P4-57Sh and P4-57Ss.

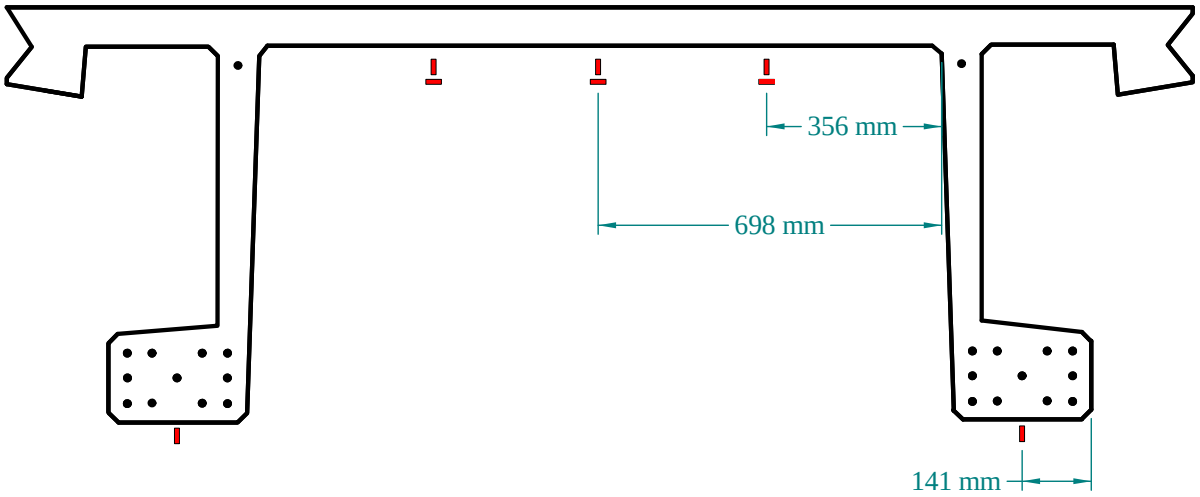

Figure 41. Illustration. Line F strain gage locations for Tests P4-57Sh and P4-57Ss.

Figure 42. Illustration. Lines C and E LVDT locations for Tests P4-57Sh and P4-57Ss.

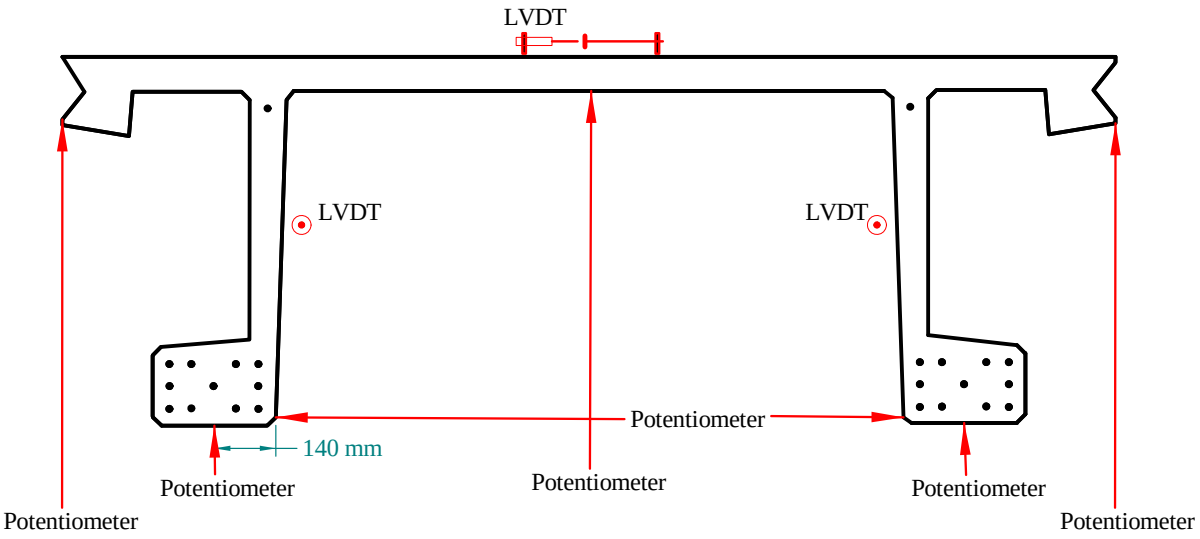

Figure 43. Illustration. Line D potentiometer and LVDT locations for Tests P4-57Sh and P4-57Ss.

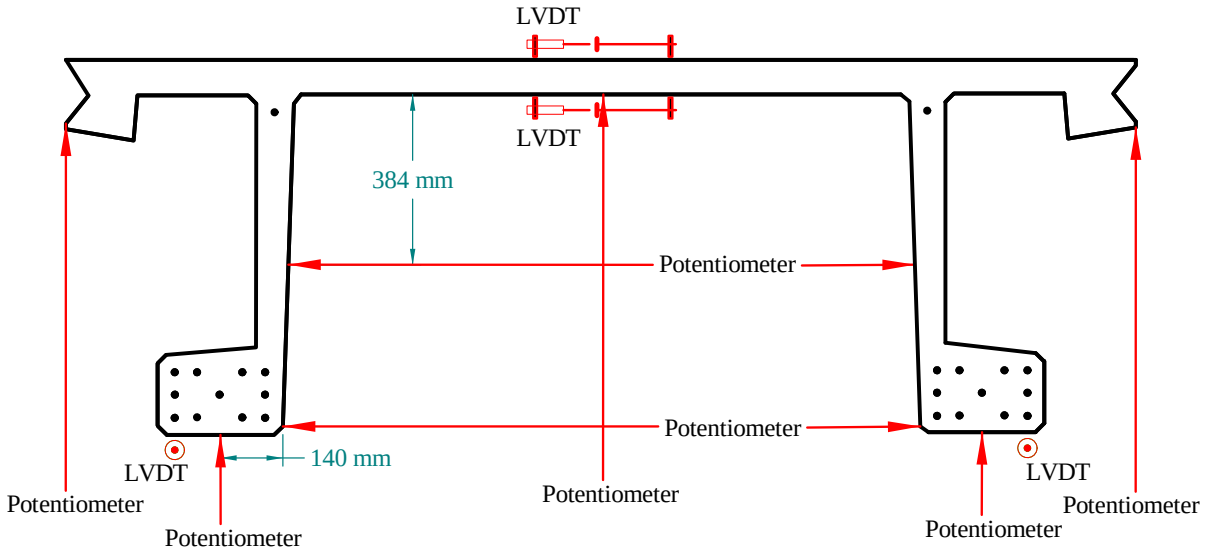

Figure 44. Illustration. Line F potentiometer and LVDT locations for Tests P4-57Sh and P4-57Ss.

Figure 45. Illustration. Line G potentiometer locations for Tests P4-57Sh and P4-57Ss.

Test P4-57Ss

Test P4-57Ss was focused on determining the shear response of this girder shape when subjected to large point loads applied above the girder webs. Test P4-57Ss was completed on the west end of Girder P4; previously the east end of Girder P4 was subjected to loading in Test P4-57Sh. The test setup for Test P4-57Ss is shown in Figure 46. The setup for this test is a mirror image (east to west) of the setup that was used for Test P4-57Sh. Loads were applied in the same

manner as presented for Test P4-57Sh and an identical instrumentation plan was implemented at Instrumentation Lines B through G. All of the strands emanating from the south bulb at the west end of the girder were instrumented with LVDTs and are named according to the same convention used for Test P2-21S. Figure 47 presents a photograph of the setup for Test P4-57Ss.

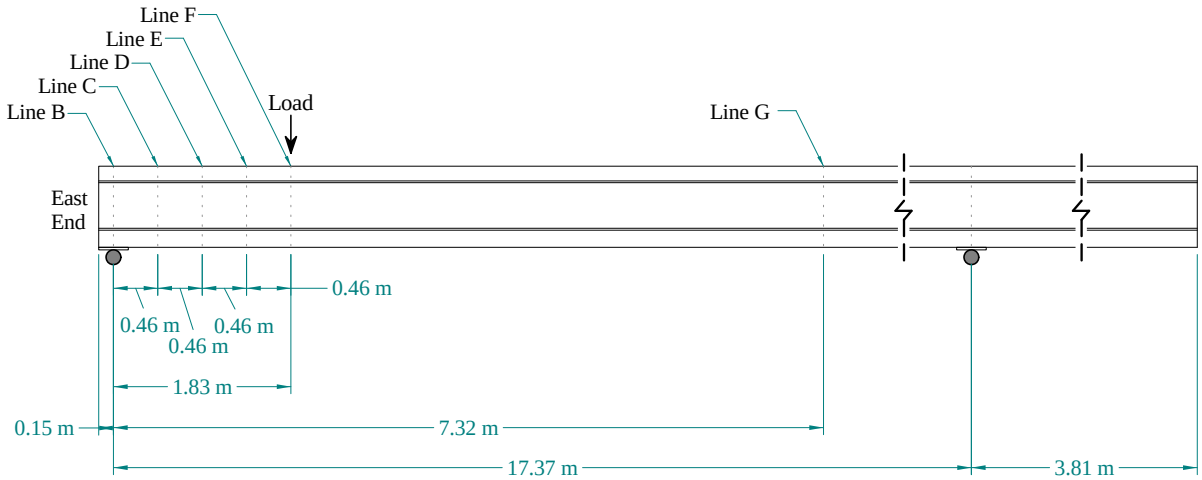

Figure 46. Illustration. Loading setup for Test P4-57Ss.

Figure 47. Photo. Setup for Test P4-57Ss.

Test P4-24T and Test P4-24D

Tests P4-24T and P4-24D were similar tests applied to relatively undamaged sections of Girder P4 after the conclusion of Test P4-45F. These tests focused on the transverse flexural behavior of the girder. The loading setup for these tests is shown in Figure 48. Figure 49 provides a photograph of the setup for Test P4-24T. Note that approximately 0.6 to 0.9 m (2 to 3 feet) of girder overhung the reaction points at each end of each girder. Remaining portions of Girder P4 which would have overhung the reaction points in these tests were cut from the girder prior to the start of testing. This created two similar specimens which did not possess any extraneous transverse flexural resistance beyond the reaction points.

In Tests P4-24T and P4-24D, loads were applied through 0.25 m by 0.51 m (10 inch by 20 inch) elastomeric pads located along the centerline of the girder and situated 0.61 m (2 ft) on either side of midspan. Loads were reacted through 0.15 m by 0.30 m (6 inch by 12 inch) elastomeric pads placed under the girder bulbs at the abutment locations. The elastomeric pads at the load points were 51 mm (2 inch) thick and at the reaction points were 25 mm (1 inch) thick.

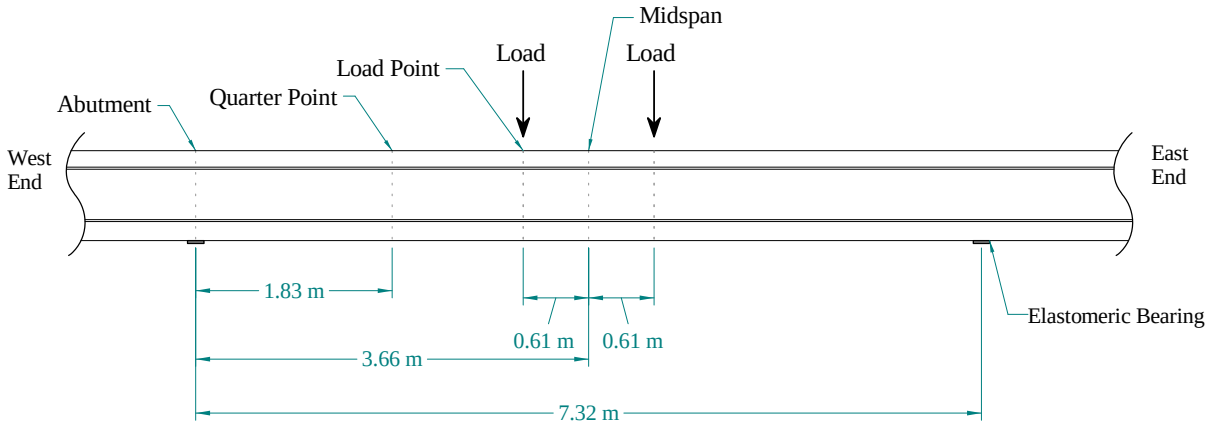

Figure 48. Illustration. Loading setup for Test P4-24T and Test P4-24D.

Figure 49. Photo. Setup for Test P4-24T.

The only difference in the test setups between P4-24T and P4-24D was that two transverse bulb movement restraining systems were installed on P4-24D. First, two approximately 76 mm by 9.5 mm (3 inch by 3/8th inch) steel straps were attached to the bottom faces of the bulbs, each located 0.46 m (18 inches) from midspan and spanning between the bulbs. These straps were composed of Grade 50 steel. The straps were epoxied and bolted to the bulbs as shown in Figure 50. The straps were instrumented with longitudinally-oriented strain gages.

The second restraining system consisted of the installation of steel angles outside of the bulbs at each reaction point. These angles were butted flush to the outside face of the bulbs and were welded to the top face of each steel abutment. Figure 51 shows the setup for Test P4-24D including these restraining angles.

Figure 50. Photo. Steel strap attachment between bulbs of Test P4-24D.

Figure 51. Photo. Setup of Test P4-24D including restraining angles at reaction points.

Strain gages, potentiometers, and LVDTs were used to capture the behavior of the girder throughout the application of loads in these tests. The instrumentation was applied to cross sections at midspan and at the load point, quarter point, and abutment toward the west end of each test setup. Figure 52, Figure 53, and Figure 54 show the locations of strain gages applied to the surface of the girder. Figure 55, Figure 56, and Figure 57 show the locations of the linear

potentiometers. Figure 58, Figure 59, and Figure 60 show the locations of the LVDTs. Note that all LVDTs were affixed such that they measured axial deformation along a surface of the girder over a predefined gage length thus allowing for a measurement of distributed strain after cracking.

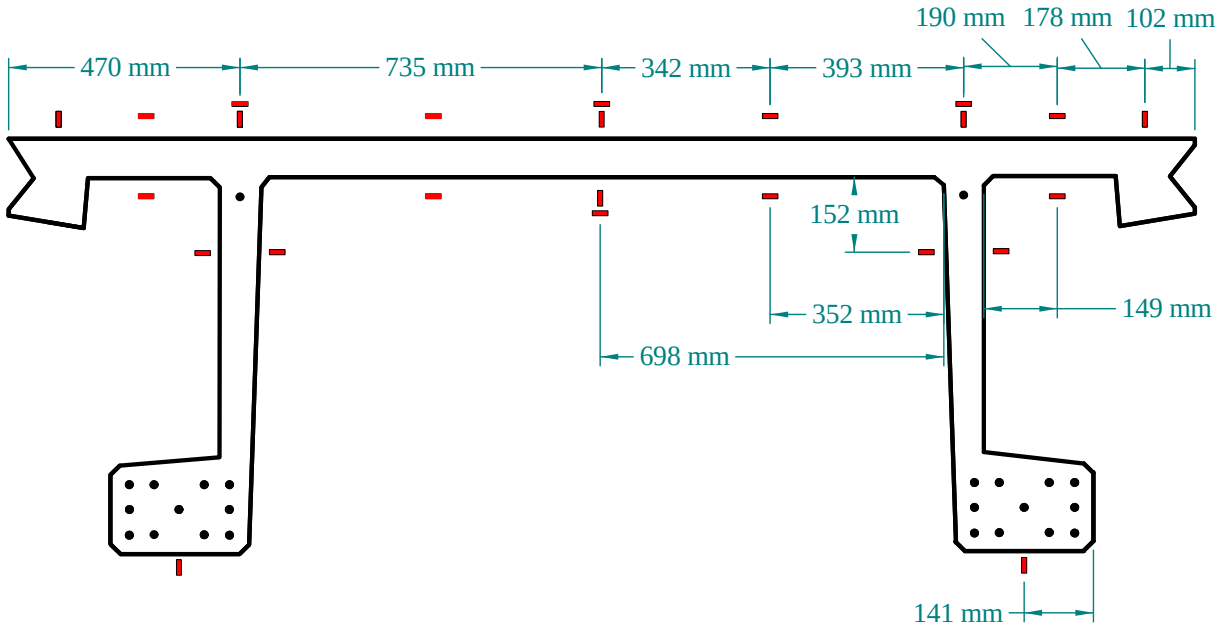

Figure 52. Illustration. Midspan strain gage locations for Test P4-24T and Test P4-24D.

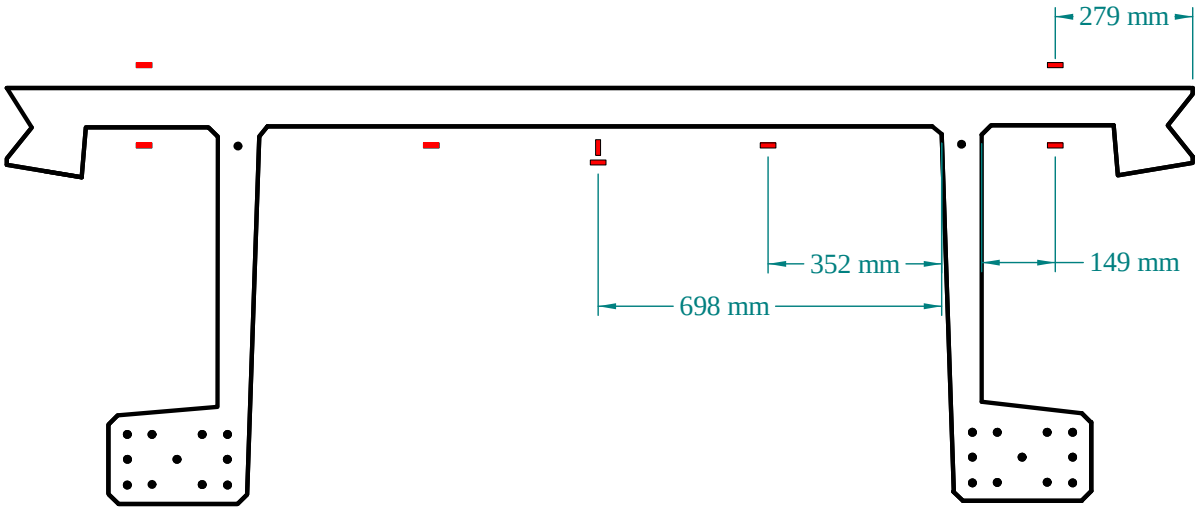

Figure 53. Illustration. Load point strain gage locations for Test P4-24T and Test P4-24D.

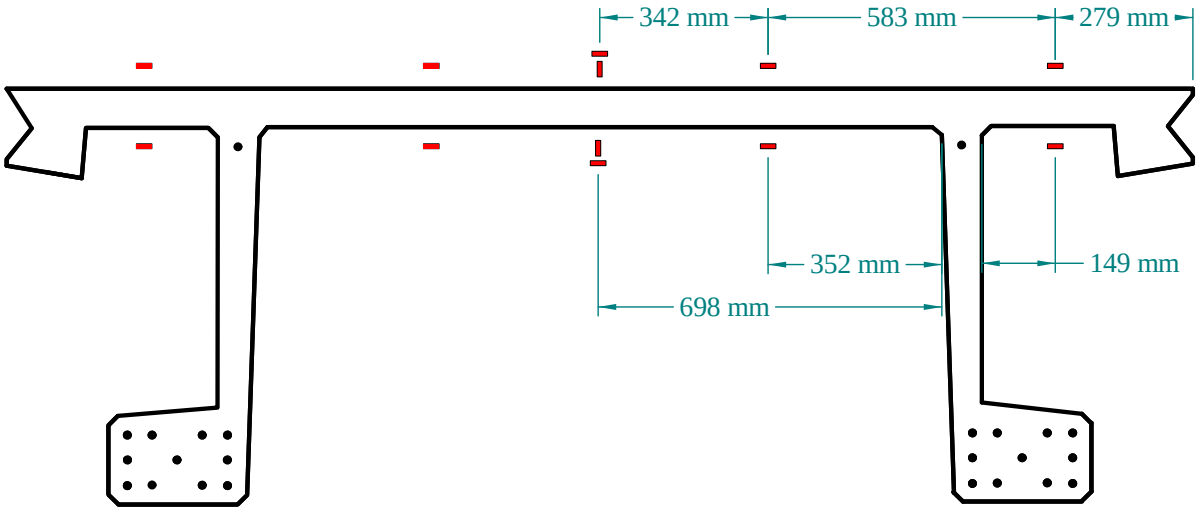

Figure 54. Illustration. Quarter point and abutment strain gage locations for Test P4-24T and Test P4-24D.

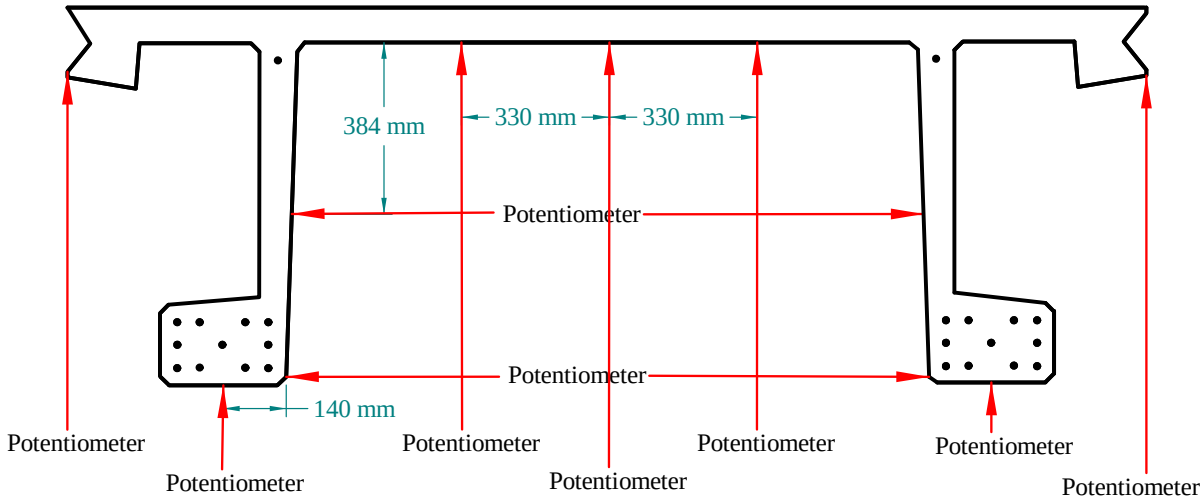

Figure 55. Illustration. Midspan potentiometer locations for Test P4-24T and Test P4-24D.

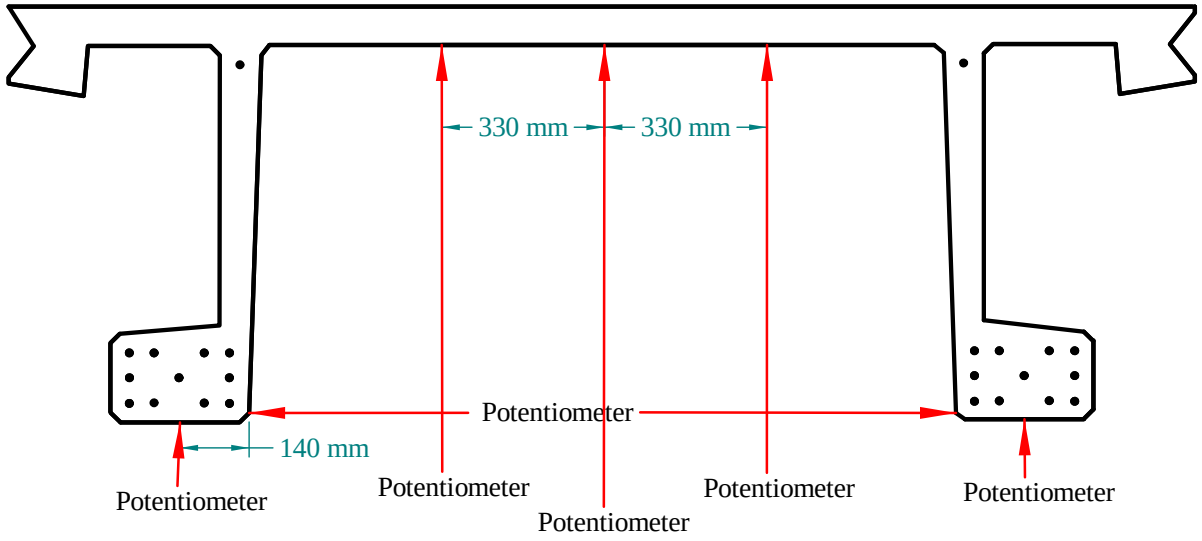

Figure 56. Illustration. Load point and quarter point potentiometer locations for Test P4-24T and Test P4-24D.

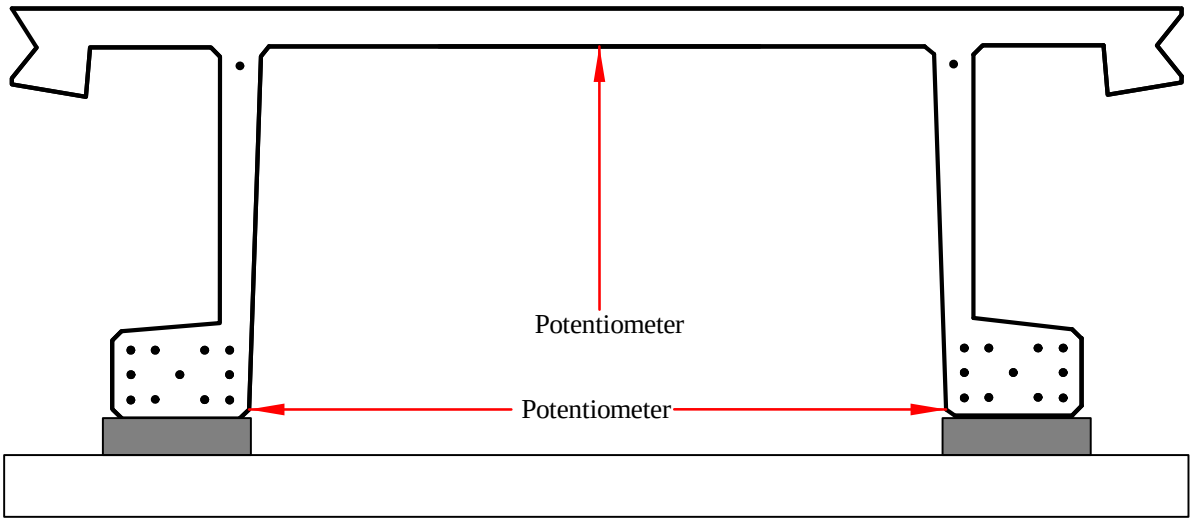

Figure 57. Illustration. Abutment potentiometer locations for Test P4-24T and Test P4-24D.

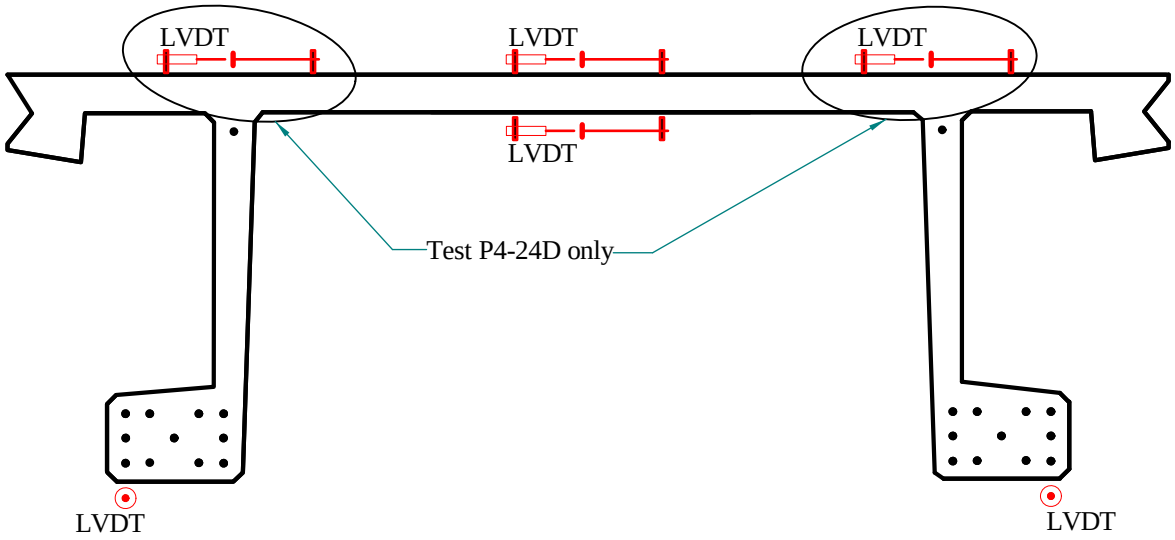

Figure 58. Illustration. Midspan LVDT locations for Test P4-24T and Test P4-24D.

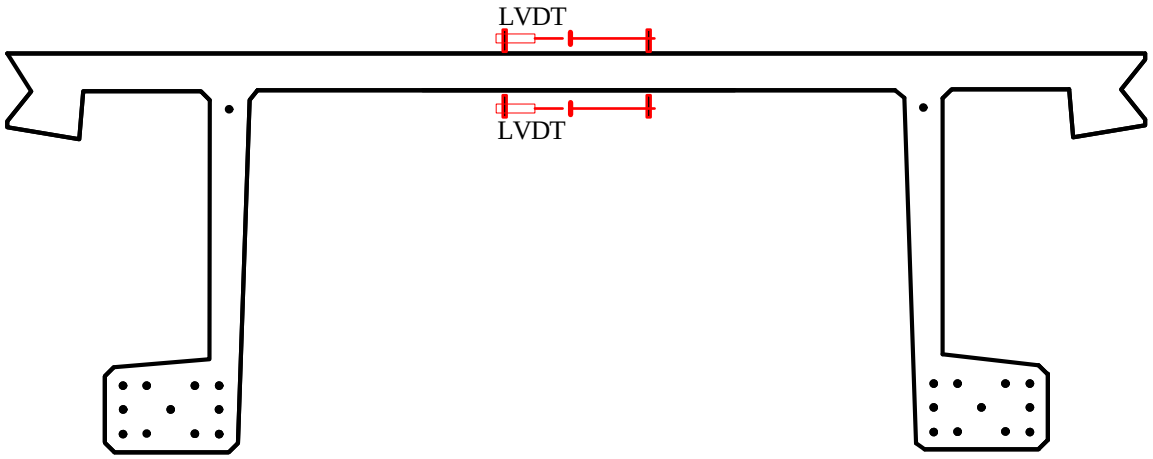

Figure 59. Illustration. Quarter point LVDT locations for Test P4-24T and Test P4-24D.

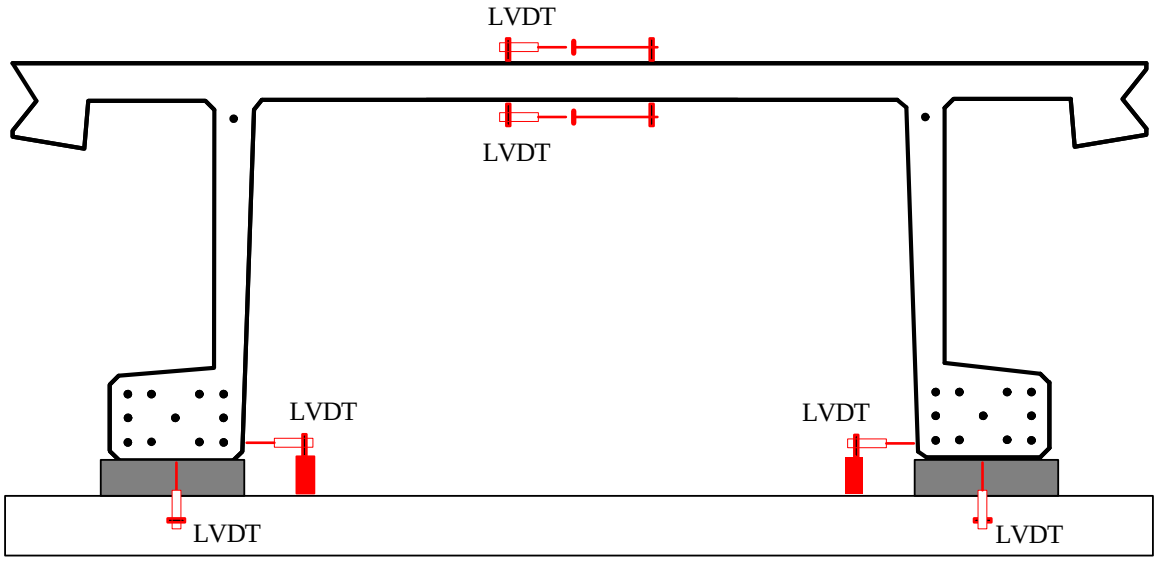

Figure 60. Illustration. Abutment LVDT locations for Test P4-24T and Test P4-24D.

CHAPTER 5. TEST RESULTS

INTRODUCTION

The results of the full-scale structural testing completed in this study are presented in this chapter. First, the load distribution testing completed on the pi-girder bridge is presented. Results from tests focused on primary flexural response of the pi-girder are then presented. The shear response of the pi-girder is presented next. Finally, the results from the transverse flexure tests are presented.

BRIDGE LOAD DISTRIBUTION TESTING

The first structural tests completed on the optimized UHPC girders focused on the behavior of the girders in a bridge configuration when subjected to symmetric and asymmetric gravity loads. The test setup, loading configurations, and instrumentation plan were described previously. The primary purpose of these tests was to investigate the load distribution behavior of the modular bridge component system.

The load distribution analysis was completed on data acquired during the application of the four loading configurations presented in Table 7 and Figure 10. The peak total loads applied during these tests four tests were 525, 273, 118, and 120 kN (118, 61, 27, and 27 kips), respectively.

The strain gages applied to the surface of the girders captured the midspan longitudinal strain profile over the depth of each girder. In terms of primary flexural behavior, these girders behaved elastically through all four tests. Thus, knowledge of the strain profile, the modulus of elasticity, and the moment of inertia of the girder allows for determination of the internal moment carried by each girder. The external moment on the bridge can be calculated based on the loads as captured by the load cells located at each load point. In all four tests, a comparison of internal and external moments agreed to within four percent.

The internal moments as distributed throughout the four girder legs resulting from the peak applied loads are shown in Figure 61. The results for Load Configuration 1 show that the loads were well distributed between the four girder legs. The results from the other load configurations show that the asymmetric load applications resulted in asymmetric moments being carried by the girder legs. Configurations 2W and 2D both show that the south girder carried approximately 85 percent of the load that was applied to it and only transferred 15 percent to the north girder. Finally, Configuration 3 shows that 95 percent of the load that was applied to the exterior leg of the south girder was carried by the south girder. Also note that this load configuration induced a small negative moment into the north leg of the north girder.

Figure 62 provides further information regarding the distribution of loads throughout the bridge. This figure shows the midspan vertical deflections of the bridge under the maximum applied load in each configuration. The measurements were collected from the bottom of each bulb and from the underside middle of each deck. The general deflected shape of the cross-section as depicted in this figure indicates that when loads are applied to the girder webs, the basic cross-section of the bridge remains mostly intact, with only translation of the cross-section occurring. However, when loads are applied between girder webs, the figure shows that the greater deflections will be

observed in the deck under the load point and that transverse flexural deformation of the cross-section occurs. These behaviors were verified through readings collected from potentiometers measuring the spreading of the girder webs throughout each test.

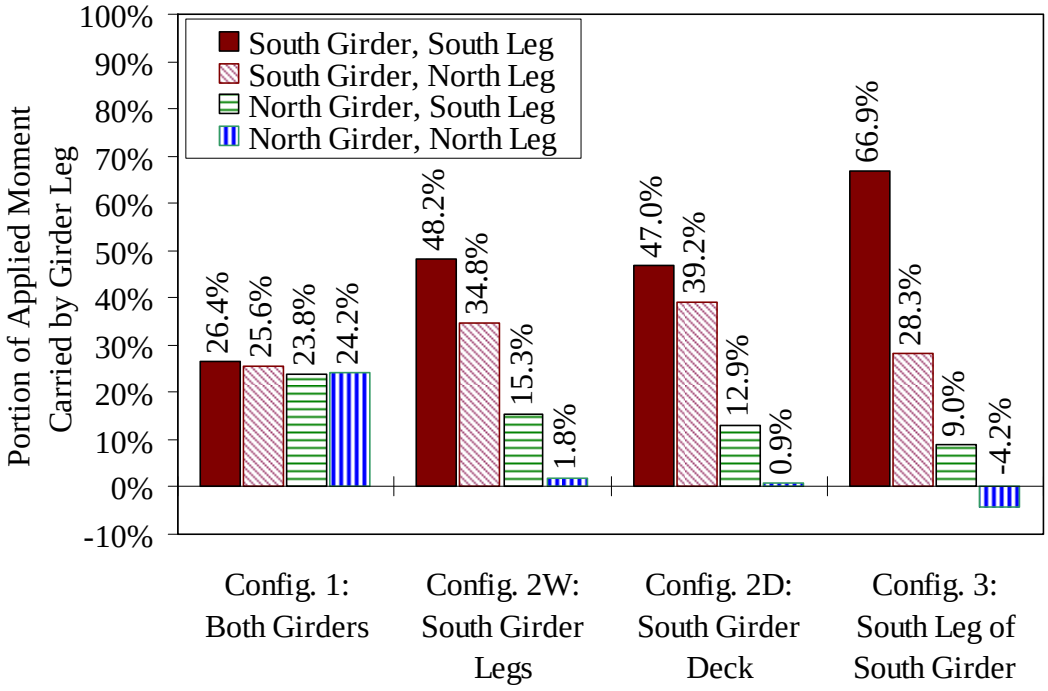

Figure 61. Chart. Proportion of applied moment carried by each girder leg.

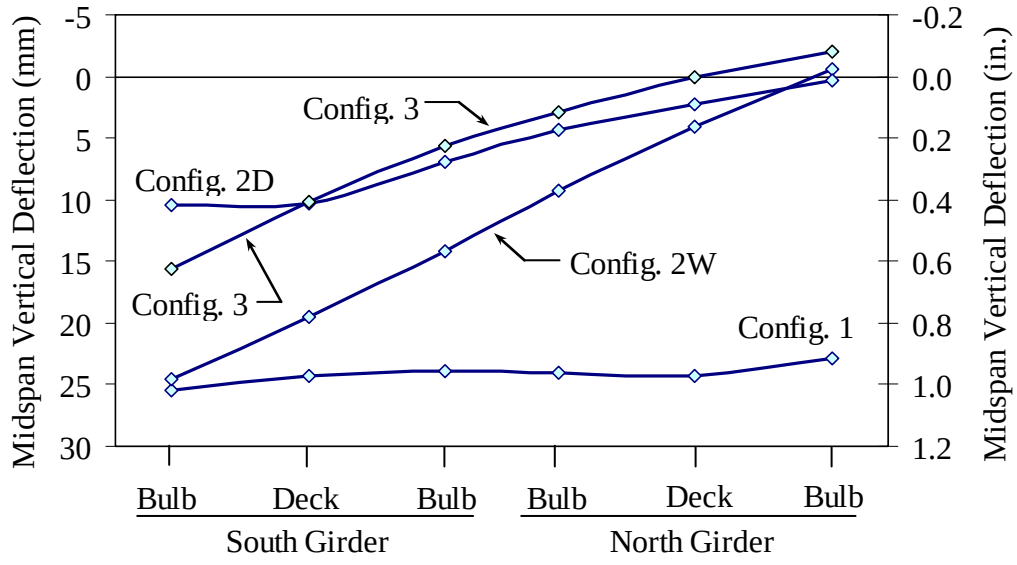

Figure 62. Chart. Midspan deflection under four loading configurations.

STATIC PRIMARY FLEXURE TESTING

A series of structural behavior tests focused on the flexural behavior of the pi-girder cross section were conducted. These tests utilized portions of Girders P2 and P4. The results of these tests are presented below.

P2-70F

Test series P2-70F focused on the primary flexural response of the pi-girder cross section. Two sets of tests were completed, with the first set focusing on load distribution behaviors resulting from asymmetric loading of the girder and the second set focusing on the flexural response of the girder through flexural failure. Recall that Girder P2 arrived at TFHRC with a negative flexure crack located 0.6 m (2 feet) east of midspan running across the deck and down into the webs. The tests discussed below were devised so as to limit the effect that this crack would have on the results obtained.

Load Distribution Testing

A series of load distribution tests were completed as part of the P2-70F tests. These tests were the first structural tests completed on Girder P2. Table 9 provides an overview of the sequence of six tests that were completed. Note that Load Configuration A represents a baseline test wherein the loads applied to the girder are symmetric, and that Load Configurations E and F are identical geometrically with the only difference being the peak total load applied to the girder. (Load Configuration F surpassed the deck's transverse flexural cracking load.) Also recall that this girder does not possess any diaphragms or cross-frames through which to assist in load-sharing between girder legs within the span; however, the girder does possess solid UHPC diaphragms at each end so as to limit any deformation of the cross-section at the support points.

The chart in Figure 63 presents the proportion of the applied moment that was carried by each leg of the girder for each of the six load configurations. The presented results pertain to the instance when the peak load was applied to the girder for each load configuration. These results are based on the internal moment carried by each leg of the girder at midspan. The underlying analysis is based on the curvature of the midspan cross section as determined from the strain gages affixed to the surface of the girder. These strain gages captured the strain profile through the depth of each girder leg.

The results presented in Table 9 show the peak total load applied to the girder in each load configuration as well as the combined load simultaneously reacted through the two south leg supports. The remainder of the load was reacted through the north leg supports. In some cases the north leg supports registered negative loads indicating that the reacted load was decreasing from its static dead load value.

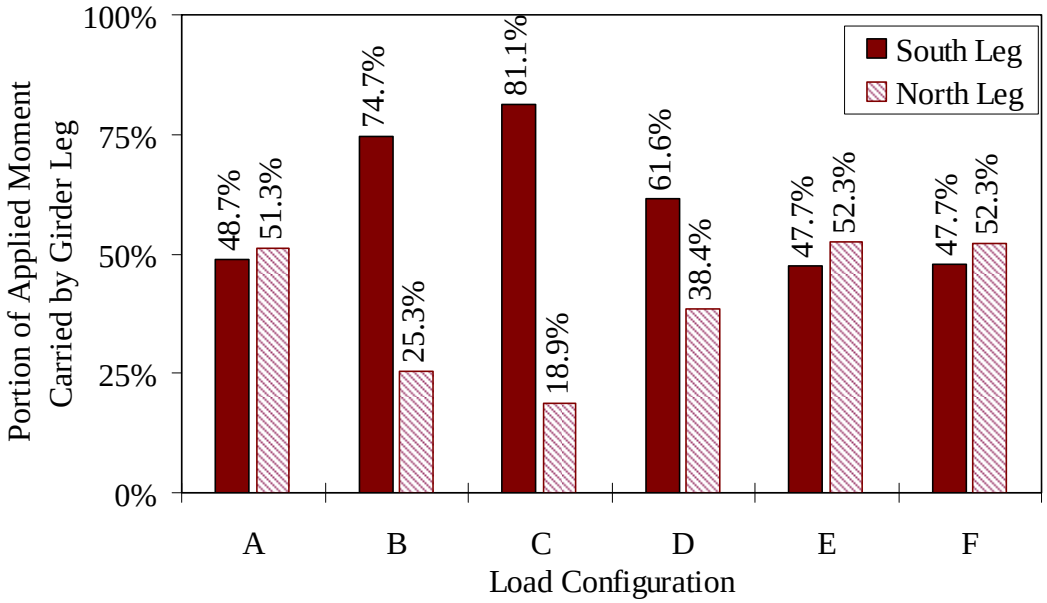

Figure 63. Chart. Proportion of applied moment carried by each girder leg.

Table 9. P2-70F load distribution test results.

Load Config.	Load Location	Peak Load Applied to Girder	Load Reacted at South Leg Supports
A	Above Both Webs	272 kN (61.1 kips)	145 kN (32.7 kips)
B	Above South Web	131 kN (29.4 kips)	135 kN (30.3 kips)
C	Along South Overhang	90 kN (20.3 kips)	106 kN (23.8 kips)
D	At Quarter Span Between Webs	136 kN (30.5 kips)	104 kN (23.4 kips)
E	At Middeck	86 kN (19.4 kips)	45 kN (10.2 kips)
F	At Middeck (Beyond Cracking)	134 kN (30.1 kips)	69 kN (15.6 kips)

The load distribution in the girder was also analyzed through the deflection and strain profiles captured across the width of the girder. As each loading configuration met or surpassed a total applied load of approximately 89 kN (20 kips), results were captured and are presented for comparison. Figure 65 presents the deflection of the midspan on the girder when subjected to the six different loading configurations. Note that the deck was uncracked in Load Configuration E, while the deck has just cracked at the presented load level for Load Configuration F.

Figure 64 shows the transverse spreading of the girder legs as measured by the potentiometer affixed to the inside of the bulbs at midspan. The plot shows the measured values from initial load application up through the peak load applied for each load configuration. Note that the first three load configurations resulted in the legs moving together, while the last three resulted in the

legs moving apart. The results from load configurations E and F are coincident up through the peak load applied in configuration E; however, immediately thereafter the results from configuration F show a noteworthy behavior. The approximately 0.15 mm (0.006 inch) increases in leg spread shown in the plot for Load Configuration F at loads of 91 kN (20.5 kips) and 133 kN (30 kips) correspond to the occurrence of discrete transverse flexural cracks in the deck as noted from audible and visual observations.

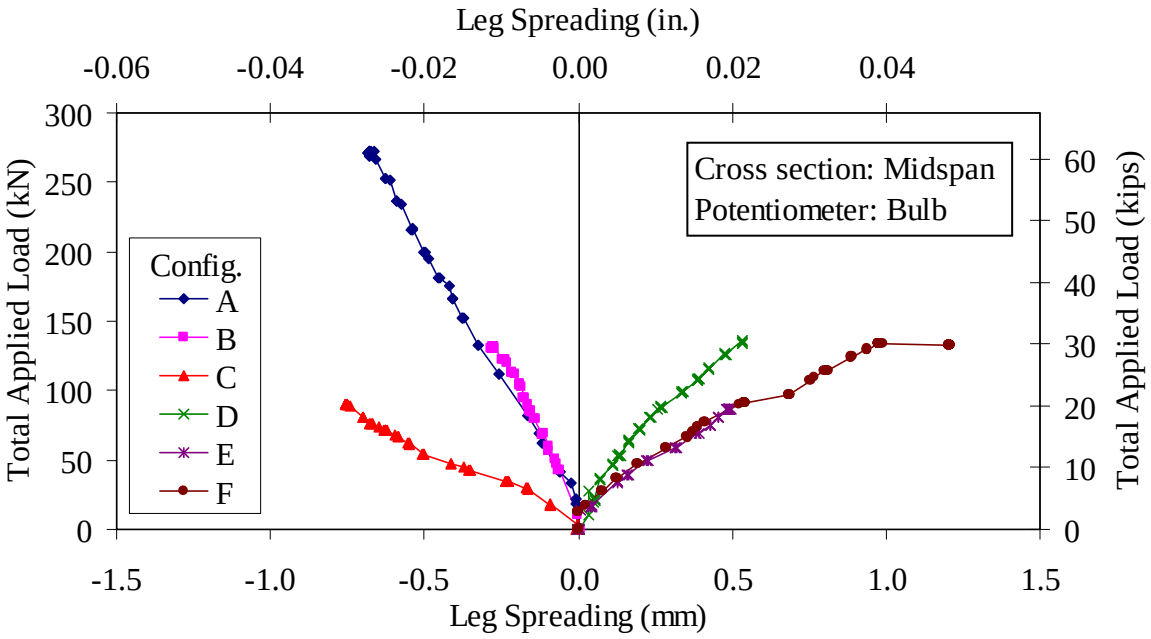

Figure 64. Graph. Spreading between legs of Girder P2-70F as measured at midspan bulbs.

Figure 66, Figure 67, and Figure 68 show strain profiles as captured for the six loading configurations. Figure 66 presents the longitudinal strain at midspan of the girder on top of the deck. Figure 67 presents the transverse strain at midspan of the girder on top of the deck. Figure 68 presents the transverse strain at midspan of the girder on the underside of the deck.

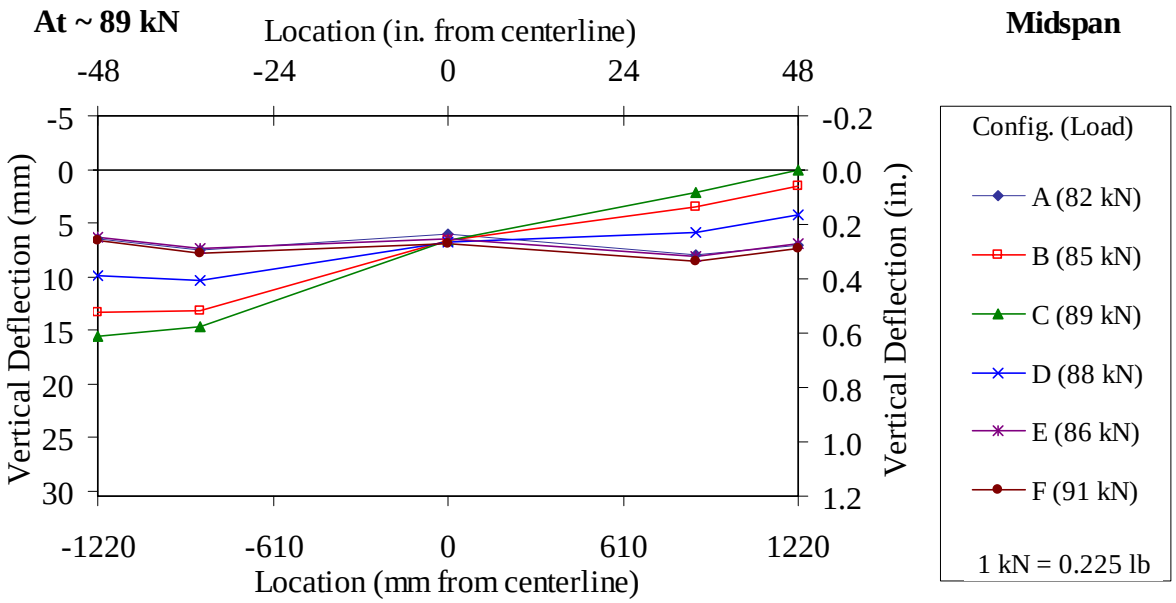

Figure 65. Graph. Midspan vertical deflection profile of Girder P2-70F.

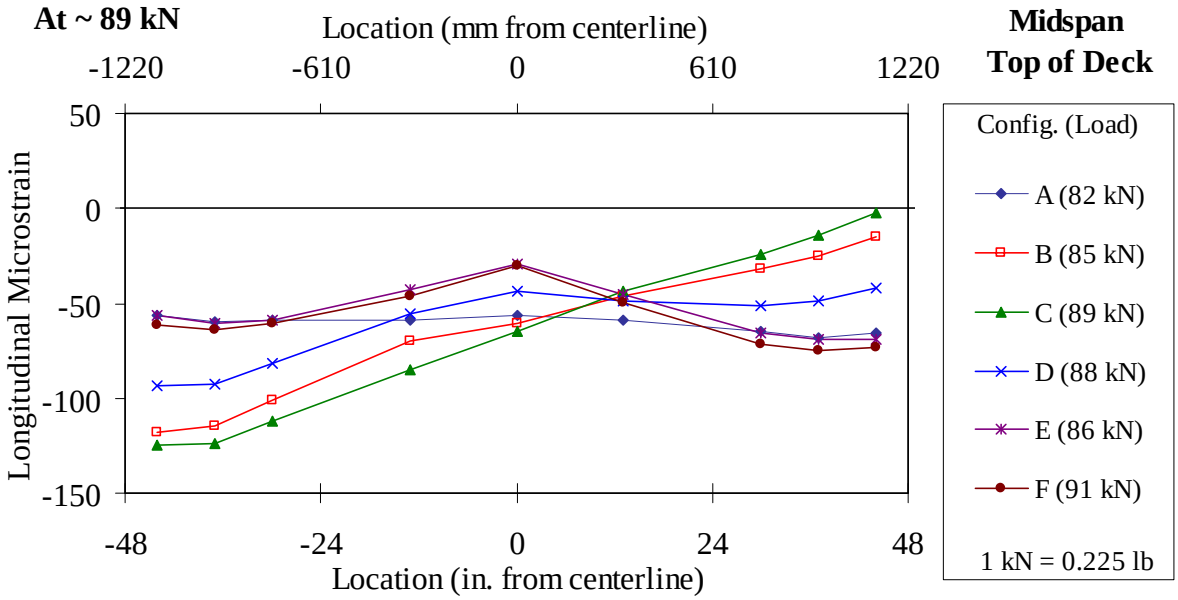

Figure 66. Graph. Midspan longitudinal strain profiles on top of Girder P2-70F deck.

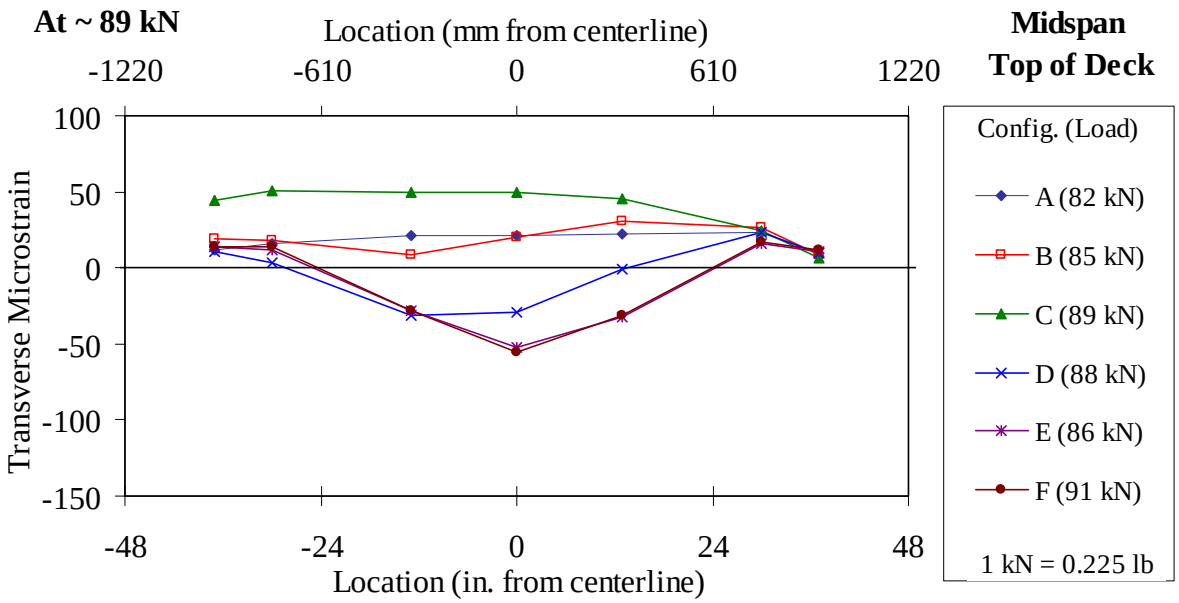

Figure 67. Graph. Midspan transverse strain profiles on top of Girder P2-70F deck.

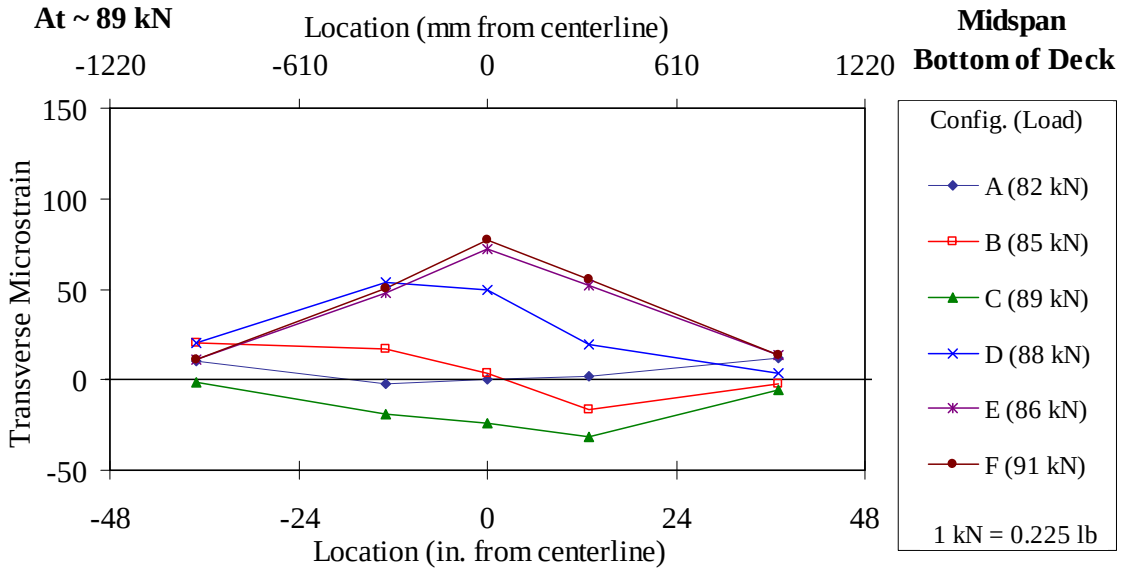

Figure 68. Graph. Midspan transverse strain profiles on bottom of Girder P2-70F deck.

Ultimate Flexural Capacity Testing

The ultimate flexural capacity testing was completed immediately after the conclusion of the load distribution testing on Girder P2. Recall that the loads were applied at four load points directly above the webs through 0.23-m (9-inch) diameter steel plates which were grouted to the deck surface. The applied load was measured through load cells placed between the hydraulic jacks and the deck. The loads were reacted through 0.18-m (7-inch) diameter steel rollers. The girder span was 21 m (69 feet).

Figure 69 shows the applied load versus vertical deflection response of the girder. The reported deflection is the average value recorded from the two potentiometers measuring the displacement of the bottom face of the girder legs. The load-deflection response shows that the girder began to soften near 400 kN (90 kips) at a deflection of approximately 38 mm (1.5 inches). The girder exhibited significant additional capacity, reaching a peak load of 738 kN (166 kips) at a deflection of 249 mm (9.8 inches). Failure occurred due to a loss of tensile capacity in the south bulb at midspan.

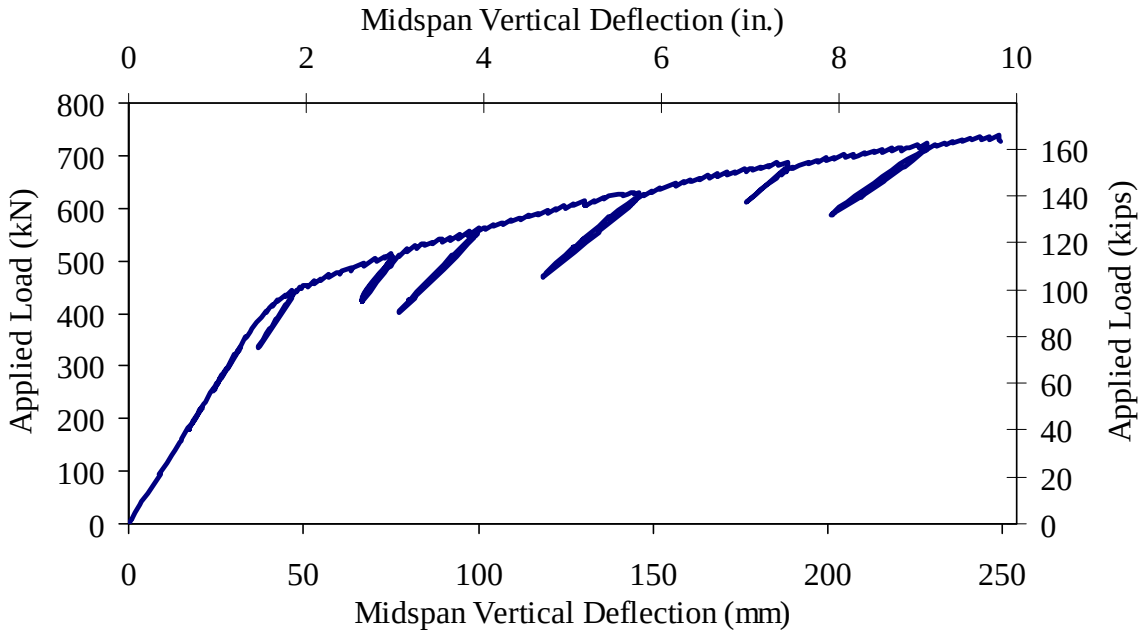

Figure 69. Graph. Load versus midspan deflection response of Girder P2-70F.

The strain gages mounted on the girder's centerline and oriented along the length of the girder were used to create a strain profile over the depth of the girder throughout the test. Individual gages were used until their readings became unreliable due to cracking of the underlying concrete. Data from each side of each leg was analyzed independently and found to be nearly coincident. The neutral axis location and curvature of the cross-section were then calculated based on these results. Figure 70 presents the neutral axis depth as measured down from the top of the girder at each load step throughout the test. Note that an elastic section analysis of the cross section indicates that the neutral axis at test initiation should have been located approximately 323 mm (12.7 inches) down from the top of the girder. The plot shows that the neutral axis began to rise at an applied load of approximately 400 kN (90 kips), quickly moved to a depth of 203 mm (8 inches), then steadily moved to a depth of 86 mm (3.4 inches) by failure. Note the stability of the neutral axis depth during the unload/reload steps.

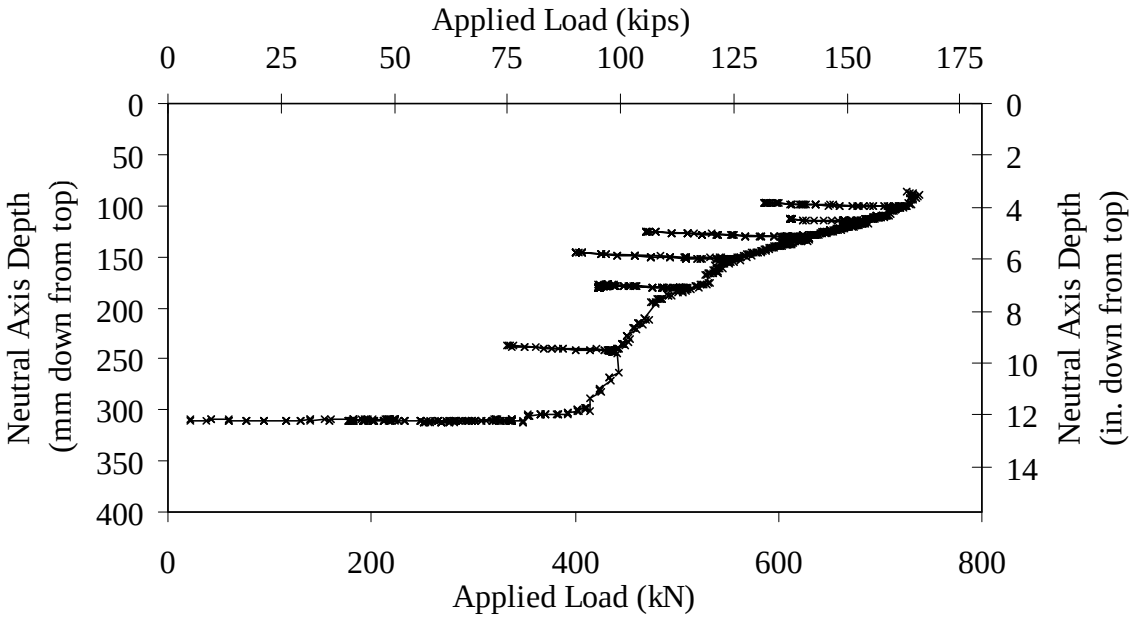

Figure 70. Graph. Midspan neutral axis depth down from the top of Girder P2-70F.

The midspan strain profiles obtained from the strain gages on each leg of the girder as well as the LVDTs affixed to the bottom faces of the bulbs provide an indication of the tensile strain in the UHPC throughout the application of load. These results are plotted in Figure 71 and Figure 72 for the south and north legs, respectively. The strain gage results are calculated based on extrapolation from operational strain gages on the midspan cross section independently in each leg of the girder. The LVDT results are based on the recorded displacement readings divided by the gage length. Note that prior to the application of load, the prestressing forces and dead load resulted in an extreme tensile face compressive strain of approximately 240 microstrain. The plots show that at peak applied load, the strain on the tensile face of the south leg was approximately 10,000 microstrain.

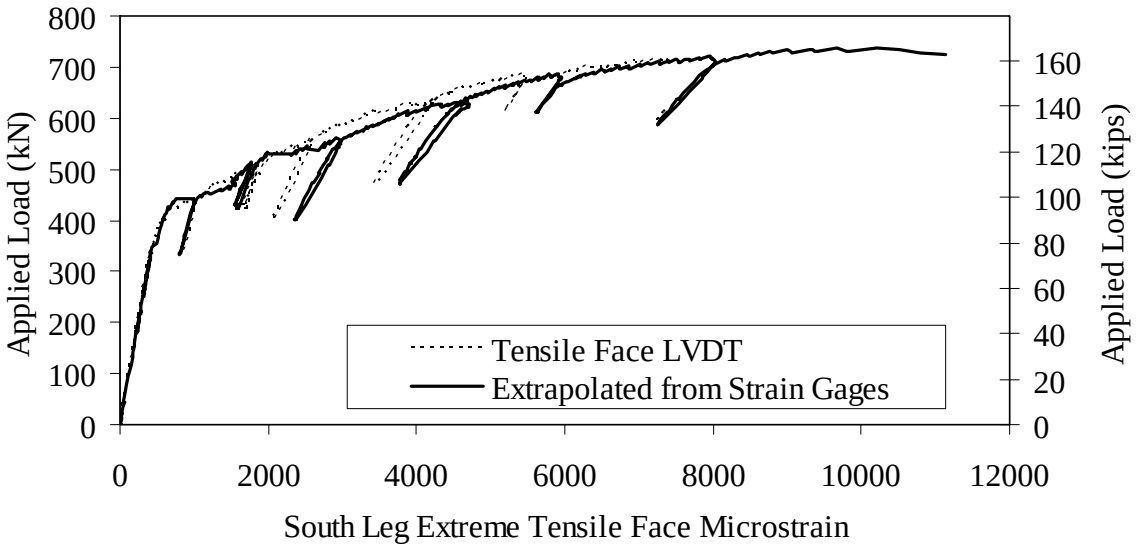

Figure 71. Graph. Midspan south leg tensile face strain in Girder P2-70F.

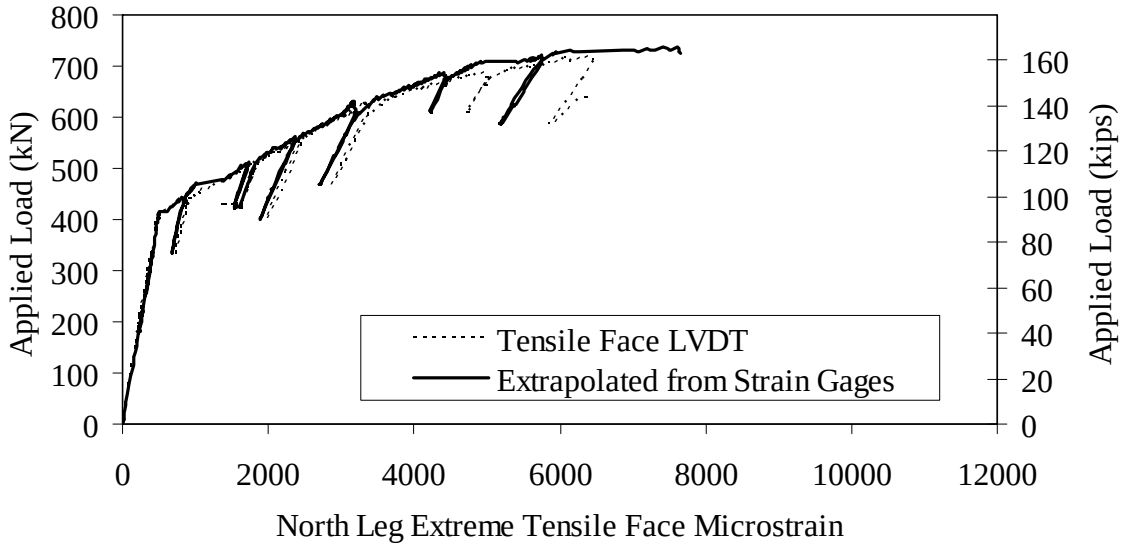

Figure 72. Graph. Midspan north leg tensile face strain in Girder P2-70F.

Figure 73 presents the results obtained from the four potentiometers installed to capture the spreading of the girder's legs throughout the test. These results show that the girder legs progressively moved toward one another as the load increased, with the largest relative movement occurring at the bottom of the midspan legs. In all cases, the legs moved less than 3 mm (0.12 inches) throughout the test, indicating that the loads were nearly symmetrically applied over the webs.

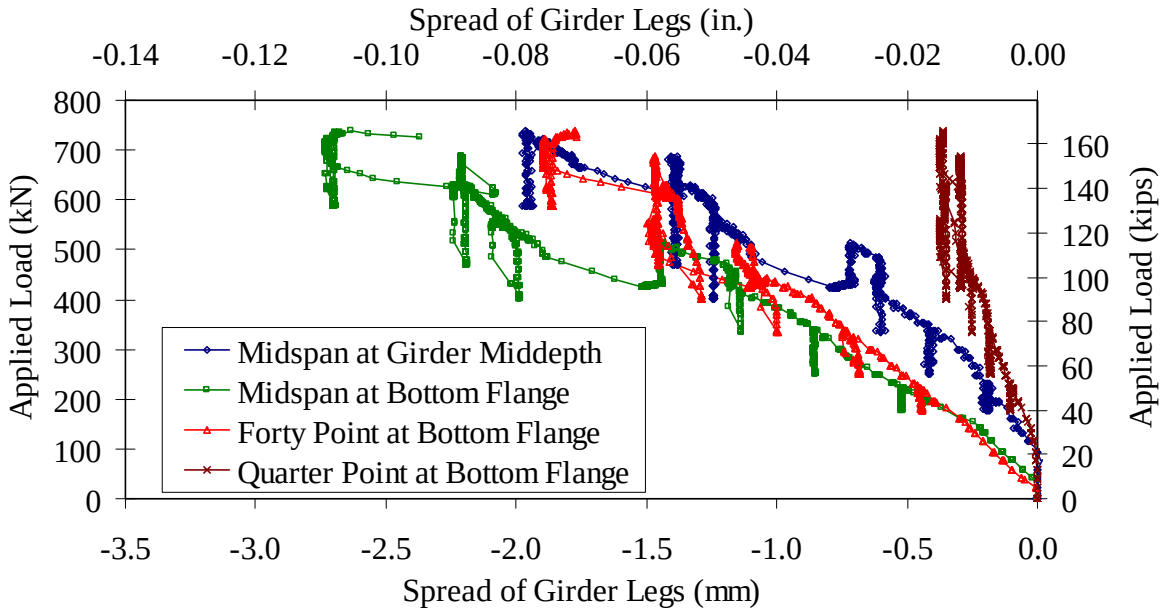

Figure 73. Graph. Spreading between webs of Girder P2-70F.

Further results related to the deflection of the girder are presented in Figure 74. This plot shows the results from the five potentiometers which measured vertical deflection of the girder at midspan. Results from the set of potentiometers at ten discrete steps throughout the test are presented. Note the lag in deflection that becomes apparent at higher load levels in the parts of the girder not directly subjected to the applied load.

Figure 75 and Figure 76 provide strain results captured from the midspan strain gages which were oriented along the girder's length above and below the deck, respectively. Results from the sets of strain gages at ten discrete steps throughout the test are presented. These figures show that the strain readings were relatively uniform across the girder until after flexural cracking of the girder had occurred. After cracking, the gages on the top of the deck showed greater variability but were still relatively consistent up through girder flexural failure. The gages below the deck demonstrate that the neutral axis did not rise into the 76 mm (3 inch) thick deck prior to failure but that it did rise into the thickened flange tips. Clearly, the flange tips were participating in the girder's resistance to the flexural forces applied.

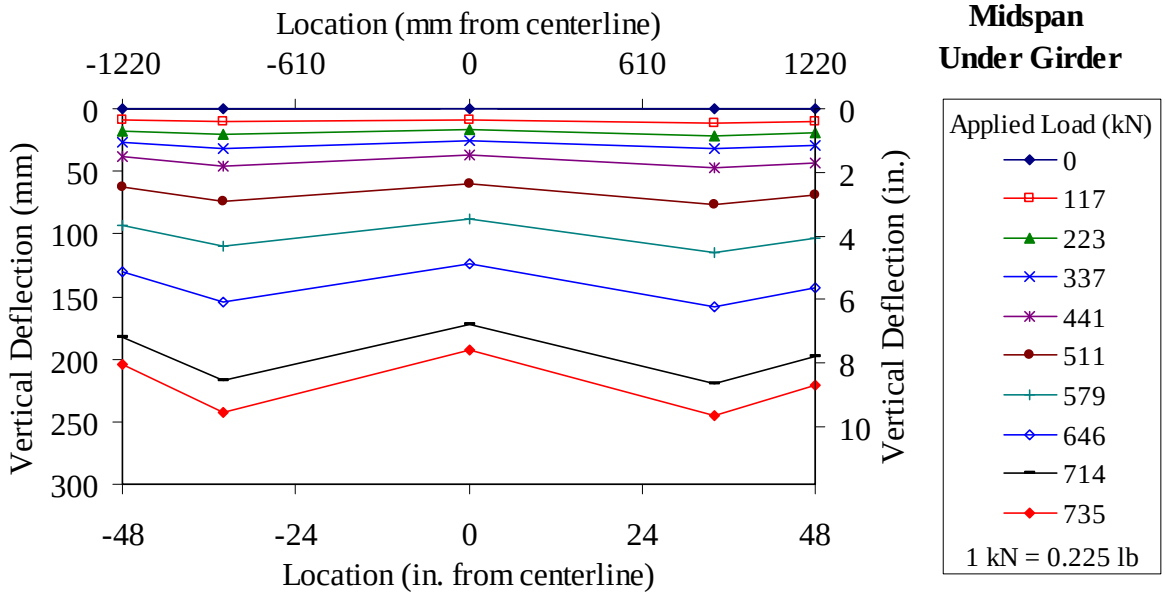

Figure 74. Graph. Midspan vertical deflection of Girder P2-70F.

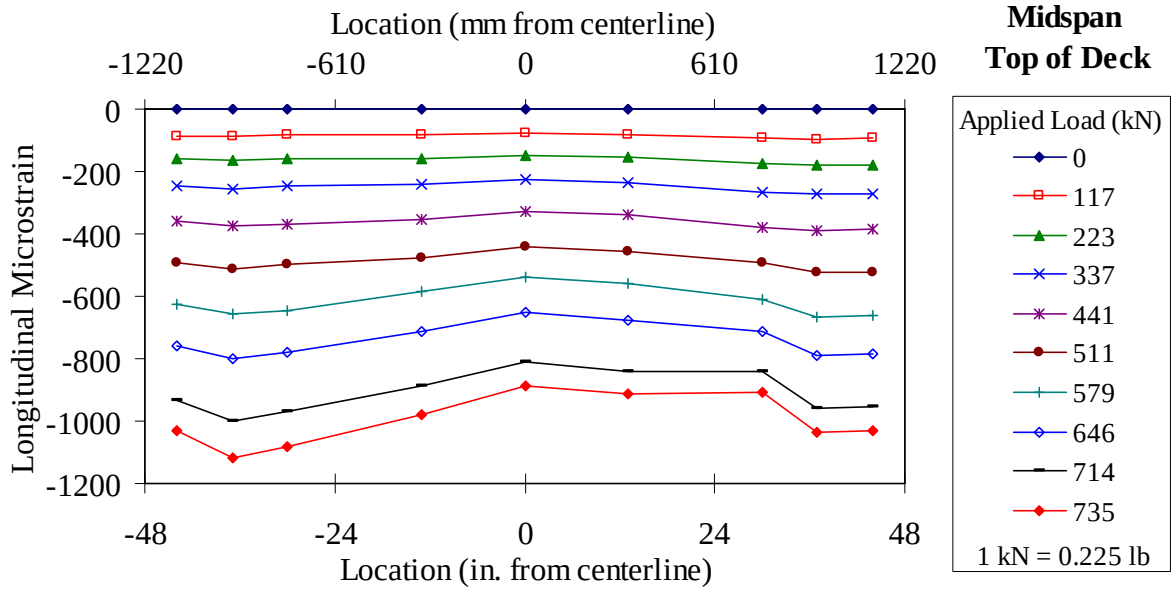

Figure 75. Graph. Midspan longitudinal strains on top of Girder P2-70F deck.

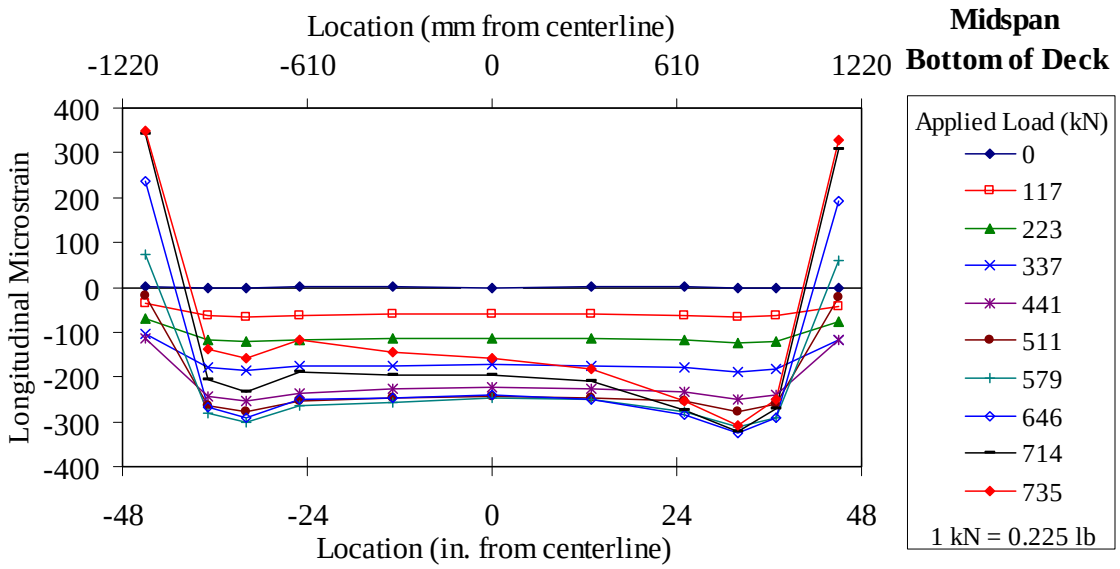

Figure 76. Graph. Midspan longitudinal strains on bottom of Girder P2-70F deck.

Significant audible cracking began at an applied load of approximately 330 kN (75 kips) and continued during loading steps throughout the remainder of the test. Assessment of the flexural cracks was completed at two applied load levels. The first assessment was completed at an applied load of 503 kN (113 kips) which corresponded to an overall midspan deflection of 76 mm (3 inches). A denatured alcohol spray was used to identify the cracks which were too small to be observed with the naked eye. The assessment marked every flexural crack on the outside of the north and south bulbs to the east of midspan. Figure 77 presents these results by summing the discrete cracks observed in each 0.3 m (1 foot) increment along the girders length. On average, there were approximately 2.3 cracks per 25 mm (1 inch) in the constant moment region. Also, extrapolation indicates that there were approximately 300 flexural cracks in each bulb, all occurring over a 5.5 m (18 foot) region centered on midspan.

The second crack assessment was completed at an applied load of 689 kN (155 kips) which corresponded to an overall midspan deflection of 191 mm (7.5 inches). The results are again presented in Figure 77 with only the south bulb having been assessed. On average there were approximately 6 cracks per 25 mm (1 inch) in the constant moment region. Extrapolating on the data indicates that there were approximately 1100 flexural cracks in each bulb, all occurring over a 9.1 m (30 foot) region centered on midspan.

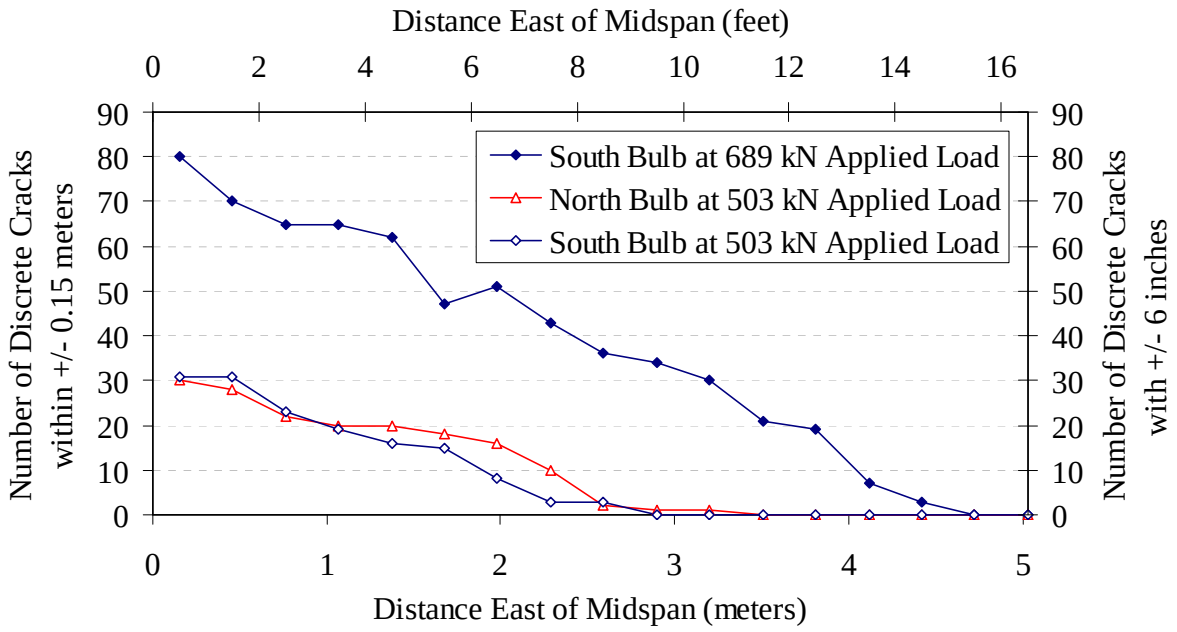

Figure 77. Graph. Flexural cracking observed on outside faces of Girder P2-70F bulbs.

This girder exhibited a significant deflection capacity prior to failure. Figure 78 shows the girder carrying a load of 716 kN (161 kips) with a resulting midspan deflection of 230 mm (9 inches). Soon thereafter, the girder reached its maximum applied load of 738 kN (166 kips) which corresponds to an applied moment of 3540 kN-m (31,350 kip-inches). The maximum combined dead and live load moment was 4250 kN-m (37,600 kip-inches).

Flexural failure of the girder occurred immediately after the fiber reinforcement bridging an individual flexural crack pulled out of the matrix thus shedding the tensile load it had been carrying into the prestressing strands. The failure crack was located at midspan in the south bulb. All eleven prestressing strands in this bulb ruptured and the crack ran up the web and into the deck. The loss of resistance on the south side of the girder allowed the hydraulic jacks to sufficiently reduce their applied load that the north bulb of the girder did not rupture. (The north side of the girder was later taken to flexural failure so as to disconnect the girder pieces and allow for the completion of future tests.)

Figure 79 shows the west face of the south bulb failure surface after the girder had been broken into two pieces. Note the pulled out fiber reinforcement and the ruptured strands. Figure 80 shows the north face of the south leg immediately after the south leg failed. Note the red instrumentation cable which is visible inside of the crack. This cable was attached to vibrating wire strain gage which was cast into the girder during fabrication. The wire ran from the middle of the deck, across the deck, and down the web into the bulb at midspan. Given that the girder failed at this location, it is likely that the ultimate flexural capacity of the girder was impacted by the presence of this cable within the web. Visual inspection of the failure surface in the vicinity of the cable indicated that the cable impeded the proper dispersion of fiber reinforcement during casting and thus precluded fibers from bridging the eventual failure crack for approximately 12 mm (0.5 inches) of width over the height of the web.

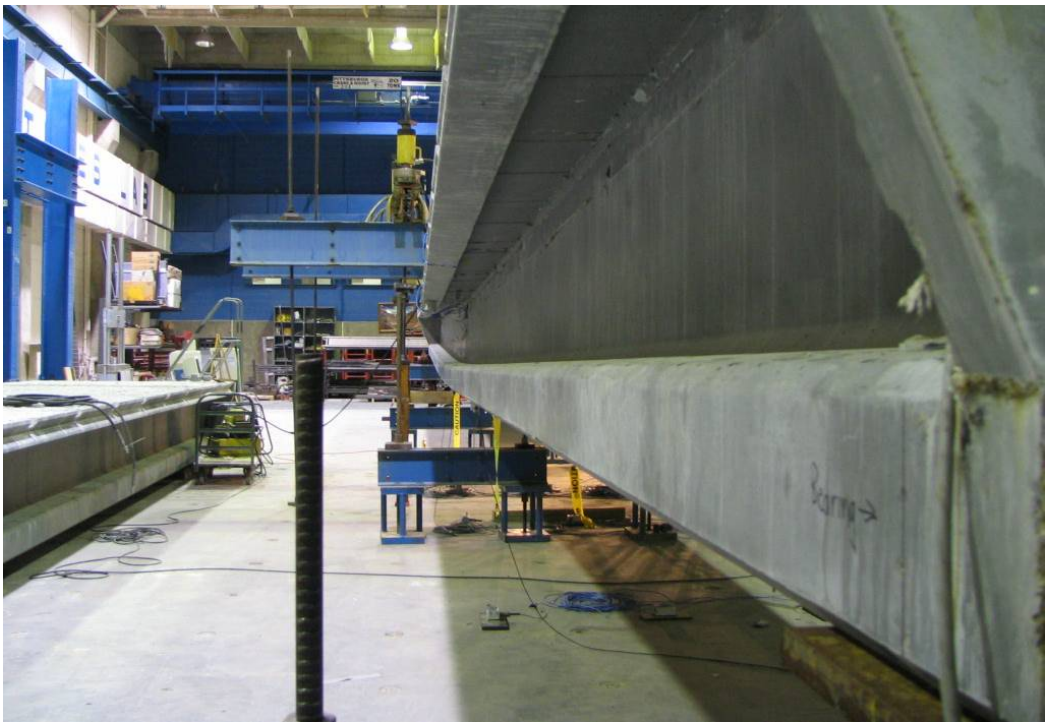

Figure 78. Photo. North face of Girder P2-70F after 230 mm (9 inches) of deflection.

Figure 79. Photo. West face of Girder P2-70F south bulb failure surface.

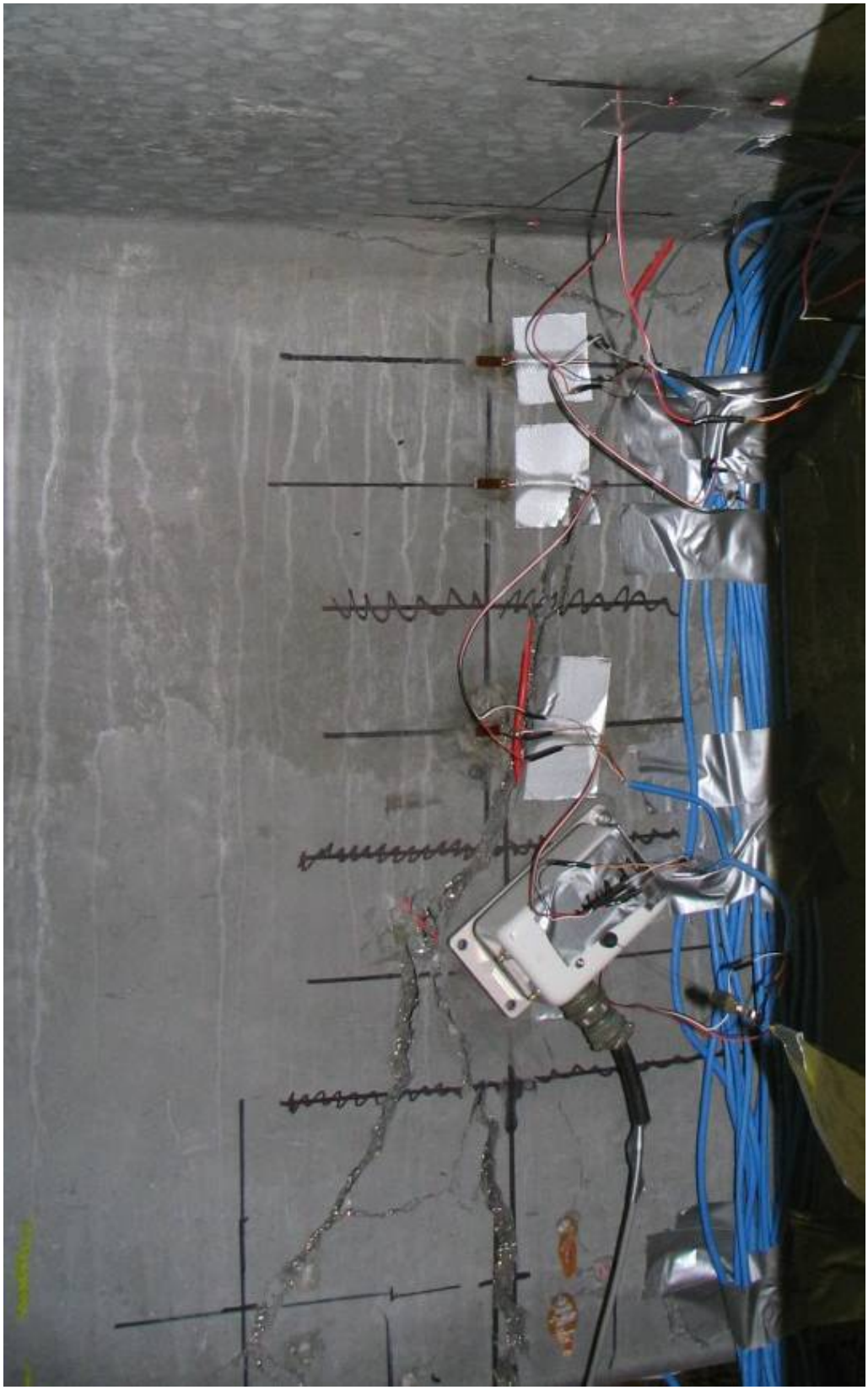

Figure 80. Photo. North face of Girder P2-70F south web immediately after failure.

P4-45F

The second ultimate flexural response test was completed on Girder P4. The setup for this test was very similar to that used for the P2-70F test, except that the total span of the girder was reduced to 13.72 m (45 feet) as shown in Figure 19. Prior to the completion of this test, both the east and west ends of this girder were subjected to shear tests as will be described later. The most significant effects of these shear tests were concentrated in the portions of the girder which overhang the P4-45F supports, thus it is not anticipated that these previous tests significantly affected the flexural response which was observed.

As in Test P2-70F, the loads were applied at four load points directly above the webs through 0.23-m (9-inch) diameter steel plates which were grouted to the deck surface. The applied load was measured through load cells placed between the hydraulic jacks and the deck. The loads were reacted through 0.18-m (7-inch) diameter steel rollers.

Figure 81 shows the applied load versus vertical deflection response of the girder. The reported deflection is the average value recorded from the two potentiometers measuring the displacement of the bottom face of the girder legs. The load-deflection response shows that the girder began to soften near 755 kN (170 kips) at a deflection of approximately 22 mm (0.87 inches). The girder exhibited significant additional capacity, reaching a peak load of 1350 kN (304 kips) at a deflection of 130 mm (5.1 inches). Failure occurred due to a loss of tensile capacity in the south bulb at midspan.

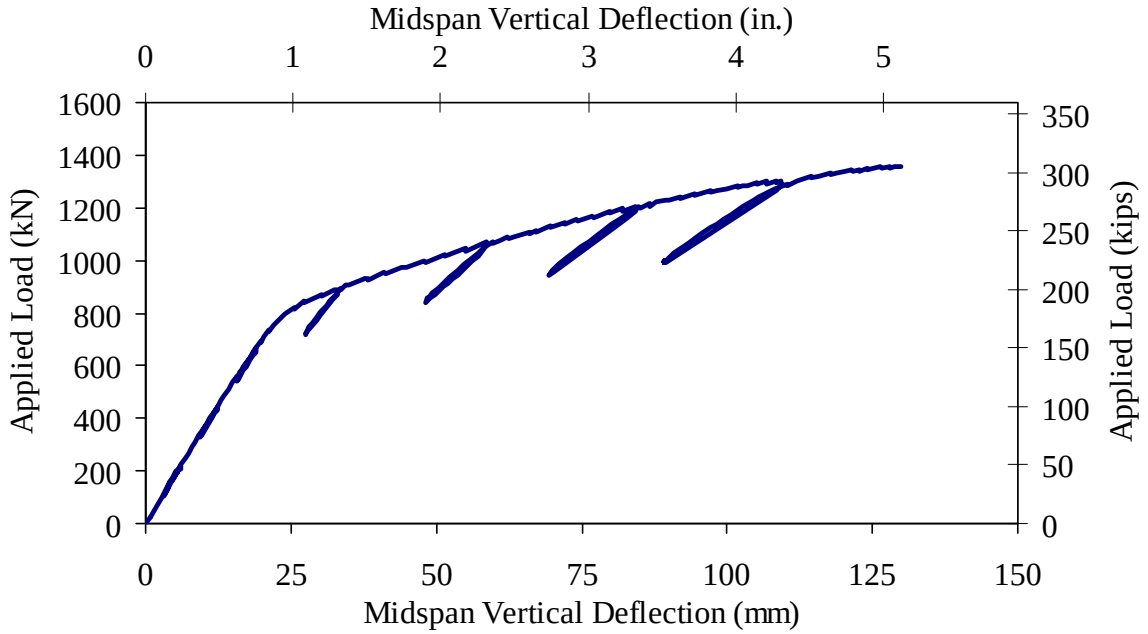

Figure 81. Graph. Load versus midspan deflection response of Girder P4-45F.

As in Test P2-70F, the strain gages mounted on the girder's centerline and oriented along the length of the girder were used to determine strain profile and neutral axis depth results. Figure 82 presents the neutral axis depth as measured down from the top of the girder at each load step

throughout the test. Note that an elastic section analysis of the cross-section indicates that the neutral axis at test initiation should have been located approximately 323 mm (12.7 inches) down from the top of the girder. The plot shows that the neutral axis began to rise at an applied load of approximately 755 kN (170 kips), quickly moved to a depth of 152 mm (6 inches), then steadily moved to a depth of 132 mm (5.2 inches) by failure. Note the stability of the neutral axis depth during the unload/reload steps.

Figure 85 presents the results obtained from the four potentiometers installed to capture the spreading of the girder's legs throughout the test. These results show that the girder legs progressively moved toward one another as the load increased, with the largest relative movement occurring at the bottom of the midspan legs. In all cases, the legs moved less than 6 mm (0.24 inches) throughout the test, indicating that the loads were nearly symmetrically applied over the webs.

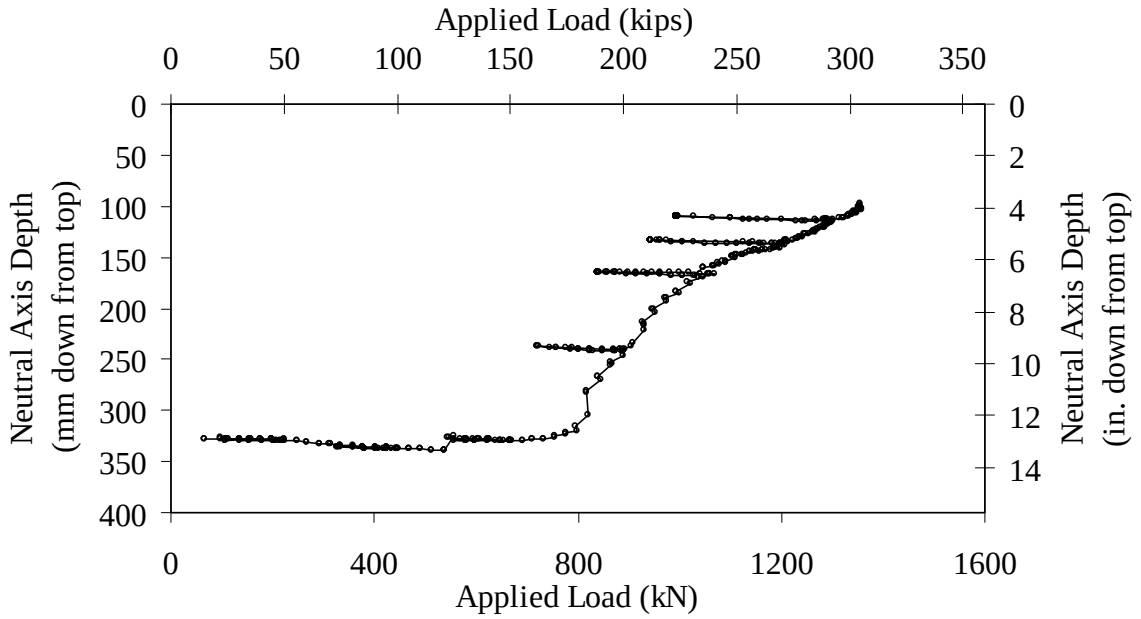

Figure 82. Graph. Midspan neutral axis depth down from the top of Girder P4-45F.

The midspan strain profiles obtained from the strain gages on each leg of the girder as well as the LVDTs affixed to the bottom faces of the bulbs provide an indication of the tensile strain in the UHPC throughout the application of load. These results are plotted in Figure 83 and Figure 84 for the south and north legs, respectively. The strain gage results are calculated based on extrapolation from operational strain gages on the midspan cross section independently in each leg of the girder. The LVDT results are based on the recorded displacement readings divided by the gage length. Note that prior to the application of load, the prestressing forces and dead load resulted in an extreme tensile face compressive strain of approximately 330 microstrain. The plots show that at peak applied load, the strain on the tensile face of the south leg was between 7,000 and 10,000 microstrain.

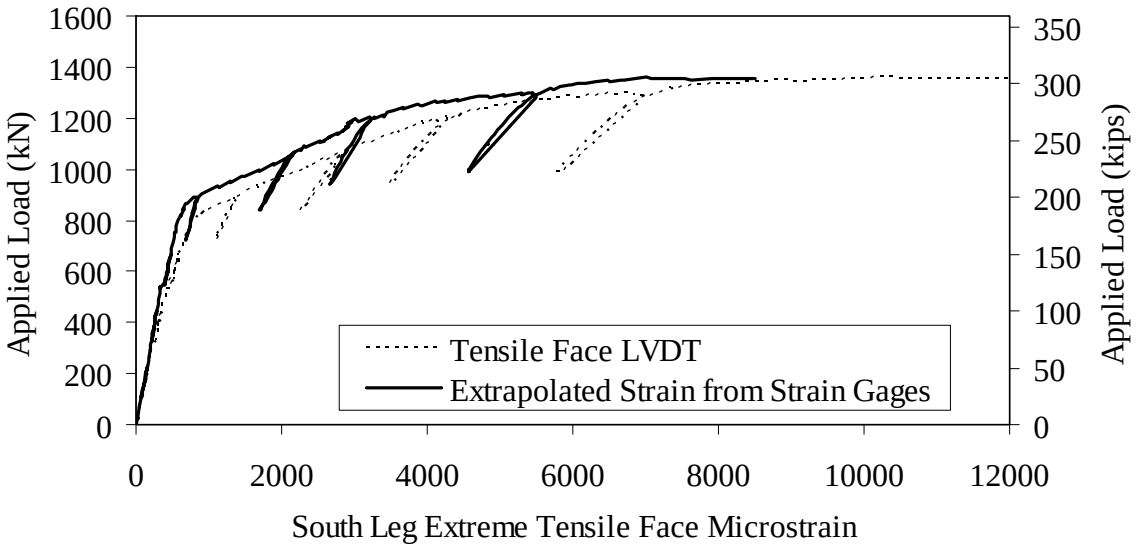

Figure 83. Graph. Midspan south leg tensile face strain in Girder P4-45F.

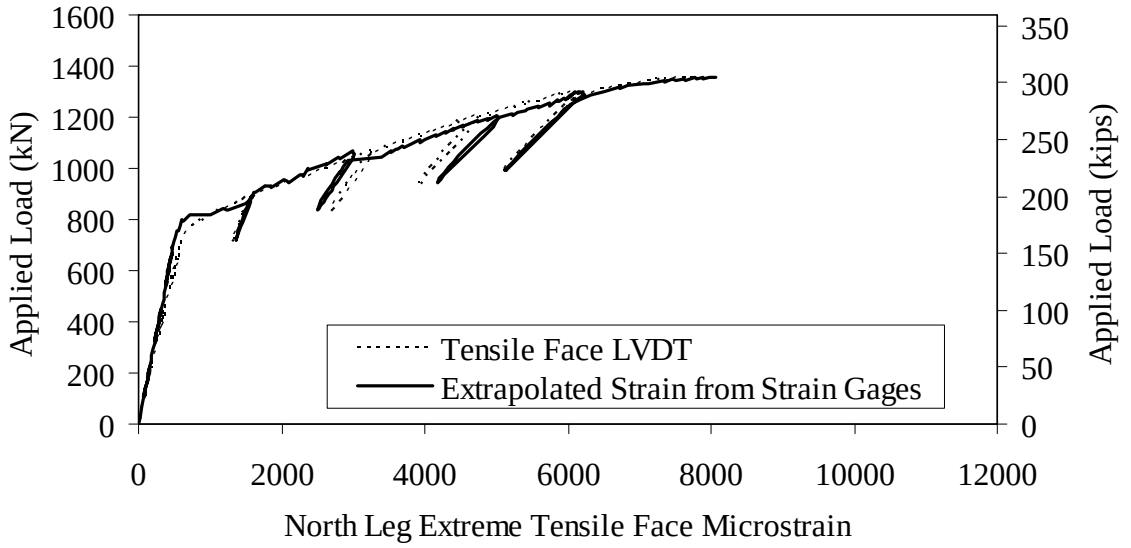

Figure 84. Graph. Midspan north leg tensile face strain in Girder P4-45F.

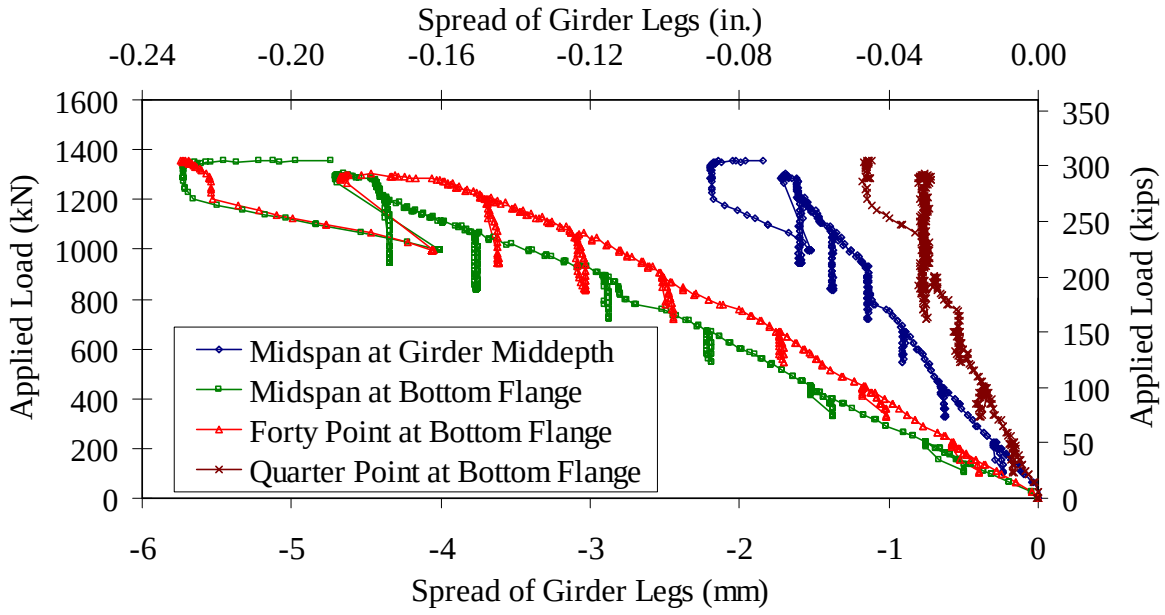

Figure 85. Graph. Spreading between webs of Girder P4-45F.

Further results related to the deflection of the girder are presented in Figure 86. This plot shows the results from the five potentiometers which measured vertical deflection of the girder at midspan. Results from the set of potentiometers at nine discrete steps throughout the test are presented. The deflections are quite consistent throughout the entirety of the load application.

Figure 87 provides strain results captured from the midspan strain gages which were oriented along the girder's length above the deck. Results from the set of strain gages at nine discrete steps throughout the test are presented. These figures show that the strain readings were relatively uniform across the girder until after flexural cracking of the girder had occurred. After cracking, the gages on the top of the deck showed some variability but were still relatively consistent up through girder flexural failure.

Significant audible cracking began at an applied load of approximately 645 kN (145 kips) and continued during loading steps throughout the remainder of the test. A quantitative assessment of flexural cracks was not completed for this test. In contrast to Test P2-70F, a clearly visible flexure crack was observed on the south face of the south leg at an applied load of 1070 kN (240 kips). This crack was located within 25 mm (1 inch) of midspan, was visible over most of the height of the web, and had a maximum width of approximately 0.25 mm (0.01 inches). By an applied load of 1200 kN (270 kips), this crack had extended higher in the web and had a maximum width of approximately 0.38 mm (0.015 inches). Figure 88 shows a photo of this crack. For reference, a 51 mm (0.5 inch) gage length strain gage is also shown in the picture. Figure 89 shows a photo of this crack just before failure of the girder.

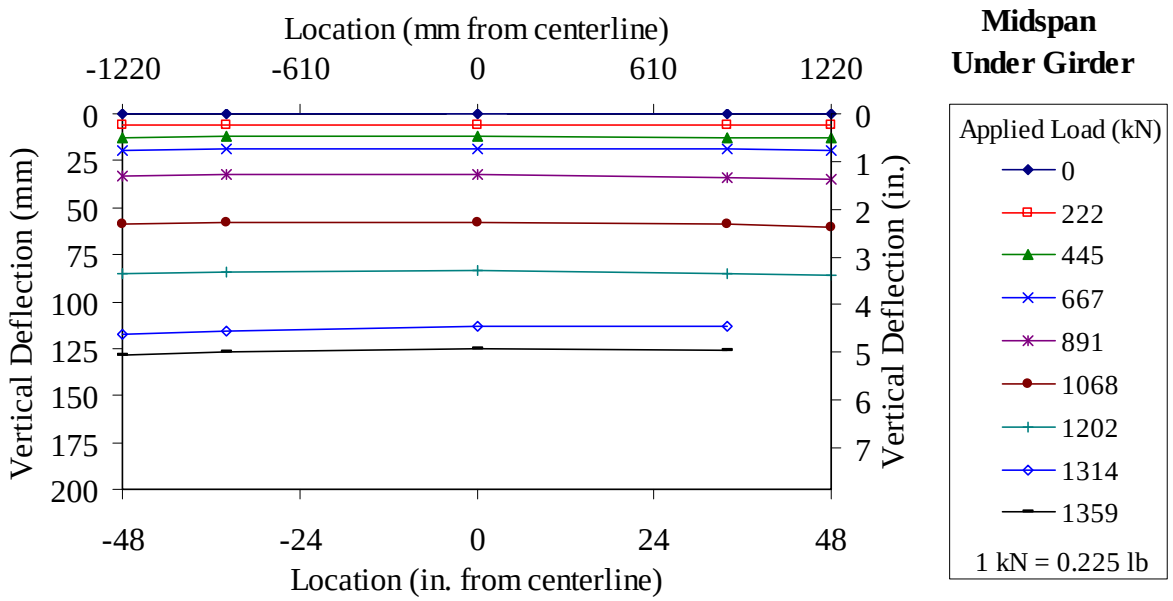

Figure 86. Graph. Midspan vertical deflection of Girder P4-45F.

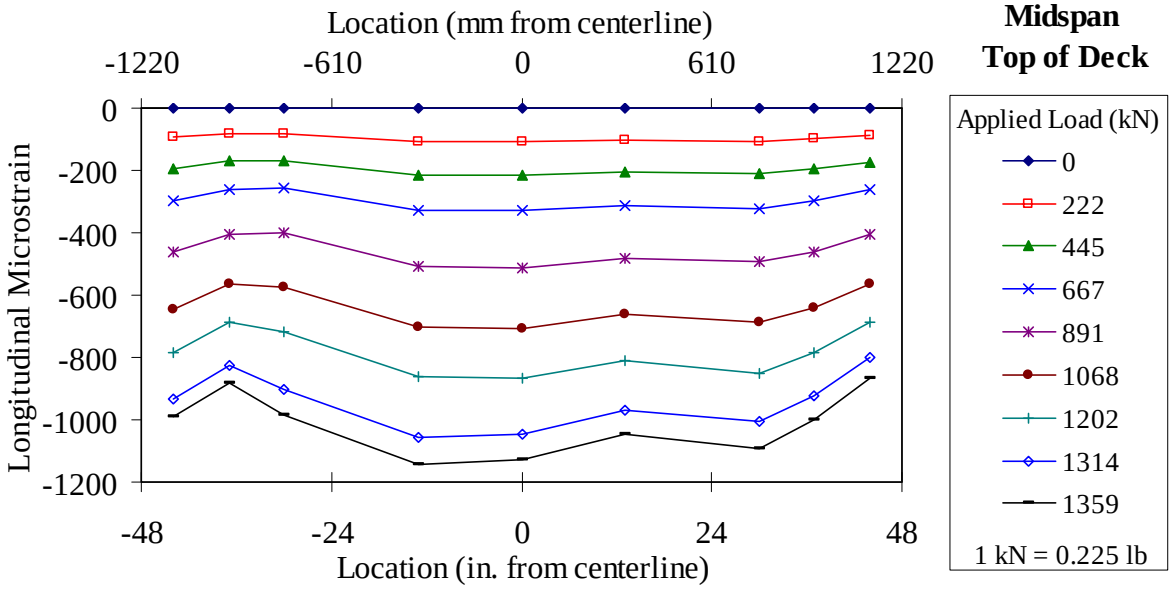

Figure 87. Graph. Midspan longitudinal strains on top of Girder P4-45F deck.

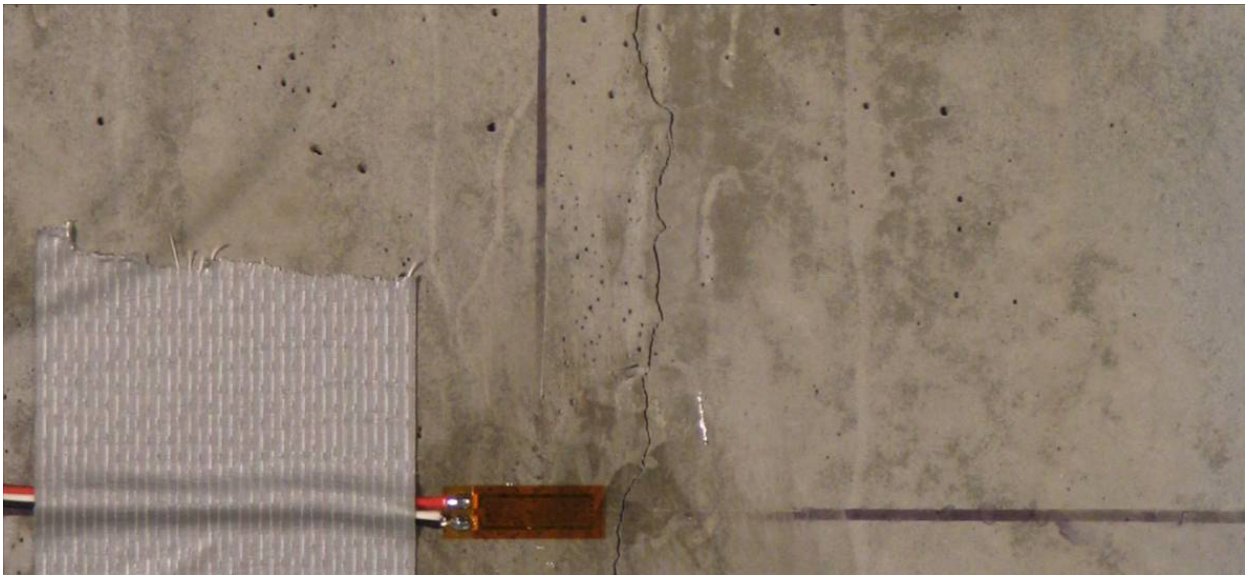

Figure 88. Photo. Crack on south face of Girder P4-45F at 1070 kN (240 kips).

Figure 89. Photo. Crack on south face of Girder P4-45F just before failure.

At a midspan deflection of 130 mm (5.1 inches), the girder reached its maximum applied load of 1350 kN (304 kips) which corresponds to an applied moment of 4040 kN-m (35,730 kip-inches). The maximum combined dead and live load moment was 4310 kN-m (38,190 kip-inches).

Flexural failure of the girder occurred when fiber pullout and strand rupture occurred across the crack discussed previously and shown in Figure 89. The south leg of the girder failed while the north leg remained intact. All eleven prestressing strands in the south bulb ruptured and the crack ran up the web and into the deck. (The north side of the girder was later taken to flexural failure so as to disconnect the girder pieces.)

Figure 90 shows the south face of the girder immediately after flexural failure of the south leg. Note the red instrumentation cables which are visible inside of the crack in the web. Figure 91 shows a close-up view of the west face of the south leg flexural failure surface. As in Girder P2, the instrumentation cables were attached to vibrating wire strain gage which were cast into the girder during fabrication. Given that the girder failed at this location, it is likely that the ultimate flexural capacity of the girder was impacted by the presence of this cable within the web. Visual inspection of the failure surface in the vicinity of the cable indicated that the cables impeded the proper dispersion of fiber reinforcement during casting and thus precluded fibers from bridging the eventual failure crack for approximately 19 mm (0.75 inches) of width over the height of the web.

Figure 90. Photo. Crack on south face of Girder P4-45F just after failure.

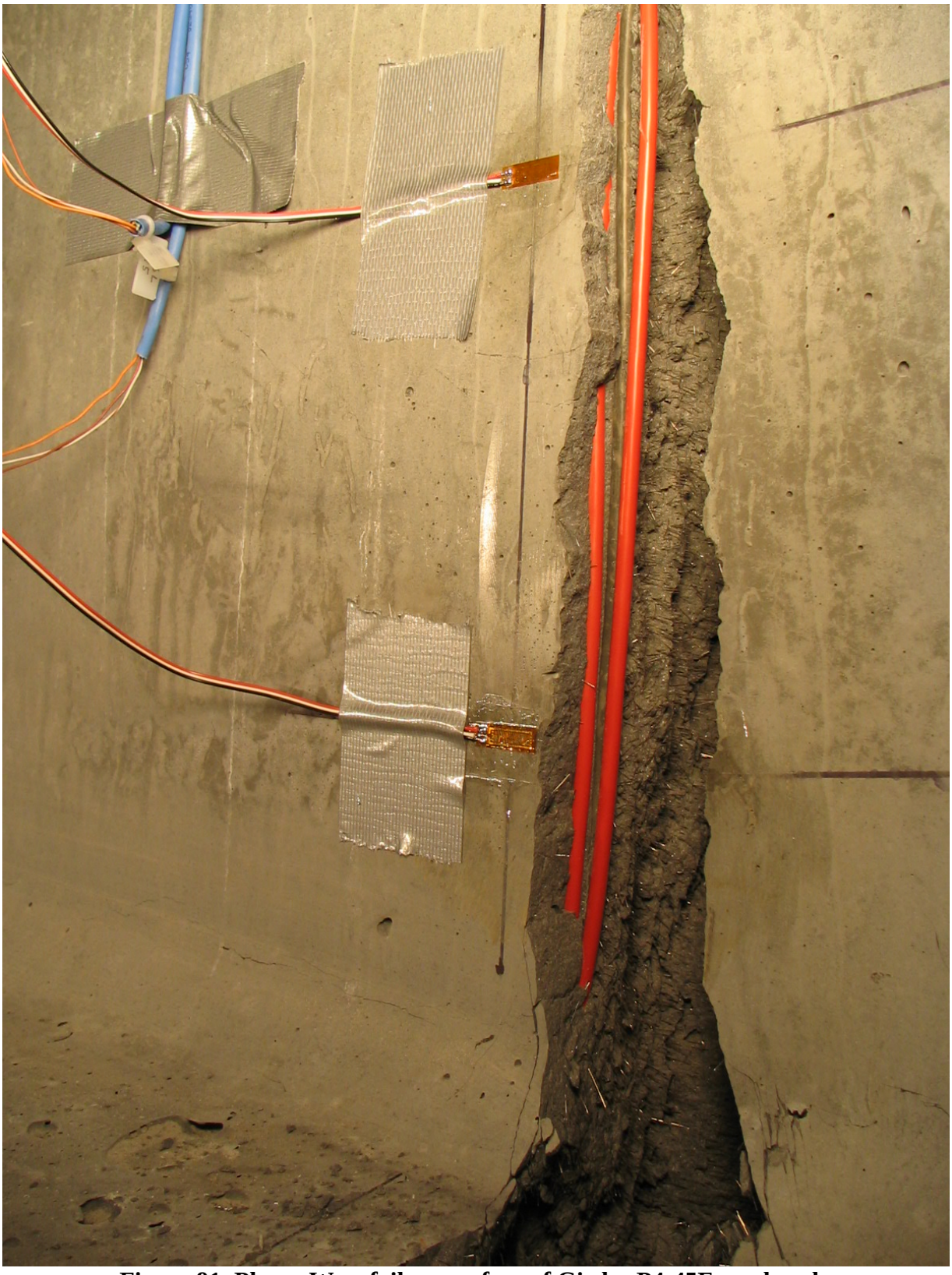

Figure 91. Photo. West failure surface of Girder P4-45F south web.

STATIC SHEAR TESTING

A series of structural tests focused on the shear behavior of the pi-girder cross section were conducted. These tests used portions of Girders P2 and P4 and the results are presented below.

P2-21S

Test series P2-21S focused on the primary shear response of the pi-girder cross section. Two sets of tests were completed, with the first set focusing on load distribution behaviors resulting from unsymmetric loading of the girder and the second set focusing on the shear response of the girder through shear failure. Recall that Test P2-21S was conducted on Girder P2 after the conclusion of Test P2-70F. The east half of Girder P2 was used for Test P2-21S. Prior to the start of testing the girder was inspected for damage. Some flexural and deck cracking was noted in the test span; however, no cracking or other damage was observed within either leg of the girder to the east of the load point.

Load Distribution Testing

A load distribution test was completed as part of the P2-21S tests prior to the completion of the ultimate strength test. Two loading configurations were used: Load Configuration A included load application by two hydraulic jacks centered over the girder webs, while Load Configuration B included load application by one hydraulic jack centered over the south web. In both cases, loads were applied through 229 mm (9 inch) diameter steel plates which were grouted to the surface of the deck. Reaction forces were measured through load cells positioned under the girder legs on the supports. Recall that this girder does not possess any diaphragms or cross-frames through which to assist in load-sharing between girder legs within the span; however, the specimen does possess a solid UHPC diaphragm at the east end so as to limit cross-sectional deformations. This test setup is shown in the photo in Figure 92.

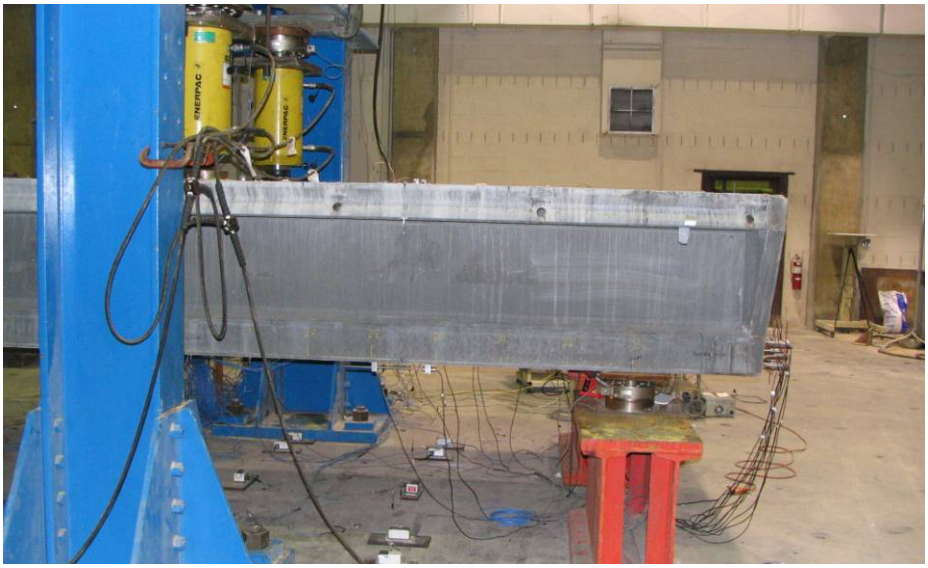

Figure 92. Photo. Load distribution test setup for Girder P4-21S.

The distribution of load resulting from Load Configuration A occurred as anticipated, with the load being appropriately distributed to the four support points. The distribution of load resulting from Load Configuration B was investigated through two means. First, the strain gages affixed to the girder webs at instrumentation lines C, D, and E as shown in Figure 24 were used to quantify the principal tensile and compressive strains at these locations. These results indicated that minimal if any shear force was being carried by the north web in the shear span. The load distribution was also investigated through the reactions observed at the support points. Figure 93 illustrates the reaction forces observed when the applied load was 360 kN (81 kips). Nearly 93 percent of the applied load is reacted through the south leg support points. Further insight into the load distribution behavior is provided through Figure 94 and Figure 95. These figures show that the north overhang at the load point cross-section deflected upward and that the longitudinal strain on top of the deck at the mid-shear span was tensile, respectively, when the specimen was subjected to the 360 kN (81 kip) load.

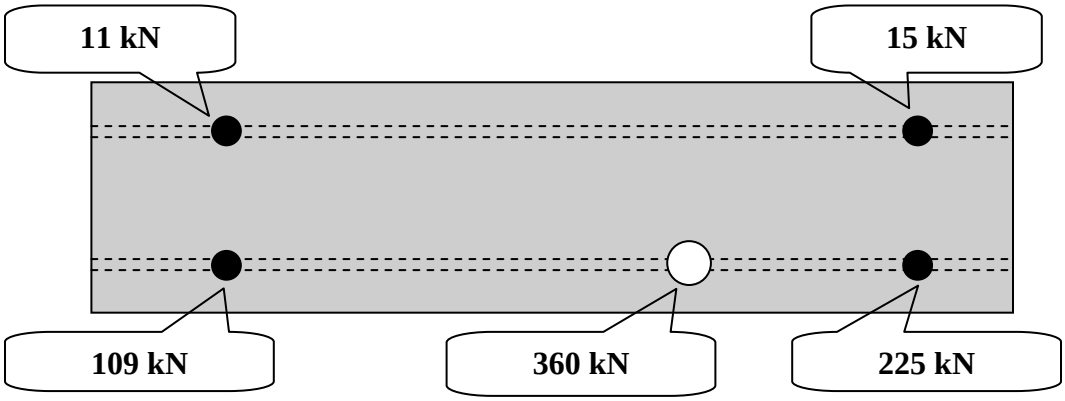

Figure 93. Illustration. Load and reactions for Girder P4-21S at 360 kN (81 kips) of load.

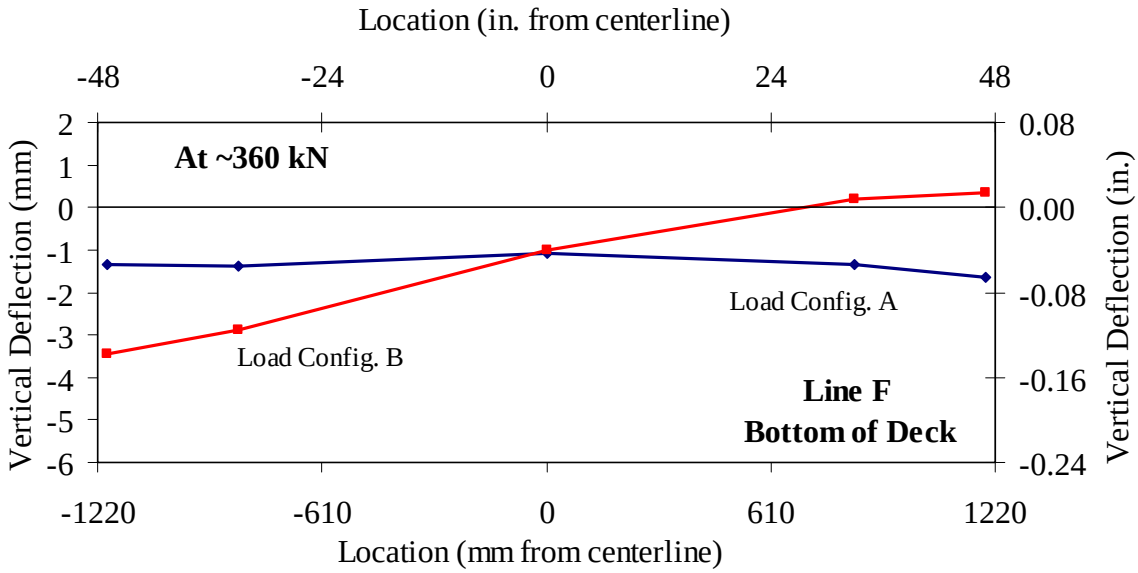

Figure 94. Graph. Vertical deflection response across Girder P2-21S at the load point.

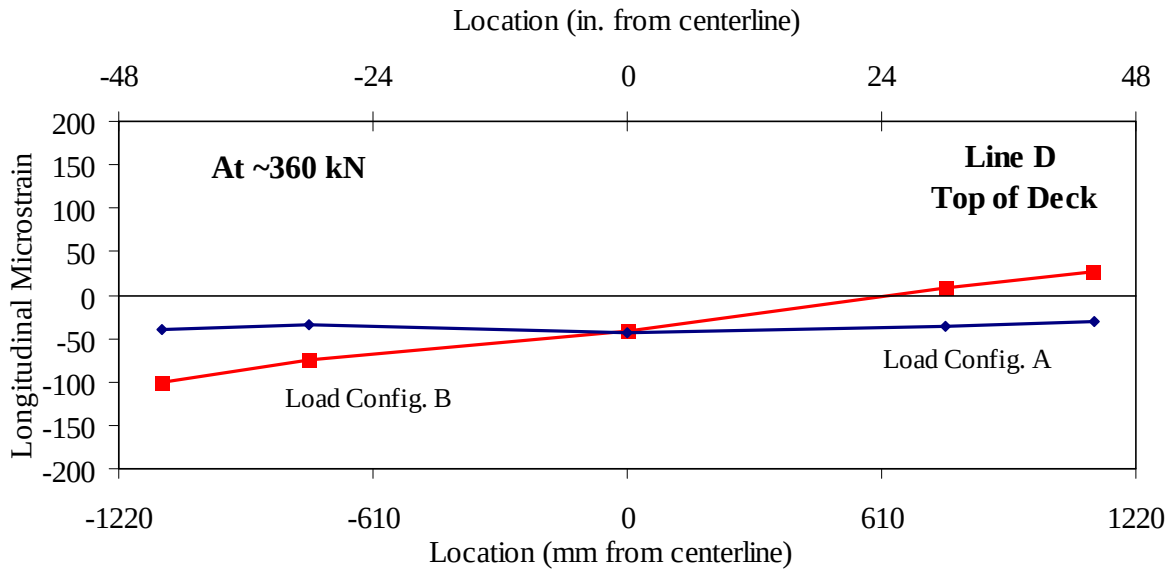

Figure 95. Graph. Longitudinal microstrain on Girder P2-21S at the mid-shear span.

Ultimate Shear Capacity Testing

The ultimate shear capacity testing was completed immediately after the conclusion of the load distribution testing on P2-21S. Recall that the loads were applied at two load points directly above the webs through 0.23-m (9-inch) diameter steel plates which were grouted to the deck surface. The applied load was measured through load cells placed between the hydraulic jacks and the reaction frame. The loads were reacted through 0.18-m (7-inch) diameter steel rollers. The girder span was 6.4 m (21 feet) and the shear span was 2.14 m (7 feet), resulting in a shear span-to-depth ratio of 2.55. The east support rollers were placed 0.61 m (2 feet) from the end of the girder to minimize the effect that debonding of the strands would have on the test results. Recall that three strands in each bulb were debonded for 0.3 m (1 foot) and two strands in each bulb were debonded for 1.8 m (6 feet).

Figure 96 shows the applied load versus vertical deflection response of the girder. The reported deflection is the average value recorded from the two potentiometers measuring the displacement of the bottom face of the girder legs. The load-deflection response shows that the girder began to soften near 1,420 kN (320 kips) of applied load at a load point deflection of approximately 5 mm (0.2 inches). The girder exhibited significant additional capacity, reaching a peak load of 2,930 kN (636 kips) at a deflection of 29.7 mm (1.17 inches). As shown in the figure, the total dead load plus live load shear in the shear span at first shear cracking was 780 kN (175 kips). The total overall dead plus live load shear in the shear span at girder failure was 1,910 kN (430 kips).

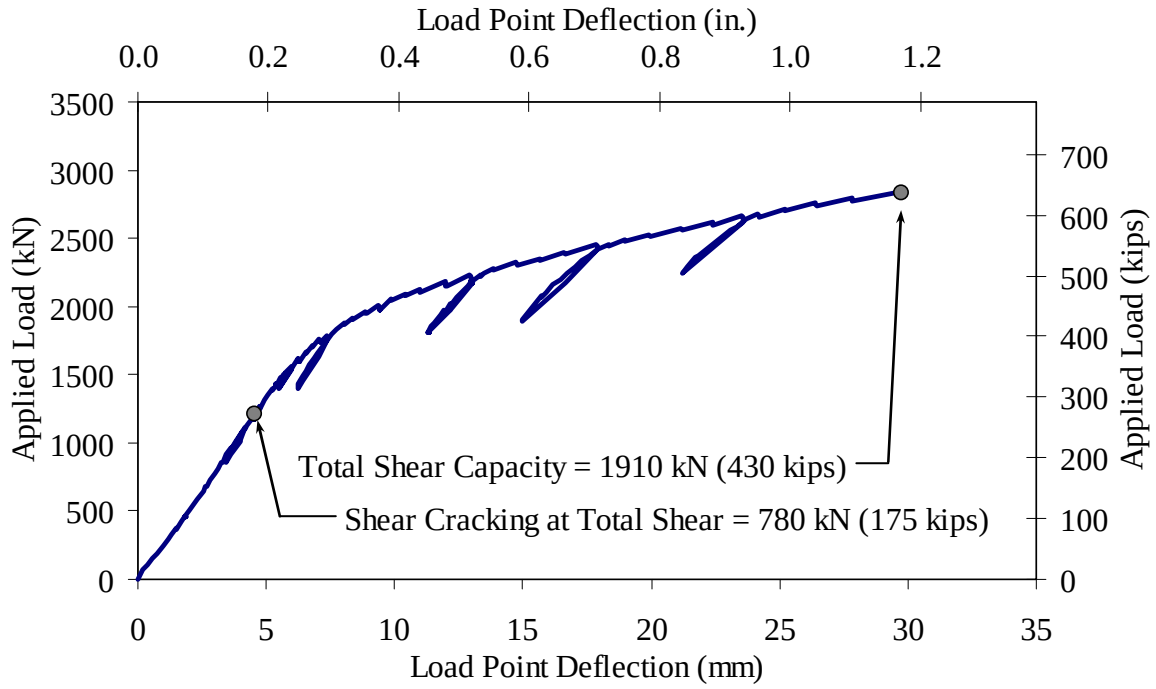

Figure 96. Graph. Load versus load point deflection response of Girder P2-21S.

Further results related to the deflection of the girder are presented in Figure 97. This plot shows the results from the five potentiometers which measured vertical deflection of the girder across the cross-section at the load point. Results from the set of potentiometers at nine discrete steps throughout the test are presented. Note the lag in deflection that becomes apparent at higher load levels in the middle of the deck.

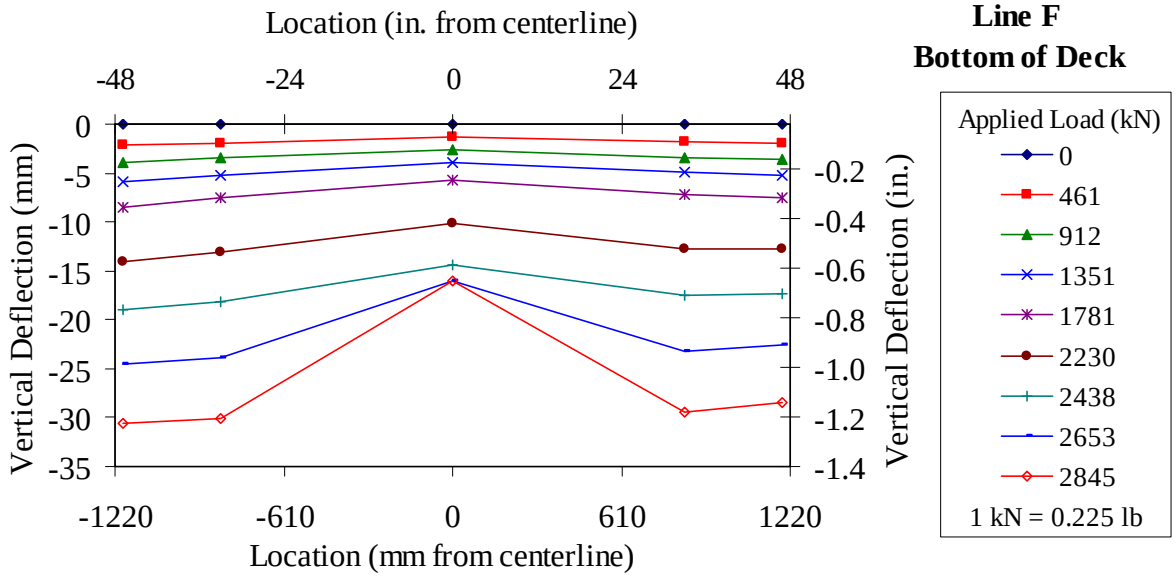

Figure 97. Graph. Load versus deflection response across P2-21S at the load point.

Figure 98 provides strain results captured from the strain gages which were oriented along the girder's length below the deck midway between the girder legs. Results from the set of strain gages at nine discrete steps throughout the test are presented. This figure shows that the behavior of the midline of the girder changed markedly after the applied load surpassed approximately 1500 kN (240 kips). The underside of the deck from the middle of the shear span to the load point begins trending toward and experiencing longitudinal tensile strains.

Recall that the eleven prestressing strands in the south bulb of the girder were instrumented near the east reaction point to measure strand slip. Figure 99 presents the results. None of the strands displayed any significant movement relative to the end of the girder.

The strain rosettes affixed to the north face of the south web and to the south face of the north web provided principal strain results in the shear span region. These rosettes were installed at instrumentation lines A, C, D, and E. The results from the rosette gages are presented in terms of principal tensile strain (Figure 100) and strain angle (Figure 101), and in terms of the principal compressive strain (Figure 102) and strain angle (Figure 103). In the figures, the south web gages are shown with solid lines and the north web gages are shown with dotted lines. The strain angle presented in the figures is measured from the horizontal with the gage location being viewed from the south looking north. Note that diagonal tensile cracking of the webs began at approximately 1,250 kN (280 kips) of applied load, thus rosette strain readings acquired after this load may be influenced by underlying cracking of the concrete.

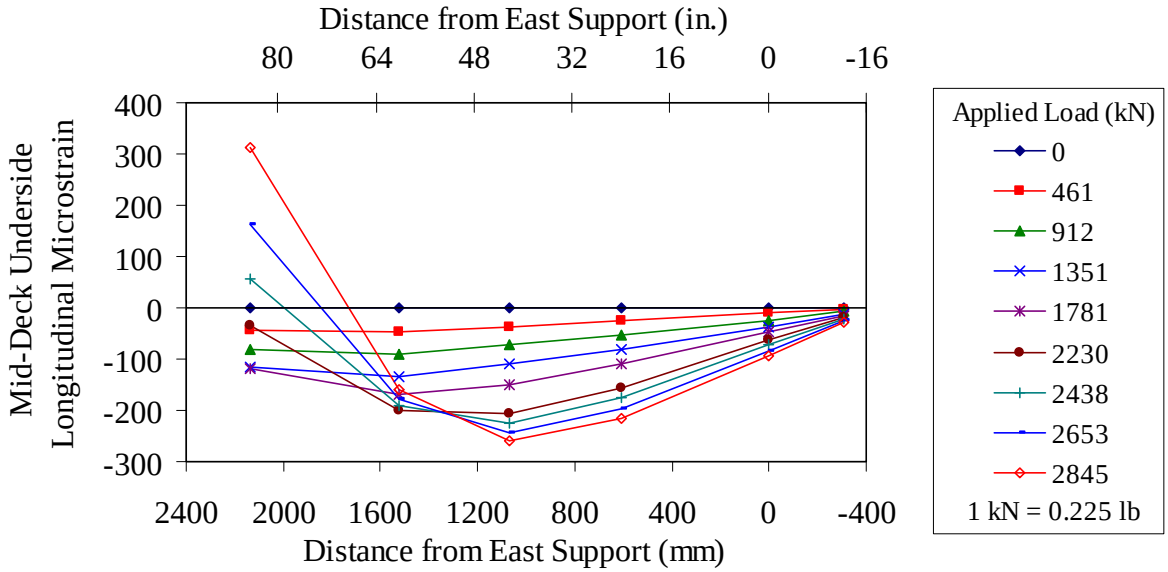

Figure 98. Graph. Longitudinal microstrain on underside of Girder P2-21S deck.

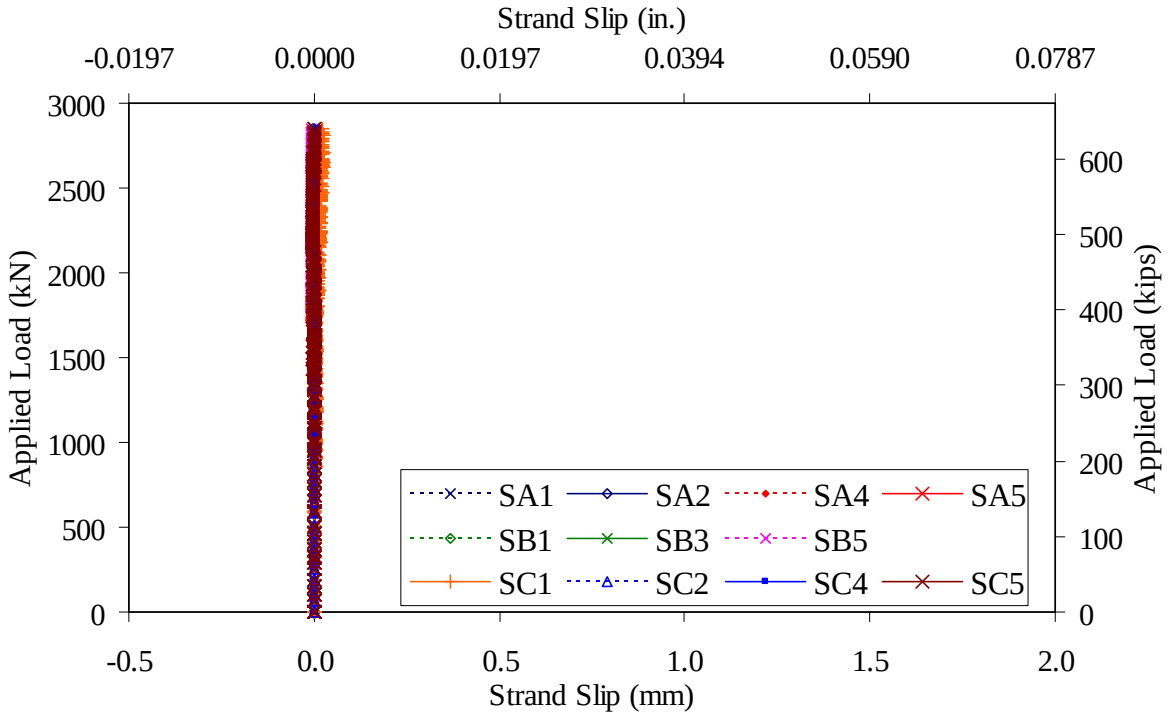

Figure 99. Graph. Strand slip in Girder P2-21S.

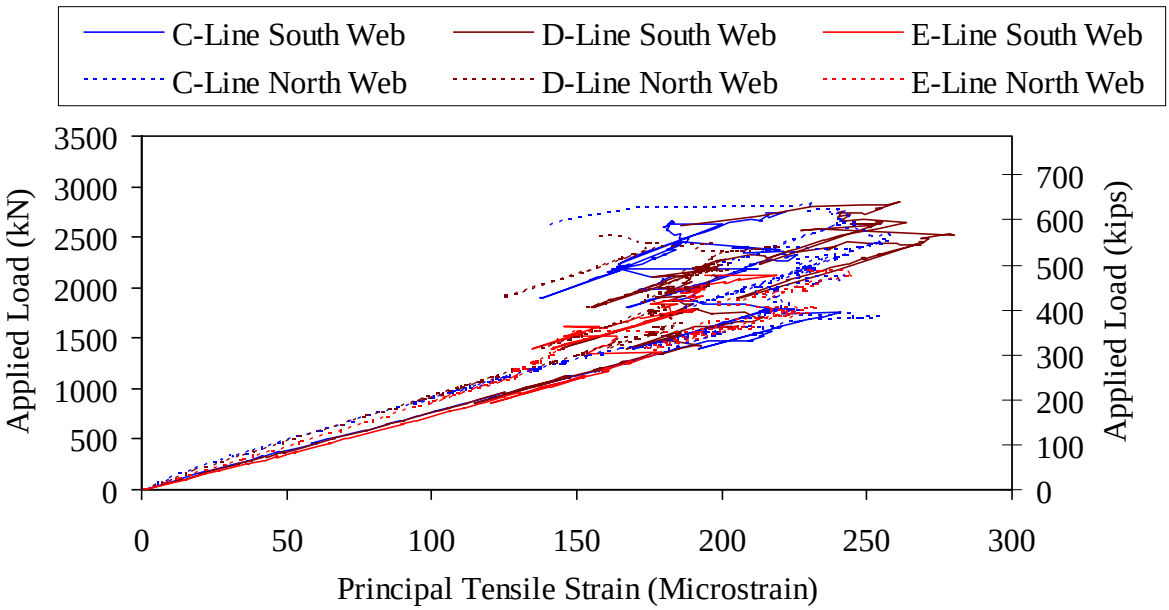

Figure 100. Graph. Principal tensile strain in the web of Girder P2-21S.

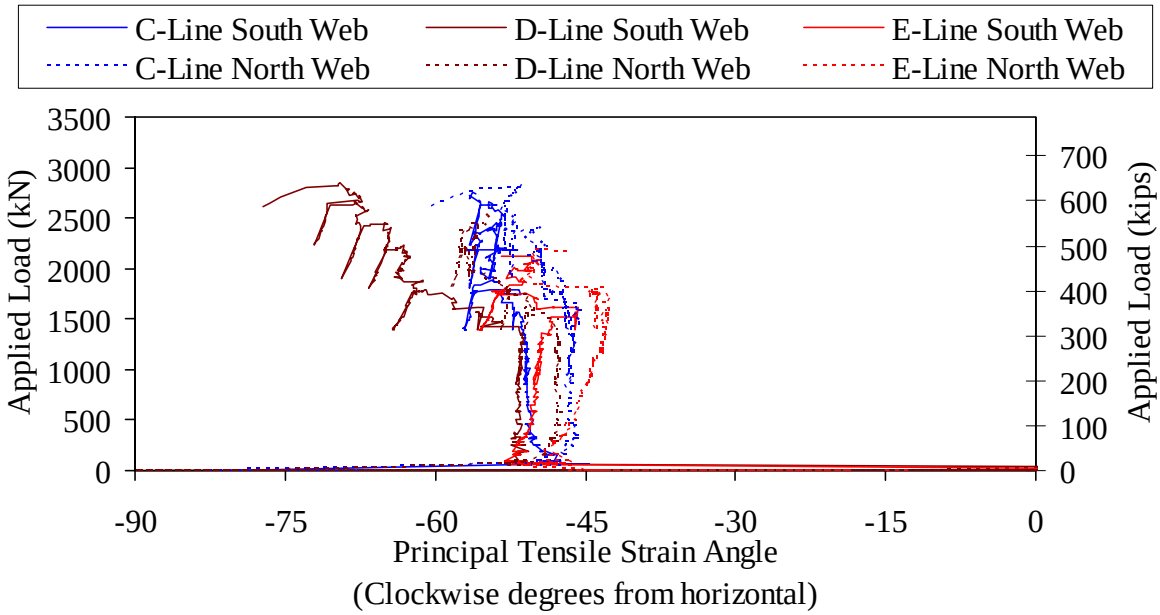

Figure 101. Graph. Principal tensile strain angle in the web of Girder P2-21S.

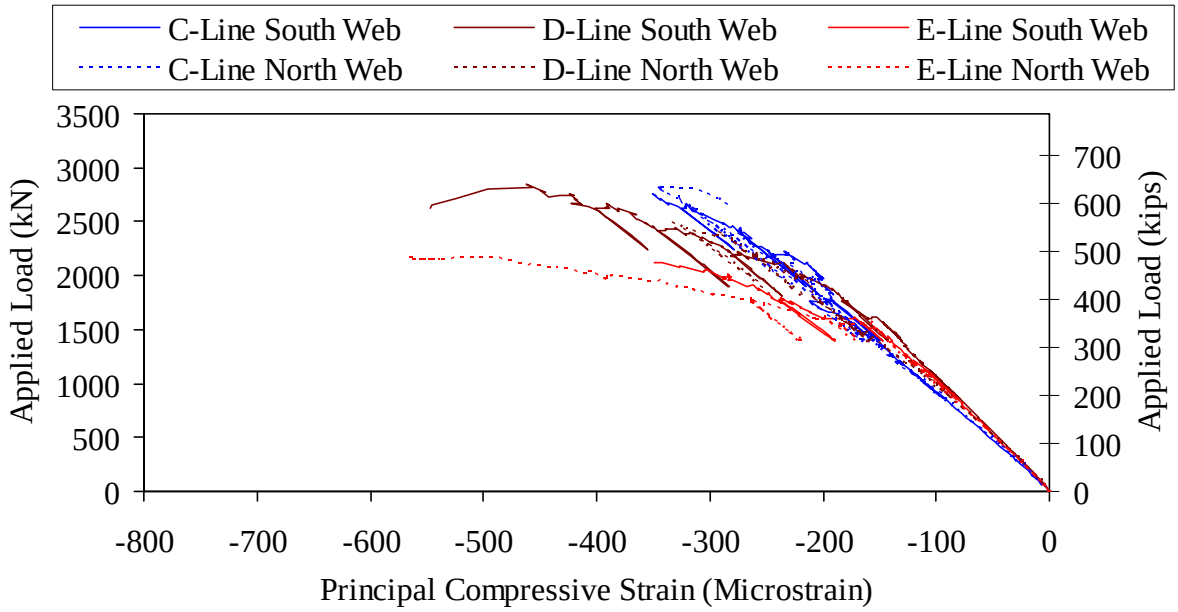

Figure 102. Graph. Principal compressive strain in the web of Girder P2-21S.

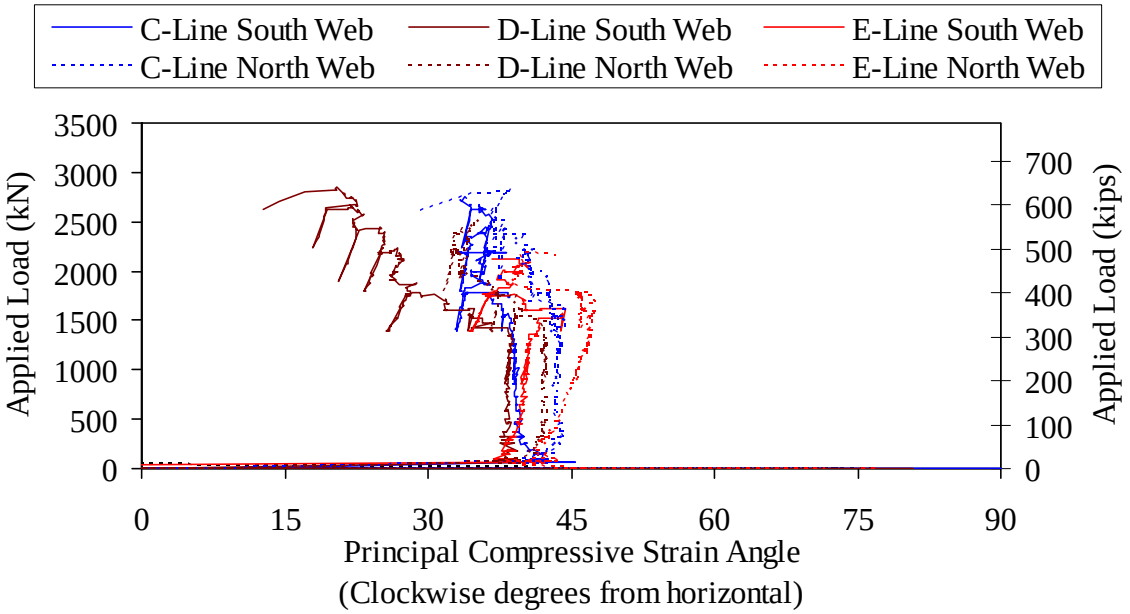

Figure 103. Graph. Principal compressive strain angle in the web of Girder P2-21S.

The diagonal tensile strains in the webs were captured through both strain rosettes affixed to the surface of the webs as well as by LVDTs which monitored deformations over predefined gage lengths. The results of greatest interest were captured along Instrumentation Line E; the shear failure plane intersected this instrumentation line precisely at the strain rosette. The results are plotted in Figure 104 and Figure 105 for the south and north webs, respectively. The principal tensile strain from the strain gage rosette is only plotted until the results become suspect due to cracking of the underlying concrete. The single LVDT on each web was installed at an orientation of 39 degrees counterclockwise from the horizontal based on the elastic principal tensile strain angle as calculated from the strain gage rosette. Note that prior to the application of load, the prestressing forces and dead load resulted in less than 50 microstrain precompression in the web along the angle of the principal tension. The plots show that at peak applied load the tensile strain in the north web (which failed) was approximately 11,000 microstrain, and the tensile strain in the south web (which remained intact) was greater than 8,000 microstrain.

Cracking of the concrete was observed audibly and visually beginning at an applied load of 1,180 kN (265 kips), with the first crack occurring in the north web within the shear span. Additional cracking was observed on loading steps through the remainder of the test. Both shear cracking in the webs as well as primary flexure cracking in the bulbs was observed. Cracks were mapped in the webs periodically in order to capture the progression of damage accumulation. The photos in Figure 106 show the progression of cracking in the north web of the shear span between the loads of 2,000 kN (450 kips) and 2,220 kN (500 kips). Note that the cracks were marked on the surface of the girder with wax crayon as they are not visible to the naked eye.

The girder continued to display additional shear and flexure cracks as the applied load approached 2,840 kN (638 kips). At this load, the south web of the girder failed in shear as shown in Figure 107. During the shear failure of the south web, a less dynamic shear failure of the north also occurred. The north web shear failure can be seen in Figure 108. The failure

surfaces in both the north and south webs ran parallel to the cracks existing prior to failure, but did not follow an individual crack over the entire length. The orientation of the cracks comprising the failure surfaces was approximately 35 degrees clockwise from the horizontal as viewed from the south.

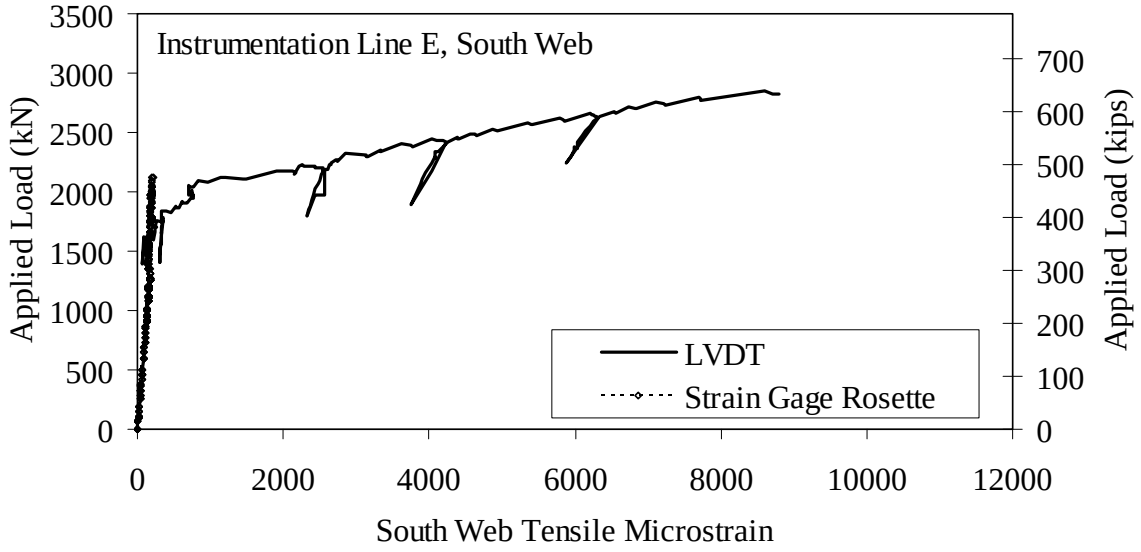

Figure 104. Graph. Web tensile strain at Line E in Girder P2-21S south leg.

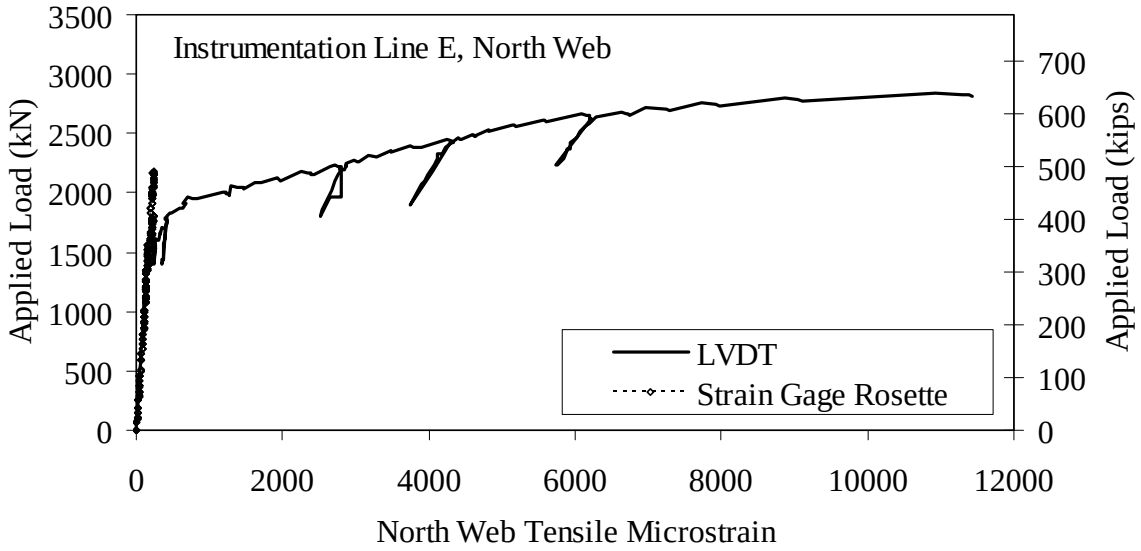

Figure 105. Graph. Web tensile strain at Line E in Girder P2-21S north leg.

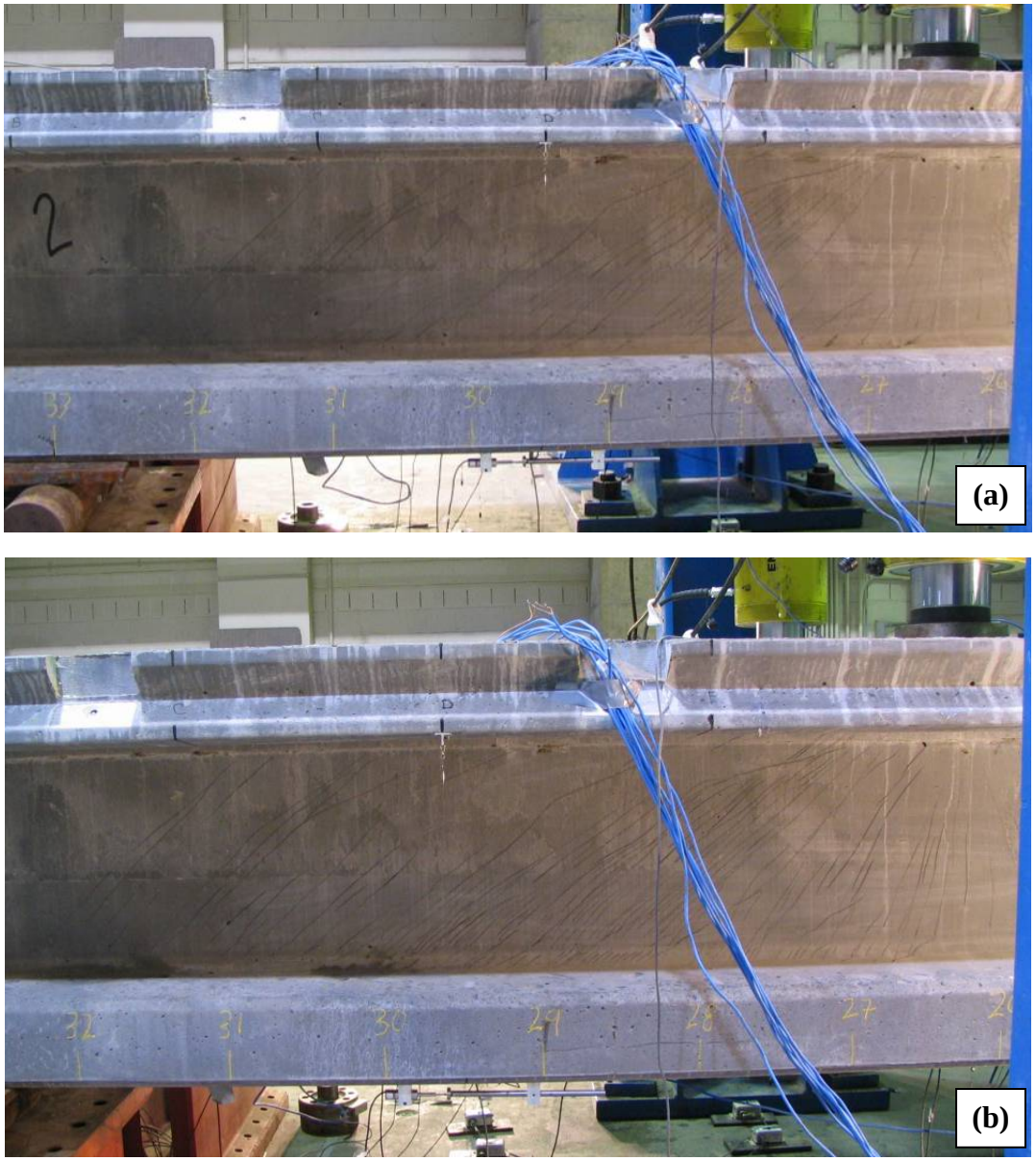

Figure 106. Photo. Web crack map for Girder P2-21S at (a) 2,000 kN and (b) 2,220 kN.

Figure 107. Photo. South face of Girder P2-21S after shear failure.

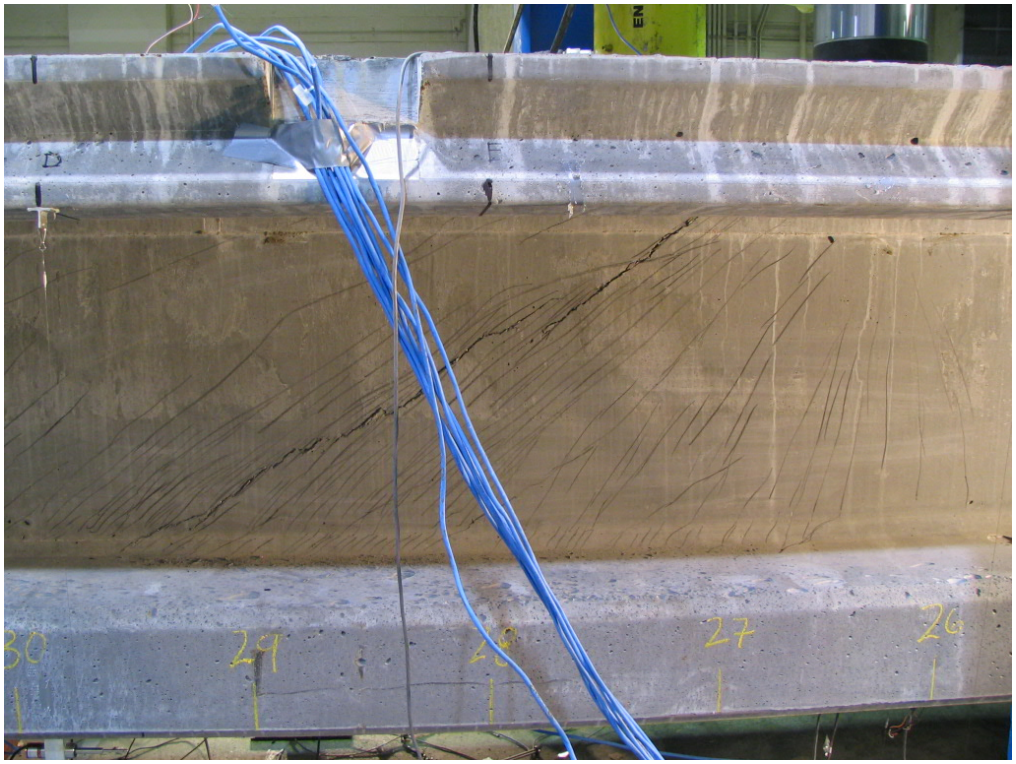

Figure 108. Photo. North face of Girder P2-21S after shear failure.

P4-57Sh

Shear response test P4-57Sh was the first structural test completed on Girder P4. This test focused on the shear response of the girder when subjected to a monotonically increasing, symmetrically applied pair of point loads. The end of Girder P4 which contained harped strands was the focus of this test. Recall that the inner three strands in each bulb were harped beginning 6.5 m (21.3 feet) from this end of the girder with the lowest strand exiting the cross-section 0.56 m (22 inches) up from the bottom of the girder. An additional two straight strands in each bulb were debonded for 1.8 m (6 feet) from the end of the girder.

The loads were applied at two load points directly above the webs through 0.3 m (12 inch) square rocker plates which were grouted to the deck surface. The rounded upper surface on the steel plates had a radius of 0.91 m (36 inches) and the maximum plate thickness was 51 mm (2 inches). The applied load was measured through load cells placed between the hydraulic jacks and the reaction frame. The loads were reacted through 0.18-m (7-inch) diameter steel rollers. The girder span was 17.4 m (57 feet) and the shear span was 1.83 m (6 feet), resulting in a shear span-to-depth ratio of 2.18. The east support rollers were centered 0.15 m (6 inches) from the end of the girder.

Figure 109 shows the applied load versus vertical deflection response of the girder. The reported deflection is the average value recorded from the two potentiometers measuring the displacement of the bottom face of the girder legs. The load-deflection response shows that the girder began to soften near 980 kN (220 kips) of applied load at a load point deflection of approximately 10 mm (0.4 inches). The girder exhibited significant additional capacity, reaching a peak load of 1740 kN (390 kips) at a deflection of 34 mm (1.35 inches). As shown in the figure, the total dead load plus live load shear in the shear span at first shear cracking was 800 kN (180 kips). The total overall dead plus live load shear in the shear span at girder failure was 1,630 kN (366 kips).

Further results related to the deflection of the girder are presented in Figure 110. This plot shows the results from the five potentiometers which measured vertical deflection of the girder across the cross-section at the load point. Results from the set of potentiometers at nine discrete steps throughout the test are presented. These results show that the deflection across the girder was relatively uniform, with a slight tendency toward decreased stiffness on the north side of the girder at higher load levels.

Figure 111 provides strain results captured from the strain gages which were oriented along the girder's length below the deck midway between the girder legs. Results from the set of strain gages at nine discrete steps throughout the test are presented. This figure shows that the behavior of the midline of the girder changed markedly after the applied load surpassed approximately 1,000 kN (225 kips). The underside of the deck from the middle of the shear span to the load point begins trending toward and experiencing longitudinal tensile strains.

Recall that the eleven prestressing strands exiting the south bulb and web of the girder were instrumented near the west reaction point to measure strand slip. Figure 112 presents the results. None of the strands displayed any significant movement relative to the end of the girder.

The strain rosettes affixed to the north face of the south web and to the south face of the north web provided principal strain results in the shear span region. These rosettes were installed at instrumentation lines C, D, and E as shown in Figure 36. The results from the rosette gages are presented in terms of principal tensile strain (Figure 113) and strain angle (Figure 114), and in terms of the principal compressive strain (Figure 115) and strain angle (Figure 116). In the figures, the south web gages are shown with solid lines and the north web gages are shown with dotted lines. The strain angle presented in the figures is measured from the horizontal with the gage location being viewed from the south looking north. Note that diagonal tensile cracking of the webs began at approximately 800 kN (180 kips) of applied load, thus rosette strain readings acquired after this load may be influenced by underlying cracking of the concrete.

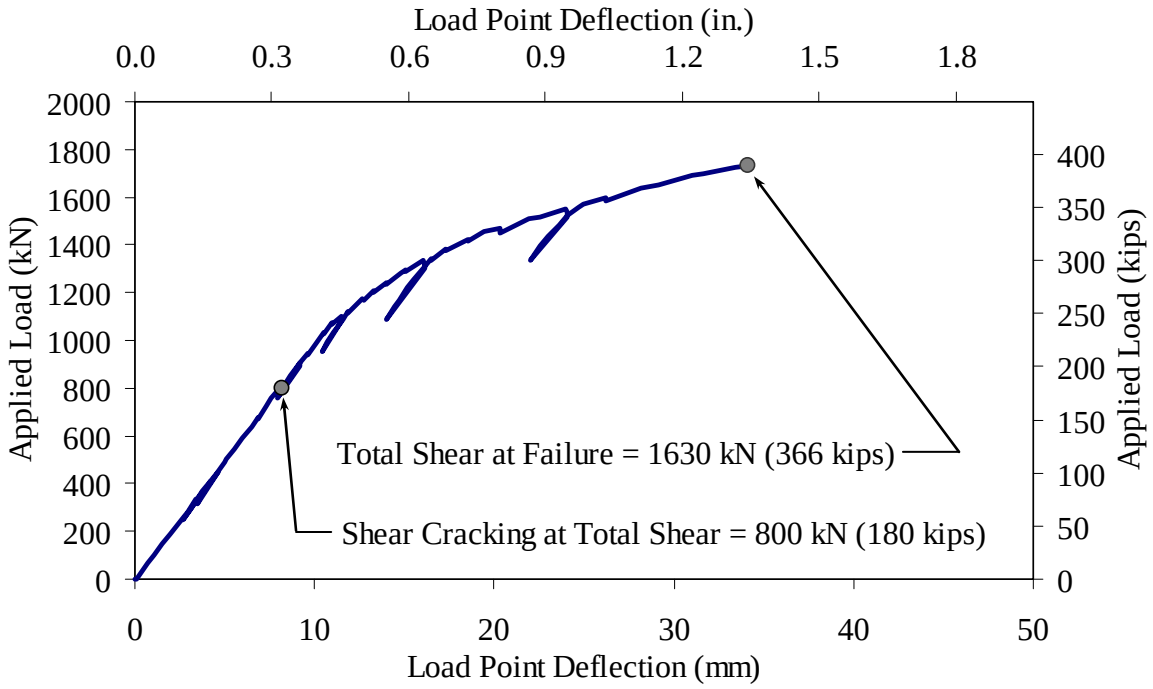

Figure 109. Graph. Load versus load point deflection response of Girder P4-57Sh.

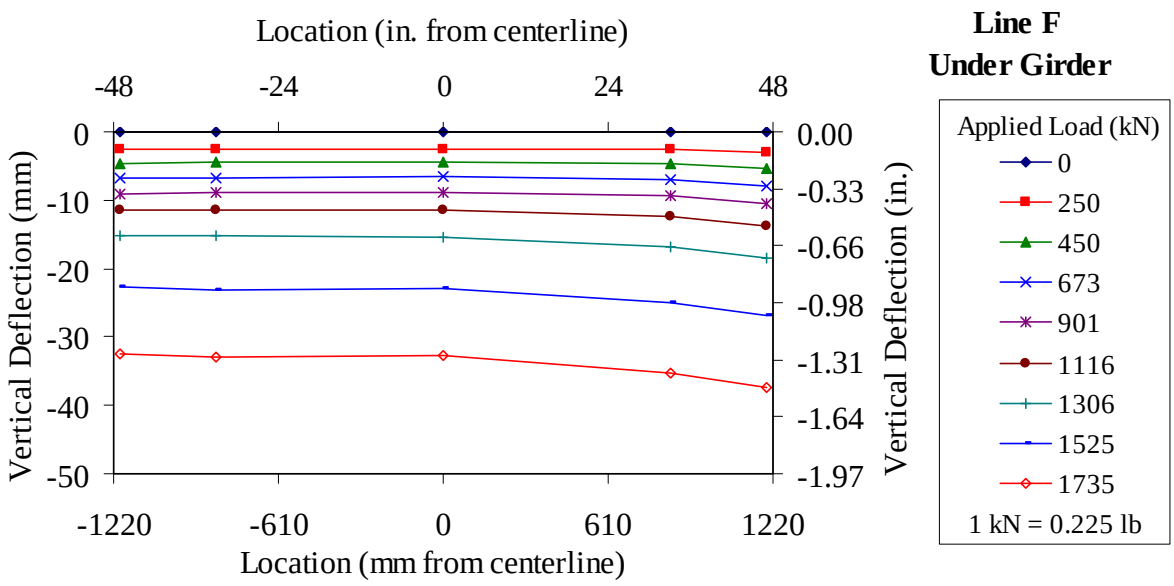

Figure 110. Graph. Load versus deflection response across P4-57Sh at the load point.

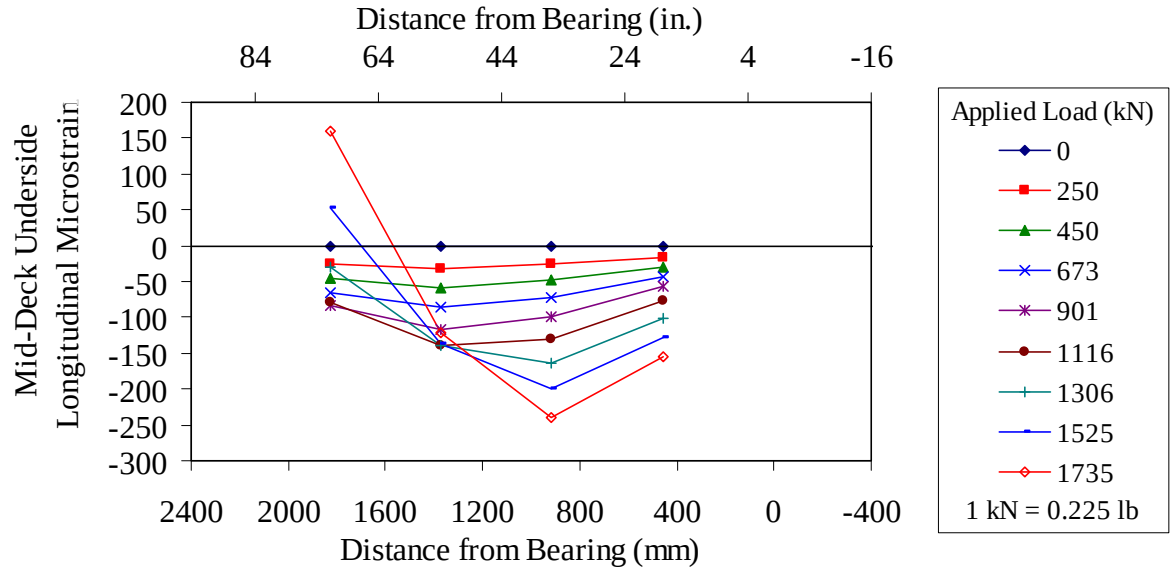

Figure 111. Graph. Longitudinal microstrain on underside of Girder P4-57Sh deck.

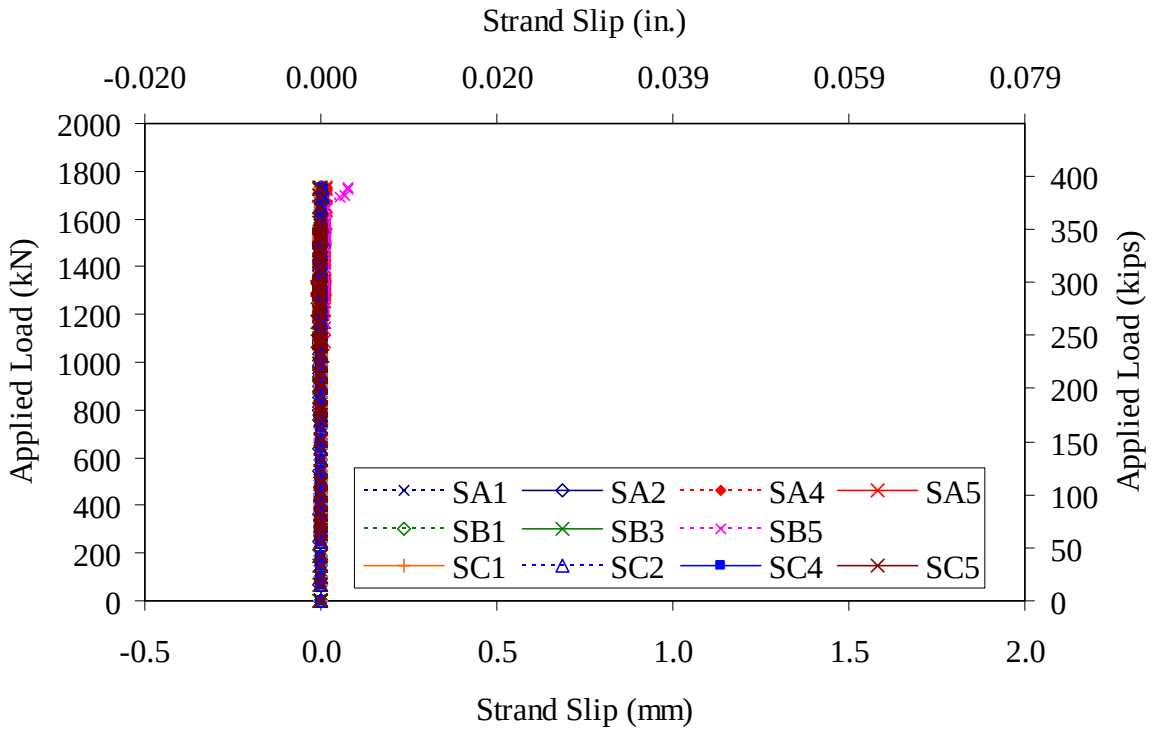

Figure 112. Graph. Strand slip in Girder P4-57Sh.

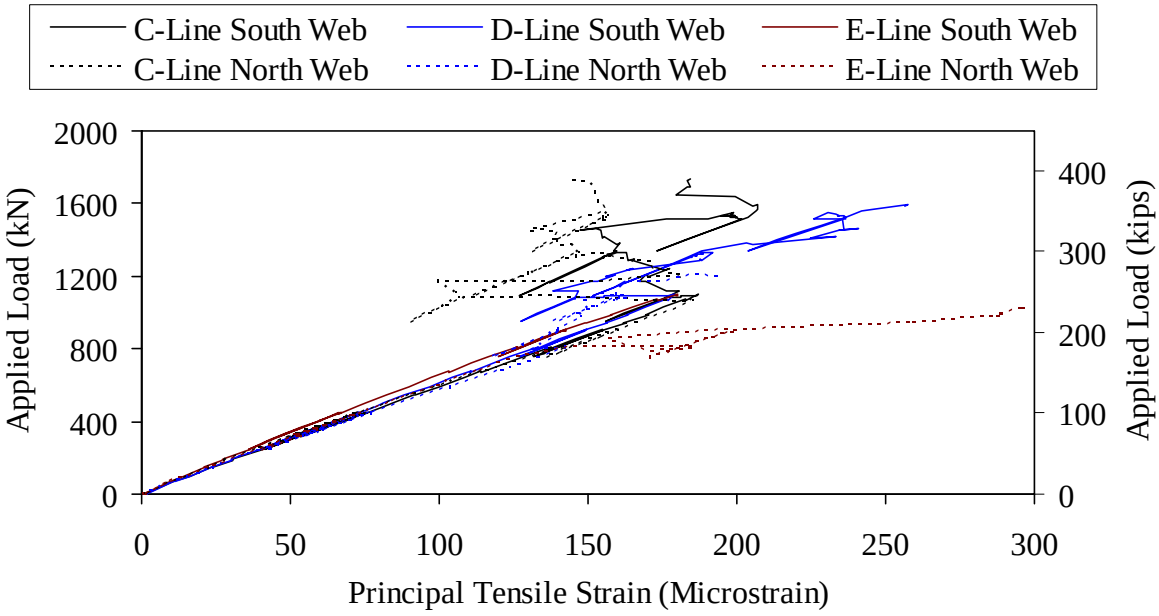

Figure 113. Graph. Principal tensile strain in the web of Girder P4-57Sh.

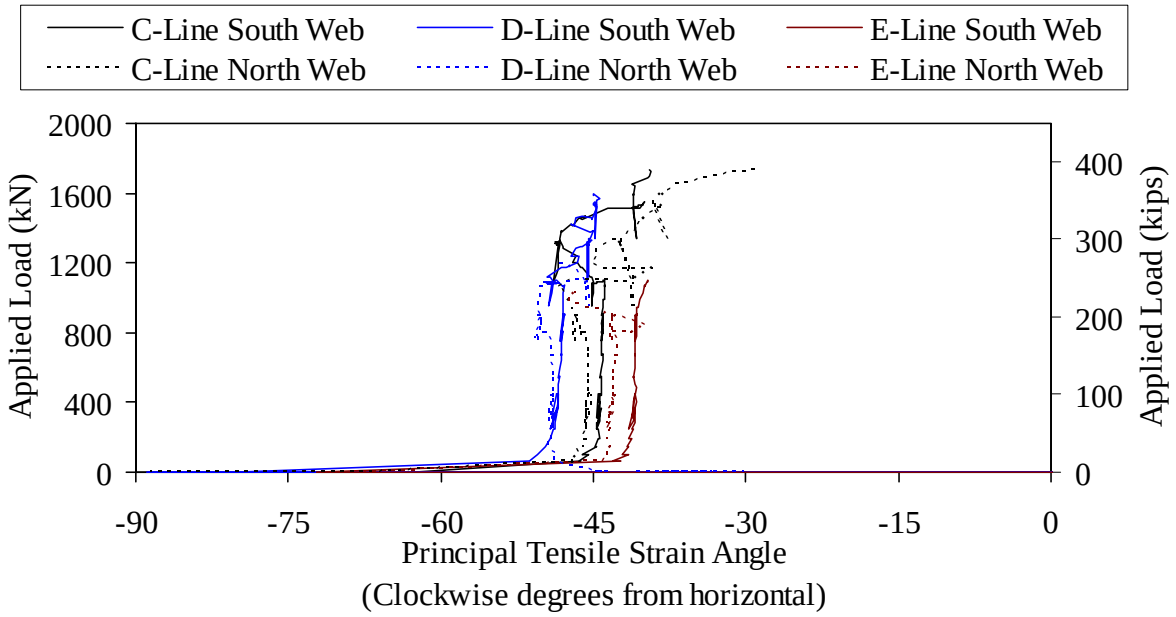

Figure 114. Graph. Principal tensile strain angle in the web of Girder P4-57Sh.

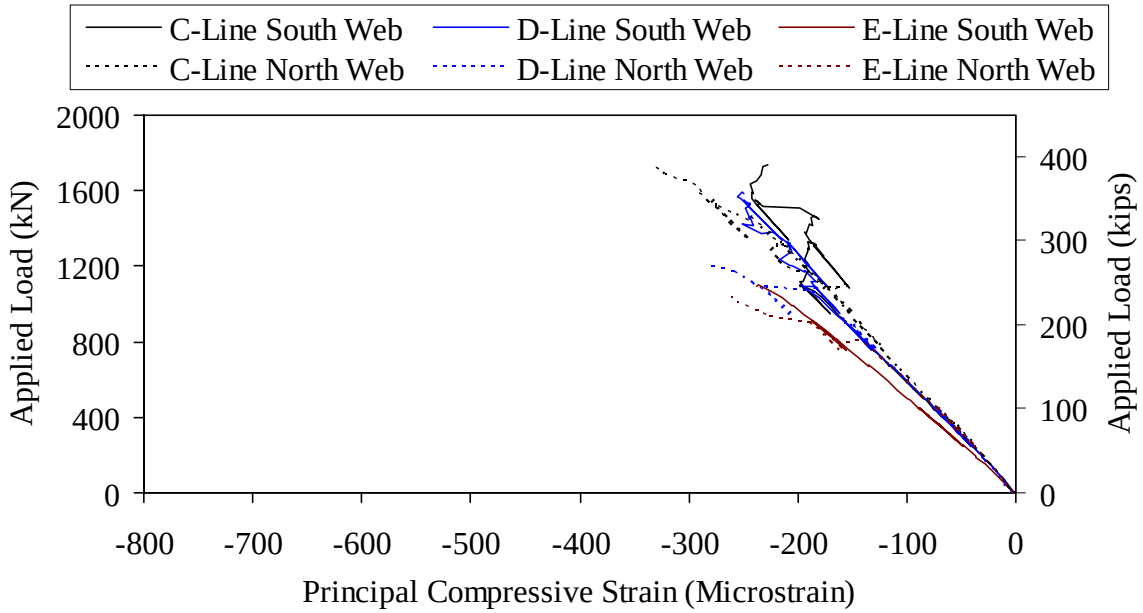

Figure 115. Graph. Principal compressive strain in the web of Girder P4-57Sh.

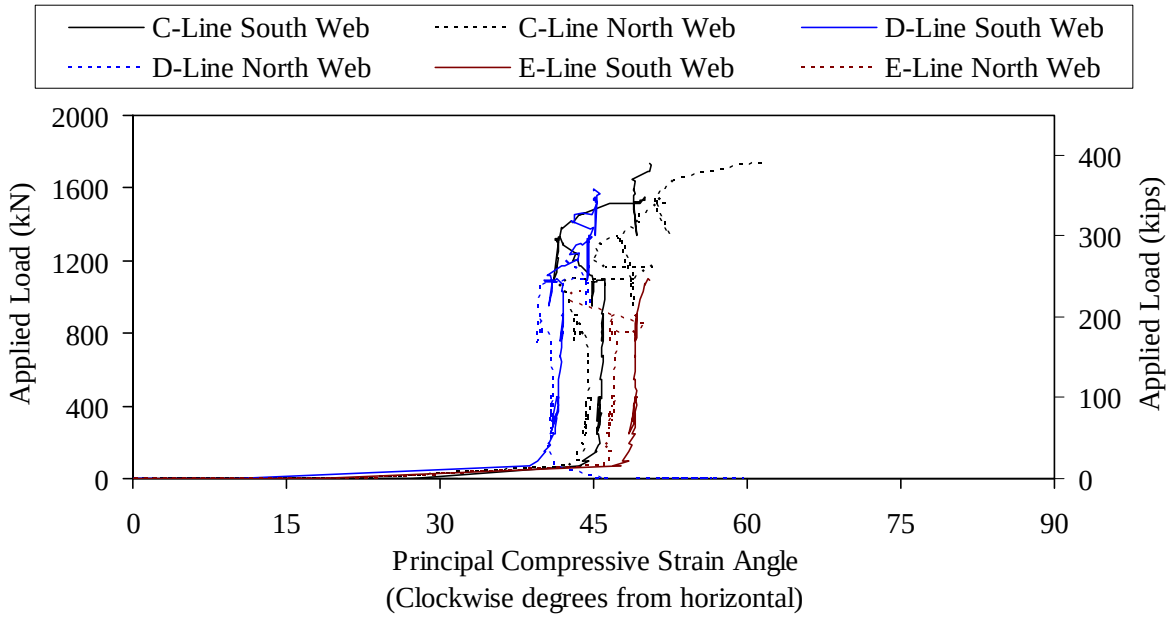

Figure 116. Graph. Principal compressive strain angle in the web of Girder P4-57Sh.

The diagonal tensile strains in the webs were captured through both strain rosettes affixed to the surface of the webs as well as by LVDTs which monitored deformations over predefined gage lengths. The results of greatest interest were captured along Instrumentation Line E; the shear failure plane passed within 50 mm (2 inches) of the strain rosette. The results are plotted in Figure 117 and Figure 118 for the south and north webs, respectively. The principal tensile strain from the strain gage rosette is only plotted until the results become suspect due to cracking of the underlying concrete. The single LVDT on each web was installed at an orientation of 45 degrees from the horizontal. Note that prior to the application of load, the prestressing forces and dead load resulted in less than 50 microstrain precompression in the web along the angle of the principal tension. The plots show that at peak applied load the tensile strain in the north web (which failed) was greater than 9,000 microstrain, and the tensile strain in the south web (which remained intact) was greater than 6,000 microstrain.

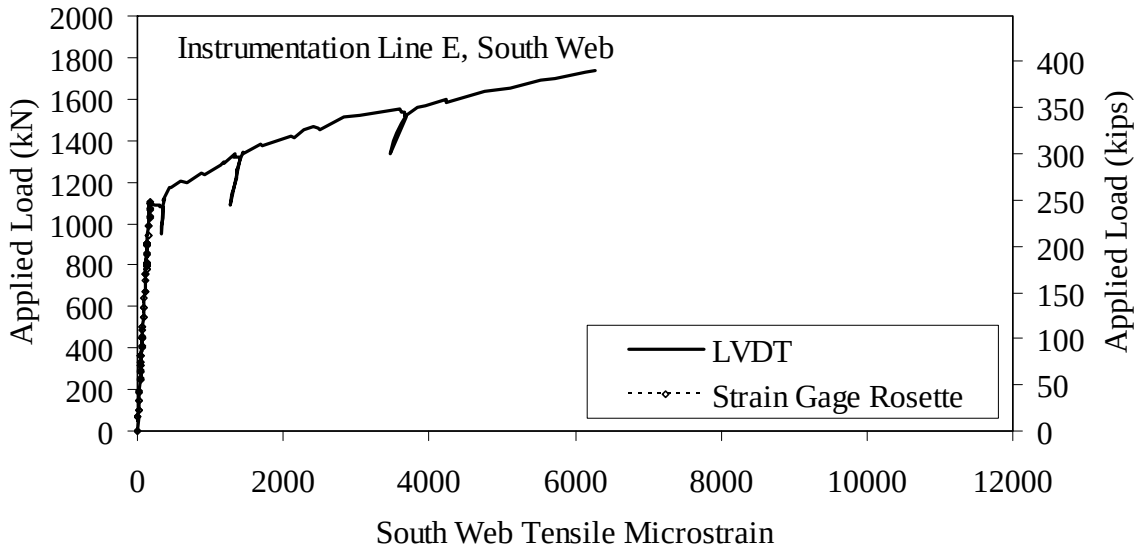

Figure 117. Graph. Web tensile strain at Line E in Girder P4-57Sh south leg.

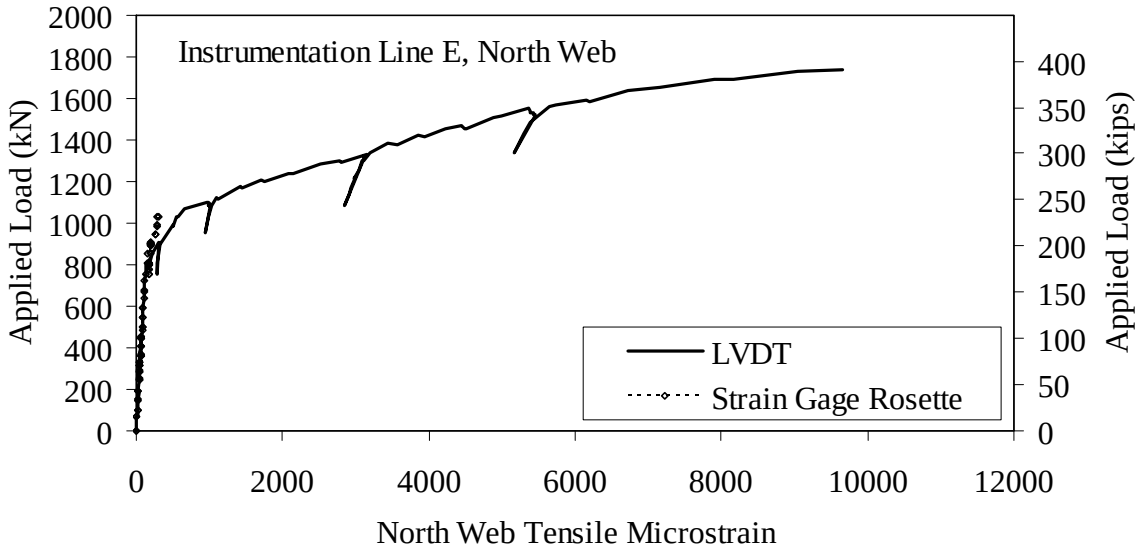

Figure 118. Graph. Web tensile strain at Line E in Girder P4-57Sh north leg.

Cracking of the concrete was observed audibly and visually beginning at an applied load of 800 kN (180 kips), with the first crack occurring in the north web within the shear span. Additional cracking was observed on loading steps through the remainder of the test. Both shear cracking in the webs as well as primary flexure cracking in the bulbs was observed. Cracks were mapped in the webs periodically in order to capture the progression of damage accumulation.

The girder continued to display additional shear and flexure cracks as the applied load approached 1,740 kN (390 kips). At this load, the north web of the girder failed in shear as shown in Figure 119 and Figure 120. The failure plane included a diagonal tensile failure progressing downward from the load point and a horizontal shear failure plane along the bottom of the web. The horizontal plane continued into the diaphragm, with tensile cracking indicating that the diaphragm had been pulled to the east by the north bulb. The south leg of the girder did not fail. The failure surfaces in the north webs ran parallel to the cracks existing prior to failure, but did not follow an individual crack over the entire length. The orientation of the cracks comprising the main diagonal shear failure surfaces was approximately 33 degrees counterclockwise from the horizontal as viewed from the north.

The crack patterns observed at the conclusion of the test on the north and south faces of both girder legs were also captured. Figure 121 and Figure 122 present the results from the north leg, while Figure 123 and Figure 124 present results from the south leg. Areas that were either not visible or were not quantitatively assessed are shown shaded in gray. Large cracks which constitute the failure plane are shown in blue, while tight cracks which were difficult or impossible to see without visual aids are shown in red. All crack maps are shown from the north looking south vantage point. The crack patterns on the north and south webs are generally similar to one another.

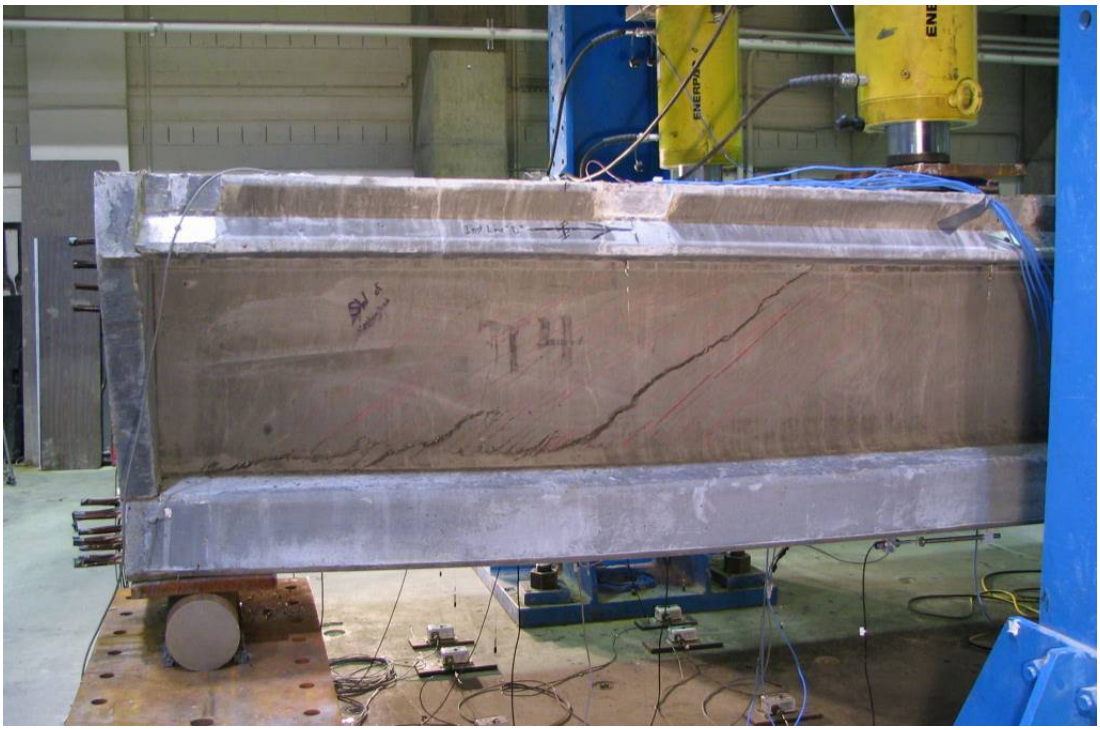

Figure 119. Photo. North face of P2-57Sh after failure.

Figure 120. Photo. Northeast end of P4-57Sh after failure.

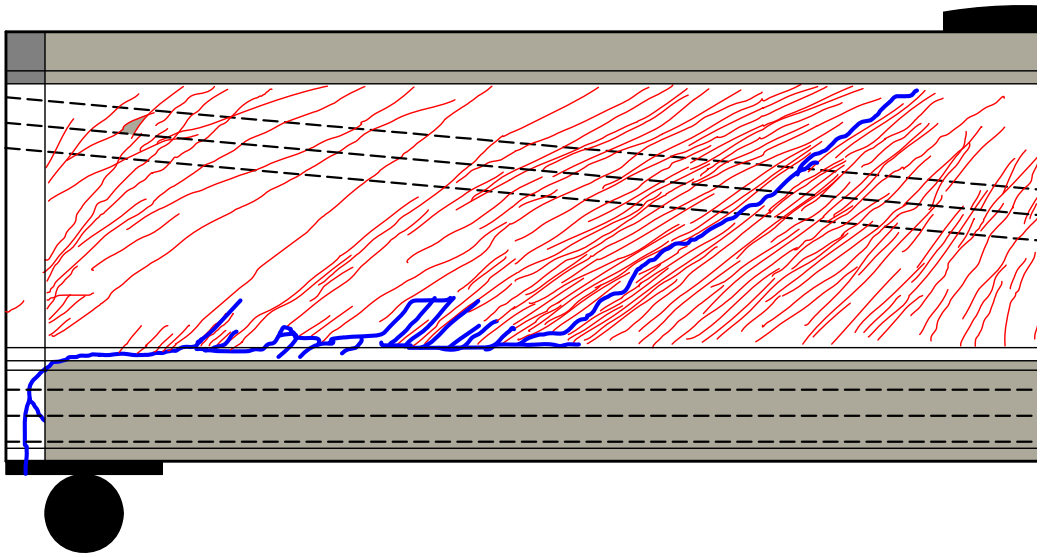

Figure 121. Illustration. Crack map from north face of P4-57Sh north leg after failure.

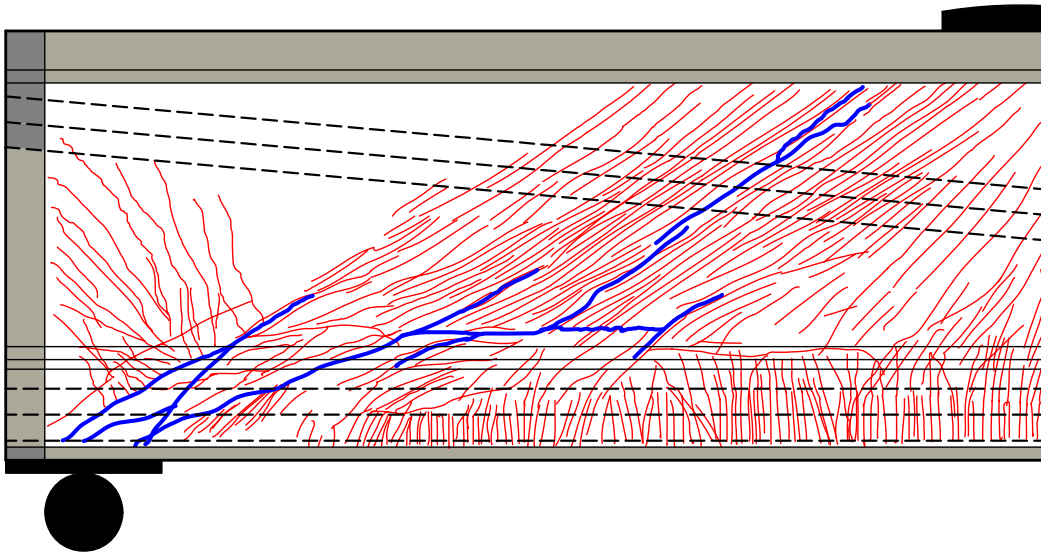

Figure 122. Illustration. Crack map from south face of P4-57Sh north leg after failure.

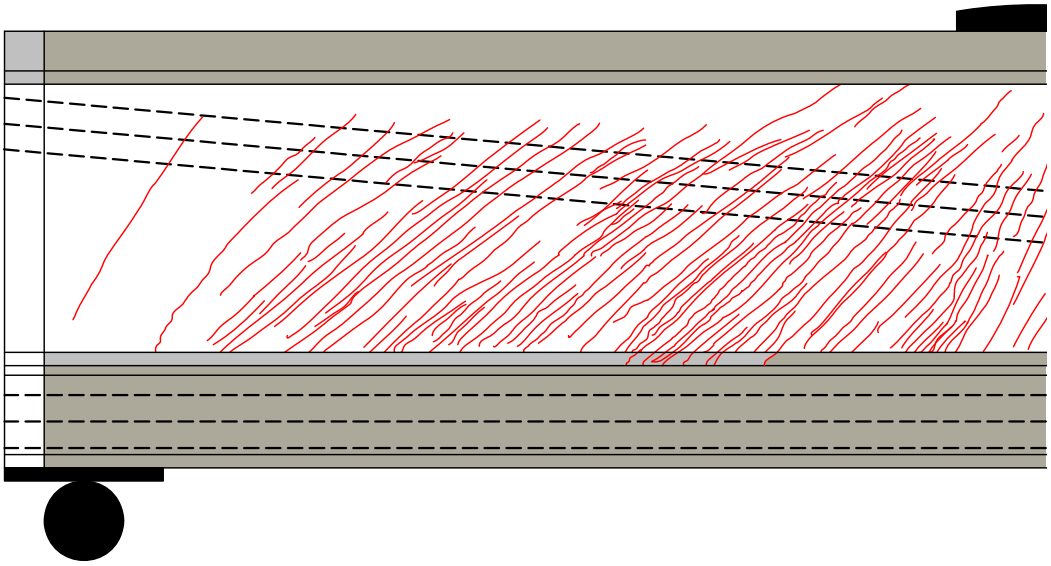

Figure 123. Illustration. Crack map from south face of P4-57Sh south leg after failure.

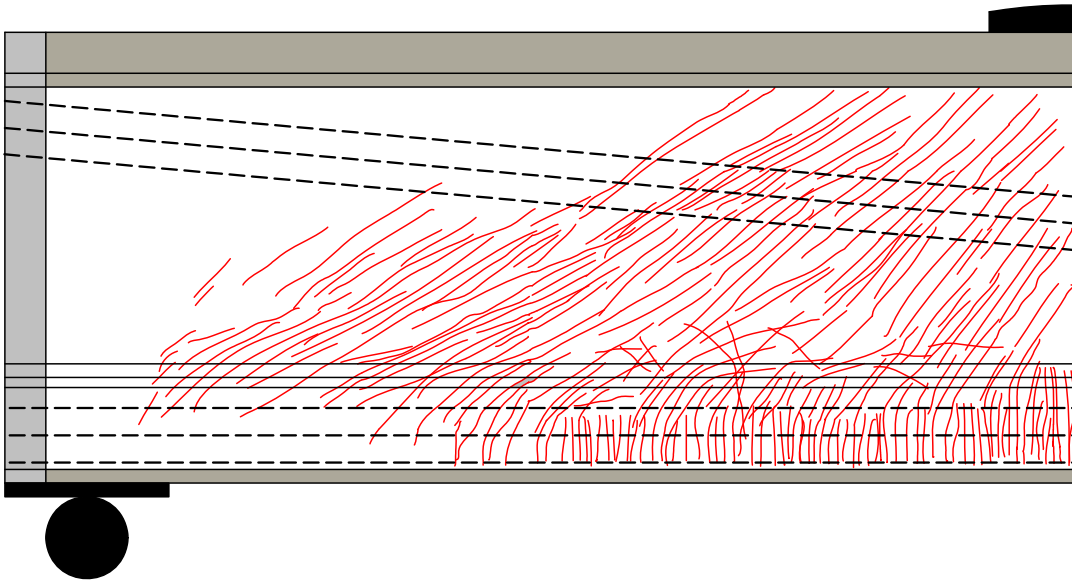

Figure 124. Illustration. Crack map from north face of P4-57Sh south leg after failure.

P4-57Ss

Shear response test P4-57Ss was the second structural test completed on Girder P4. As with the prior test, this test focused on the shear response of the girder when subjected to a monotonically increasing, symmetrically applied pair of point loads. The end of Girder P4 which contained no harped strands was the focus of this test. As with test P2-21S, two strands in each bulb were debonded for 1.8 m (6 feet) and three strands were debonded for 0.3 m (1 foot) from the end of the girder.

The load as support setup was identical to that previously described for test P4-57Sh. The girder span was 17.4 m (57 feet) and the shear span was 1.83 m (6 feet), resulting in a shear span-to-depth ratio of 2.18. The west support rollers were centered 0.15 m (6 inches) from the end of the girder.

Figure 125 shows the applied load versus vertical deflection response of the girder. The reported deflection is the average value recorded from the two potentiometers measuring the displacement of the bottom face of the girder legs. The load-deflection response shows that the girder began to soften near 1,160 kN (260 kips) of applied load at a load point deflection of approximately 11 mm (0.45 inches). The girder exhibited significant additional capacity, reaching a peak load of 2,450 kN (550 kips) at a deflection of 70 mm (2.75 inches). As shown in the figure, the total dead load plus live load shear in the shear span at first shear cracking was 910 kN (205 kips). The total overall dead plus live load shear in the shear span at girder failure was 2,270 kN (510 kips).

Further results related to the deflection of the girder are presented in Figure 126. This plot shows the results from the five potentiometers which measured vertical deflection of the girder across the cross-section at the load point. Results from the set of potentiometers at nine discrete steps

throughout the test are presented. These results show that the deflection across the girder was relatively uniform, with a slight tendency toward decreased stiffness on the south side of the girder at higher load levels.

Recall that the eleven prestressing strands exiting the south bulb of the girder were instrumented near the east reaction point to measure strand slip. Figure 127 presents the results. No strand movement was observed until after 2,000 kN (450 kips) of load was applied to the girder. By the conclusion of the test, both 1.83 m (6 foot) debonded strands had moved 1 mm (0.04 inch) and two of the three 0.3 m (1 foot) debonded strands had moved 0.5 mm (0.08 inch). The fully bonded strands that were further out in the bulb tended to show more relative movement; however, the recorded movements were still exceptionally small.

The strain rosettes affixed to the north face of the south web and to the south face of the north web provided principal strain results in the shear span region. These rosettes were installed at instrumentation lines C, D, and E as shown in Figure 46. The results from the rosette gages are presented in terms of principal tensile strain (Figure 128) and strain angle (Figure 129), and in terms of the principal compressive strain (Figure 130) and strain angle (Figure 131). In the figures, the south web gages are shown with solid lines and the north web gages are shown with dotted lines. The strain angle presented in the figures is measured from the horizontal with the gage location being viewed from the south looking north. Note that diagonal tensile cracking of the webs began at approximately 930 kN (210 kips) of applied load, thus rosette strain readings acquired after this load may be influenced by underlying cracking of the concrete.

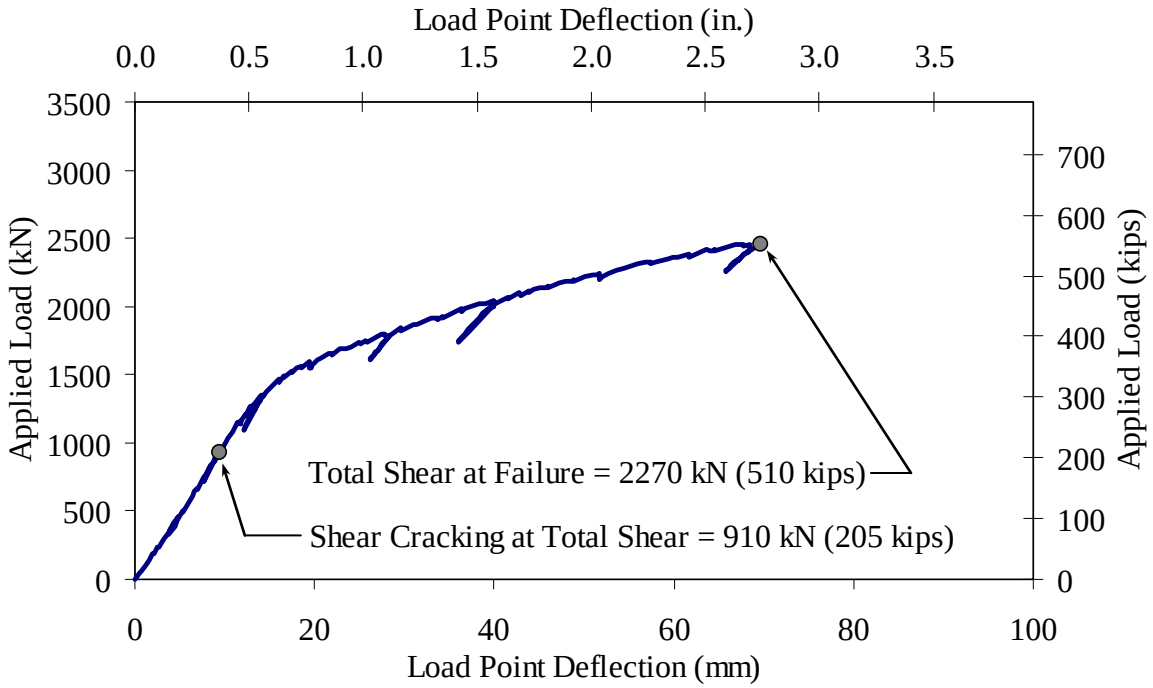

Figure 125. Graph. Load versus load point deflection response of Girder P4-57Ss.

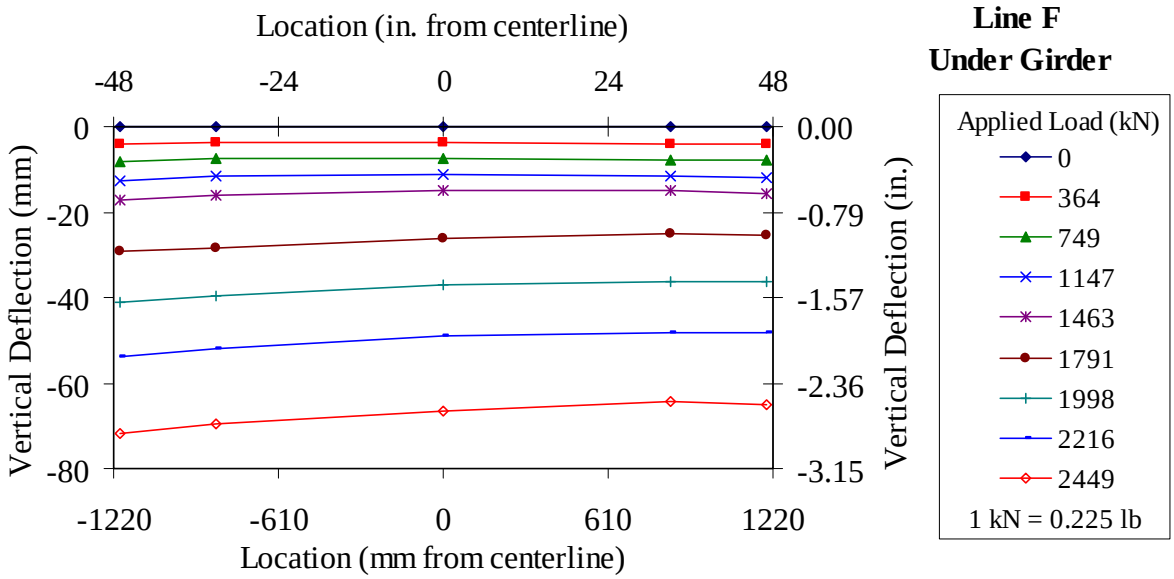

Figure 126. Graph. Load versus deflection response across P4-57Ss at the load point.

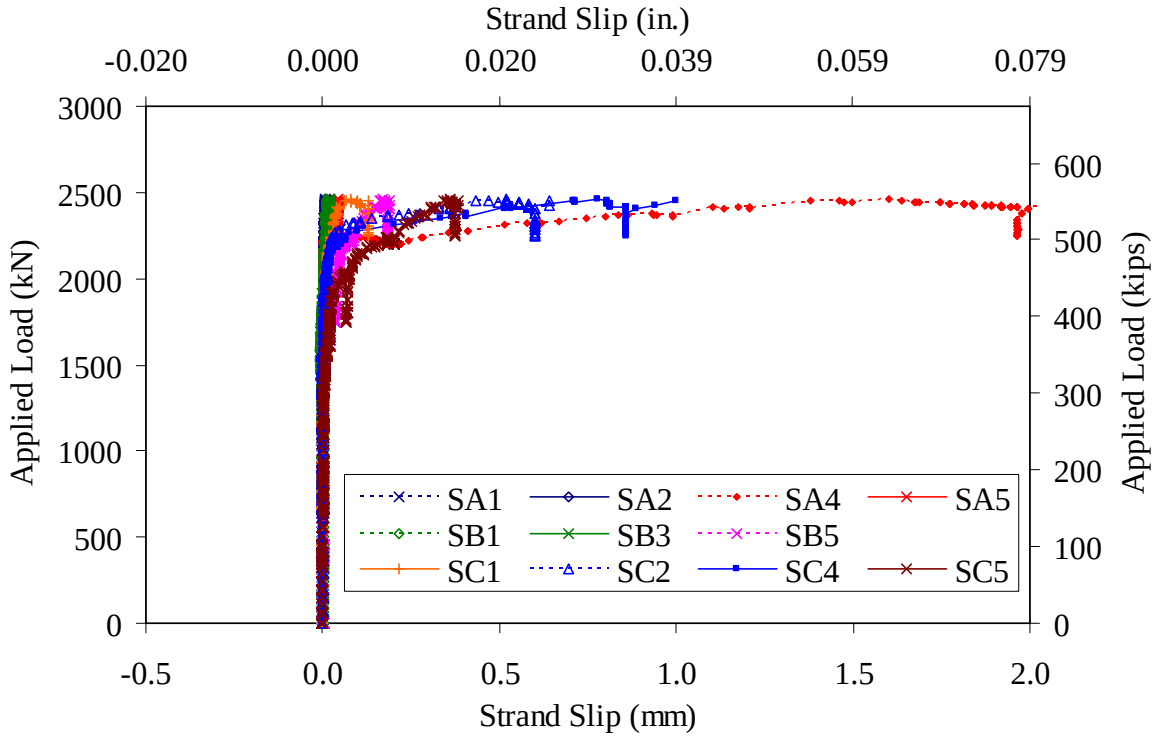

Figure 127. Graph. Strand slip in Girder P4-57Ss.

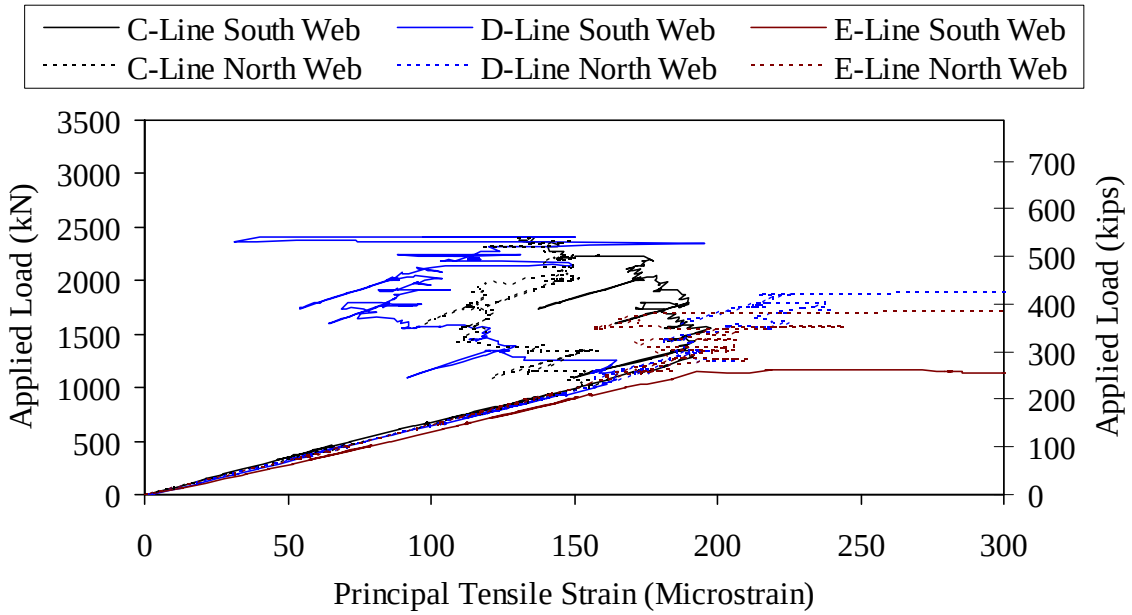

Figure 128. Graph. Principal tensile strain in the web of Girder P4-57Ss.

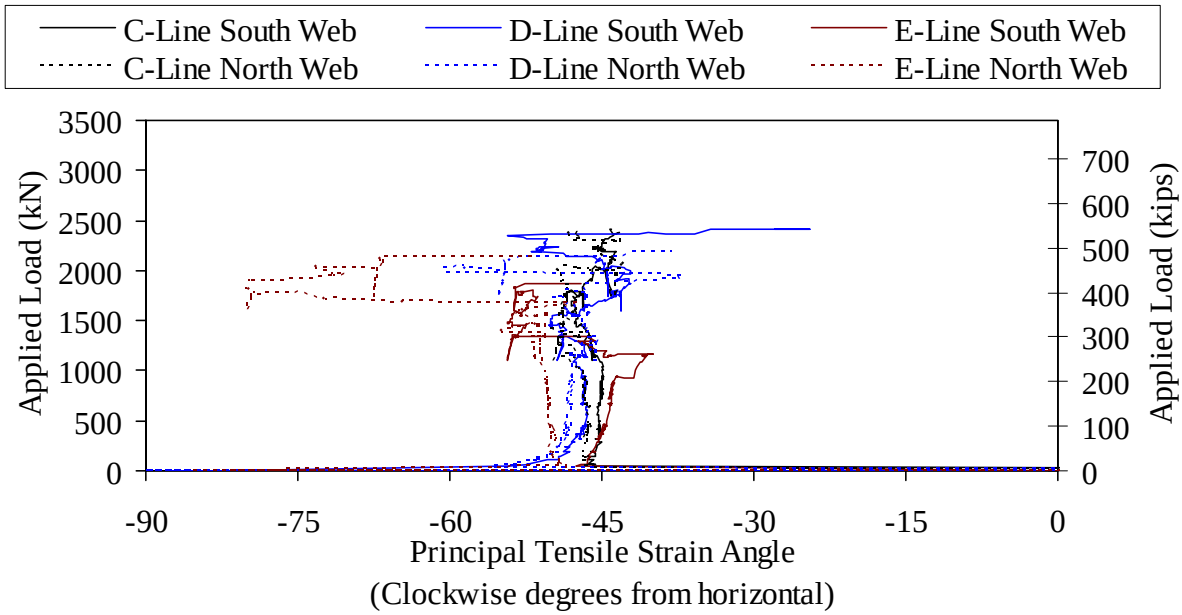

Figure 129. Graph. Principal tensile strain angle in the web of Girder P4-57Ss.

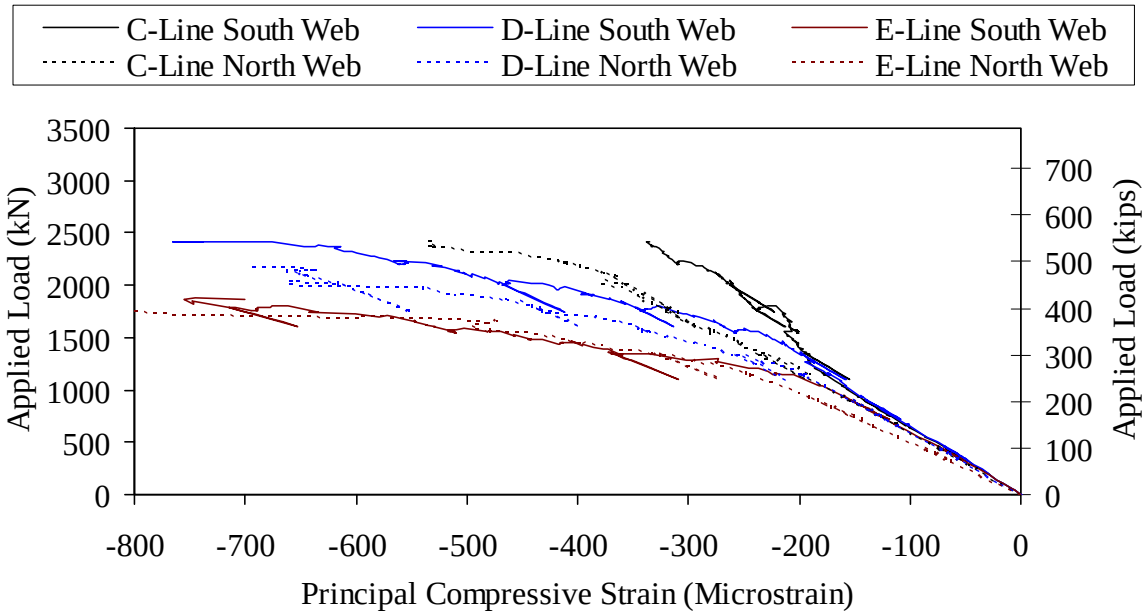

Figure 130. Graph. Principal compressive strain in the web of Girder P4-57Ss.

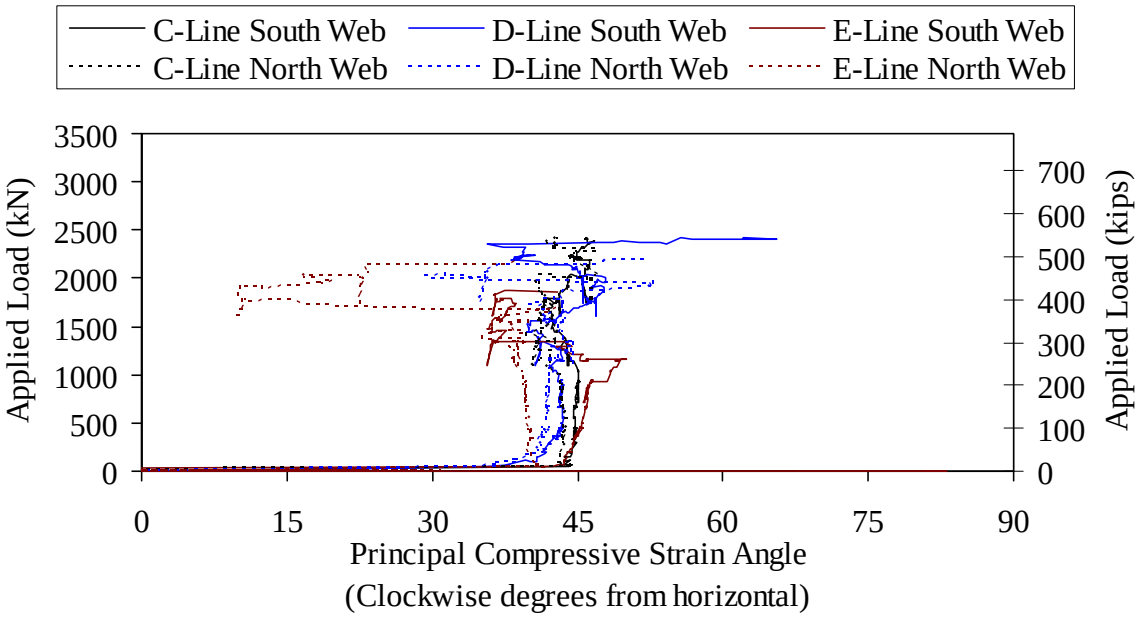

Figure 131. Graph. Principal compressive strain angle in the web of Girder P4-57Ss.

The diagonal tensile strains in the webs were captured through both strain rosettes affixed to the surface of the webs as well as by LVDTs which monitored deformations over predefined gage lengths. The results of greatest interest were captured along Instrumentation Line E as this is where the shear failures of P2-21S and P4-57Sh occurred. The results are plotted in Figure 132 and Figure 133 for the south and north webs, respectively. The principal tensile strain from the strain gage rosette is only plotted until the results become suspect due to cracking of the

underlying concrete. The single LVDT on each web was oriented at an angle of 45 degrees from the horizontal. Note that prior to the application of load, the prestressing forces and dead load resulted in less than 50 microstrain precompression in the web along the angle of the principal tension. The plots show that at peak applied load the tensile strain in the both the north and south webs was greater than 7,000 microstrain.

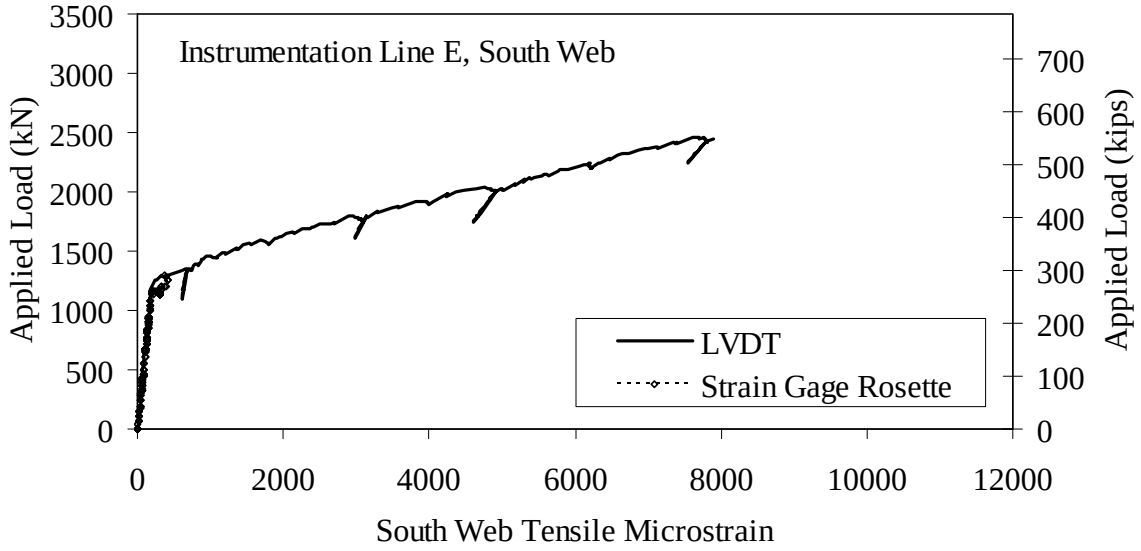

Figure 132. Graph. Web tensile strain at Line E in Girder P4-57Ss south leg.

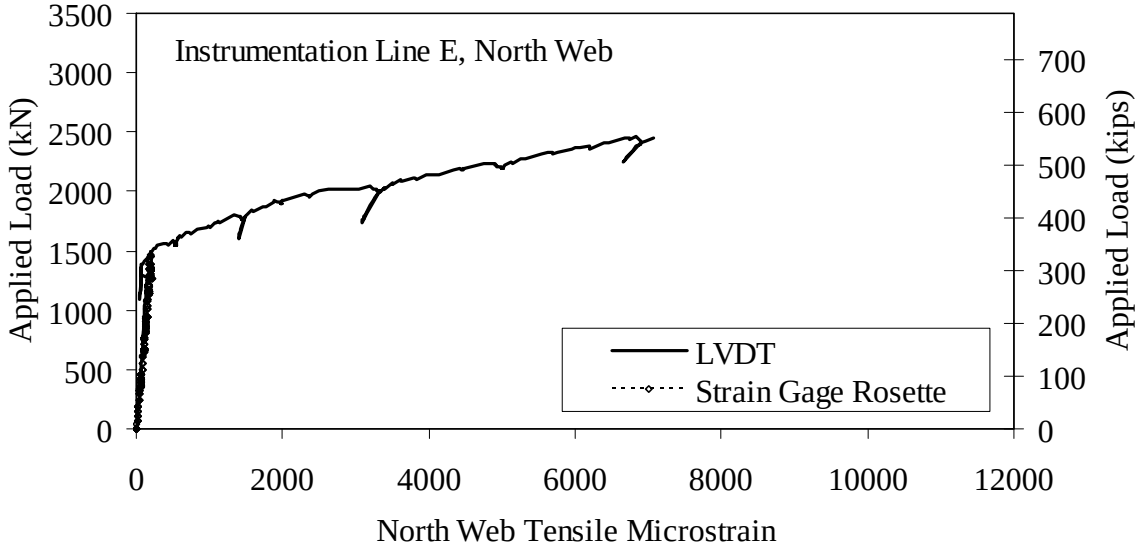

Figure 133. Graph. Web tensile strain at Line E in Girder P4-57Ss north leg.

Cracking of the concrete was observed audibly and visually beginning at an applied load of 930 kN (210 kips), with the first crack occurring in the south web within the shear span. Additional cracking was observed on loading steps through the remainder of the test. Both shear cracking in the webs as well as primary flexure cracking in the bulbs was observed. Cracks were mapped in the webs periodically in order to capture the progression of damage accumulation. The photo in Figure 134 shows the large number of tightly spaced shear cracks existing in the south web at an applied load of 2,000 kN (450 kips). The photo shows the entire height of the web over the region from the middle of the shear span to the load point. Denatured alcohol was sprayed on the surface in order to make the cracks temporarily visible. The distance between discrete cracks in this photo is approximately 2 to 3 mm (0.08 to 0.12 inches). The web shear cracks visible on the exterior faces of the webs were oriented at approximately 40 degrees counterclockwise from the horizontal as viewed from the south.

The girder continued to display additional shear and flexure cracks as the applied load approached 2,450 kN (550 kips). At this load, the south leg of the girder failed in flexure as shown in Figure 135. The total dead plus live load moment in the girder at failure was 4,150 kN-m (36,720 kip-inches).

The flexural failure of the girder at a location where uniaxial strain was being monitored provides another opportunity to investigate the strain in UHPC at tensile failure. The strains on the bottom faces of the bulbs at the line of load application were captured through LVDTs as well as individual strain gages. These results are plotted in Figure 136 and Figure 137 for the south and north legs, respectively. The strain gage results are individual gage readings and thus are influenced by cracking of the underlying concrete. The LVDT results are based on the recorded displacement readings divided by the gage length. Note that prior to the application of load, the prestressing forces and dead load resulted in an extreme tensile face compressive strain of approximately 280 microstrain. The plots show that at peak applied load, the strain on the tensile face of the south leg was greater than 9,000 microstrain.

Figure 134. Photo. Cracking on south face of P4-57Ss web at 2,000 kN applied load.

Figure 135. Photo. Flexural failure of P4-57Ss south leg.

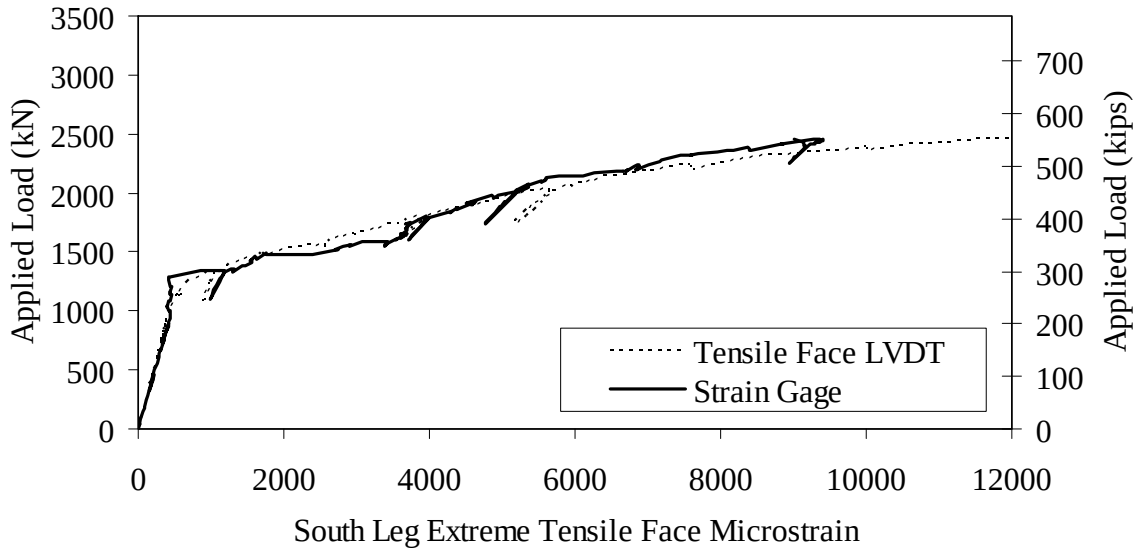

Figure 136. Graph. Load point south leg tensile face strain in Girder P4-57Ss.

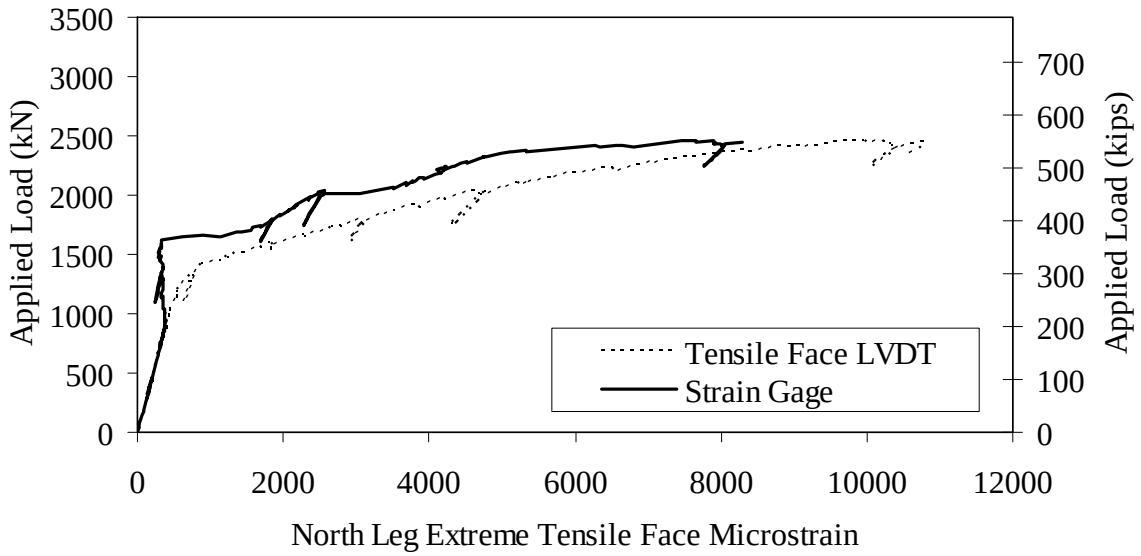

Figure 137. Graph. Load point north leg tensile face strain in Girder P4-57Ss.

STATIC TRANSVERSE FLEXURE TESTING

Two structural tests were completed with the aim of investigating the response of the girder cross-section to loads applied midway between the webs. Both of these tests were completed on sections of Girder P4 after the completion of tests P4-57Sh, P4-57Ss, and P4-45F. The two tests, P4-24T and P4-24D, differed only in that P4-24D contained supplemental restraining mechanisms that were intended to limit the outward movement of the bulbs during the test.

P4-24T

Test P4-24T was intended to investigate the transverse flexural response of the girder cross section. The test was completed using an approximately 8.5 m (28 foot) long portion of Girder P4. As shown in Figure 9, the girder section tested includes the length of Girder P4 running from the P4-57Ss load point to midspan of P4-45F. Both ends of the girder test section sustained significant damage during the earlier structural tests, while the middle of the test section was observed to possess some structural cracking in the deck and the legs.

The setup for the test included a 7.3 m (24 foot) span, two point loads applied in the middle of the deck with each being 0.61 m (2 feet) from midspan, and four reaction points centered under the bulbs. Recall that the loads were applied through a pair of stacked 25 mm (1 inch) thick elastomeric pads and were reacted through single 25 mm (1 inch) thick elastomeric pads. Loads were monitored through load cells mounted between the hydraulic jacks and the reaction frame.

Figure 138 shows the applied load versus vertical deflection response of the midspan cross section of the girder. Longitudinal cracking of the underside of the deck was first observed at a total applied load including all loading apparatus of 109 kN (24 kips). The peak load applied to the girder was 257 kN (58 kips). Observe the significant difference between the deflection responses of the girder legs and the mid-deck, with the deck experiencing multiple times more deformation. This behavior is also shown in Figure 139 where the results from the seven potentiometers measuring vertical deflection of the midspan cross section are presented at ten discrete load steps from throughout the test. Figure 140 presents similar information from the five potentiometers measuring vertical deflection at the quarter point of the test span.

Additional observations related to the global deformation of the girder are presented in Figure 141 and Figure 142. Figure 141 presents the results from the four potentiometers which were measuring the spreading between the legs. Note that the spreading responses at the inside of the bulbs at the quarter point, the forty point, and at midspan are very similar. Figure 142 combines the three bulb spreading results with the results from the LVDTs which measured lateral movement of the bulbs at the west reaction points. These results show that the reaction points provided little lateral restraint and the bulbs spread nearly as much at the supports as they did at midspan.

Results from the gages which monitored the transverse strain in the deck at midspan are presented in Figure 143 and Figure 144. Figure 143 shows the results from the seven gages affixed to the top of the deck. The transverse strains in the top of the deck between the girder webs increase up through cracking of the deck, with the mid-deck gages showing between two and three times the strain at the gages located one quarter of the distance between the webs. After cracking, the mid-deck strains continue increasing while strains recorded at the remaining six locations remain relatively static. Figure 144 shows the results from the five gages affixed to the underside of the deck. This figure shows that the transverse strains in the underside of the deck increased up through initial deck cracking, then began to decrease as loads continued to increase. Note that none of these gages were directly intercepted by discrete cracks which formed in the deck.

As the applied load was increased from the initial cracking load toward the eventual peak load, additional longitudinal cracking of the deck occurred. All of the longitudinal cracking observed in the deck tended to be wider and more widely spaced than the flexure and shear cracks which were observed in the previous girder tests. The longitudinal crack about which failure of the deck occurred was directly down the centerline of the girder. This crack continued to grow wider as the load was increased with a significant amount of the rotation of the two cross section halves occurring about this point. By the time the peak load had been applied, this crack had extended over the entire length of the girder. The deformation of the cross section at peak load can be seen in Figure 145. Figure 146 shows the failure crack at midspan after the conclusion of the test, while Figure 147 shows the crack where it intersected the east end of the test specimen. A crack assessment after the conclusion of the test indicated the failure crack and other cracks adjacent to it were generally parallel and approximately 50 to 75 mm (2 to 3 inches) distant.

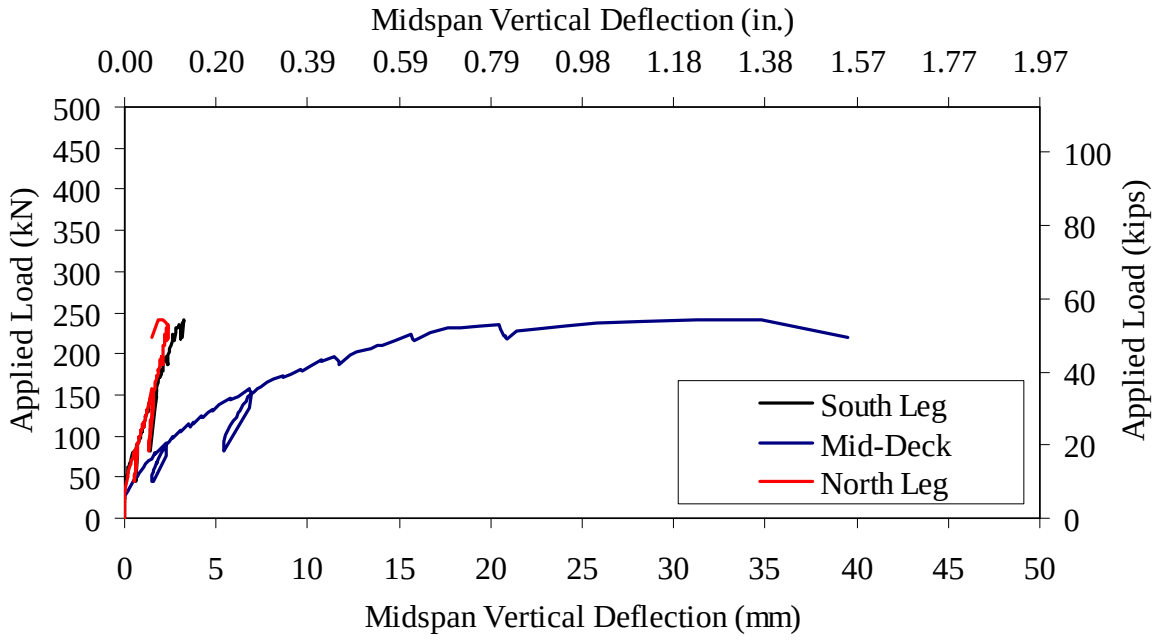

Figure 138. Graph. Load versus midspan deflection response of Girder P4-24T.

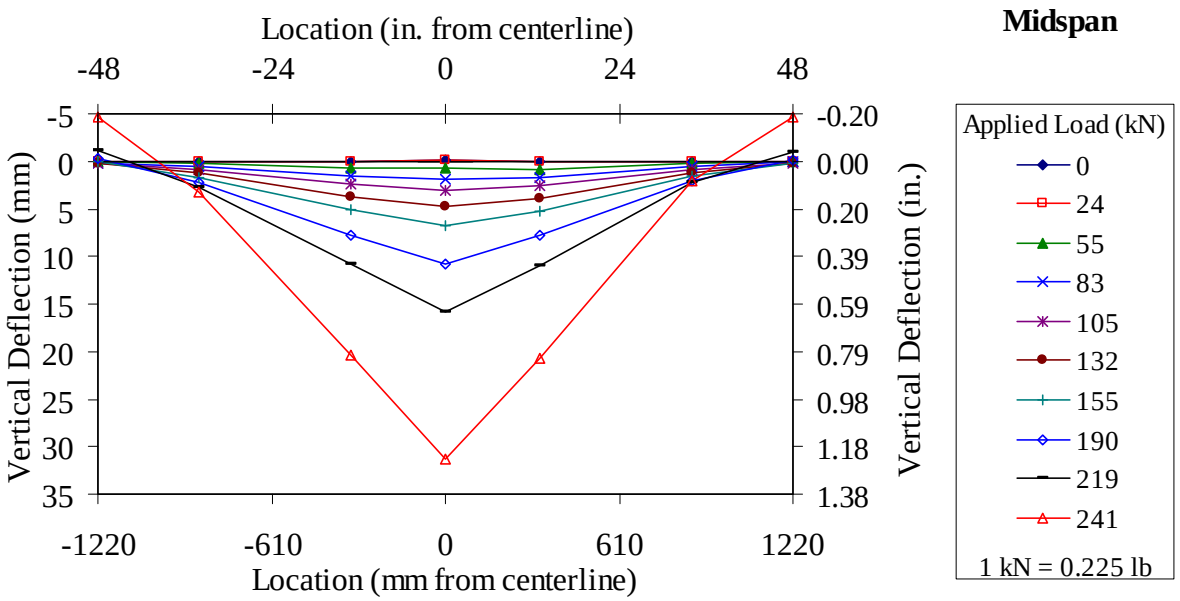

Figure 139. Graph. Load versus deflection response across Girder P4-24T at midspan.

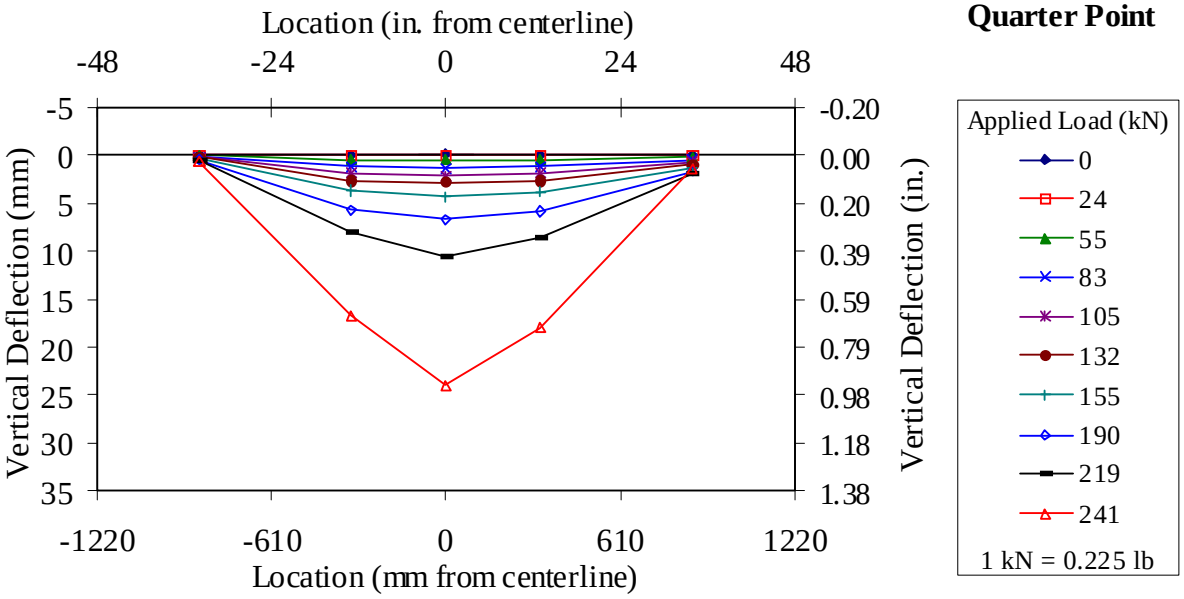

Figure 140. Graph. Load versus deflection response across Girder P4-24T at quarter span.

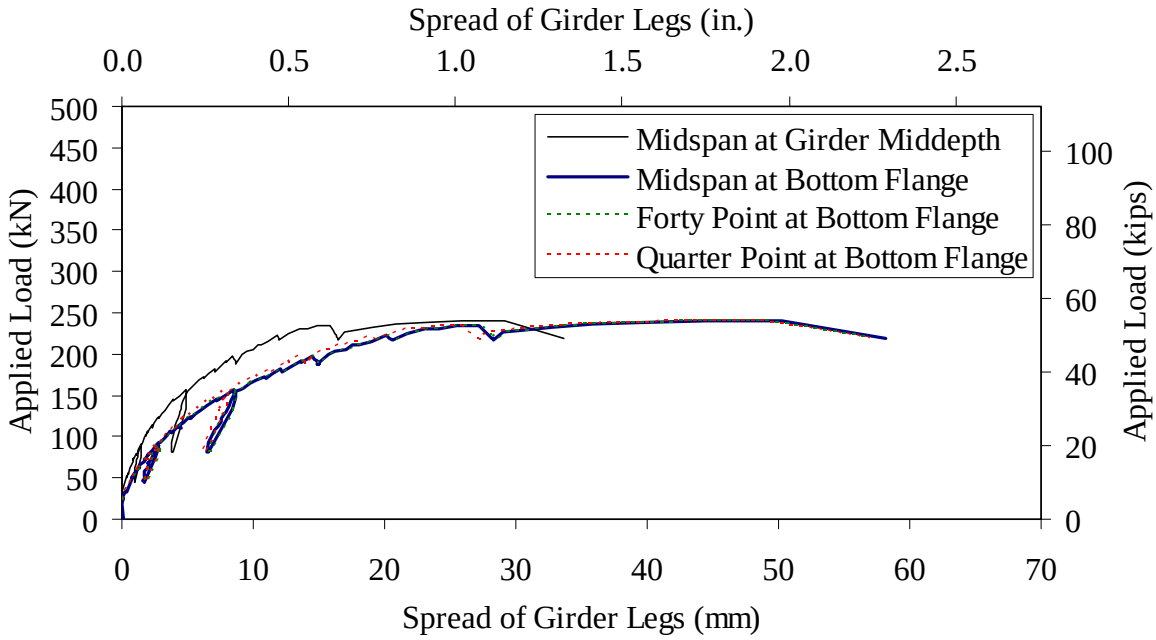

Figure 141. Graph. Spreading between legs of Girder P4-24T.

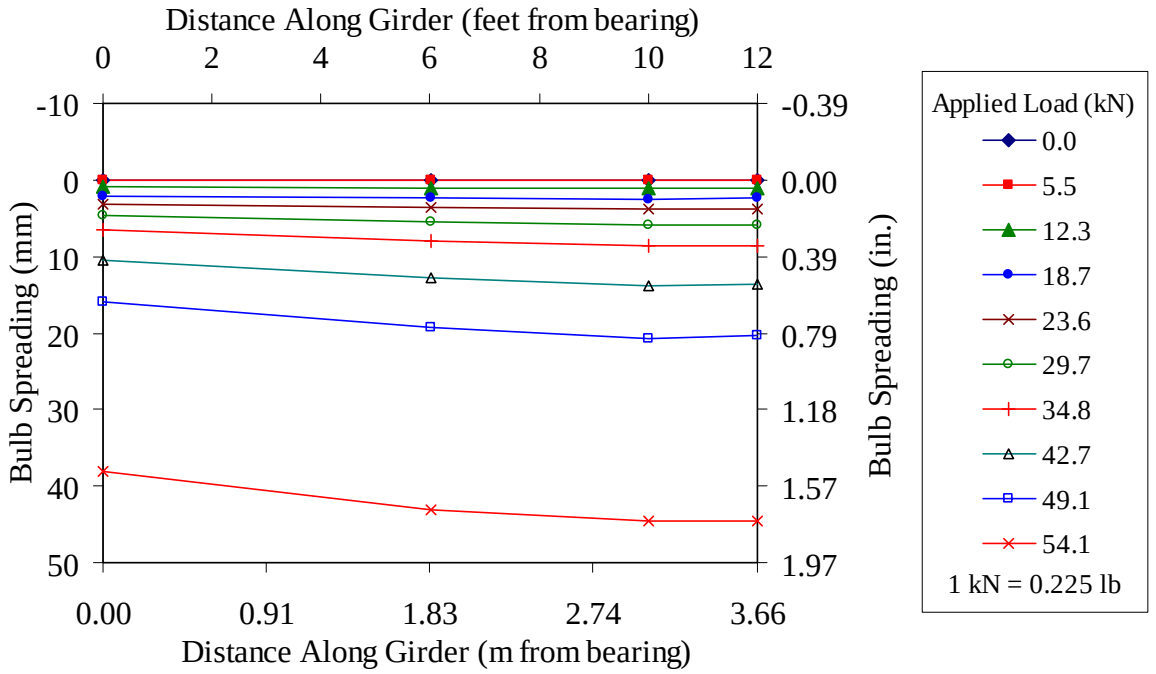

Figure 142. Graph. Bulb spreading along length of Girder P4-24T.

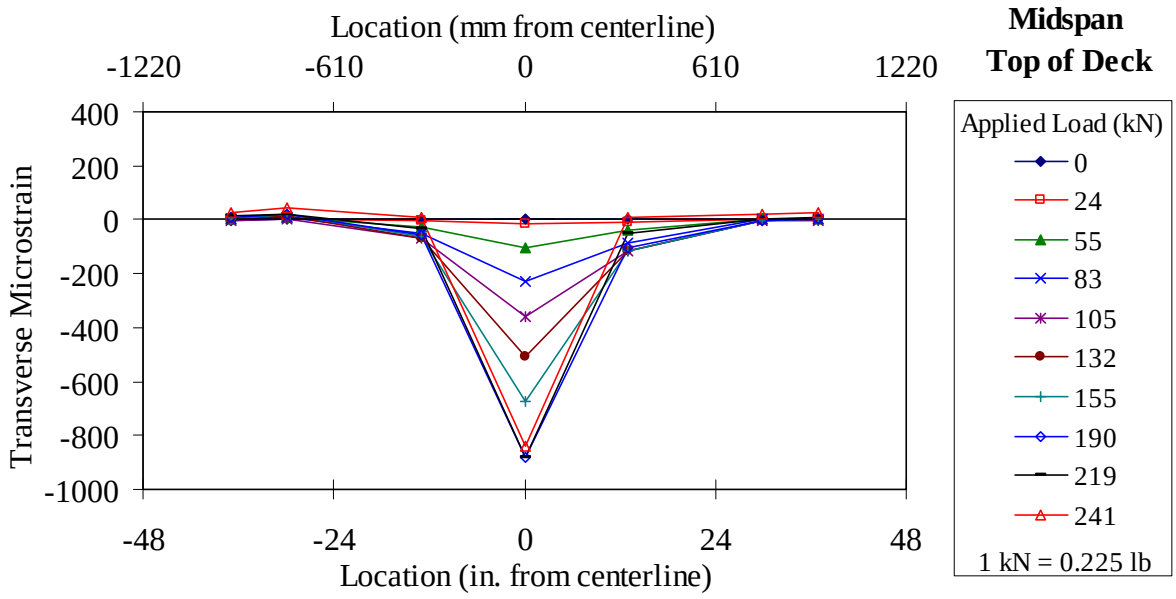

Figure 143. Graph. Transverse strain on top of deck across midspan of Girder P4-24T.

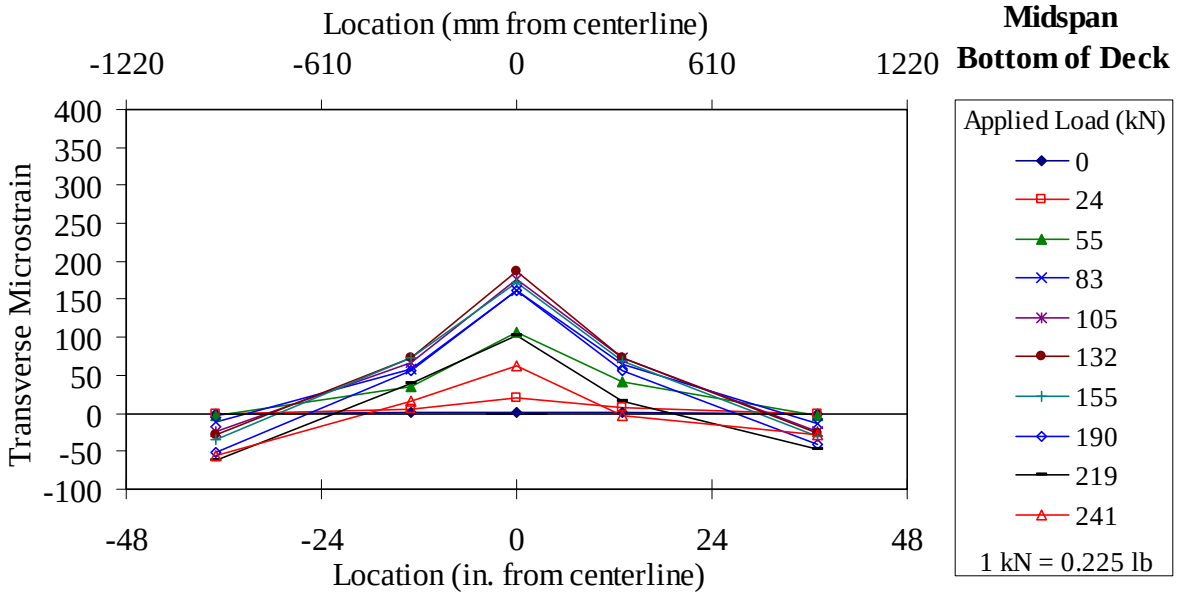

Figure 144. Graph. Transverse strain on bottom of deck across midspan of Girder P4-24T.

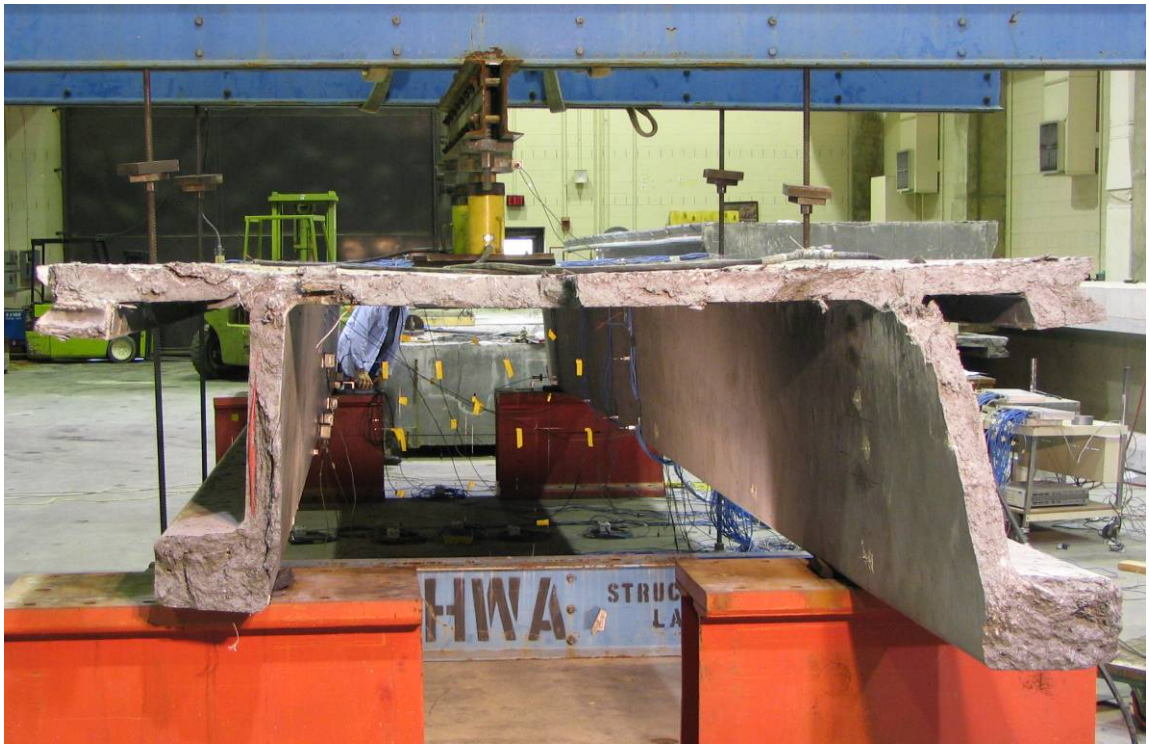

Figure 145. Photo. Girder P4-24T east elevation view at peak applied load.

Figure 146. Photo. Longitudinal mid-deck crack on P4-24T after conclusion of test.

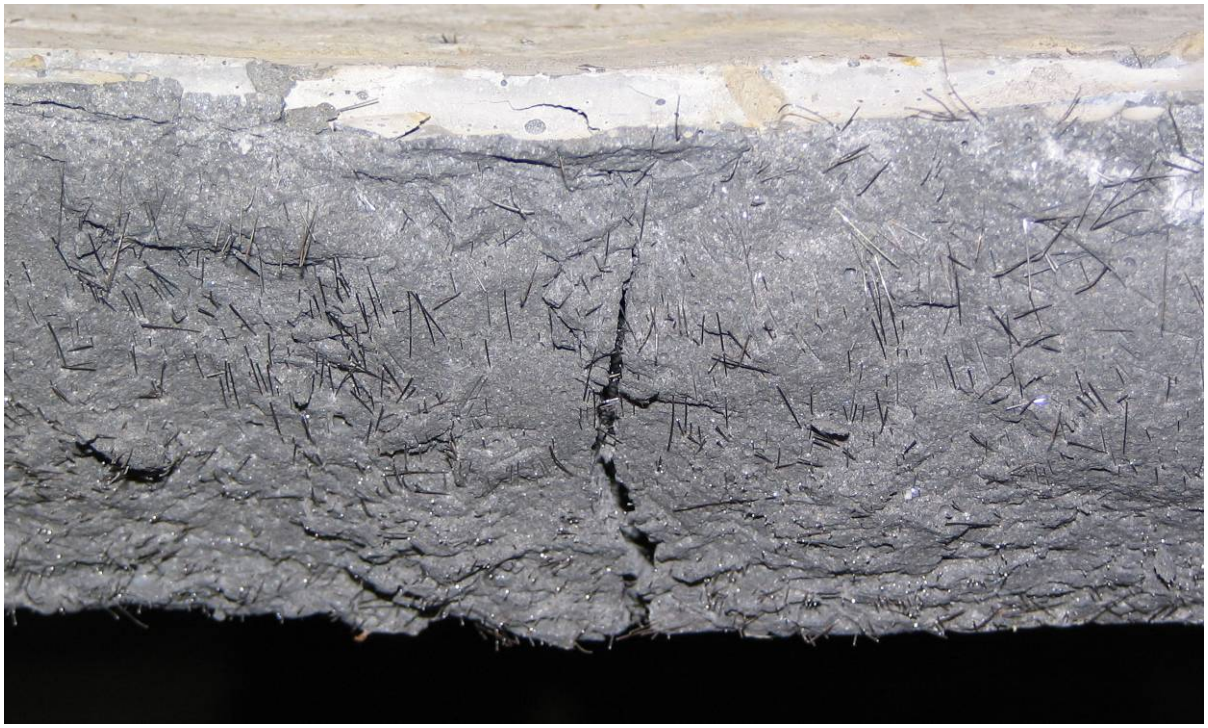

Figure 147. Photo. Failure crack in P4-24T as observed after conclusion of test.

P4-24D

Test P4-24D was a reprise of P4-24T with the only modification being in the supplemental restraint provided to the bulbs in order to resist lateral spreading. The test was completed using an approximately 8.5 m (28 foot) long portion of Girder P4. As shown in Figure 9, the girder section tested includes the length of Girder P4 running from the P4-57Sh load point to midspan of P4-45F. Both ends of the girder test section sustained significant damage during the earlier structural tests, while the middle of the test section was observed to possess some structural cracking in the deck and the legs.

Restraint was provided to the legs through two specific means. First, steel angles were abutted to the outside of the bulbs at the four reactions then welded to the support structure. These stops minimized the ability of the legs to spread outward at the reaction points. Second, two steel straps were attached to span between the bottom faces of the bulbs, with each located 0.46 m (18 inches) from midspan. Recall that the straps were 9.5 mm (0.375 inch) thick and were approximately 76 mm (3 inches) wide. They were attached to the bulbs using mechanical anchors and structural grade epoxy.

Figure 148 shows the applied load versus vertical deflection response of the midspan cross section of the girder. Longitudinal cracking of the underside of the deck was first observed at a total applied load including all loading apparatus of 116 kN (26 kips). The peak load applied to the girder was 409 kN (92 kips). Observe the significant difference between the deflection responses of the girder legs and the mid-deck, with the deck experiencing significantly more

deformation. This behavior is also shown in Figure 149 where the results from the seven potentiometers measuring vertical deflection of the midspan cross-section are presented at ten discrete load steps from throughout the test. Figure 150 presents similar information from the five potentiometers measuring vertical deflection at the quarter point of the test span.

Additional observations related to the global deformation of the girder are presented in Figure 151 and Figure 152. Figure 151 presents the results from the four potentiometers which were measuring the spreading between the legs. Note that the largest initial deformations are observed at the quarter point while later the middepth of the webs as midspan shows the greatest deformation. Figure 152 combines the three bulb spreading results with the results from the LVDTs which measured lateral movement of the bulbs at the west reaction points. These results show that neither the steel angles nor the steel straps fully restrained the outward movement of the legs.

Figure 153 plots the force observed in the two steel straps against the load applied to the girder. The force in the straps was calculated based on the strain readings captured, the strap cross-sectional area, and an assumed steel modulus of elasticity of 200 GPa (29,000 ksi). It was not clear whether the larger loads carried by the west strap were the result of a partial connection failure on the east strap or of non-symmetric behaviors on the part of the test girder. At the peak applied load, the total restraining force provided by the straps was greater than 111 kN (25 kips).

Results from the gages which monitored the transverse strain in the deck at midspan are presented in Figure 154 and Figure 155. Figure 154 shows the results from the seven gages affixed to the top of the deck. The compressive strains in the top of the deck at mid-deck and the tensile strains above the webs increase uniformly up through cracking of the deck, after which the middeck compressive strains continue increasing while the tensile strains above the web remains relatively constant. Figure 155 shows the results from the five gages affixed to the underside of the deck. This figure shows that the transverse strains in the underside of the deck increased up through initial deck cracking, then remain relatively constant through the remainder of the test. Note first that none of these gages were directly intercepted by discrete cracks which formed in the deck and second that the results from the peak applied load are not plotted as some of the readings from these sets of gages were unreliable.

As the applied load was increased from the initial cracking load toward the eventual peak load, additional longitudinal cracking of the deck occurred. These cracks tended to be wider and more widely spaced than the flexure and shear cracks which were observed in the previous girder tests. The longitudinal crack about which failure of the deck occurred was directly down the centerline of the girder. This crack continued to grow wider as the load was increased. Figure 156 shows the failure crack at midspan on the under side of the deck after the conclusion of the test. Figure 157 shows the damage apparent on the top of the deck at midspan after conclusion of the test, including chipping/crushing of the concrete along mid-deck and flexural tensile cracking above each web. A crack assessment after the conclusion of the test indicated that the failure crack and those adjacent to it on the underside of the deck were generally parallel and approximately 50 to 75 mm (2 to 3 inches) distant.

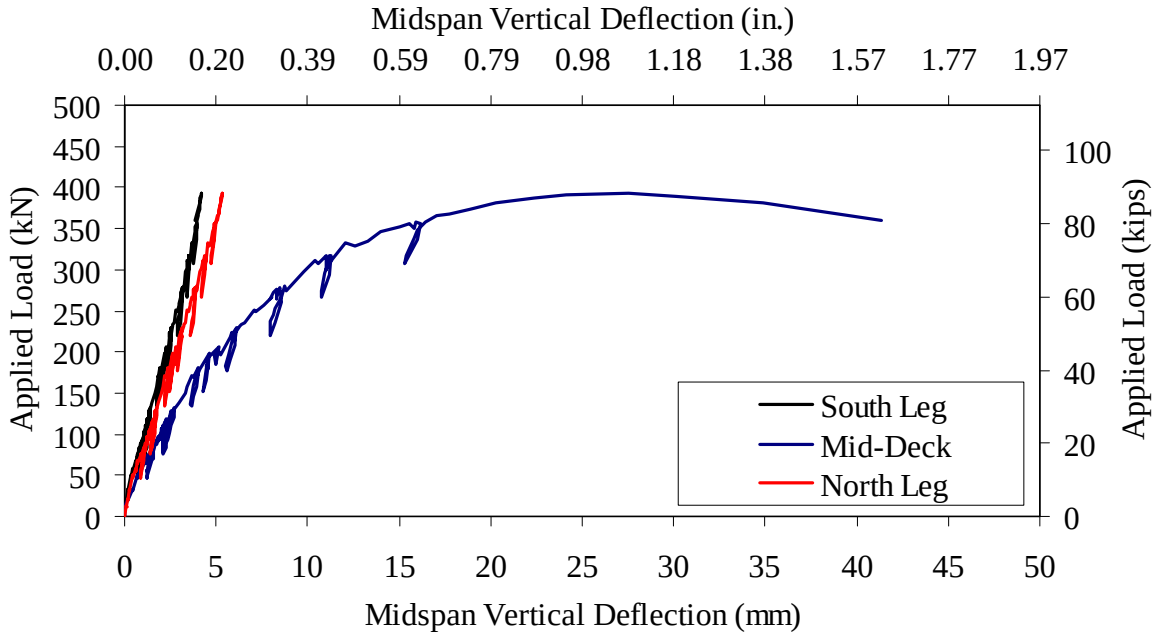

Figure 148. Graph. Load versus midspan deflection response of Girder P4-24D.

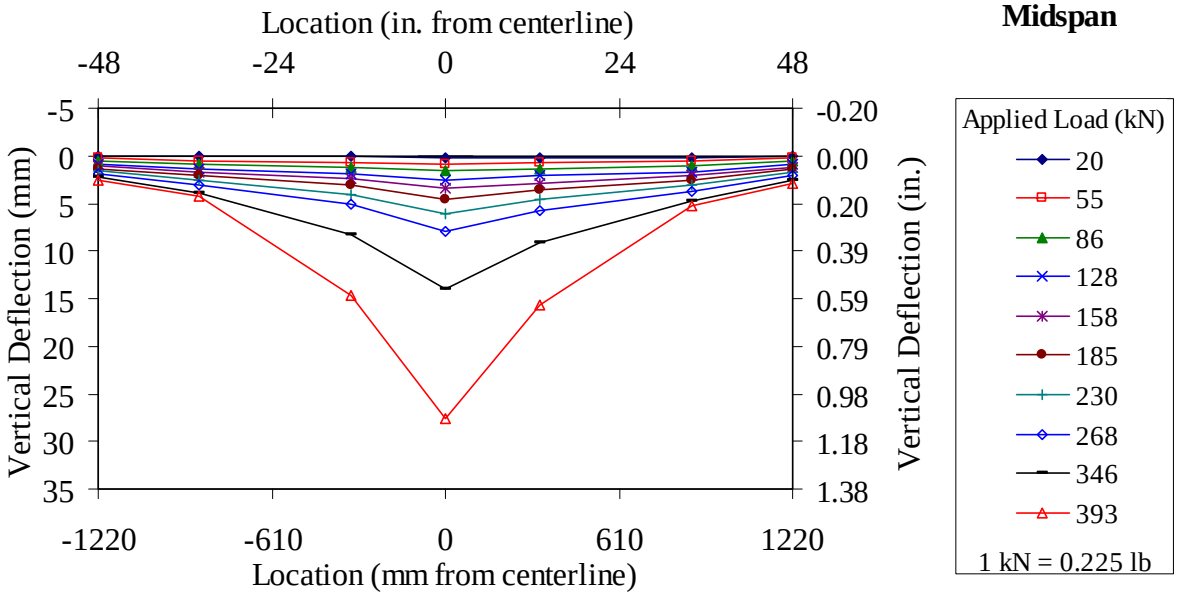

Figure 149. Graph. Load versus deflection response across Girder P4-24D at midspan.

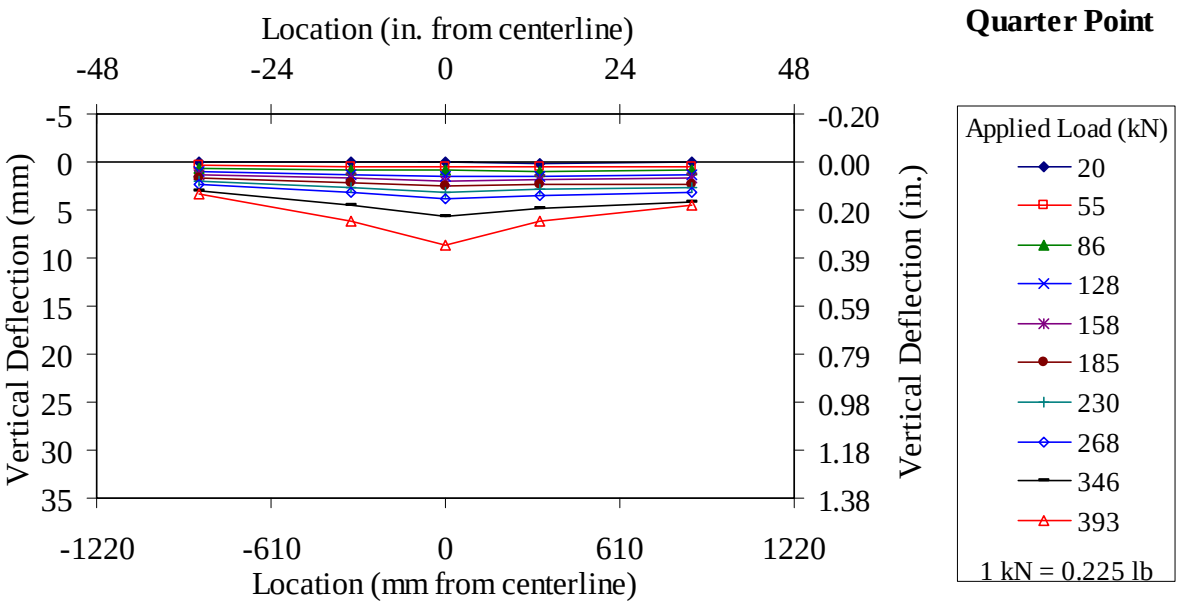

Figure 150. Graph. Load versus deflection response across Girder P4-24D at quarter span.

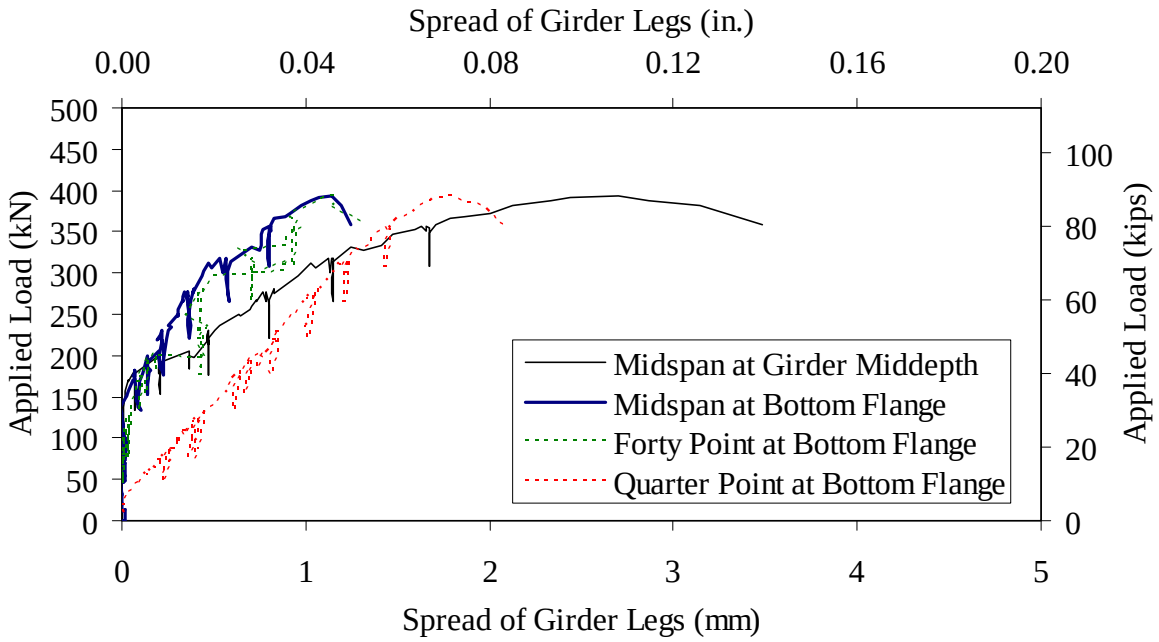

Figure 151. Graph. Spreading between webs of Girder P4-24D.

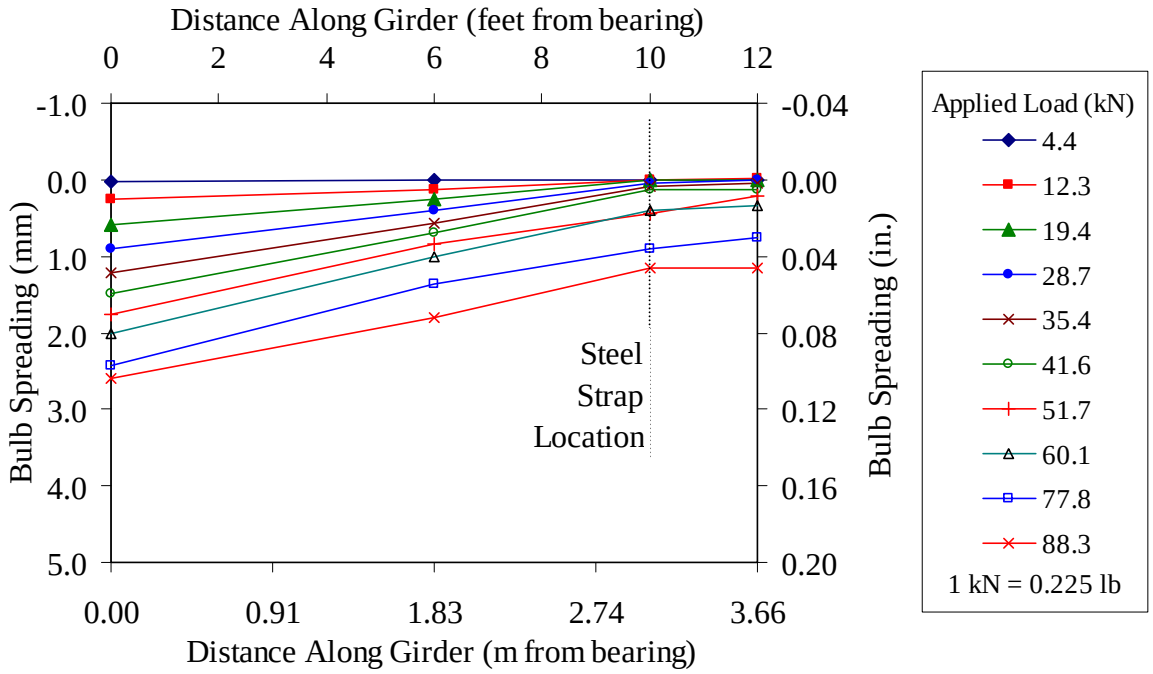

Figure 152. Graph. Bulb spreading of Girder P4-24D.

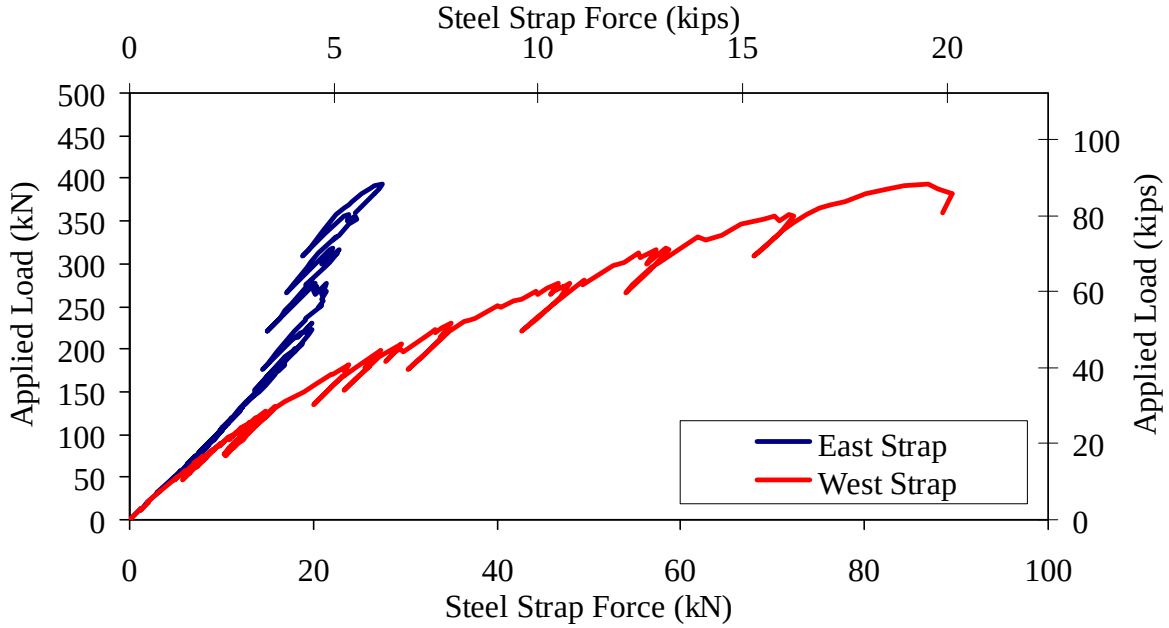

Figure 153. Graph. Strap force in Girder P4-24D.

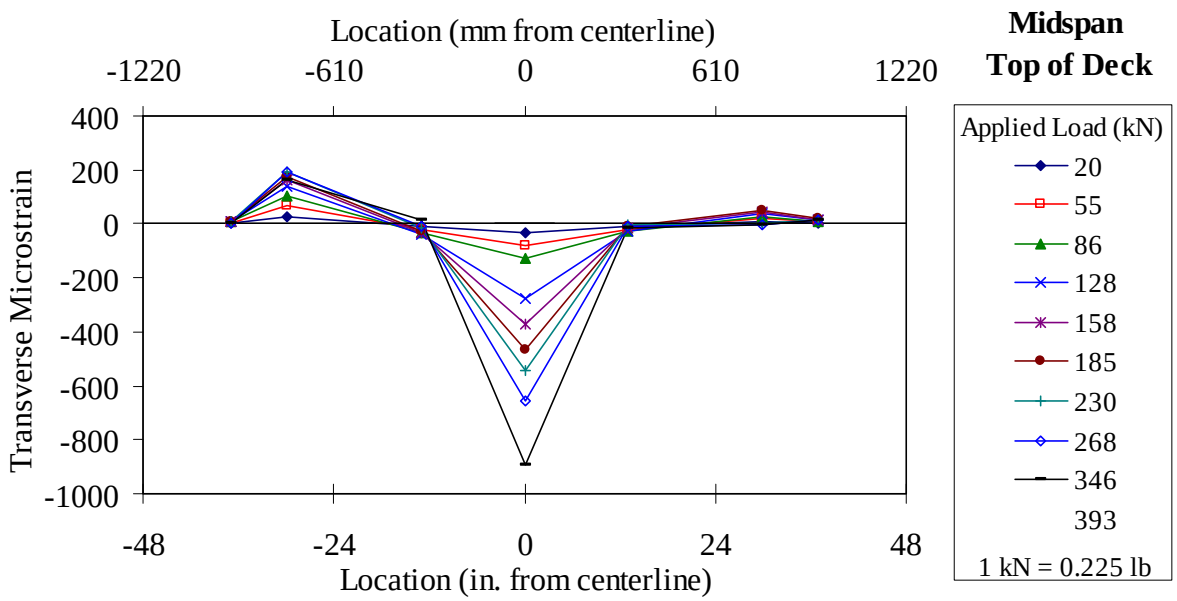

Figure 154. Graph. Transverse strain on top of deck across midspan of Girder P4-24D.

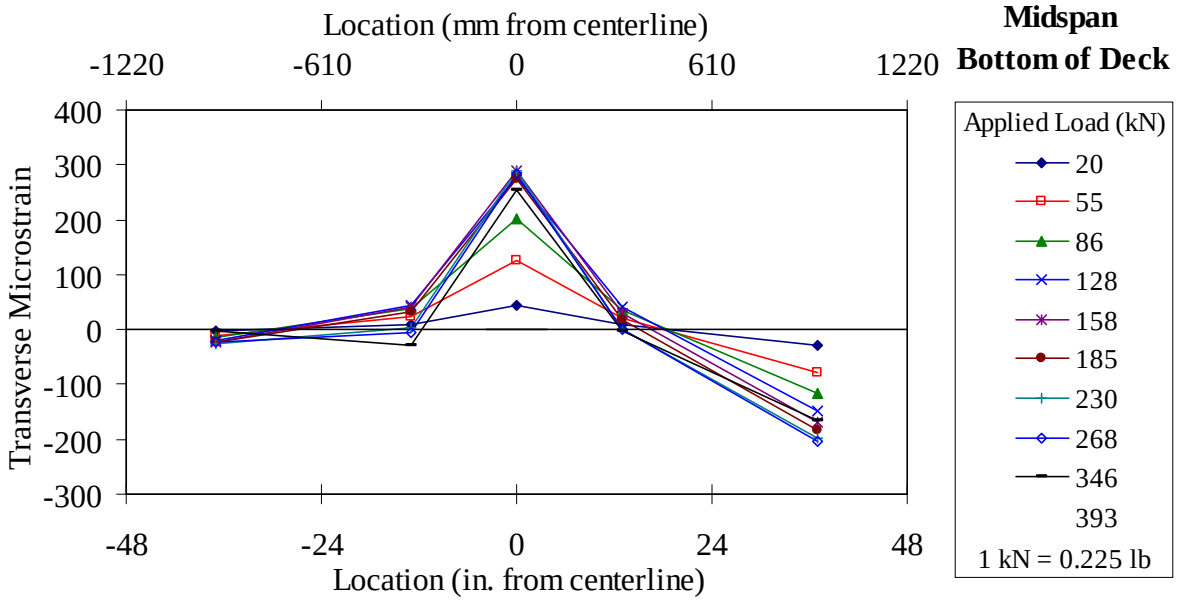

Figure 155. Graph. Transverse strain on bottom of deck across midspan of Girder P4-24D.

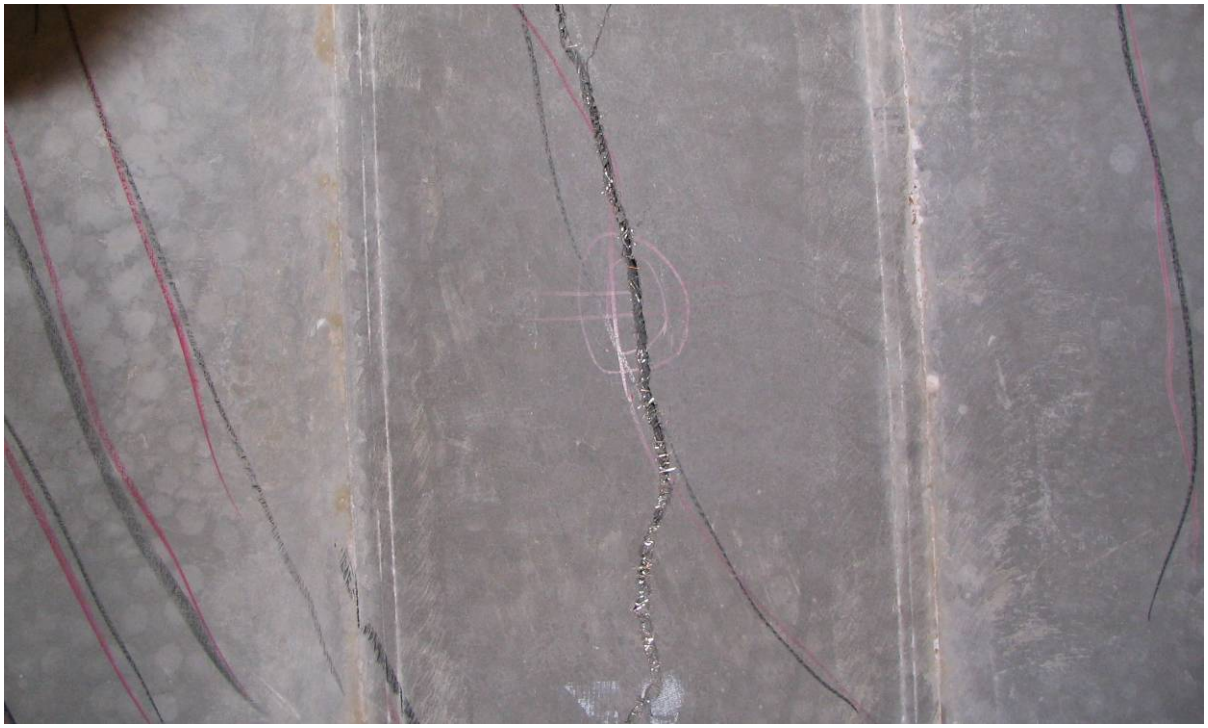

Figure 156. Photo. Longitudinal mid-deck crack on P4-24D after conclusion of test.

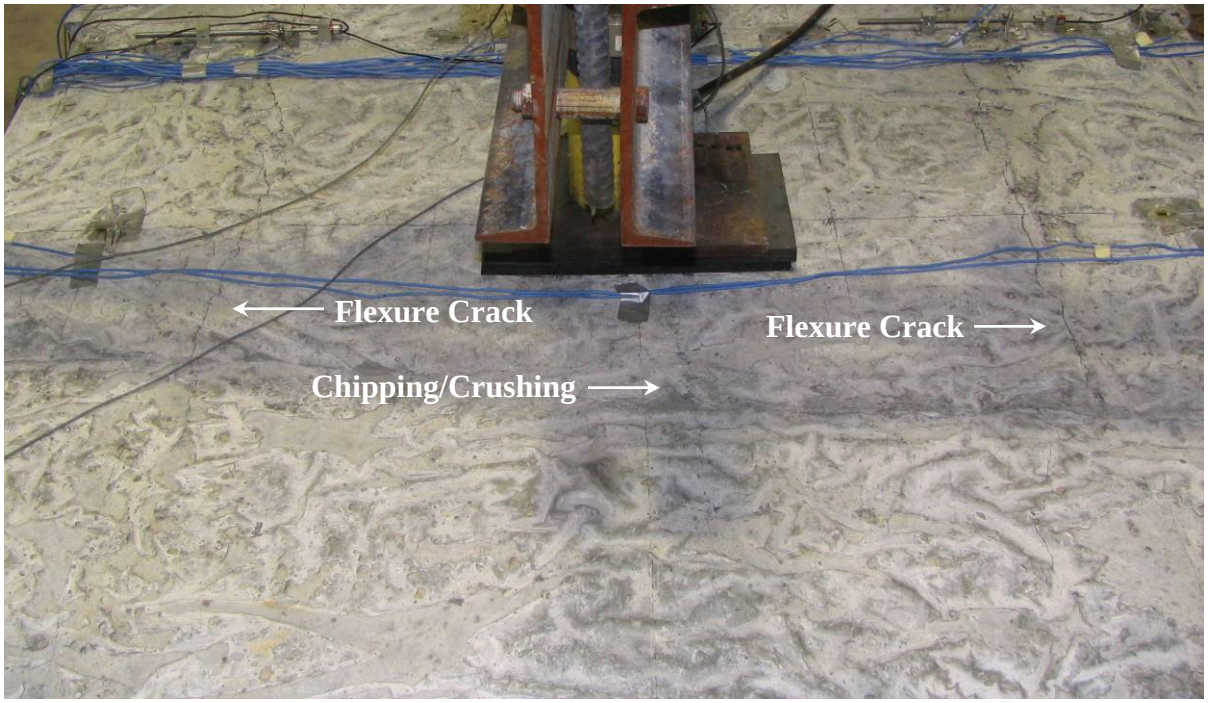

Figure 157. Photo. Damage on top of P4-24D deck after conclusion of test.

CHAPTER 6. DISCUSSION OF RESULTS

INTRODUCTION

This chapter presents an analysis and discussion of the results from the physical tests conducted in this research program. The chapter is divided into four sections which focus on the four major topics addressed in this test program, namely primary flexural response, shear response, transverse flexural response, and load distribution behaviors of the prototype UHPC pi-girder.

FLEXURAL RESPONSE OF A UHPC PI-GIRDER

Results from three of the girder tests conducted provide information relevant to describing the overall flexural response of the UHPC pi-girder. The tests P2-70F and P4-45F were both designed to focus on flexural response. Test P4-57Ss also provides relevant information as this girder, although loaded to induce large shear forces, failed in flexure.

As these are prestressed girders, the prestressing forces on the members must be delineated prior to discussing the flexural response. As presented previously, the strands in these girders were initially stressed to 70.7 percent of their ultimate capacity which equates to 1316 MPa (190.8 ksi). Aside from this higher stressing force, the fabrication of these girders as related to the strand tensioning and detensioning was similar to that conducted for the casting of the AASHTO Type II girders whose results are presented in Graybeal[(2)]. Thus, the prestressing loss, inclusive of shrinkage, creep, and relaxation and exclusive of elastic shortening, is assumed to be 139 MPa (20.2 ksi). The elastic shortening loss for these girders was calculated to be 117 MPa (17.0 ksi). In total, the prestressing forces and losses combine to create an internal prestressing moment in each girder of 1,525 kN-m (13,500 kip-inches) in the fully developed regions of each girder.

First flexural cracking of P2-70F was audibly observed at a combined dead plus live load moment of 2,330 kN-m (20,600 kip-inches). Similarly, P4-45F occurred at 2,200 kN-m (19,500 kip-inches). A first flexural cracking result was not obtained for P4-57Ss as this test setup was not conducive to isolating shear and flexural cracking behaviors. Combined, these two results indicate that the total cracking moment of the girder was approximately 2,260 kN-m (20,000 kip-inches). Considering the prestressing moment in the girders, the applied moment beyond decompression at first cracking was approximately 735 kN-m (6,500 kip-inches). Given a girder moment of inertia of 37.1×10^9 mm^4 (89,060 in^4) and an elastic neutral axis depth 307 mm (12.1 inches) down from the top of the girder, an elastic analysis indicates that the stress in the tensile face of the UHPC girder was 10.3 MPa (1.5 ksi) at first cracking.

The ultimate flexural capacities of the three girders were 4,250 kN-m (37,600 kip-inches), 4,310 kN-m (38,190 kip-inches), and 4,150 kN-m (36,720 kip-inches) for P2-70F, P4-45F, and P4-57Ss, respectively. These results include both the dead and live loads on the girders at the time of failure. The average ultimate flexural capacity is 4,235 kN-m (37,500 kip-inches); however, note that this value includes the result from P4-57Ss which may have been reduced by the presence of debonded strands near the failure location.

In P2-70F, P4-45F, and P4-57Ss, the girder failure was precipitated by the loss of tensile capacity in a bulb resulting from fiber pullout across a discrete crack. Strain readings captured during these tests indicate that the total strain in the bulbs at failure in each of the three cases was between 7,000 and 10,000 microstrain. The strain in each of the non-failing bulbs at peak load applications was in the same range. Results from a previously conducted UHPC I-girder flexure test also indicated that tensile fiber pullout occurred at approximately 10,000 microstrain.[2] Combined, these results indicate that a limiting tensile strain of 0.007 may be reasonable for heavily reinforced UHPC flexure members.

A capacity analysis of this girder was completed according to the requirements of the AASHTO LRFD Bridge Design Specifications[13]. A 21.3 m (70 foot) simple span was considered since this is the span for which the included quantity of prestressing strand was initially designed. Due to the limited capability of the prototype pi-girder to distribute loads laterally between girders, the demand on the girder was calculated by considering the critical load cases on half of a girder as depicted in Figure 158. The lever rule was used to distribute loads. The girder's own self weight load was supplemented by an additional 122 kg/m^2 (25 lb/ft^2) applied load to account for a thin wearing surface. Multiplying the demands by two allows for easy comparison to the test results which pertain to the symmetric loading of the as-fabricated prototype pi-girder. The Service III and Strength I demands for an as-fabricated girder are 2250 kN-m (19940 kip-inches) and 4470 kN-m (39600 kip-inches), respectively. The experimentally observed flexural cracking in Tests P2-70F and P4-45F was approximately equal to the Service III demand. The experimentally observed ultimate flexural capacity of this girder is approximately 5 percent less than the demand, indicating that additional prestressing force is necessary in order to meet the flexural requirement.

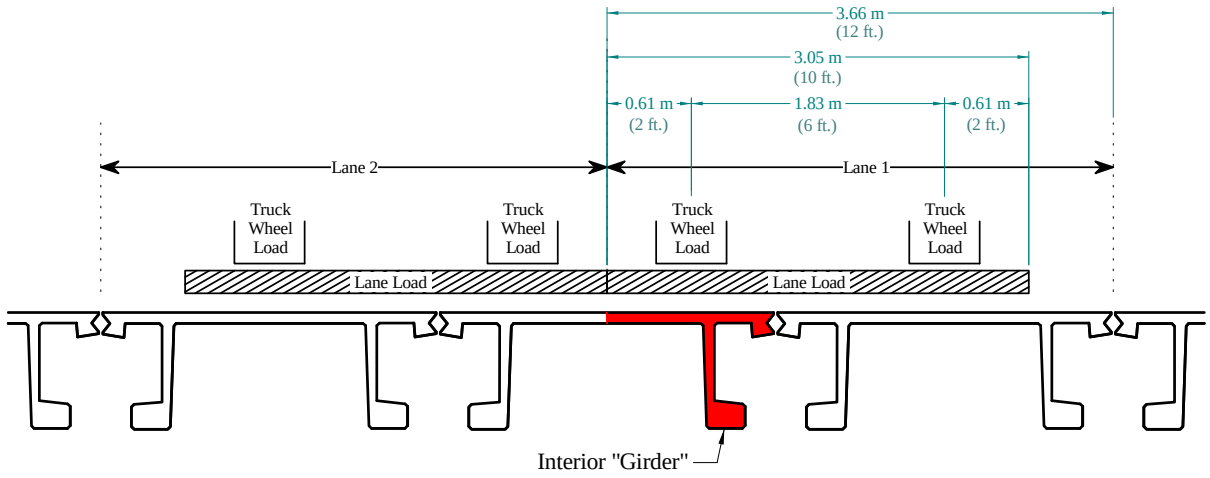

Figure 158. Illustration. Loading configuration for interior "girder".

A deflection analysis was also completed using the optional deflection provisions of the AASHTO LRFD Bridge Design Specifications. The considered loading included the design truck with impact factor on the 21.3 m (70 foot) simple span. The resulting applied moment on an as-fabricated girder is 1,740 kN-m (15,440 kip-inches). The recommended deflection limit

obtained by dividing the span length by 800 is 26.7 mm (1.05 inch). In Test P2-70F at this applied moment, the average observed midspan deflection of the girder bulbs was 34.3 mm (1.35 inch). Clearly, the prototype pi-girder does not meet the recommended deflection provisions. Recognize, however, that this analysis involves conservatively applying an entire truck load to the 2.4 m (8 ft) wide girder, whereas there is inevitably some level of load distribution transversely across the bridge.

Finally, an analysis was completed to quantify the effective moment of inertia of the pi-girder as observed through Tests P2-70F and P2-45F. The unload/reload cycles applied to these girders throughout the tests allow for an estimation of the flexural stiffness of the entire girder through the use of the vertical deflection observations obtained. The analytical procedure used was identical to that described in detail in reference (2). A constant modulus of elasticity of 55.8 GPa (8100 ksi) was assumed for the analysis. The results obtained are shown on load deflection plots from their respective tests in Figure 159 and Figure 160.

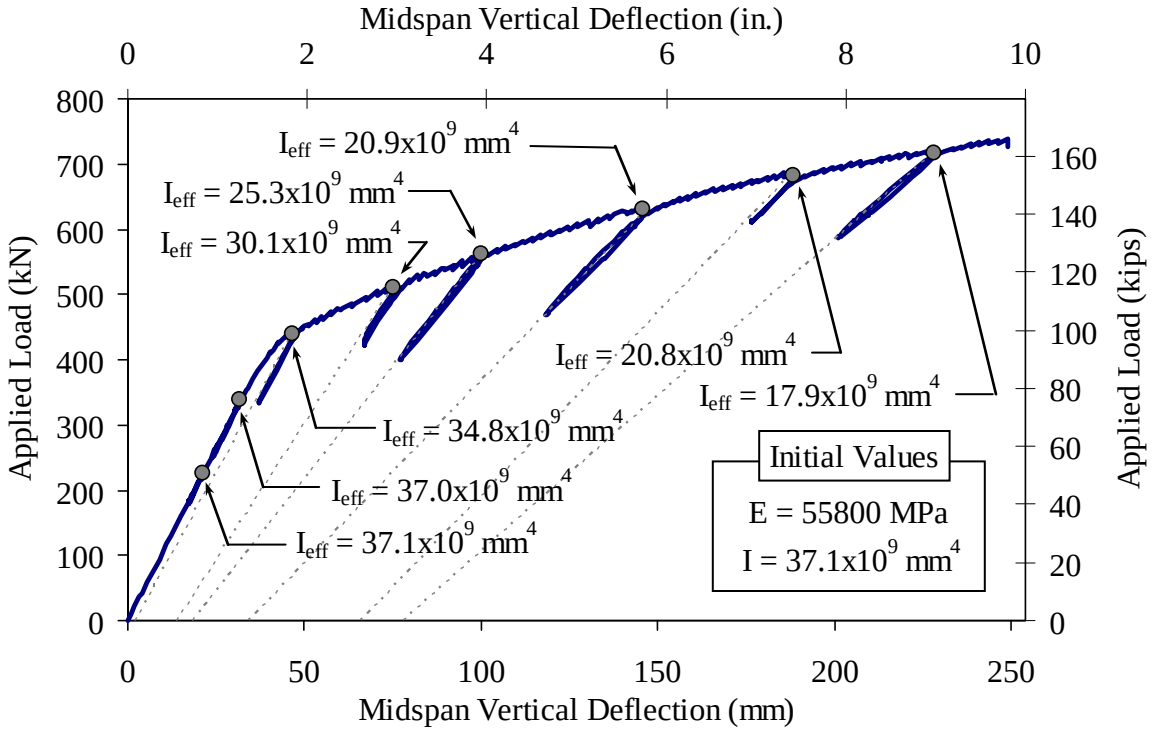

Figure 159. Graph. Effective moment of inertia from Test P2-70F.

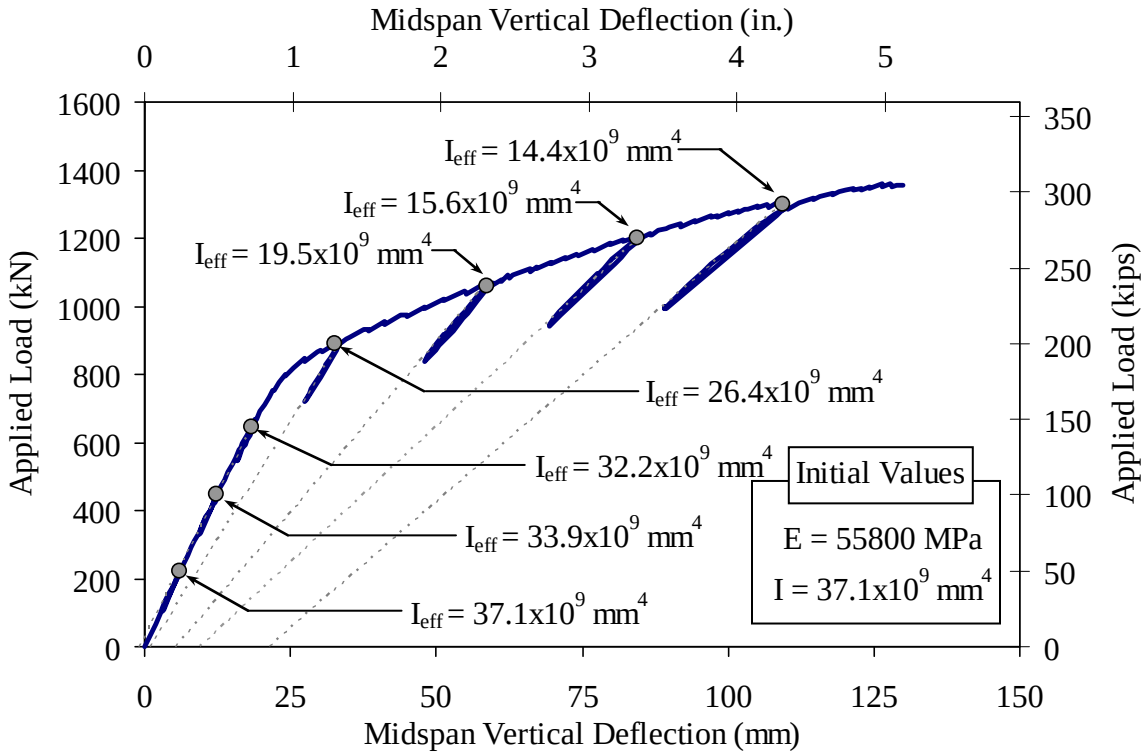

Figure 160. Graph. Effective moment of inertia from Test P4-45F.

SHEAR RESPONSE OF A UHPC PI-GIRDER

Results from three of the girder tests conducted provide information relevant to describing the overall shear response of the UHPC pi-girder. Recall that tests P2-21S, P4-57Sh, and P4-57Ss were all designed to induce large shear forces into the girder cross section. Test P2-21S resulted in a shear failure of a girder web at a total dead plus live load shear of 1,910 kN (430 kips). Test P4-57Sh resulted in a shear failure of a girder web at a total dead plus live load shear of 1,630 kN (366 kips). Test P4-57Ss resulted in a flexural failure of the girder when the total dead plus live load shear in the girder was 2,270 kN (510 kips).

In Tests P2-21S and P4-57Sh, the girder failure was precipitated by the loss of diagonal tensile capacity in a web resulting from fiber pullout across a discrete crack. Strain readings captured during these tests indicate that the total strain in the webs at failure in these two cases was between 9,000 and 11,000 microstrain. Other webs which were heavily loaded in shear but did not fail showed strains between 6,000 and 8,500 microstrain.

The shear capacity of this girder was assessed using a similar methodology to the flexural capacity analysis discussed above. The Service III demand for a 2.44-m (8-foot) width of a 21.3-m (70-foot) long bridge is 459 kN (103.2 kips), while the Strength I demand is 916 kN (206 kips). All experimentally observed shear capacities are at least 75 percent greater than the Strength I demand.

The ultimate shear capacity of this girder was also analyzed using basic engineering principles as presented in Graybeal[(2)]. Note that this method of analysis is a modified version of the design

provisions presented in the Association Française de Génie Civil *Interim Recommendations for Ultra High Performance Fiber-Reinforced Concretes* [14]. The analysis assumes that the girder webs carry all of the shear forces and that the diagonal tensile force, which can be resolved from the shear force, acts uniformly over the relevant cross-sectional area of the webs. At peak shear load, the angles of the web shear cracks in the three girder tests were approximately 35 degrees from the horizontal. This angle pertained to the failure plane in Tests P2-21S and P4-57Sh, while it pertained to the average crack angle in Test P4-57Ss. The entire 0.56 m (22 inch) depth of web and the 0.14 m (5.5 inch) average web width were assumed to be uniformly effective in resisting the diagonal tensile force. From these values, the average direct tensile force carried across the critical shear crack at failure can be determined. The calculated diagonal tensile capacities were 14.6 MPa (2.1 ksi) in P4-57Sh, 17.2 MPa (2.5 ksi) in P2-21S, and 20.3 MPa (2.9 ksi) in P4-57Ss.

TRANSVERSE FLEXURAL RESPONSE OF A UHPC PI-GIRDER

Tests P4-24T and P4-24D were both focused on the transverse flexural response of the UHPC pi-girder. In both cases, a pair of wheel patch loads was applied along the midline of the girder near midspan in a configuration consistent with the design tandem detailed in the AASHTO LRFD Bridge Design Specifications[13]. In P4-24T the only supplemental restraint provided to the bulbs to resist transverse displacement was the shearing resistance provided by the elastomeric bearing pads at the support points. In P4-24D additional passive restraint was provided through blocking installed outside of the bulbs at the support points and through steel straps installed between the bottom faces of the bulbs near midspan.

In Test P4-24T, the girder exhibited first cracking of the deck at total applied loads of 53 kN (12 kips) per loading patch (i.e., 106 kN (24 kips) total applied load). A slightly higher load of 58 kN (13 kips) per loading patch (i.e., 116 kN (26 kips) total applied load) caused first cracking in Test P4-24D. These results are sufficiently close to one another to indicate that the supplemental transverse restraint provided little restraint prior to first cracking. Note that the load capacity at first cracking is approximately equivalent to the design tandem wheel patch live loads defined in the AASHTO LRFD[13], but that the capacity is insufficient to account for impact factors or lane loads prior to cracking.

The midspan middeck vertical deflection response of the two test girders is shown in Figure 161. The figure shows that the responses were similar until first cracking, after which P4-24T shows significantly increased vertical deflection per load increment applied. The peak load carried by P4-24D is 60 percent greater than the peak load carried by P4-24T with both girders undergoing similar magnitude deflections prior to failure.

Visual observations and data recorded during and after failure indicate that the responses of the two girders differed significantly. In P4-24T, the girder seemed to exhibit behaviors consistent with one-way bending of a deck which was simply supported at the girder legs. In P4-24D, the girder seemed to exhibit behaviors consistent with one-way bending of a deck which was restrained at the leg-to-deck interface. These different responses were most clearly depicted in the bulb spreading response of the two girders, through the flexural cracking above the legs in P4-24D, and in the steel strap forces observed in P4-24D.

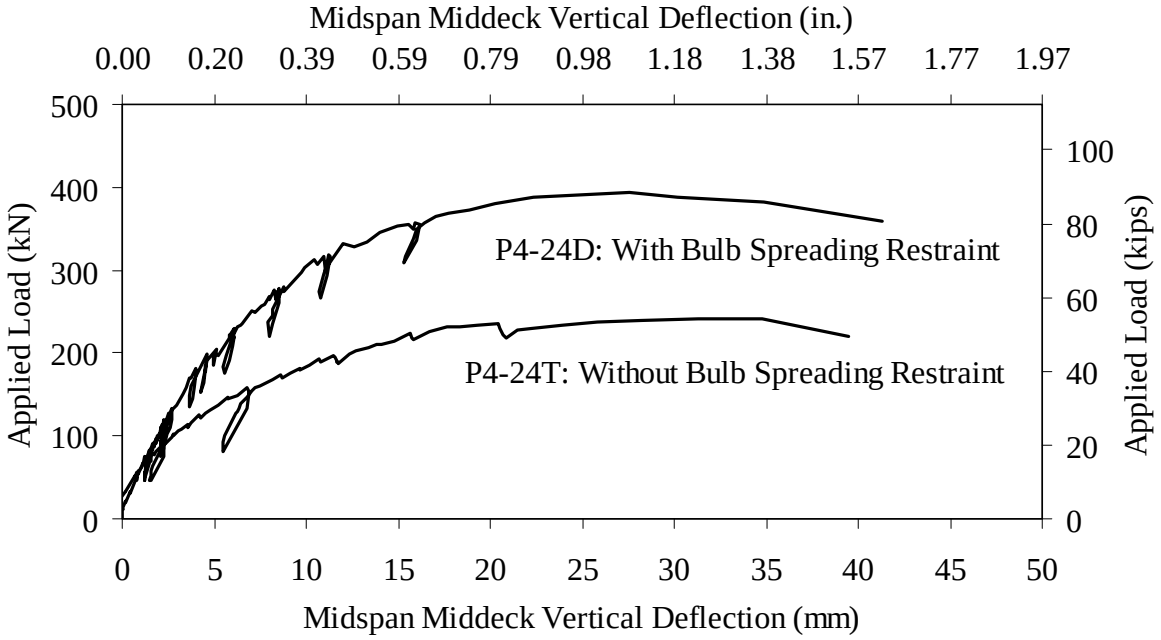

Figure 161. Graph. Midspan middeck vertical deflection results from two transverse flexural response tests.

LOAD DISTRIBUTION BEHAVIOR OF A UHPC PI-GIRDER

Three of the tests completed in this research program focused on the load distribution behavior of the UHPC pi-girder. These included the load distribution testing of the UHPC pi-girder bridge, the testing of P2-70F, and the testing of P2-21S. In each of these cases, elastic level loads were applied to the test specimens in both symmetric and asymmetric configurations in order to investigate the ability of the pi-girder cross section to share applied loads transversely across a bridge.

It must be recognized that the girder configurations tested present more sever situations that would be encountered in practice. In the field, a minimal width two-lane bridge would require at least three of these UHPC pi-girders to be connected transversely across the bridge. Thus, the opportunity for load sharing between girders and the resistance to unrestrained deck flange tip vertical movement would necessarily be increased.

The bridge test presents the most informative results related to load distribution. These results demonstrated that, in terms of flexural response, there is limited transfer of applied loads across the bridge structure. For point loads applied to an exterior leg of and exterior girder, approximately two-thirds of the load is carried in flexure by that leg and the remaining one-third can conservatively be assumed to be carried by the adjacent leg. For point loads applied midway between two girder legs, the load can be conservatively assumed to be carried equally by the adjacent legs. For point loads applied above interior legs, half of the load can be assumed to be carried by the loaded leg and one-quarter can be distributed to each of the two adjacent legs. Alternatively, recognizing that each girder leg effectively acts as an individual ‘girder’ for the

purposes of the definition, the Lever Rule as defined in the AASHTO LRFD Bridge Design Specification[13] can provide a conservative approximation of live load moment distribution.

The load distribution testing associated with P2-21S provides some limited information on the ability of the girder cross section to laterally distribute loads applied in traditionally high shear regions of a span. As shown in Figure 93, the large majority of the load applied above the south girder leg is directly reacted by the supports under this leg. The cross section displays limited ability to laterally distribute applied point loads in high shear portions of the span. The Lever Rule can provide an approximation of live load shear distribution, again assuming that each girder leg acts as an individual 'girder' for the purposes of the definition.

CRACKING RESPONSE OF UHPC UNDER STRUCTURAL LOADING

Tensile cracking of UHPC is an easily observed feature which can provide significant information related to the behavior of the material and the structure. Three specific tensile cracking responses were observed in the series of structural tests discussed in this report. The cracking responses included flexural cracking in a girder subjected to primary bending, shear cracking in a girder subjected to primary shear, and flexural cracking in a girder subjected to transverse bending. In all cases, the observed cracks resulted from mechanical stresses generated through the application of structural loads.

Tests P2-70F and P2-45F demonstrated the tight crack spacing and small crack widths normally associated with the bulb of a prestressed UHPC girder loaded to induce flexural failure. Figure 77 shows that at a total dead plus live load moment equivalent to 94 percent of the moment that caused failure, the bulb of the girder near midspan had approximately 1 crack every 4 mm (6.7 cracks per inch). In both of these tests and as commonly observed in conventional concrete flexural members, tighter crack spacings and crack widths were observed in the bulbs as opposed to in the webs immediately above the bulbs.

Tests P2-21S, P4-57Sh, and P4-57Ss demonstrated the tight crack spacings and crack widths associated with diagonal tensile response of UHPC girders subjected to high shear forces. This behavior is best illustrated in Figure 134 where the space between adjacent cracks is between 2 and 3 mm (0.08 to 0.12 inches). In this figure, the applied shear is approximately 82 percent of the total dead plus live load shear in the girder at failure.

A significantly different cracking response was observed in Test P4-24T and P4-24D wherein the transverse flexural response of the girder cross-section was investigated. In these tests, long, discrete cracks formed on the underside of the deck running the length of the girder. Multiple cracks formed, each generally running parallel to the length of the girder and being approximately 25 to 50 mm distant (1 to 2 inches) from its neighboring cracks. These cracks were also unique in that many were visible to the naked eye. Similar longitudinal cracks also formed over the webs in the top of the deck in Test P4-24D.

These disparate cracking behaviors demonstrate that the UHPC investigated in this study does not necessarily exhibit higher uniaxial tensile strength after cracking than it does prior to cracking. The results demonstrate that supplemental restraint, which may be provided in a particular cracked region through prestressing strands in the bulbs or through upper and lower

flanges in shear panel but which is largely absent in a thin, flat integral deck, significantly influences the post cracking tensile response of UHPC.

FAILURE MECHANISMS OF UHPC UNDER STRUCTURAL LOADING

The tests completed as part of this study were intended to investigate the structural mechanical response of the UHPC pi-girder from initial load application through structural failure. All tests which progressed through structural failure resulted in the same fundamental failure mechanism, namely tensile failure through fiber pullout. Whether in primary flexure, primary shear, or transverse flexure, the UHPC material itself at the local level in each eventual failure region progressed from elastic tensile straining, to tensile cracking, to engagement of the internal fiber reinforcement, until the straining of the fiber reinforcement exceeded its capacity to remain bonded within the UHPC matrix. Figure 162 shows three photographs captured immediately after the failures of P2-70F, P4-45F, and P2-21S. In these figures it is apparent that the fiber reinforcement which bridged the eventual failure crack and provided post-cracking tensile capacity to the cross section has pullout out from the UHPC matrix on the mating side of the failure surface.

As the fiber reinforcement begins to pullout, local tensile capacity in the cross section is lost and the resulting load must be redistributed or the member will fail. In the case of primary flexural response, the initiation of fiber pullout results in transfer of tensile force into the prestressing strands which bridge the eventual failure crack. In Tests P2-70F, P2-45F, and P2-57Ss, these strands were unable to sustain the additional tensile force and, soon thereafter, one bulb of the girder failed through instantaneous rupture of all bonded prestressing strands bridging the crack. In the case of primary shear response as observed in Tests P2-21S and P4-57Sh, the initiation of fiber pullout resulted in a loss of diagonal tensile capacity and an immediate tensile shear dislocation across the crack. In the case of transverse flexural response as observed in Tests P4-24T and P4-24D, the initiation of fiber pullout at the most highly stressed location in the bottom of the deck results in crack widening and increased tensile stress being applied to fibers located higher in the deck cross section. This behavior progresses as additional fibers pullout and the effective flexural depth of the eventual failure cross section continues to decrease.

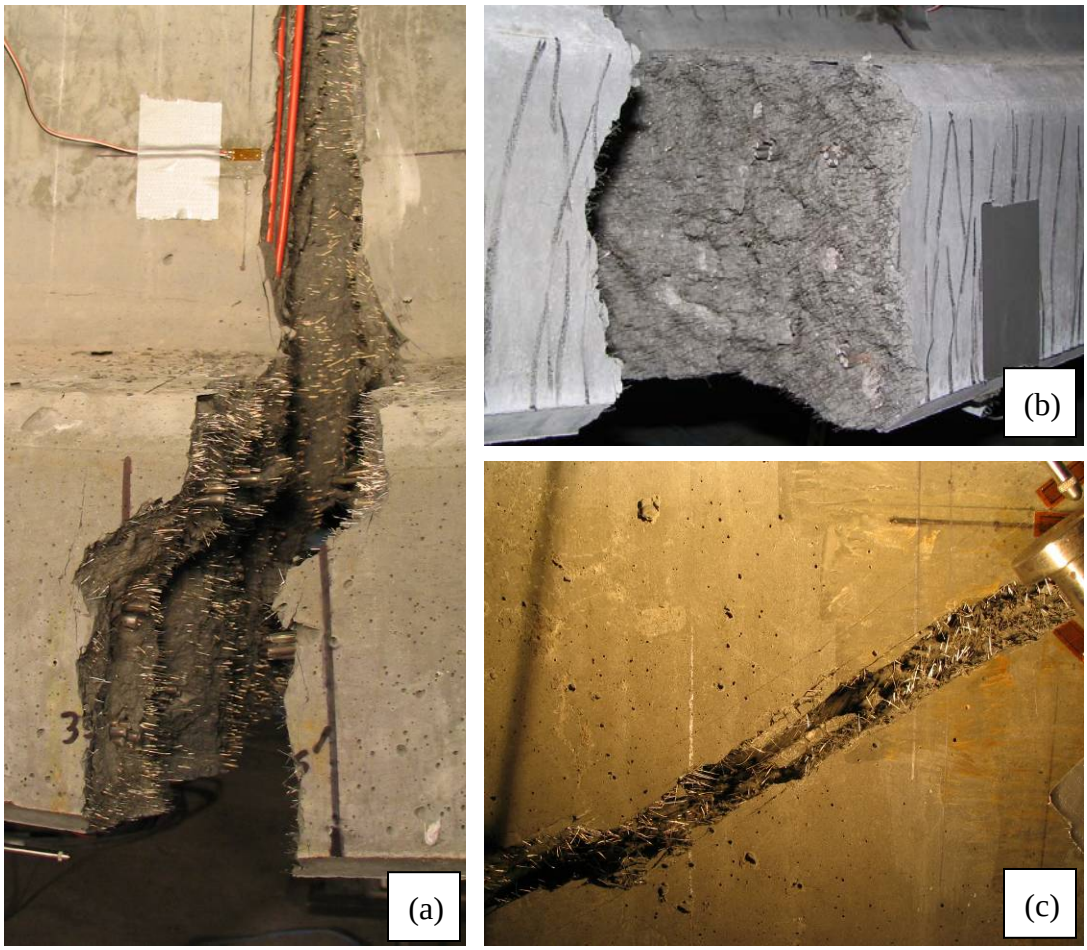

Figure 162. Photo. Failure surfaces including (a) bulb of P4-45F, (b) bulb of P2-70F, and (c) web of P2-21S.

CHAPTER 7. CONCLUSIONS

INTRODUCTION

This experimental investigation focused on the structural behavior of a newly developed highway bridge girder cross section, namely the pi-girder. This girder was developed and optimized specifically to exploit the advanced mechanical and durability properties of UHPC. Structural testing was completed on girders and sections of girders so as to investigate the flexural response, the shear response, and the transverse flexural response of the girder. Conclusions resulting from this study are presented below. A brief discussion of ongoing and potential future research related to this topic is presented immediately thereafter.

CONCLUSIONS

The following conclusions are presented based on the research presented in this report.

1. The 0.84 m (33 inch) deep, 2.44 m (96 inch) wide prototype UHPC pi-girder exhibited an average primary flexural capacity of 4,235 kN-m (37,500 kip-inches). This capacity is slightly less than the flexural loading requirements of the AASHTO LRFD Bridge Design Specification[13] for a span of 21.3 m (70 feet). The flexural capacity could easily be increased through adding additional prestressing force.

2. In three full-scale tests, the prototype UHPC pi-girder exhibited a minimum dead load plus live load shear capacity of 1,630 kN (366 kips). This capacity is 75 percent greater than the demand required by the AASHTO LRFD Bridge Design Specification[13] for a 2.44-m (8-foot) wide tributary area in a span of 21.3 m (70 feet).

3. The transverse flexural response of the prototype pi-girder was insufficient to carry the full live load plus impact of the AASHTO LRFD Bridge Design Specification[13] defined tandem load without undergoing tensile cracking and inelastic deformation of the cross section. The addition of passive restraint to the cross-section did not significantly increase the load at which the underside of the deck cracked. After cracking, the passive restraint provided by steel straps tying the bulbs together in conjunction with additional lateral restraint at the support locations combined to allow for a 60 percent increase in the applied load ultimate capacity.

4. The prototype pi-girder has a limited capability to transfer primary flexure and shear forces laterally across a bridge. The Lever Rule in the AASHTO LRFD Bridge Design Specification[13] provides a reasonable method for proportioning loads laterally in a bridge. When completing load distribution analyses, each half of the pi-girder cross section should be assumed to act as an individual ‘girder’.

5. The flexural deflection of the prototype pi-girder on a 21.3 m (70 feet) span is greater than the deflection limit recommended in the AASHTO LRFD Bridge Design Specification[13].

6. The tensile response of UHPC when subjected to structural loading can vary depending on available alternate load paths and supplemental geometric cross sectional restraint provided in the system. In primary flexure and shear, the bottom flange and web of the prototype pi-girder exhibited high crack densities and tight crack widths. In transverse flexure where alternate load paths are limited, the deck exhibited relatively large crack spacings with cracks of comparatively large width.

7. In addition to the commonly recognized structural failure mechanisms in reinforced concrete of concrete crushing and reinforcing steel tensile yielding and fracture, the additional tensile failure mechanism of fiber reinforcement pullout warrants consideration for UHPC structures. All structural failures observed in this study were precipitated by the steel fiber reinforcement across a critical crack reaching a pullout strain and debonding from the UHPC matrix. This loss of tensile capacity across a critical crack resulted in load redistribution and member failure.

8. A limiting tensile strain of 0.007 may be reasonable for heavily reinforced UHPC flexure members. A similar limiting tensile strain may also be reasonable for the diagonal principal tensile strain in the web of a prestressed girder. Tensile fiber pullout was observed to occur in the three primary flexure failures between strains of 0.007 and 0.010 and in the webs of two shear failures between strains of 0.009 and 0.011.

9. The fabrication of a structurally-optimized UHPC pi-girder can be successfully completed in a conventional precast concrete girder production facility. Special attention must be given to the proper mixing and placing of fresh UHPC, and to the temperature and shrinkage demands of setting UHPC.

10. Obstructions inside the formwork of a structural element can impede the flow of fresh UHPC and have a significant effect on the local dispersion of fiber reinforcement. In both of the full-scale primary flexural response tests completed in this study, the girders failed at cross sections which contained instrumentation wires running vertically up the girder web. The UHPC matrix was observed to lack fiber reinforcement in the immediate vicinity of the instrumentation wires.

ONGOING AND FUTURE RESEARCH

The results of this study demonstrate that the UHPC pi-girder presents a viable solution for the implementation of UHPC in the highway bridge infrastructure. The development and testing of a second generation UHPC pi-girder is underway. This second generation pi-girder has been specifically modified so as to rectify the structural deficiencies associated with transverse flexural behavior in the prototype girder. Additionally, the second generation pi-girder contains cross-sectional modifications which simplify the fabrication of the girder and reduce stress concentrations at reentrant corners.

REFERENCES

1. Graybeal, B.A., "Material Property Characterization of Ultra-High Performance Concrete," Federal Highway Administration, Report No. FHWA-HRT-06-103, August 2006, 186 pp.

2. Graybeal, B.A., "Structural Behavior of Ultra-High Performance Concrete Prestressed I-Girders," Federal Highway Administration, Report No. FHWA-HRT-06-115, August 2006, 104 pp.

3. Behloul, M., G. Causse, and D. Etienne, "Ductal® Footbridge in Seoul," First fib Congress, Osaka, Japan, October 2002, 11 pp.

4. Chuang, E., "Ductility Enhancement of High Performance Cementitious Composites and Structures," Massachusetts Institute of Technology, 2002, 319 pp.

5. Park, H., "Model-Based Optimization of Ultra High Performance Concrete Highway Bridge Girders," Massachusetts Institute of Technology, 2003, 139 pp.

6. Soh, M., "Model-Based Design of a Ultra High Performance Concrete Prototype Highway Bridge Girder," Massachusetts Institute of Technology, 2003, 64 pp.

7. Chuang, E., and F. Ulm, "Two-Phase Composite Model for High Performance Cementitious Composites," *Journal of Engineering Mechanics*, V. 128, No. 12, 2002, pp. 1314-1323.

8. AASHTO, *AASHTO LRFD Bridge Design Specifications, 2nd Edition*, American Association of State Highway and Transportation Officials, 2002.

9. ASTM C39, "Standard Test Method for Compressive Strength of Cylindrical Concrete Specimens," American Society for Testing and Materials Standard Practice C39, Philadelphia, PA, 2001.

10. ASTM C469, "Standard Test Method for Static Modulus of Elasticity and Poisson's Ratio of Concrete in Compression," American Society for Testing and Materials Standard Practice C469, Philadelphia, PA, 2002.

11. Graybeal, B., "Practical Means for the Determination of the Tensile Behavior of Ultra-High Performance Concrete," *Journal of ASTM International*, V. 3, No. 8, December 2006, 9 pp.

12. ASTM C496, "Standard Test Method for Splitting Tensile Strength of Cylindrical Concrete Specimens," American Society for Testing and Materials Standard Practice C496, Philadelphia, PA, 2002.

13. AASHTO, *AASHTO LRFD Bridge Design Specifications, 4th Edition*, American Association of State Highway and Transportation Officials, 2007.

14. Association Française de Génie Civil, Interim Recommendations for Ultra High Performance Fibre-Reinforced Concretes, 2002.

NTIS DISCLAIMER

- This document has been reproduced from the best copy furnished by the sponsoring agency.